Biochemical and Regulatory Aspects of DNA Double-Strand Break Repair

---

Dissertation

zur Erlangung der naturwissenschaftlichen Doktorwürde

(Dr. sc. nat.)

vorgelegt der

Mathematisch-naturwissenschaftlichen Fakultät

der

Universität Zürich

von

Julia Eileen Godau

aus

Deutschland

Promotionskommission

Prof. Dr. Alessandro A. Sartori (Vorsitz und Leitung der Dissertation)

Prof. Dr. Joao Matos

PD. Dr. Pavel Janscak

Prof. Dr. Matthias Altmeyer

Zürich, 2018

Contents

Abbreviations **v**

Summary **vii**

Zusammenfassung **ix**

1 Introduction **1**
1.1 Genome instability - A hallmark of cancer 1
1.2 DNA damage response 2
1.3 DNA repair 3
1.3.1 DSB repair 4
1.3.2 Meiotic recombination 6
1.3.3 Fanconi anemia pathway of ICL repair 7
1.4 Post-translational modifications 10
1.5 CtIP 11
1.5.1 Sae2/Ctp1/CtIP protein family 11
1.5.2 CtIP promotes DNA-end resection 13
1.5.3 Regulation of CtIP by PTMs 15
1.5.4 CtIP and its connection to cancer development and therapy 18
1.6 SLX4 - A nuclease scaffold 19
1.7 PIN1 22
1.7.1 PIN1 - A molecular switch regulating diverse pathways 22
1.7.2 PIN1 and its role in tumorigenesis 25
1.8 *P. tetraurelia* as a model organism to study DSB repair 27

2 Aims **31**

3 Material and Methods **33**

4 Results **41**
4.1 Investigating the biochemical function of CtIP in DSB repair 41
4.1.1 Identification of a miniature Sae2/Ctp1/CtIP ortholog from *Paramecium tetraurelia* required for sexual reproduction and DNA double-strand break repair 41

Supplementary Figures 79

4.1.2 *Paramecium* CtIP stimulates MRE11 nuclease activity 85
4.2 Deciphering the potential regulation of SLX4 by PIN1-mediated isomerization 89
4.2.1 Validation of the PIN1-SLX4 interaction 89
4.2.2 Identification of the PIN1-interaction motif in SLX4 89
4.2.3 Establishing a phospho-SLX4 (T1315) antibody 97
4.2.4 Investigating the potential role of PIN1 in regulating SLX4 function . 98

5 Discussion and Outlook **109**
5.1 Investigating the biochemical function of CtIP in DSB repair 109
5.2 Deciphering the potential regulation of SLX4 by PIN1-mediated isomerization 115

Bibliography **119**

Acknowledgments **147**

Appendix **149**
Curriculum Vitae 150
Publication: A Short BRCA2-Derived Cell-Penetrating Peptide Targets RAD51 Function and Confers Hypersensitivity toward PARP Inhibition. 152

Abbreviations

ALT	alternative lengthening of telomeres
AML	acute myeloid leukemia
Aph	aphidicolin
ATM	ataxia-telangiectasia mutated
ATR	ataxia-telangiectasia and Rad3-related
BER	base excision repair
CDC25	cell division cycle 25 family members
CDK	cyclin-dependent kinase
CFS	common fragile sites
CO	crossover
CPT	camptothecin
CTD	C-terminal domain
CtIP	CtBP-interacting protein
DDR	DNA damage response
dHJ	double Holliday junction
DNA	deoxyribonucleic acid
DNA-PKcs	DNA-dependent protein kinase catalytic subunit
ds	double-stranded
DSB	double-strand break
Ess1	essential in yeast 1
FA	fanconi anemia
FAAP24	FA-associated protein 24 kDa
GSK3	glycogen synthase kinase 3
HJ	Holliday junction
HR	homologous recombination
ICL	interstrand crosslink
IES	internal eliminated sequences
IP	immunoprecipitation
IR	Ionizing radiation
JNK	Jun-N-terminal protein kinase
LE	long exposure
MAC	macronucleus
MAPK	mitogen-activated protein kinases
MEF	mouse embryonic fibroblasts
MIC	micronucleus
MMC	mitomycin C
MMR	mismatch repair

MRE11	meiotic recombination 11 homolog A
MRN	MRE11-RAD50-NBS1
NBS1	nijmegen breakage syndrome 1
NER	nucleotide excision repair
NHEJ	non-homologous end joining
NIMA	never in mitosis A
NTD	N-terminal domain
PARP	poly(ADP-ribose) polymerase
PD	pulldown
PIKK	phosphatidylinositol 3-kinase-like protein kinase
PLK1	polo-like kinase 1
PPase	protein phosphatase
PPIase	peptidyl-prolyl *cis/trans* isomerase
PTMs	posttranslational modifications
RB	retinoblastoma
RBBP8	retinoblastoma binding protein 8
Rtt107	regulator of Ty1 transposition
ROS	reactive-oxygen species
RPA	replication protein A
Sae2	sporulation in the absence of Spo11 protein 2 homolog
SC	synaptonemal complex
SE	short exposure
SIM	SUMO interaction motif
SLX	synthetic lethal of unknown function
Spo11	sporulation-specific protein 11
ss	single-stranded
SSB	single-strand breaks
ssc	single-stranded circular
S/T-P	serine/threonine-proline
SUMO	small ubiquitin-related modifiers
TLS	translesion synthesis
UV	ultraviolet light
wt	wild type

Summary

Faithful transmission of genetic information to daughter cells is fundamental for all living cells. DNA lesions resulting from exogenous or endogenous sources are potent driving forces of genomic instability and tumorigenesis. To maintain genome integrity, cells have evolved a complex network of DNA damage signaling and repair pathways, referred to as the DNA damage response (DDR). CtIP and SLX4 are key DDR factors, contributing to the error-free survival of cells in response to genotoxic stress. However, our mechanistic understanding about how these DNA repair proteins operate at the molecular level and how their activities are regulated during the cell cycle is very limited.

Human CtIP is crucial for the resection and repair of DNA double-strand breaks (DSBs), one of the most cytotoxic lesions a cell can encounter. At the molecular level, the function of CtIP in DSB repair is not fully understood and the lack of high-resolution structures precludes any detailed insights into its biochemical features. Recently, our lab identified two open reading frames in the ciliate *Paramecium tetraurelia*, representing the shortest known orthologs of CtIP in evolution. In the course of our studies, we investigated the DNA binding properties of recombinant PtCtIP and its functional interplay with the MRE11-RAD50 nuclease complex. Specifically, we find that PtCtIP binds with high affinity to replication fork-like DNA structures but lacks any detectable intrinsic nuclease activity. Moreover, DNA binding, but not MRE11-RAD50 interaction, strongly depends on a highly conserved RHR motif located in the evolutionarily conserved C-terminus. Additionally, using genetically engineered cells stably expressing a CtIP DNA binding mutant, we provide evidence that the RHR motif mediates recruitment of CtIP to sites of DNA damage, thereby ensuring efficient DNA-end resection and homology-directed repair of DSBs. In collaboration with the lab of Dr. Mireille Bétermier, we further unveiled that

PtCtIP is required for the processing of Spo11-dependent meiotic DSBs in *P. tetraurelia*. Together, these results establish that PtCtIP is a true homolog of CtIP and that a short DNA-interaction motif is crucial for its function in DSB repair.

In the second part of my Ph.D. thesis, we sought to decipher the potential regulation of SLX4 by PIN1-mediated prolyl isomerization. PIN1 catalyzes the isomerization of proline peptide bounds adjacent to phosphorylated serines or threonines (pS/T-P) to either *cis* or *trans* configuration, thereby controlling protein function. We previously discovered various DDR factors in a proteomic screen for potential PIN1 targets, including the DNA repair endonuclease scaffold SLX4. Human SLX4 is involved in the cleavage of DNA interstrand-crosslinks (ICL) and resolution of Holliday junctions (HJs) as well as in the trimming of telomeric loops. Our results hitherto suggest that PIN1 binds to SLX4 in a direct and phosphorylation-dependent manner. Moreover, fine-mapping of the PIN1 interaction motif in SLX4 points towards multiple pS/T-P sites as critical sites for PIN1 recognition. However, overexpression or knockdown of PIN1 does neither alter established SLX4 protein-protein interactions required for ICL repair and HJ resolution nor its telomeric localization, indicating that PIN1 potentially controls other biological aspects involving SLX4.

Zusammenfassung

Jeden Tag wird unser Erbgut - DNS genannt - geschädigt, sei es durch UV-Strahlung, Tabakrauch oder andere toxische Substanzen, die bei normalen zellinneren Prozessen entstehen. Jede Veränderung der DNS birgt die Gefahr entscheidende Mechanismen, welche die Zellteilung und das Zellwachstum kontrollieren, ausser Gefecht zu setzen. Dies kann zu Zellentartung und schliesslich Krebs führen.
Umso entscheidender ist, dass jede einzelne Zelle mit einem vielfältigen Repertoire an DNS Reparaturmechanismen ausgestattet ist, welche die Integrität des Genoms schützen. Das Zusammenspiel einzelner Faktoren in diesem hoch komplexen Netzwerk - unter ihnen Schlüsselproteine wie CtIP und SLX4 - ist jedoch bei weitem nicht aufgeklärt.
CtIP ist ein evolutionär hochkonserviertes Protein, welches eine essentielle Rolle in der Reparatur von DNS Doppelstrangbrüchen (DSB) spielt. Auch wenn in den letzten Jahren viele Erkenntnisse über CtIP gewonnen wurden, fehlen immer noch entscheidende Mosaikstücke um die Funktion von CtIP im Detail zu verstehen. Erschwerend kommt hinzu, dass die Kristallstruktur von CtIP noch nicht aufgeklärt werden konnte. Diese würde uns wichtige Anhaltspunkte zum besseren Verständnis der biochemischen Eigenschaften von CtIP liefern. Der erste Teil meiner Arbeit beschreibt die Charakterisierung von CtIP des Pantoffeltierchens (*Paramecium tetraurelia*). PtCtIP besteht größtenteils nur aus den wichtigsten konservierten Domänen und stellt mit einer Länge von 198 Aminosäuren das kleinste bisher beschriebene CtIP Ortholog dar. Zusammen mit der Forschungsgruppe von Dr. Mireille Bétermier zeigen wir, dass PtCtIP essentiell für die sexuelle Reproduktion in *P. tetraurelia* ist. Wir charakterisieren die biochemischen Eigenschaften von aufgereinigtem, rekombinantem PtCtIP und demonstrieren, dass das RHR Motiv im C-terminus des Proteins maßgeblich für die Bindung an die DNS verantwortlich ist, aber selbst keine

DNS schneiden kann, eine Eigenschaft welche für andere CtIP Proteine umstritten ist. Ausserdem liefern wir Beweise, dass ein intaktes RHR Motiv sowohl für die Lokalisierung des CtIP Proteins an beschädigte DNS als auch für die DSB Reparatur wichtig ist.
Der zweite Teil meiner Doktorarbeit basiert auf früheren Ergebnissen unserer Arbeitsgruppe, in denen SLX4, ein Adapterprotein für verschiedene Nukleasen, als neuer Bindungspartner der Peptidyl-Prolyl-Isomerase PIN1 identifiziert wurde. SLX4/FANCP wird als Fanconi Anemia Gen kategorisiert, dessen Mutation mit der gleichnamigen Erkrankung assoziiert ist. Mittels verschiedener Experimente bestätigen wir, dass PIN1 und SLX4 direkt und abhängig von bestimmten Phosphorylierungsmotiven (S/T-P) miteinander interagieren. Weitere Resultate deuten darauf hin, dass PIN1 keinen Effekt auf andere Interaktionspartner von SLX4 hat und auch nicht die Lokalisierung von SLX4 im Zellkern beeinflusst. Die Frage nach der biologischen Bedeutung der PIN1-SLX4 Interaktion wird uns also noch eine Weile beschäftigen.
Zusammenfassend liefern unsere Resultate neue Einblicke in die Funktion von CtIP auf molekularer und zellulärer Ebene und schaffen eine vielversprechende Basis die Funktion der SLX4-Isomerisierung für die Genomstabilität weiter zu erforschen.

Introduction

1.1 Genome instability - A hallmark of cancer

The genome is defined as an organism's complete set of genetic material. It consists of deoxyribonucleic acid (DNA), which is present in almost every cell of the human body[1]. The human genome, which is stored in the nucleus of a cell, comprises 3 x 10^9 nucleotides of DNA and carries all the information necessary to build and maintain the organism by governing cell division and survival. Therefore, it is of utmost importance to preserve genomic stability to faithfully propagate genetic information to subsequent generations. Failure to do so can lead to the development of cancer – a disease characterized by abnormally proliferating cells that can invade beyond normal tissue boundaries and metastasize to distant organs[2].

A major underlying cause driving carcinogenesis is the accumulation of multiple mutations and clonal expansion[3]. Mutations can alter the DNA sequence with base pairs being substituted, changed or deleted but can also affect the structure or number of individual chromosomes (e.g. translocations, fusions and duplications). The number of mutations can differ from a considerably small number to hundreds or thousands. Accordingly, mutations can be either passenger mutations, having a rather modest effect for the cell, or driver mutations, changing key factors of basic cellular processes[4]. Consequently, mutations can affect the function of oncogenes and tumor suppressor genes in a normal cell[5]. Oncogenes are genes, which hyperactivation have the potential to cause cancer, whereas the term tumor suppressor refers to those genes whose loss-of-function leads to tumor development[5]. Notably, cancer evolves over time and all its stages, ranging from precancerous lesions to already malignant tumors cell, and the underlying mu-

tational processes are highly diverse[6]. Germline mutations in genes employed in DNA repair and the maintenance of genomic integrity predispose their carriers to an increased risk of cancer[7,8]. To name one example, women carrying mutations in the BRCA1 gene are at increased lifetime risk for developing breast cancer of 72% compared to 12% in normal population and for ovarian cancer of 44% compared to 1.5%[9,10]. In conclusion, genome instability is a hallmark of cancer cells[11,12].

1.2 DNA damage response

Maintaining genetic stability is essential for cell survival and division. Nevertheless, our genome is constantly exposed to intrinsic or extrinsic factors, provoking different types of DNA lesions. DNA alterations can arise from exposure to ionizing radiation (IR), ultraviolet light (UV) or chemical compounds, such as ingredients of tobacco smoke or chemotherapeutic drugs. Moreover, DNA damage can also be induced by DNA replication errors or by endogenously generated reactive-oxygen species (ROS), free radicals and nitrogen species[13]. It has been estimated that each cell of the human body is challenged by 25 highly dangerous DNA double-strand breaks (DSBs) per day[14]. Paradoxically, DSB induction is also a fundamental process in generating biological diversity. During meiosis or development of the immune system, hundreds of DSBs are deliberately induced and subsequently repaired to generate novel combinations of genes[15].

To ensure genomic integrity, eukaryotic cells have evolved a sophisticated signaling network, termed the DNA damage response (DDR). The DDR can be described as a cascade of sequentially activated sensor proteins at sites of DNA lesions, signal transmitters, and effector proteins to pause cell cycle progression by activating cell cycle checkpoints and provide time for DNA repair[16]. If repair fails or cell cycle progression is paused for too long, the DDR triggers programmed cell death (apoptosis) or senescence to avert tumorigenesis[17].

Upon DNA damage lesion-specific sensing complexes, including MRN complex (MRE11, meiotic recombination 11 homolog A; RAD50; and NBS1, Nijmegen breakage syndrome 1) and RPA (replication protein A), initiate the DDR by activating signal transducer pro-

teins of the phosphatidylinositol 3-kinase-like protein kinase (PIKK) family, mainly ATM (ataxia-telangiectasia mutated), ATR (ataxia-telangiectasia and Rad3-related) and DNA-PKcs (DNA-dependent protein kinase catalytic subunit)[18,19]. ATM and ATR amplify the signal by phosphorylation of downstream transducers like the checkpoint kinases CHK1 and CHK2[20]. To transiently pause the initiation of DNA replication, CHK1 and CHK2 act on a variety of substrates, amongst others CDC25 (cell division cycle 25 family members) and the kinase Wee1. These in turn, promote the inhibition of CDKs (cyclin-dependent kinases), which are responsible for progression and proper timing of the cell cycle[21]. Importantly, CDKs have recently emerged as key players in the regulation of DNA repair pathways[22,23]. Furthermore, CHK1, CHK2 and ATM promote stabilization of p53, a key tumor-suppressor protein triggering cell cycle arrest, altered transcription and apoptosis[24].

1.3 DNA repair

Each cell is equipped with a toolkit of DNA repair mechanisms. Base excision repair (BER) facilitates repair of aberrant DNA bases, such as deaminated cytosines, oxidized guanines and alkylated adenines[25]. Nucleotide excision repair (NER) is suited to remove bulky DNA lesions, such as the ones formed during exposure to UV light[26]. The mismatch repair pathway (MMR) is responsible for the detection and excision of nucleotides misincorporated during replication[27,28]. To overcome obstacles faced during replication, cells employ specialized translesion synthesis (TLS) polymerases, a process that bears an increased risk of causing mutagenesis[29]. Finally, DSBs are mainly repaired by non-homologous end joining (NHEJ) or homologous recombination (HR)[30]. Evidently, repair pathways can overlap. For instance, DNA interstrand cross-links (ICLs) are repaired by the concerted actions of NER, HR and TLS[31]. Given the fact that most cancer cells have lost one or more DDR pathways render them more dependent on the remaining ones. This vulnerability is currently exploited in targeted cancer treatment based on the concept of synthetic lethality[17,32,33].

1.3.1 DSB repair

DSBs are considered the most cytotoxic lesions, because the two complementary strands of the DNA helix are disrupted simultaneously at approximately the same place. Cells have evolved two major DSB repair mechanisms: non-homologous end-joining (NHEJ) and homologous recombination (HR)(Figure 1.1). NHEJ is active throughout the cell cycle and directly ligates broken DNA ends. DSB repair by classical NHEJ is initiated by binding of the KU70/80 heterodimer to two juxtaposed DNA ends that are subsequently rejoined by the XRCC4-XLF-DNA ligase IV complex[31,34,35]. In S/G2 phase, however, when an intact sister chromatid is present for repairing DSBs in an homology-dependent manner, HR competes with NHEJ[31]. In mammals, HR is initiated by the MRN complex, which recognizes the DSB and recruits CtIP (CtBP-interacting protein), preventing the association of KU70/80[36,37]. Together with CtIP, MRN tethers the broken DNA and initiates processing of the DSB ends[37,38]. A bidirectional DNA-end resection model was proposed, in which CtIP stimulates the endonucleolytic activity of MRN to generate a nick in the 5' strand. In a second step, Mre11 continues to exonucleolytically trim the DNA in a 3' to 5' direction from the nick towards the DSB. Meanwhile, exonucleases such as Exo1 (exonuclease 1) and Dna2 (together with the helicase BLM) resect the same strand in 5' to 3' direction away from the nick[39–41]. Generated 3' ssDNA-overhangs are immediately protected from degradation and stabilized by the heterotrimeric replication protein A (RPA). With the help of a BRCA1-BARD1-PALB2-BRCA2 recombination mediator complex, RPA is subsequently replaced by the recombinase Rad51 to form nucleoprotein filaments that initiate homology search and catalyze invasion of the intact duplex DNA sequences, ultimately resulting in the formation of a DNA structure called double Holliday junction (dHJ)[42]. After DNA synthesis, the dHJs can be processed by different mechanisms to complete HR, generating either non-crossover or crossover recombination products, depending whether the flanking DNA of the break is exchanged or not[43]. In the presence of type IA topoisomerase (BLM-TOP3A in mammals) and a DNA helicase dHJ dissolution generates non-crossover products by facilitating branch migration and decatenation of the JH. In absence of BLM, dHJs are processed by structure-specific resolvases, giving raise to either non-crossover or crossover products[44].

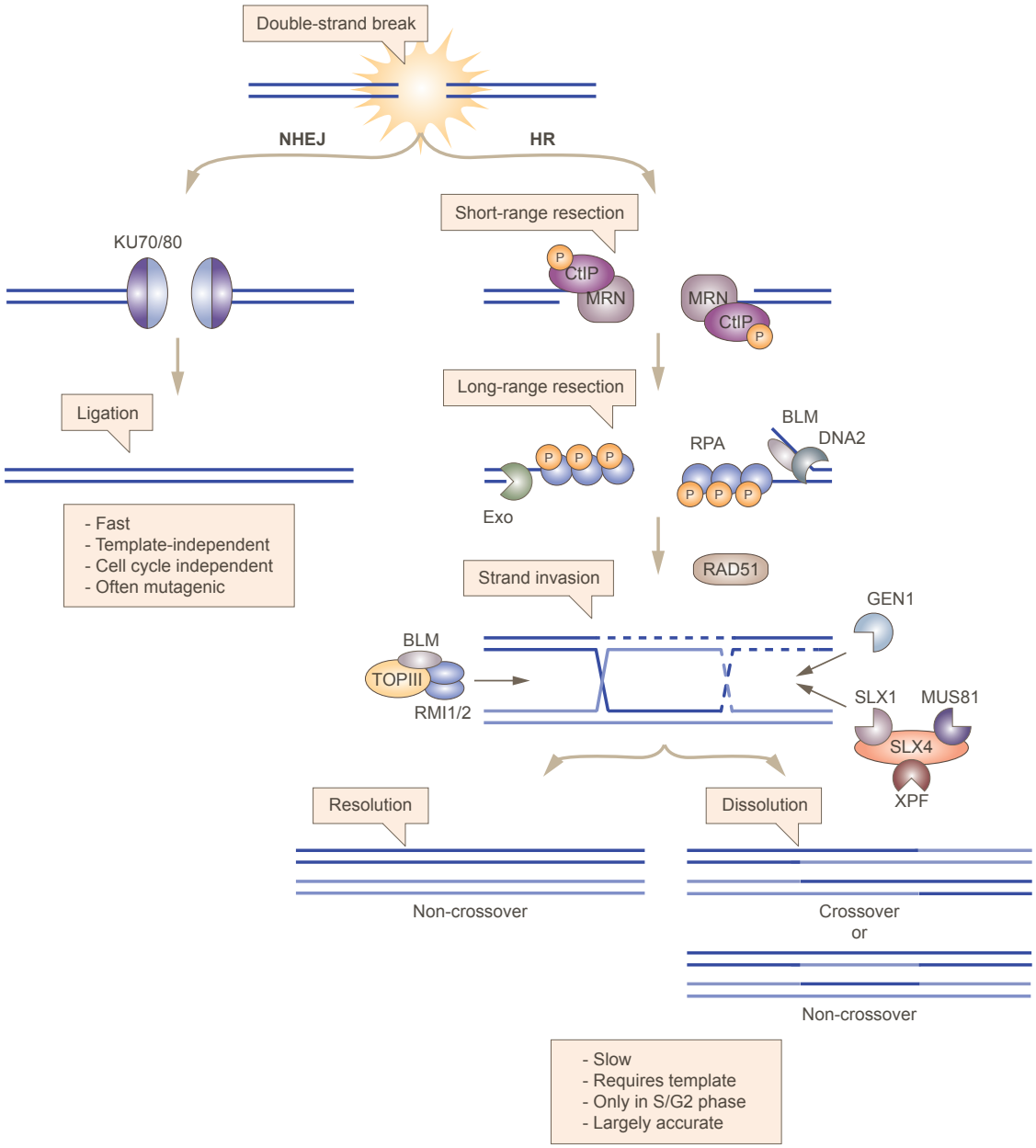

Figure 1.1: Schematic representation of DSB repair pathways. After a DSB occurs, the Ku70/80 heterodimer rapidly associates to the DSBs to facilitate repair by NHEJ. NHEJ is considered to be active throughout the cell-cycle and does not depend on the presence of template for repair, but is therefore often mutagenic. Alternatively, the break can be repaired by HR, which is restricted to S/G2. After MRN senses the DSB, CtIP is recruited to the sites of the break to initiate short-range resection, generating 3' ssDNA overhangs – a step which ultimately inhibits NHEJ and catalyzes further processing by HR. ssDNA stretches are immediately protected by RPA while EXO1 or BLM, in conjunction with DNA2, facilitate long-range resection. Next, RPA is displaced by RAD51, which mediates strand invasion into the homologous DNA template leading to the formation of a double Holliday junction (dHJ). dHJ resolution by BLM, topoisomerase IIIα, and RMI1 results in non-crossovers. In contrast endonucleolytic cleavage and dissolution of the dHJ by GEN1 or the SLX4 protein complex can lead to non-crossovers and crossovers depending on the incision pattern of the two strands.

The output strongly depends on which resolvase is employed for the endonucleolytic cleavage of the dHJ. Key proteins mediating dHJ resolution by introduction of two single-stranded (ss) incisions are the resolvase GEN1 and a multi-subunit nuclease complex consisting of SLX1-SLX4 and MUS81-EME1[45–47].

1.3.2 Meiotic recombination

Meiosis is a specialized form of cell division that generates haploid gametes in most sexually reproducing organisms[48]. The genetic information is reshuffled to facilitate genetic diversity in progeny. During the first meiotic division, homologous chromosomes of both maternal and paternal origin undergo replication to form pairs of sister chromatids. Next, sister chromatids conglomerate in bivalent pairs, which are stabilized by the synaptonemal complex and cohesion proteins[49,50]. The bivalent association is crucial for the later formation of crossovers, i.e. the reciprocal exchange of chromosome arms, which occur by recombination events. In contrast to HR repair in somatic cells, where genome maintenance has priority and therefore non-crossovers are preferred, meiotic recombination promotes generation of at least one crossover per chromosome to mix genetic information[51] (Figure 1.2). In the last step, the spindle is formed and chromosomes line up along the metaphase plate before being separated into two daughter cells. Recombination failures or obstacles occurring during metaphase often lead to meiotic arrest and failure in correct chromosome segregation, ultimately having negative consequences on fertility[49]. Recombination is initiated by the induction of DSBs in a programmed manner – another major difference to DSBs induced by DNA damage[52]. Self-inflicted DSBs during meiosis are catalyzed by the type II-topoisomerase Spo11, which is highly conserved from yeast to human[53,54]. Upon cleavage of both DNA strands, Spo11 stays covalently attached to the 5' ends of the break. Subsequently, Spo11 is released from DSB ends by endonucleolytic single-strand cleavage on each side of the break[48,55]. This so-called 'clipping' of Spo11 is mediated by the MRN complex in concerted action with CtIP and allows subsequent resection and recombination[40]. In yeast, the CtIP homolog Sae2 and the nuclease activity of Mre11 are essential for the removal of Spo11 and DNA resection[56]. In a first step, CtIP enhances MRE11-dependent cleavage activity to clip the protein-blocked DSB

ends, and subsequently induces long-range resection to facilitate homology search and repair of the DSB[57–59]. In contrast to DSB repair by HR in somatic cells, meiotic recombination requires the replacement of RPA by both Rad51 and the meiosis-specific strand exchange protein Dmc1. Data from *S. cerevisiae* suggest that Rad51 and Dmc1 cooperate during meiotic recombination with Rad51 being crucial for recombination while Dmc1 serves as a supporting factor to stimulate strand exchange activity[60,61]. Next, the nucleoprotein filament invades selectively the homologous chromosome instead of the sister-chromatid, leading to the formation of HJ, which are preferentially resolved producing crossovers. Thus, key players facilitating the incision of HJ during meiosis are the structure-specific SLX4 nuclease complex and the GEN1 resolvase[47,62].

	Meiotic cell	Vegetative cell
DSB breaks	**Programmend, SPO11-induced**	**Accidential**
Repair template	**Homologous chromosome**	**Sister chromatid**
Strand-exchange protein:	**RAD51, DMC1**	**RAD51**
Genetic outcome	**≥ one crossover/chromosome**	**Non-crossover prefered**
Function	**Exchange of genetic information**	**Maintenance of genome instability**

Figure 1.2: An overview of the major differences between HR in meiotic and vegetative cells.

1.3.3 Fanconi anemia pathway of ICL repair

ICLs are defined as covalent and irreversible linkages between DNA bases residing in opposite strands of the double helix. ICLs can have catastrophic consequences for the cell because they prevent separation of the DNA strands, thereby blocking essential metabolic processes such as replication or transcription[63]. Rapidly proliferating cells, including cancer cells, are hypersensitive to ICLs mainly due to DNA replication interference, ultimately triggering apoptosis. Thus, ICL-forming agents, such as cisplatin or mitomycin C, are among the most widely used antitumor drugs[64,65]. Moreover, ICLs can also be induced during normal cell metabolism by aldehydes that are produced as by-products of lipid peroxidation[66,67].

ICL removal during S-phase is achieved by combination of three classical DNA repair mechanisms - HR, NER and TLS - coordinated by the Fanconi anemia (FA) pathway[31]. ICL repair can be divided into the following steps: sensing of the lesion, incision and unhooking of the crosslink and DSB formation, followed by translesion synthesis and repair completion by HR[68,69] (Figure 1.3A).

FA is a rare chromosomal instability syndrome affecting 1 in 100'000 individuals[83]. Patients commonly suffer from bone marrow failure, congenital abnormalities and an extremely high risk of developing leukemia or solid tumors[84]. FA is an autosomal recessive disease and the susceptibility to cancer is associated with an abnormal response to DNA damage and genomic instability. Mutations in FA genes confer extreme cellular hypersensitive to ICL-inducing agents[7,69]. Currently, nineteen genes specifically mutated in FA patients are known, with most of them carrying out additional functions in other DNA repair transactions (Figure 1.3B).

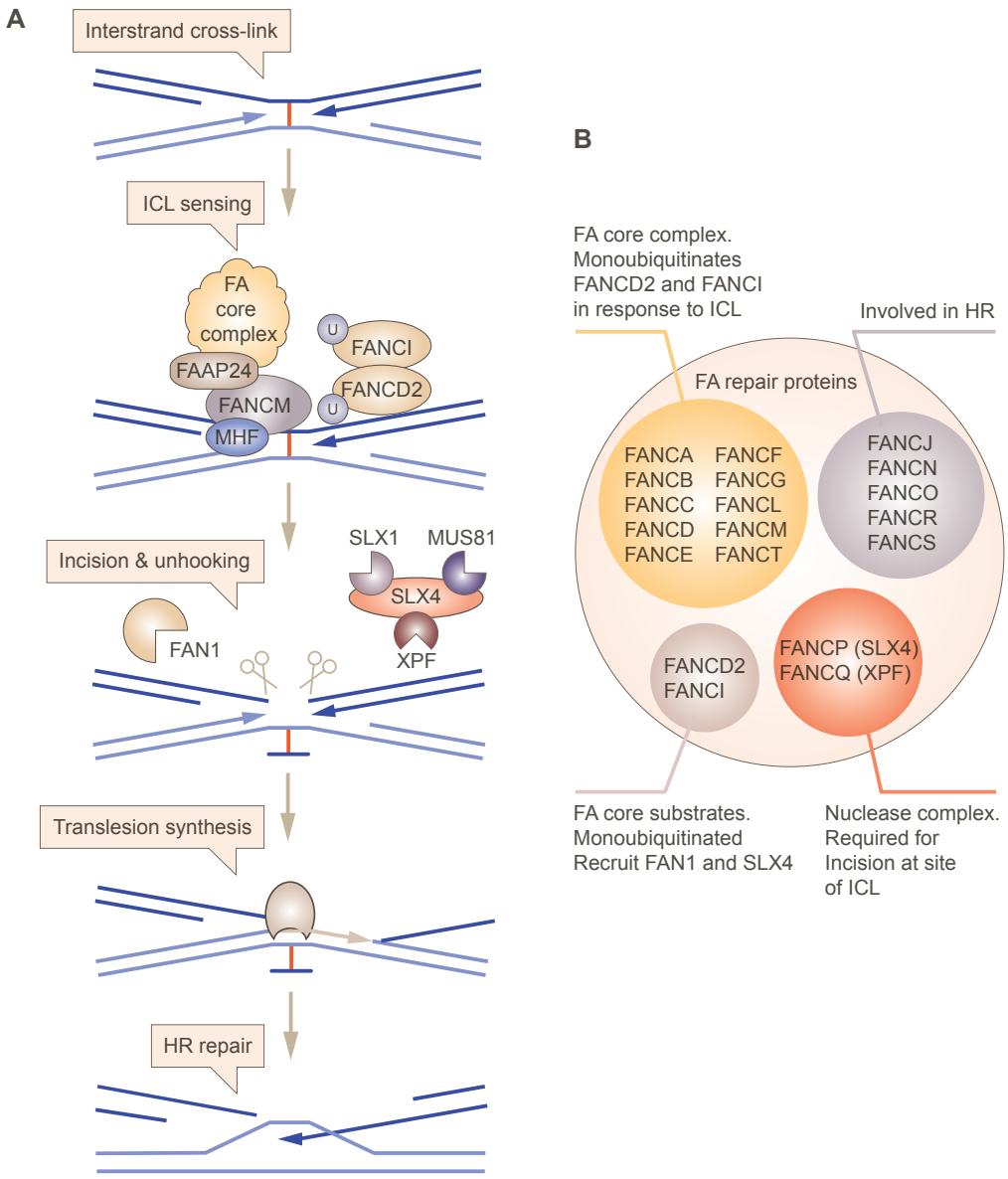

Figure 1.3: Model of ICL repair and list of FA proteins. (**A**) When a replication fork encounters an ICL, the translocase FANCM together with FAAP24 (FA-associated protein 24 kDa) and MHF1/2 is recruited to the DNA, which initiates ATR-mediated checkpoint signaling and subsequently leads to the loading of the FA core complex[70–72]. The FANCL subunit then catalyzes monoubiquitination of FANCD2 and FANCI[73–75]. Ubiquitination of FANCD2 triggers the accumulation of additional proteins that coordinate DNA repair, including the endonuclease FAN1 and the scaffold protein SLX4 (alias FANCP)[76,77]. ERCC1-XFP and MUS81-EME1 are SLX4-associated structure-specific nucleases and, together with the FAN1, assumed to mediate the incision at both 5' and 3' sides of the DNA strand flanking the crosslink, resulting in unhooking of the lesion[78]. Still, a crosslinked base is adducted on one strand, thus TLS has to be used to replicate over the adducted base. Nucleotide excision repair (NER) removes the bulky base and the gap in the opposite sister strand is repaired by HR, using the sister chromatid, which has been repaired by TLS, as a template[79]. (**B**) List of FA proteins and their implication in DNA repair. Most of the FA proteins (FANCA, B, C, D, E, F, G, L, M and T) build the FA core complex. The FANCL harboring ubiquitin ligase activity ubiquitinates FANCD2 and FANCI to initiate ICL repair[80,81]. Adapted from[80] and[82].

1.4 Post-translational modifications

Cells need to rapidly react to internal and external cues to facilitate proper cell cycle progression and development. To ensure accurate and timely communication of metabolic pathways, most proteins are tightly regulated by post-translational modifications (PTMs). PTMs are crucial for determining the fate of a protein, its localization, activity or stability and facilitate interaction with other proteins, often in a dynamic and reversible manner[85]. More than 300 different PTMs are known, adding another layer of complexity to the signaling network[86]. PTMs are described as the covalent attachment of molecules to amino acid side chains or as conversion of a protein into a different isomer[87]. The former includes addition of a chemical group (like phosphorylation) or polypeptides (SUMOylation or Ubiquitination), the latter can be *cis-trans* isomerization[88–90]. Moreover, proteins can be modified on more than one residue that are in constant crosstalk with each other.

Phosphorylation is the best-characterized and most extensively encountered PTM. It is estimated that one third of all eukaryotic proteins are phosphorylated[91]. Protein phosphorylation is the covalent addition of a phosphate group donated from ATP to the hydroxyl group of serines, threonines and tyrosines with a distribution of 1800:200:1 in vertebrates[92]. Addition of the charged, dianionic, tetrahedral phosphate group to a neutral OH side chain alters the chemical environment of the protein and can induce conformational changes[93]. Consequently, change of the chemical microenvironment surrounding modified residues can foster enzymatic activity, interaction with other proteins or influence other PTMs[85]. The attachment and removal of the phosphate group is catalyzed by protein kinases and phosphatases (PPases), respectively. The family of kinases is extensive and highly diverse with over 500 members. In contrast, PPases only count 150 family members[94,95].

Prominent serine/threonine kinases are ATM, ATR, CDKs and MAPKs[22,23,96–99]. CDKs and MAPKs are tightly regulated during the cell cycle and specifically phosphorylate serine or threonine residues preceding prolines (S/T-P motifs). Strikingly, prolyl peptide bond isomerization is tightly intertwined with phosphorylation and is catalyzed by peptidyl-prolyl *cis-trans* isomerases (PPIase), such as PIN1, which constitutes a crucial

post-phosphorylation signaling mechanism (see chapter 1.7.1)[100].

1.5 CtIP

1.5.1 Sae2/Ctp1/CtIP protein family

First studies in *S. cerevisiae* described the CtIP ortholog Sae2 as 'sporulation in the absence of Spo11 protein 2 homolog' with its mutation resulting in hampered progression of meiosis at prophase presenting first hints towards its crucial role in DNA-end resection[101,102]. CtIP is highly conserved among organisms ranging from yeast to human. Several studies identified orthologs in *S. cerevisiae* (Sae2), *S. pombe* (Ctp1), *C. elegans* (COM-1), *A. thaliana* (AtCOM1), *X. laevis* (xCtIP), *G. gallus* and *M. musculus*[37,103–106]. Members of the CtIP protein family vary extremely in size, with the stripped-down version expressed in *Paramecium tetraurelia* (PtCtIP) representing the smallest known ortholog (Figure 1.4).

At the molecular level, human CtIP is a 125 kDa nuclear protein comprised of 897 amino acids (Figure 1.4). Members of the Sae2/Ctp1/CtIP protein family are predicted to be largely intrinsically disordered, with exception of the N-terminal coiled-coil domain (NTD) that mediates tetramerization of homodimers, and the highly-conserved C-terminal domain (CTD)[107–109]. Both terminal domains of CtIP have been reported to interact independently with the MRN complex[110]. CtIP's role in DNA-end resection has mainly been attributed to its physical and functional interaction with MRN[37]. This versatile protein complex consists of a highly conserved MRE11-RAD50 heterodimer and NBS1 functioning as a signal transducer to foster activation of the ATM kinase[111–113]. Furthermore, Nbs1 coordinates the interaction of Mre11 with fission yeast Ctp1 at the vicinity of the break by recognizing phosphorylated Ctp1 and subsequently linking it to the MRN complex via its FHA domain[114,115]. A similar mechanism has been proposed for human NBS1 although the MRN complex is not strictly required for CtIP recruitment to DSBs[110,116]. Yeast cells lacking one of the components of the MRN complex are viable but present growth defects, hypersensitivity to DSB-inducing agents and failure in meiosis progression[117]. However, in mice all proteins of the MRN complex are essential for survival as

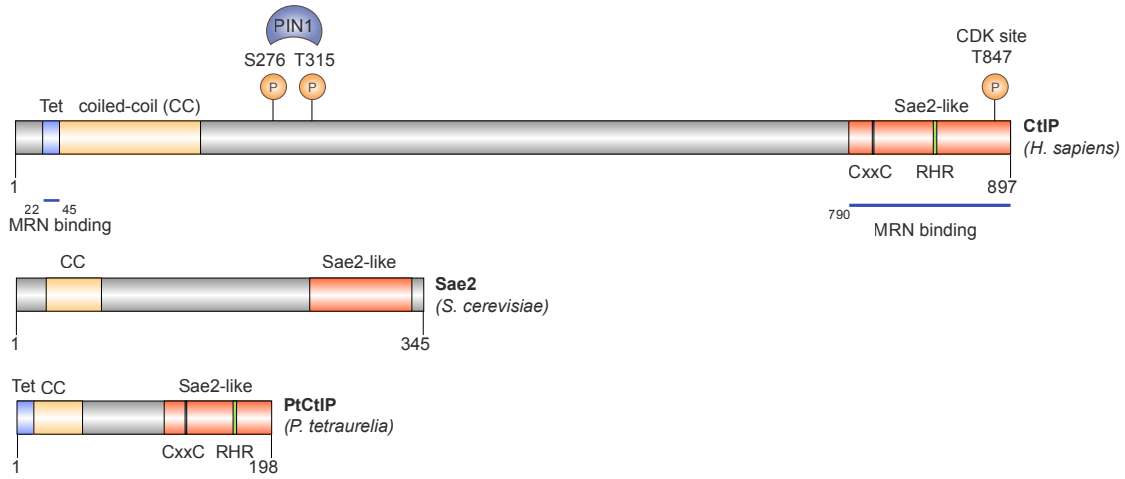

Figure 1.4: Schematic depiction of human CtIP and its orthologs in *S. cerevisiae* (Sae2) and *P. tetraurelia* (PtCtIP) including the most important domains, motifs and PTMs. The N-terminus of CtIP contains the tetramerization domain (blue) within a coiled-coil (yellow) followed by an intrinsically disordered middle region (grey). The peptidyl-prolyl isomerase PIN1 interacts with phosphorylated residues S276 and T315. The C-terminal part (Sae2-like domain, orange) contains the CDK phosphorylation site T847 and the CxxC and the RHR motif, which is required for DNA binding. MRN-binding regions are located in both N- and C-terminal regions of CtIP.

knockout mice display embryonic lethality[118–120]. Recent *in vitro* findings highlighted CtIP as a co-factor of MRN nuclease function and identified phosphorylation at T847 to promote CtIP-dependent stimulation of the MRE11 endonuclease activity[57]. Furthermore, a study in *C. elegans* demonstrated that COM-1 is not essential for MRN dependent resection but rather important to inhibit NHEJ during meiosis[121]. Taken together, CtIP is thought to play additional roles than stimulating MRE11. Yeast strains bearing null mutations of Sae2 were more sensitive to DNA-damaging agents than cells expressing the nuclease dead version of Mre11. Additionally, mouse embryos lacking CtIP die at day 3.5-4 compared to animals exhibiting MRE11 nuclease dead, which survive to day 7.5-9.5[122–125]. Moreover, CtIP directly interacts with and stimulates BLM helicase via its residues 161-369, indicative for a role not only in short-end resection (in concerted action with MRN) but also in promoting long-range resection[126]. Similarly, EXO1 is recruited in a CtIP-dependent manner accompanied by MRN suggesting that CtIP restrains EXO1 activity *in vitro*[127].

CtIP tetramer assembly is critical for its function in DNA-end resection[108,128]. Detailed biochemical studies have demonstrated that amino acids 45-160 compose a coiled-coil

structure facilitating CtIP homodimerization. The preceding residues 20-45 have been found to compose the tetramerization domain. Disruption of dimers or mutation of the tetramerization motif resulted in abrogated localization of CtIP to DSB breaks, impaired HR and strong resection defects[108,128,129]. Interestingly, a shortened version of CtIP, comprising residues 1-296, fused to Cas9 endonuclease enhanced homology-directed repair efficiency, thereby potentially improving CRISPR-based precise genome editing[130]. A small region within the CtIP CTD displays the highest degree of amino acid similarity among all members[37,131]. Remarkably, the congenital microcephaly syndromes Seckel and Jawad are caused by mutations in the CtIP gene, leading to the expression of a C-terminally truncated form of CtIP[132]. C-terminal deletion of CtIP abrogates MRN interactions, DNA-end resection and activates the G2-M checkpoint[37,108]. The C-terminal region was found to be critical for the stimulation of the MRN endonuclease activity, in particular mediated by the highly conserved T847 CDK phosphorylation site[133,134]. Closer examination of the CTD of all orthologs revealed the presence of a so-called 'RHR' motif, shown to be important for DNA binding *in vitro*[107]. Fission yeast strains expressing a Ctp1 mutant with disrupted RHR motif were sensitive to various genotoxic agents and showed chromosomal defects, further emphasizing the importance of this motif for proper DNA-end resection[107]. In addition, CtIP orthologs harbor a highly conserved CxxC motif in their C-termini, which is associated with zinc-binding. Human CtIP contains an additional N-terminal CxxC (amino acid 82-92), which is thought to stabilize the protein structure[108]. Although depletion of the CxxC sensitizes fission yeast to multiple DNA damaging agents, such as hydroxyurea, CPT or UV, the precise function of the CxxC motif is unknown[104]. Finally, two phosphorylation sites (S276 and T315) mediate the CtIP isomerization by PIN1. Consequently, PIN1-mediated isomerization influences CtIP stability by promoting its ubiquitination and proteasomal degradation[135].

1.5.2 CtIP promotes DNA-end resection

CtIP and its orthologs have emerged as key factors in response to DSBs with multi-functional roles. Most importantly, CtIP is implied in DNA-end resection and removal of protein-blocked ends in conjunction with the MRN complex[37,56,57,136,137]. Yet, the pre-

cise mechanistic role of CtIP in promoting HR still remains controversial. It has been demonstrated that CtIP either stimulates MRN activity or functions itself as a nuclease. Three studies have reported that purified recombinant CtIP and Sae2 exhibit structure-specific nuclease activity[138–140]. However, these results could not be confirmed by other groups, failing to detect any nuclease activity associated with recombinant CtIP, Sae2 and Ctp1[57,107,126,136]. Alternatively, it was found that CtIP proteins functions as cofactors of the MRE11 endonuclease, mainly facilitating the removal of protein-blocks at DNA ends *in vitro*[57,136]. These findings are supported by data showing that Sae2 and Ctp1 are required for the removal of covalently attached Spo11 from the 5' DNA ends to allow further strand resection and meiotic recombination[137,141,142].

Besides actively promoting DNA-end resection, several groups proposed a crucial role for Sae2 in the removal of attached MRX from sites of the DNA break, which would otherwise prevent strand invasion and HR[123,143,144]. Intriguingly, it has been suggested that the protein architecture of multimeric CtIP might be suited to physically link DNA molecules, as it was reported for purified Sae2 and Ctp1 *in vitro*[107,145]. CtIP/Sae2/Ctp1 binds DNA mostly via its C-terminal domain, although studies in fission yeast show that the N-terminal domain alone exhibits weak DNA binding activity[107,108,139]. Examining the bridging ability using various Ctp1 mutants revealed that integrity of the intrinsically disordered region, the RHR motif and the NTD are all required for DNA bridging[107]. Thus, rather than acting as a nuclease itself, the DNA binding and bridging function of CtIP are proposed to modulate the nucleolytic activity of a flexibly linked MRN-DNA complex[107,108]. Notably, also the MR complex can bridge DNA, emphasizing the importance of keeping DNA-ends in close proximity to facilitate DSB repair[111,113,146,147]. It has been proposed that DNA-bridging by MRN is a prerequisite of Ctp1-mediated tethering and subsequent DSB processing[107]. In line with this, Ctp1 interacts with the FHA/BRCT domain of Nbs1 to hold the DSB ends in proximity and facilitate resection[115,148]. However, the exact mechanism of DNA bridging is still not fully understood. Functional roles of CtIP and its orthologs contributing to DSB repair are summarized in Figure 1.5.

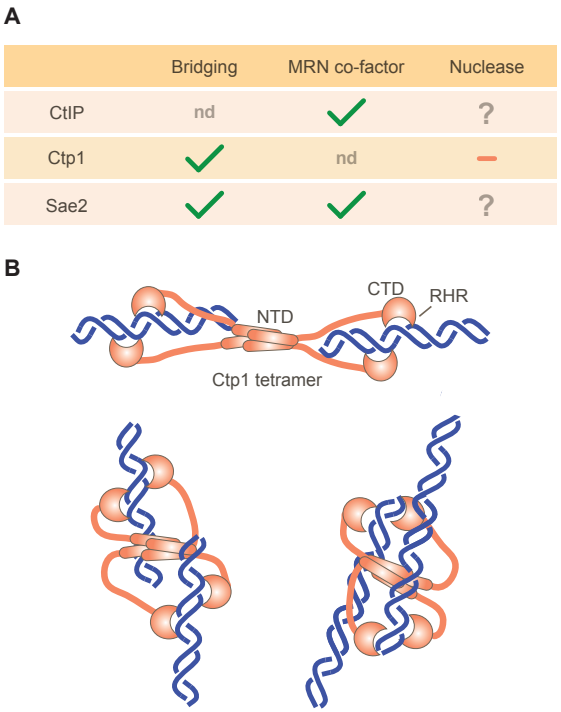

Figure 1.5: Functional roles of CtIP, Ctp1 and Sae2 in DSB repair. (**A**) Biochemical activities of CtIP homologs. Ctp1 and Sae2 were identified to harbor DNA bridging activity. CtIP and Sae2 act as MRN cofactors. Ctp1 does not exhibit nuclease activity, and characterization studies of the Sae2 and CtIP protein have conflicting results. (**B**) Schematic model of three possibilities how Ctp1 tetramers could bridge DNA breaks. NTD = N-terminal domain, CTD = C-terminal domain, RHR = DNA binding motif. Adapted from [107].

1.5.3 Regulation of CtIP by PTMs

Human CtIP was first discovered as a binding partner of the transcriptional corepressor CtBP, which is associated with cell proliferation and tumorigenesis [149]. Interestingly, CtIP was also identified as a protein interacting with the retinoblastoma protein (RB), thus alternatively named retinoblastoma binding protein 8 (RBBP8) [150]. CtIP binding to RB promotes dissociation of RB from the E2F-responsive promotor. Consequently, CtIP regulates its own transcription as well as the expression of E2F target genes, including cyclin D1, triggering S phase entry. Moreover, CtIP was shown to facilitate G1 to S phase transition by recruiting the transcription factor TFIIB to its own promotor leading to a further increase of its own transcriptional level [151,152]. To ensure that DSB resection and HR only take place when an intact DNA template is available for repair, CtIP expression levels are highly cell-cycle regulated, increasing during S and G2 phase and decreasing following

mitotic exit[153].

Moreover, CtIP's resection function is tightly governed by multiple PTMs, including phosphorylation, ubiquitination and SUMOylation. For example, CtIP recruitment to sites of damage is dependent on both ATM and ATR protein kinases. In response to DSBs, DNA-end resection is launched after ATM-mediated phosphorylation of CtIP at S664, S745 and T859[110,154], meanwhile CtIP binding to chromatin requires phosphorylation of T859 by ATR[155]. CtIP does not only possess ATM/ATR phosphorylation sites but also 12 potential CDK sites. CDK-mediated phosphorylation of T847 is essential for DNA-end resection[133,134]. However, the phosphomimetic T847E mutation only partially restored resection in the absence of CDKs, indicating that additional sites on CtIP or on associated proteins are needed for optimal processing of the DNA ends[156]. Indeed, a cluster of CDK phosphorylation sites (S233, T245, S276) is required to efficiently stimulate HR when the CtIP fragment is brought already to sites of the break by fusion to Cas9[110,130]. Of note, upon DNA damage, the same cluster of CDK sites promotes interaction with NBS1, stimulating ATM-mediated phosphorylation and activation of CtIP[157].

Complete impediment of the phosphorylation by mutation of T847 to alanine, did not abrogate the binding with MRE11, suggesting that other interactions occur in the C-terminus[134]. However, the underlying mechanism of how CtIP-T847 phosphorylation supports meiotic and mitotic recombination still remains unclear. Interestingly, located in close proximity to T847, K896 gets sumoylated by CBX4, thereby promoting CtIP's accrual at damaged DNA. Although CtIP is sumoylated probably at more than one site, conjugation of SUMO to K896 seems to be fundamental for DNA-end resection function as depletion of CBX4 or mutation of K896 results in reduced HR and increased genomic instability[158]. Furthermore, the authors claim that only a small pool of CtIP is sumoylated – the pool available for DNA-end resection – and that modifications occur sequentially with CDK-mediated phosphorylation downstream of K896 SUMOylation[159]. Emphasizing the intricate network of CtIP regulation, Y842 within a highly conserved FRY motif was shown to be required for KLHL15-CUL3-mediated CtIP ubiquitination and subsequent proteasomal degradation, representing a fine-tuning mechanism to regulate DNA-end resection[160].

PTMs are also implicated in mediating CtIP protein interactions. During S/G2, CDK-dependent phosphorylation of S327 triggers its association with the tumor-suppressor BRCA1[161,162]. However, the CtIP-BRCA1 interaction is dispensable for DNA-end resection, because cells with abrogated CtIP-BRCA1 interaction were still able to resect DNA and mice expressing CtIP mutant polypeptides grew normally and did not develop cancer[163,164]. CtIP mutant cells rather displayed defects in removal of topoisomerase II-DNA adducted breaks and further studies showed that the BRCA1-CtIP complex accelerates resection speed, controls DNA damage-induced G2/M transition checkpoint and inhibition of NHEJ[163,165,166].

In contrast to the functions and activation of CtIP in S/G2, the regulatory mechanisms in G1 are largely unknown. In G1, the polo-like kinase 3 (PLK3) phosphorylates CtIP at residues S327 and T847 upon damage, fostering DNA repair by alt-NHEJ[167].

Furthermore, constitutive acetylation at residue K432, K526 and K604 inhibits CtIP during G1. It has been found that CtIP is a direct substrate of the deacetylase SIRT6. Depletion of SIRT6 renders cells sensitive to DSB inducing-agents and suppressed DNA-end resection. Expression of deacetylated CtIP restored HR-mediated repair concluding that SIRT6-dependent deacetylation promotes DNA-end resection[168].

As mentioned above, CtIP protein levels are suppressed in G1 phase and peak during S and G2 phase, suggesting that CtIP turnover is cell-cycle-dependent. Indeed, our lab recently showed that CtIP is proteasomally degraded by the anaphase-promoting complex/cyclosome-Cdh1 (APC/C^{Cdh1}) E3 ubiquitin ligase. Upon damage in G2 or following mitotic exit APC/C^{Cdh1} controls CtIP turnover ensuring low levels of CtIP during G1, consequently contributing to limit HR to S/G2[169].

In addition, another E3 ubiquitin ligase SIAH-1 was found to trigger degradation of CtIP although the physiological impact remained unsolved[170].

Notably, it was shown that CtIP stabilization is negatively regulated by PIN1-mediated isomerization. PIN1-mediated isomerization requires phosphorylation at two sites, S276 and T315, probably mediated by CDK2. PIN1 isomerization controls CtIP turnover by promoting polyubiquitination of CtIP and subsequently proteasomal degradation, representing a regulatory mechanism for DNA repair pathway choice[135].

1.5.4 CtIP and its connection to cancer development and therapy

The very first studies associated CtIP with the *bona fide* tumor suppressor proteins BRCA1 and RB[150,171]. However, the role of CtIP in tumorigenesis is highly debated and the link between CtIP mutation, loss and overexpression in cancer is not yet clarified. Mice lacking CtIP die at a very early embryonic stage, indicating that CtIP is essential for development. Notably, heterozygous animals were viable, but their life span was shortened by the development of multiple tumors, particularly B and T cell lymphomas, suggesting that haploinsufficiency of CtIP leads to tumorigenesis[151]. The preference for lymphoma development may be explained by the fact that lymphocyte development relies on intact DNA repair during rearrangements of antigen receptor genes[172]. In other cancer, such as colorectal or endometrial cancers, frameshift mutations of CtIP and other components of the DSB repair machinery caused by microsatellite instability could be detected[173,174]. On the other hand, the fact that CtIP expression levels are very low in breast cancer cells and downregulation of CtIP is associated with resistance to tamoxifen, support the idea of CtIP being a tumor suppressor[153,175].

In contrast, recent findings suggest CtIP to promote tumorigenesis, as it was shown that heterozygous mice did not display increased tumor susceptibility and CtIP depletion resulted in decrease of mammary tumorigenesis[176]. Along the same line, Lin *et al.* demonstrated that triapine, a small molecule inhibitor of ribonucleotide reductase, sensitized cells to PARP inhibitors by inhibiting the BRCA1-CtIP-MRN interaction, subsequently disrupting CtIP-mediated HR of DNA breaks[177].

A recently published study connected CtIP phosphorylation to breast cancer by revealing CtIP to be a substrate of the protein kinase p38α, a MAPK kinase which acts as a tumor suppressor. P38α possibly phosphorylates CtIP at T847 and depletion of p38α in breast cancer cells resulted in increased replication fork stalling and elevated DNA damage, thereby negatively impacting tumor proliferation[178]. Knockdown of CtIP sensitized breast cancer cells to taxanes, commonly used chemotherapeutic drug inducing chromosomal instability. Moreover, p38α inhibitors enhanced the effect of taxanes, suggesting a potential clinical interest for a simultaneous use of p38α inhibitors with chemotherapeutic drugs[178].

Recently, whole-genome sequencing data of BRCA1-deficient breast cancer cells revealed that combined mutation of BRCA1 and p53 triggers the increase of distinct tandem duplication phenotypes (TDP), characterized by rearrangements of segmental tandem repeats. According to a characteristic pattern for disruption of tumor suppressor genes or activation of oncogenes the authors identified six TDP groups. Remarkably, decreased copy number levels of CtIP were found to be significantly associated with TDP group 2[179]. Conclusively, design of CtIP-specific small molecule inhibitors or by cell-penetrating peptides could be of great use to increase the efficacy of radio- and chemotherapy and one step towards targeted cancer therapy.

1.6 SLX4 - A nuclease scaffold

Slx4 (synthetic lethal of unknown function 4) was first identified in a yeast synthetic-lethal screen for proteins that are essential in absence of Sgs1 helicase[180]. Human SLX4 protein comprises 1834 amino acids with a calculated molecular mass of 200 kDa. Biallelic mutation of SLX4 causes a subtype of FA in humans and disruption of SLX4 in mice phenocopies many key features of FA, hence it was renamed FANCP[181,182]. In addition, it is hypothesized that monoallelic defects in SLX4 might predispose carriers to develop hereditary breast cancer[183,184].

Over the past years, SLX4 (also known as BTBD12) has been established as a scaffold protein loaded with and controlling the activity of different structure-specific endonucleases - and is therefore referred to as the 'molecular toolkit for DNA repair'[76]. The multi-domain protein SLX4 interacts with and enhances the activity of three distinct nucleases[76]: SLX1, XPF-ERCC1 and MUS81-EME1 (Figure 1.6). In complex with these endonucleases, SLX4 is involved in the cleavage of various DNA structures including ICLs, stalled replication forks and HJ[185,186].

Cleavage of complex DNA secondary structures is an important step during various DNA repair and recombination processes. Consequently, cells lacking SLX4 are hypersensitive to ICL and DSB-inducing agents[46,186,187]. SLX4 coordinates the function of the interacting endonucleases appropriately to the type of induced DNA lesion. For instance,

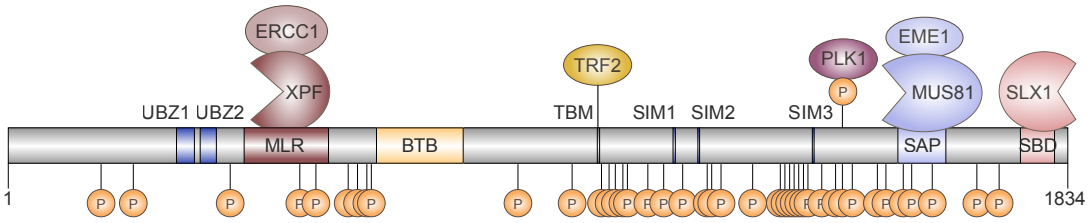

Figure 1.6: Schematic representation of SLX4 including its binding partners and conserved domains. Human SLX4 serves as a scaffold for multiple proteins, including the XPF-ERCC1, MUS81-EME1 and SLX1 nucleases. Those interactions are attributed to the conserved domains MLR, SAP and SBD, respectively. The BTB domain mediated protein dimerization. SLX4 interacts with TRF2 via its TBM domain, which is responsible for the telomeric localization of SLX4. A CDK consensus site at S1453 mediates its interaction with PLK1. Additionally, SLX4 contains motifs required for SUMO- and ubiquitin binding. Furthermore, SLX4 reveals two UBZ domains and three SUMO interaction motifs (SIMs). Notably, SLX4 contains 41 S/T-P phosphorylation motifs, with almost two thirds located in the low complexity region between residues 788 and 1540.

XPF-ERCC1 is required for ICL repair, meanwhile MUS81-EME1 in complex with SLX4 is critical in response to cisplatin-induced DNA damage[188]. Moreover, both MUS81-EME1 and SLX4-SLX1 nuclease functions are essential for resolving HJs during recombinatorial repair[47,189]. Unprocessed HJ pose a crucial threat demonstrated by the synthetic lethality of SLX4 and BLM or GEN1 in mitosis[189]. Furthermore, studies confirmed that the processing of persistent recombinant intermediates by GEN1 (or YEN1 in yeast) is timely restricted by inhibitory phosphorylation to the onset of meiosis II, ensuring that chromosomes can be properly separated[190,191]. If inhibition fails, activation of the resolvase leads to premature resolution of intermediates and premature crossovers. Along the same lines, SLX4-MUS81 emerged to be a key player in resolving persistent replication intermediates ensuring that DNA replication and mitosis occur sequentially[192]. At the onset of mitosis, CDK1 and PLK1 phosphorylate SLX4 leading to its assembly with MUS81, which cleaves persistent DNA intermediates. The complex assembly and subsequent activity occurs only in mitosis and is controlled by the kinase WEE1. Accordingly, inhibition of Wee1 leads to the catastrophic pulverization of S phase chromosomes caused by unrestrained processing activity of SLX4-MUS81[192].

Human SLX4 contains two closely spaced UBZ domains (UBZ-1 and UBZ-2) (see Figure 1.6). Recent studies revealed that only the UBZ-1 binds to ubiquitin chains, being required for SLX4 recruitment to ICLs. In contrast, the UBZ-2 was not found to bind ubiquitin *in vitro* and rather than contributing to ICL repair, manages HJ resolution[193].

In addition, the intrinsically disordered region of SLX4 comprises three SUMO interaction motifs (SIM) shown to be important for its recruitment to sites of DNA damage and localization to telomeres maintained by the alternative lengthening of telomeres (ALT-) pathway[194,195]. Recently, SLX4 has been found to be a SUMO E3 ligase itself, mediating SUMOylation of the nuclease XPF and triggering autoSUMOylation[194,196]. However, it was demonstrated that levels of SUMOylation of SLX4 itself and XPF does not change in response to DNA damage. Also, these SUMO-dependent functions of SLX4 are dispensable for ICL repair since the SLX4 SIM mutant could rescue the sensitivity against ICL-inducing MMC in clonogenic survival assays. Instead, SLX4 SIM domains play a role during the response to local replication stress. Upon inhibition of DNA replication using aphidicolin, SLX4 localizes at common fragile sites (CFS) to mediate faithful chromosome segregation, which requires its intact SIM domains[196].

Besides its recruitment to DNA damage, SLX4 plays an important role in telomere biology. Via interaction with TRF2, which is a member of the Shelterin-complex, it assembles at telomeres and negatively regulates telomere length[197]. In mammals, TRF2-RAP1 directs SLX4 localization to telomeres via PARP1 to protect telomeres from inappropriate processing by HR[198]. Loss of SLX4 leads to telomere fragility, indicative that SLX4 is important for telomere maintenance[199]. Moreover, an oligomerization motif, the BTB domain, facilitates homodimerization of SLX4 and is required for its telomeric localization as well as for the recruitment of associated nucleases. Disruption of the BTB domain leads to increased sensitivity to DNA interstrand crosslink agents and defects in telomeric maintenance[200].

A critical step in the activation of SLX4 is its phosphorylation by the polo-like kinase 1 (PLK1). PLK1 phosphorylates and activates SLX4 at S1453, which positively influences the interaction between PLK1 and XPF[46]. PLK1 activation promotes the association of the SLX4 complex to stalled replication forks in order to nucleolytically process various DNA structures[201]. It has been proposed that SLX4 is involved in the recovery of stalled forks upon replication stress, a function strongly intertwined with its recruitment by the regulator of Ty1 transposition (Rtt107)[202,203]. In yeast, fork bypass is orchestrated by the concerted action of SLX4-Rtt107 by counteracting the function of the Rad53 kinase ac-

tivator Rad9 leading to the inhibition of the Rad53-mediated DNA checkpoint response, consequently suggesting a role of SLX4 in controlling the checkpoint reponse[204–207].
Of note, 41 *in vivo* S/T-P phosphorylation sites of SLX4 were identified by mass spectrometry (www.phosphosite.org), pinpointing to a regulation by proline-directed kinases, which constitutes the prerequisite of PIN1-mediated isomerization. Taken together, the versatile functions of SLX4 are regulated by interaction with a broad range of proteins and depend on various PTMs.

1.7 PIN1

1.7.1 PIN1 - A molecular switch regulating diverse pathways

For steric reasons, the great majority of peptide bonds in proteins is found in a *trans* state, with the CO-NH/omega-angle assuming a value of 180°. However, peptide bonds preceding a proline residue have the unique ability two exist in two different conformations. Since the ring structure on the peptide backbone leads to steric similarities between the carbon atoms of the proline side chain and the backbone atoms, both *cis* and *trans* forms of proline peptide groups are almost isoenergetic[208]. Indeed, X-ray crystal structure analyses of proteins reveal that about 6% of all prolyl peptide bonds exist in the *cis* state. In contrast, the frequency of the *cis* state is only 0.04% in non-proline peptides[209]. However, the interconversion between the two conformations of prolyl peptide bonds is an intrinsically slow reaction, which can be greatly enhanced by peptidyl-prolyl *cis-trans* isomerases (PPIases). PPIases are grouped into three families: FKBPs (FK506 binding proteins), cyclophilins and parvulins[210,211]. PIN1 belongs to the family of parvulins and is composed of 163 amino acids with a molecular weight of 18 kDa[212]. It is a two-domain enzyme - its N-terminal WW domain mediates the phosphorylation-dependent binding to its substrate, whereas the C-terminal PPIase domain is responsible for the isomerization activity[213]. The N-terminally located residues Y23 and W34 form an aromatic clamp necessary for PIN1 binding. Innes *et al.* suggest that the WW domain, unlike the PPIase domain, preferentially targets binding sites with a proline at the +1 position[214]. The residues R68 and R69, located in the catalytic domain, are responsible for a unique

phosphorylation-specificity and together with K63 form a positively charged phosphate-binding hook[215–218]. In other words, PIN1 isomerizes only proline peptide bonds adjacent to phosphorylated serines or threonines (S/T-P motif), a unique feature among the PPIases (Figure 1.7).

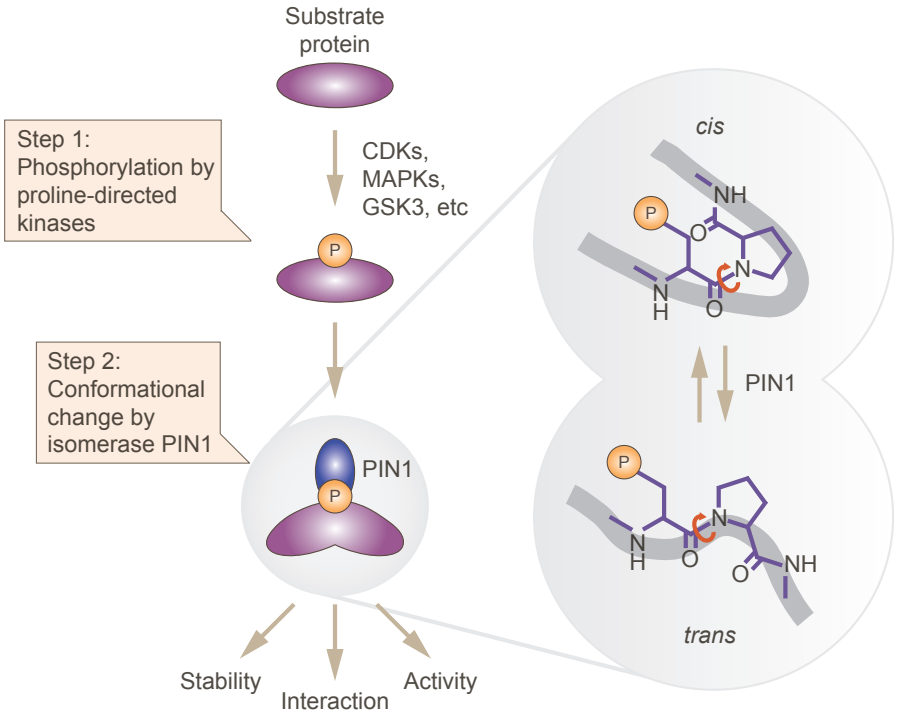

Figure 1.7: Two-step model of prolyl *cis-trans* isomerization by PIN1 after phosphorylation. Phosphorylation of a protein substrate is mediated by proline-directed kinases. Subsequently, this enables PIN1 to bind and catalyze the isomerization of the prolyl peptide bond, with various possible effects for its substrate. The zoom pictures show the conformational change of a phosphorylated serine-proline peptide bond. The grey background line represents the protein backbone. Modified from[219,220].

These S/T-P motifs are critical and play an important regulatory role for many cell cycle-regulated proteins including kinases and phosphatases. In fact, many kinases like CDKs, MAPKs, and GSK3s (Glycogen synthase kinase 3), JNKs (Jun-N-terminal protein kinases) and PLKs (polo-like kinases) act on S/T-P motifs.

Although PIN1 contributes to the activation or inhibition of many regulatory proteins during G1/S phase, namely cyclin D, cyclin E and p27, its role in mitosis is investigated the most (Figure 1.8)[210,221,222].

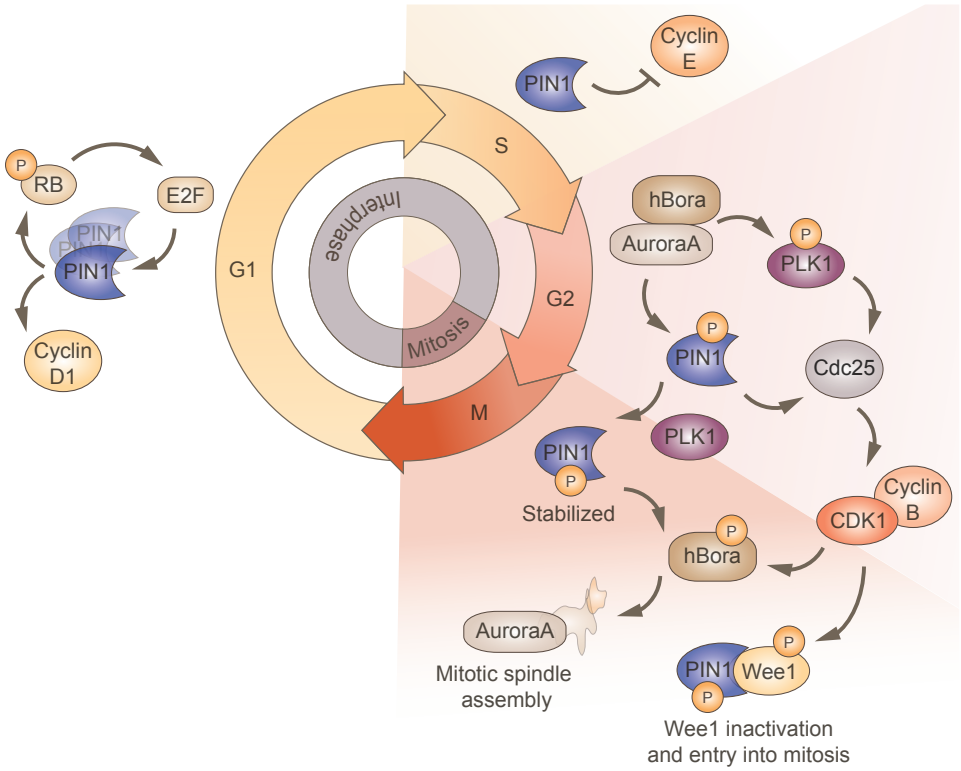

Figure 1.8: Role of PIN1 during mitosis. During G2/M transition, PIN1 is phosphorylated at Ser16 by the kinase AuroraA, leading to its translocation into the cytosol, thus preventing PIN1-mediated degradation of phosphorylated hBora, which is a crucial factor for mitotic entry[223–225]. AuroraA associates with hBora to phosphorylate PLK1, which in turn activates cdc25 and downregulates the kinases Myt1 and Wee1[226]. After mitotic entry, PLK1 restores activation of PIN1 by phosphorylation of Ser65, leading to degradation of hBora. Restored activation of PIN1 in M-phase also promotes binding and isomerization of Wee1, a suppressor of CDK1. Because CDK1 is important to cycle through mitosis, Wee1 must be inhibited during M-phase, which is achieved by PIN1-mediated isomerization[227]. Modified from[225].

PIN1 was originally identified as a negative regulator of mitosis that interacts with and inhibits the ability of NIMA (G2-specific protein kinase nimA), a mitotic regulator protein, to induce mitotic catastrophe[212]. Along the same line, deletion of the ortholog Ess1 (essential in yeast) in *S. cerevisiae* induces terminal mitotic arrest[228]. In contrast to its lethality in yeast, PIN1 knock-out mice develop normally up to the age of seven months until they display cell proliferative abnormalities (e.g. decreased body weight, testicular and retinal atrophies, mammary gland proliferative impairment and low bone mass)[229]. Moreover, PIN1$^{-/-}$ mouse embryonic fibroblasts (MEFs) were found to grow slower and show deficiencies in restarting proliferation in response to serum starvation after G0 arrest[230,231]. In addition, overexpression of PIN1 in *Xenopus* egg extracts prevents entry into mitosis,

whereas depletion leads to premature entry into G2/M, suggesting that PIN1 is mediating mitotic checkpoint control[232,233]. Studies in HeLa cells substantiate the findings that PIN1 depletion leads to premature entry into mitosis and mitotic arrest and its overexpression inhibits the G2/M transition, thus it is surprising that expression levels of PIN1 are constant throughout the cell cycle[224,232–234]. Underscoring evidence that PIN1 drives mitotic progression comes from a recent study displaying PIN1 as the mitosis promoting factor in spermatogonial stem cells[235].

Consequently, because PIN1 level do not significantly vary during the cell cycle, PIN1's action on mitosis-promoting factors must be timely restricted and tightly controlled by PTMs of its substrates but also of itself.

Furthermore, PIN1 was found to control a broad range of cell-cycle regulatory proteins including PLK1, cdc25 and cyclin D[221,234,236]. In addition, PIN1 is involved in the regulation of cell growth, immune response and neuronal differentiation in response to various cellular stresses[100,237–239] (Figure 1.9).

Collectively, the concerted action of protein kinases and PIN1 isomerization is a two-step mechanism in which proline-directed kinases first phosphorylate the S/T-P motif, thus allowing PIN1 to act on its substrate. Consequently, a change of the protein structure can have profound regulatory effects for the substrate's activity, affinity to binding partners and stability or can modulate the interplay of PTMs[240].

1.7.2 PIN1 and its role in tumorigenesis

PIN1 controls numerous cancer-driving pathways due to its stabilizing, destabilizing, activating and inhibiting effects on a broad spectrum of important oncoproteins. Plausibly one of the best described PIN1 substrate is the tumor suppressor protein p53[241–243]. Recently, the p53-RS (R249S) mutant, harboring an extra PIN1 docking site, which facilitates its nuclear localization, was frequently detected in human hepatocellular carcinoma[244].

PIN1 functions are critical during mitosis and it was shown that PIN1 overexpression leads to abnormal spindle formation, chromosome instability and finally can induce breast cancer in mice[235]. Notably, PIN1 is significantly overexpressed in many human cancers including breast, cervical, prostate and lung cancer, as well as melanoma and is also

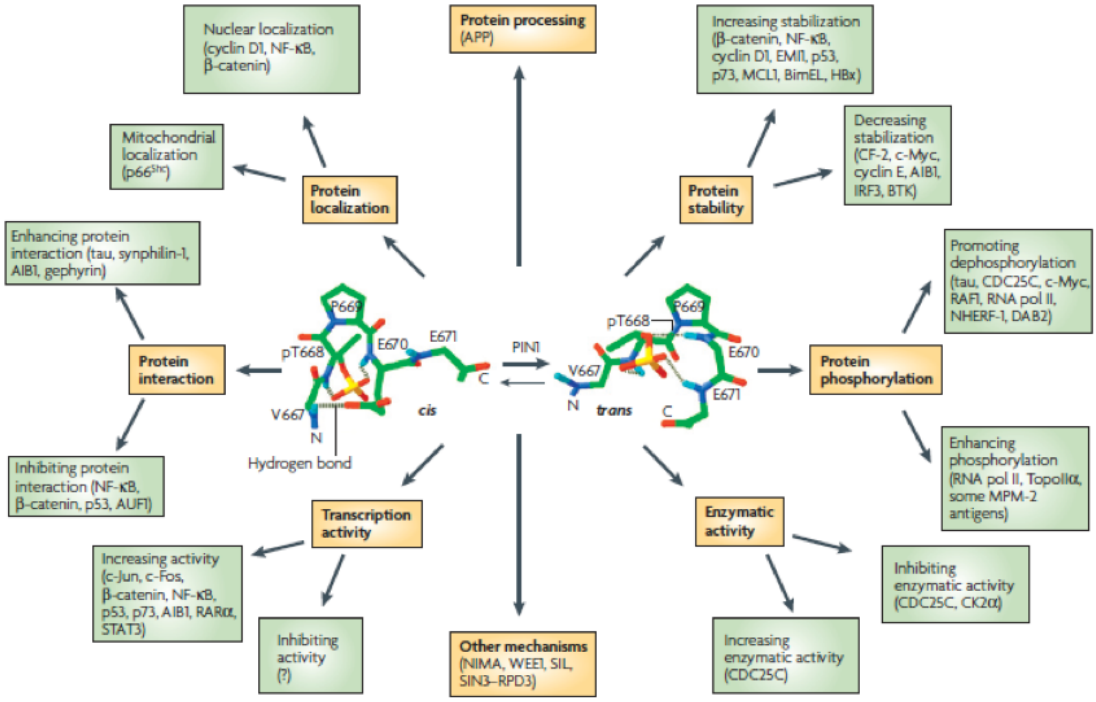

Figure 1.9: PIN1 acts on various substrates. PIN1-mediated isomerization can have crucial effects on the activity, stability, protein interaction or localization of its target substrate. Importantly, many factors regulated by PIN1 play an important role in tumorigenesis, such as cyclins, Wee1 or p53. Adapted from[240].

associated with a higher risk of tumor relapse after tumordissectomy[238,239,245–247]. Given that PIN1 overexpression is most likely a prevalent and defined event in human cancer to promote tumor growth, it is reasonable and nowadays well-established to use PIN1 expression as a prognostic marker in prostate cancer[245].

PIN1 is a critical modifier of multiple signaling pathways with important roles in cancer stem cells[248,249]. For example, PIN1 sustains Notch signaling by preventing Notch1 and Notch4 proteasomal degradation. Consequently, constantly active Notch signaling triggers tumor growth and self-renewal in breast cancer stem cells[250]. Importantly, in patient-derived primary breast cancer cells, knockdown of PIN1 suppressed expansion and tumor growth *in vitro* and in xenograft models[251]. The fact that PIN1 knockdown can suppress tumor growth and cancer stem cell expansion renders it as an attractive target for therapeutic strategy. But these attempts are hampered by the versatility of PIN1, considering a high risk of possible off-target effects and rather low specificity. Nevertheless,

first trials were completed with success. It was reported that the therapeutic effects of all-trans retinoic acid (ATRA), which is clinically used to suppress leukemia, breast and liver cancer by targeting PIN1, can be potentiated by the combination with arsenic toxide[252]. Similarly, Campaner *et al.* identified the PIN1 inhibitor KPT-6566 covalently binding to the catalytic site of PIN1, which induces ROS-dependent DNA damage specifically only in PIN1 cancer cells, resulting in suppression of lung metastasis *in vivo*[253].

To identify novel PIN1-interacting proteins mass spectrometry analyses of pulldown assays revealed more than 600 potential candidates, among them a vast majority of DSB response factors, supporting a role of PIN1 in the DDR[135,254]. The kinase ATR has been reported to be a direct target of PIN1 with implications in response to UV light. Besides its nuclear function, ATR exhibits antiapoptotic activity associated at the mitochondria. Hilton *et al.* showed that PIN1-mediated isomerization suppresses its mitochondrial activity and UV light exposure initiates inhibition of PIN1 by DAPK1 leading to stabilization of active ATR[255]. Furthermore, one study confirmed a simultaneous overexpression of PIN1 and hyper-phosphorylated RB, a protein important for cell cycle progression and DNA damage response in human breast cancer cells. The authors propose an underlying mechanism in which PIN1-mediated isomerization of RB prevents its dephosphorylation by PP2A[256].

However, the impact of PIN1-mediated prolyl isomerization on different substrates is still poorly addressed, thus more research is required aimed to elucidate the function of PIN1 in tumor development and its interaction with substrate proteins.

1.8 *P. tetraurelia* as a model organism to study DSB repair

Paramecium tetraurelia, belonging to the ciliate phylum, is a unicellular eukaryotic organism naturally found in aquatic habitats. It feeds on bacteria, yeast and algae and can be easily cultivated in laboratories, where it serves as a useful model organism to study basic cellular processes of life[257]. Growing cells can duplicate by binary fission, but once they find a mating partner, or in response to starvation, initiate sexual processes[258]. *Paramecium* possesses two modes of sexual reproduction: Conjugation (cross-fertilization) and

autogamy (self-fertilization), which can be induced by controlling food uptake, thus allowing to study basic molecular processes during meiosis.

Like all ciliates, *Paramecium* harbors a characteristic nuclear dimorphism and undergoes spectacular genome-wide genetic rearrangements during development. Its genome is separated into distinct types of nuclei with somatic and germline function. One large, highly polyploid somatic macronucleus (MAC, 800*n*) responsible for gene transcription during vegetative growth, and two micronuclei (MIC, 2*n*) undergoing meiosis during each sexual cycle[259,260] (Figure 1.10). Importantly, during meiosis, the parental MAC degrades and differentiates from copies of the zygotic nucleus after fertilization. MAC development involves the massive amplification (from 2*n* to 800*n*) of the zygote and requires two types of DNA elimination events to remove 25%-30% of MIC DNA. On the one hand, imprecise elimination of 100-200 regions of several kb repeated sequences from the germline genome leads to chromosome fragmentation[261]. On the other hand, precise excision deletes ∼45'000 internal eliminated sequences (IES), which can be regarded as short (26-882 bp) noncoding 'introns'. IES excision is initiated by creation of a DSB at IES sites, mediated by the sequential action of PiggyMac, a domesticated (= recruited by their hosts to perform novel functions) piggyBac transposase[262].

Recently, proteins involved in DSB repair by NHEJ were found to play important roles during the cut-out of IES, such as the Ku70 and Ku80 paralogs, which mediate the religation of the DNA ends[10,263]. With regards to recombinatorial repair, a recent inventory of meiosis-specific genes in ciliates revealed the presence of two gene copies for each *PtMRE11* and *PtCtIP*, consistent with multiple whole-genome duplication events in the early stages of *P. tetraurelia* evolution[264,265]. In evolution, MRE11 and CtIP were found to be strictly required for the removal of covalently attached Spo11 from the break site, and by that initiating DNA-end resection[59,137,266].

Remarkably, with a length of only 198 amino acids, PtCtIP paralogs constitute the smallest Sae2/Ctp1/CtIP protein family members that have been identified so far (see Figure 1.4). PtCtIP is a potential candidate to be implicated in the processing of DSBs during genome rearrangements. Therefore, *P. tetraurelia* serves as an attractive model to study programmed rearrangements during meiosis and DSB repair.

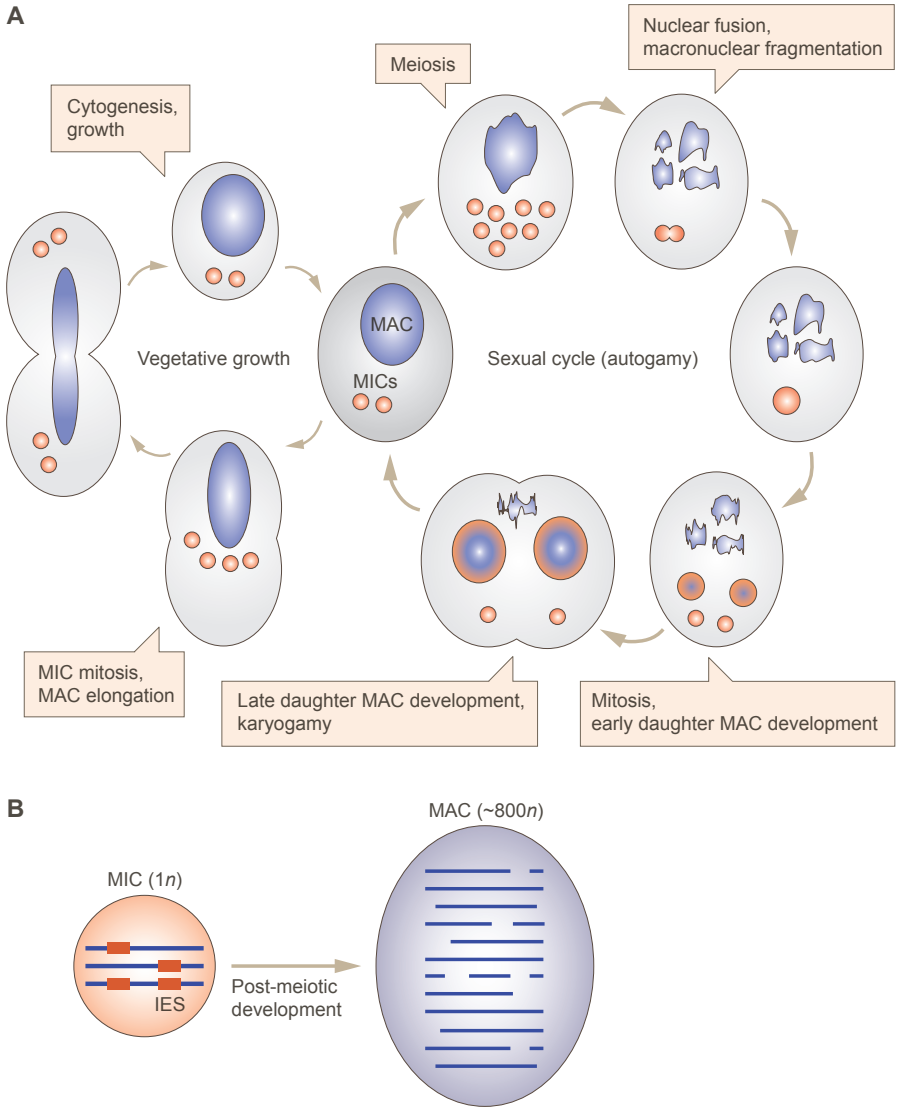

Figure 1.10: Nuclear dimorphism and the life cycle of *P. tetraurelia*. (**A**) Stages of *P. tetraurelia* development. *Left*: The vegetative growth is illustrated. The two micronuclei (MICs) undergo mitosis, while the macronucleus (MAC) elongates and splits into two. *Right*: Upon starvation or having a mating partner to conjugate with in proximity *P. tetraurelia* initiates autogamy or the sexual cycle. First, the MICs undergo meiosis resulting in eight haploid products. Two of them fuse to build a zygote, while the others are degraded. The zygote undergoes two round of mitosis to form two future MICs and two daughter MACs. During each sexual cycle, the MAC is completely degraded. (**B**) A newly somatic MAC is build from a germline MIC by genome amplification (from 2*n* to 800*n*), chromosomal fragmentations and removal of internal eliminated sequences (IES). The IES are depicted in dark orange and are removed from the coding genome (dark blue) during MAC development. Modified from [267,268].

Aims

Genomic instability drives tumor progression by enabling the acquisition of core and emerging hallmarks of cancer[12,11]. Many current therapeutic regiments for treating cancer, like ionizing radiation or chemotherapy, rely on the induction of DNA damage to trigger programmed cell death of cancer cells. Nonetheless, these agents cause severe side effects and often become ineffective when resistance develops. Therefore, a more in-depth understanding of the DDR is essential to improve the efficacy of existing therapies and to suggest novel treatment strategies.

Aim 1: Investigating the biochemical function of CtIP in DSB repair

Upon DNA damage, proliferating cells activate a signaling network to arrest the cell cycle and enable DNA repair. We and others have reported previously that CtIP is a key player in the DNA double-strand break (DSB) repair by promoting DNA-end resection and homologous recombination (HR). How members of the Sae2/Ctp1/CtIP protein family functionally integrate with the Mre11-Rad50 (MR) nuclease complex to initiate the processing of DNA double-strand breaks (DSBs) is not fully understood. Moreover, high-resolution structural analysis of CtIP is hampered, as it consists of a large intrinsically disordered region and an N-terminal coiled-coil domain that self-assembles into higher-order oligomers in solution.

We identified an ortholog of CtIP in the ciliate *Paramecium tetraurelia*, named PtCtIP, which represents the shortest known CtIP ortholog of the CtIP/Sae2/Ctp1 protein family with only 198 amino acids. Therefore, we wanted to uncover the biochemical properties of PtCtIP in more detail and aimed to translate our findings to the human ortholog. Moreover, we wanted to uncover the biochemical and biological properties of PtCtIP in more

detail and aimed to translate our findings to the human ortholog (in collaboration with Dr. Mireille Bétermier, Institut de Biologie Intégrative de la Cellule, France). In summary, we identified a miniature Sae2/Ctp1/CtIP ortholog from *Paramecium tetraurelia* that owns a conserved DNA-binding motif required for DNA-end resection (manuscript submitted to the scientific journal of DNA Repair).

Aim 2: Deciphering the regulation of human SLX4 by phosphorylation-dependent isomerization

In a previous study, our lab found that CtIP functions in the DSB repair are controlled by PIN1, a peptidyl-prolyl isomerase (PPIase), which can catalyze the *cis-trans* conformation of prolyl peptide bonds adjacent to phosphorylated serines or threonines (S/T-P motifs)[135]. In a proteomic screen for potential PIN1 substrates, we discovered several DNA damage response (DDR) proteins including SLX4. SLX4 (alias FANCP) serves as a docking platform for different structure-specific endonuclease complexes, thereby orchestrating Holliday junction (HJ) resolution during HR, DNA crosslink processing during ICL repair, restoration of stalled replication forks and regulation of telomere length homeostasis. However, if and how SLX4 conformation regulates its function is not yet known. Thus, we aim to validate the PIN1-SLX4 protein interaction and to identify the potential pS/T-P motif in SLX4 mediating its interaction with PIN1. Lastly, we want to address the effects of PIN1-mediated isomerization for SLX4 function in telomere homeostasis and DNA repair.

Material and Methods

Immunoblotting, immunoprecipitation, far-Western, GST-pulldown and phosphatase treatment

If not specified otherwise, cell extracts were prepared in NP40 buffer (50 mM Tris-HCl, pH 7.5, 120 mM NaCl, 1 mM EDTA, 6 mM EGTA, 15 mM sodium pyrophosphate and 1% NP-40 supplemented with phosphatase inhibitors (20 mM NaF, 1 mM sodium orthovanadate) and protease inhibitors (1 mM benzamidine and 0.1 mM PMSF)). For efficient cell lysis, the suspensions were snap-frozen, thawed on ice and sonicated in a Bioruptor® (Diagenode). Lysates were cleared by centrifugation at 14000 g before determining protein concentration by Bradford assay. Proteins were separated by SDS–PAGE and transferred to nitrocellulose. Detection of proteins was carried out using the appropriate antibodies and proteins were visualized applying the WesternBright (Advansta) and imaged on a FusionSolo (Witec AG).

Unless otherwise stated, a total of 0.5 – 1 mg of lysate was used for immunoprecipitation. FLAG-Epitope tagged constructs were immunoprecipitated using the agarose anti-FLAG resin (Sigma-Aldrich) overnight at 4C. Beads were washed twice with NTEN300 buffer (20 mM Tris-HCl pH 7.4, 0.1 mM EDTA, 0.5% NP-40, 300 mM NaCl), twice with NTEN500 buffer (20 mM Tris-HCl pH 7.4, 0.1 mM EDTA, 0.5% NP-40, 500 mM NaCl), followed by a single wash with TEN100 (20 mM Tris-HCl pH 7.4, 0.1 mM EDTA, 100 mM NaCl), boiled in SDS-sample buffer and analyzed by immunoblotting. HA-epitope tagged proteins were immunoprecipitated using anti-HA affinity resin (Sigma) and immunocomplexes were washed three times with NP40 buffer. GFP-TRAP was performed using anti-GFP coupled to agarose beads (ChromoTek) according to manufacturer's protocol.

Far-Western blot analysis was performed as described previously[153]. To enrich for FLAG-SLX4, proteins were immunoprecipitated and eluted in TEN100 buffer supplemented with FLAG-peptides according to manufacturer's instructions (Sigma).
GST-pulldown assay was performed by coupling GST-PIN1 (wt or W34A expressed in *E. coli* as previously described[135] to Sepharose beads for 2 h at 4℃. Recombinant GST-PIN1 was a kind gift of Stefano Ferrari (University of Zurich, Switzerland). Coupled resin was washed three times with PBS-1% TritonX before incubation with 0.5 mg protein extract for 1 h at 4℃. Beads were washed once with NTEN300, twice with NTEN500, once with NTEN300 and once with TEN100. Recovered complexes were boiled in SDS sample buffer and analyzed by SDS–PAGE followed by immunoblotting.
For phosphatase treatment, proteins bound to agarose anti-FLAG resin were dephosphorylated on beads. In brief, 20 µl beads with bound FLAG-SLX4 constructs were incubated with 50 µl PMP buffer (NEB) supplemented with $MnCl_2$, benzamidine, PMSF (and in case of PPase inhibitors plus NaF and sodium orthovanadate) containing 2 µl Lambda-PPase (NEB) for 30 min at 30℃. Beads were washed twice with PMP buffer prior to elution using 3xFLAG peptides (Sigma-Aldrich).

Antibodies

Primary antibodies used in this study are listed in table 3.1. Secondary HRP-conjugated anti-mouse and anti-rabbit antibodies were purchased from GE-Healthcare and used in a dilution of 1:5000. AlexaFluor-488, -594 and -647-conjugated secondary antibodies were bought from Invitrogen and diluted to 1:500 -1000.

Cell culture and transfection

U2OS, HeLa and HEK293T cells were maintained in Dulbecco's modified Eagles medium (DMEM, Thermofisher) supplemented with 10% fetal calf serum (FCS, Thermofisher). HeLa and U2OS clones stably expressing doxycycline (Dox)-inducible siRNA-resistant forms of YFP-SLX4 were generated as described previously[196] using the Flp-In T-REx system (Invitrogen, Life Technologies) according to manufacturer's protocol. Resistant clones were selected and YFP-SLX4 expression was analyzed by both immunofluores-

Antibody target	Reference/Supplier	Dilution	Application[a]
α-Tubulin	T-9026 (Sigma Aldrich)	1:20000	IB
CtIP (D-4)	sc-271339 (Santa Cruz)	1:250 - 500	IB
cyclinD1	RB-010-P1 (Neomarkers)	1:1000	IB
FLAG	F3165 (Sigma)	1:1000	IB
GAPDH	MAB374 (Millipore)	1:40000	IB
GFP	ab290 (Abcam)	1:1000/1:500	IB/IF
HA	Sc-7392 (Santa Cruz)	1:500	IB
PIN1	2136-1 (Epitomics)	1:1000	IB
PLK1	P5998 (Sigma)	1:1000	IB
pT1315	Creative Biolabs (Custom made)	1:500	IB
H3pS10	06-570 (Millipore)	1:1000/1:500	IB/flow cytometry
TRF2	NB110-57130 (Novus)	1:1000/1:500	IB/IF
SLX4	A302-270A (Bethyl)	1:1000	IB

[a] IB: Immunoblot, IF: Immunofluorescence

Table 3.1: Primary antibodies

cence microscopy and immunoblotting. YFP-SLX4 expression was induced with 1 µg/ml Doxycycline (Sigma) for 24 - 48 h.

Plasmids (5 µg) were transfected either by using the calcium phosphate method or FuGENE 6 transfection reagent (Promega) according to the manufacturer's instructions. Transfection of indicated siRNA oligos was carried out using Lipofectamine RNAiMAX (Life Technologies).

To assess protein turnover, cells were treated with cycloheximide (C7698) purchased from Sigma and used as indicated.

RNA interference sequences

The following siRNA sequences were used in this study (sequences in 5' to 3'): siluc (CGUACGCGGAAUACUUCGA) (used in[269], siSLX4 (AAACGUGAAUGAAGCAGAAUU) (used in[46,269] and siPIN1-3'UTR (CCGUCACACAGUAUUUAUU) (used in[135]), all purchased from Microsynth.

Plasmids

The pDEST/FRT/TO-based expression vector encoding doxycycline (Dox)-inducible siRNA-resistant YFP-SLX4 wt was kindly provided by Dr. Henri Gaillard (Centre National de la Recherche Scientifique, France)[196]. The pDEST/FRT/TO-based Venus-FLAG-SLX4 wt, 6A, 19A, 22A and 35A expression constructs were a kind of Dr. Joao Matos (ETH Zurich, Switzerland)[192]. The pHAGE plasmids containing HA-FLAG-SLX4 full-length and truncated mutants (covering SLX4 amino acid sequence 1-800, 1-1520, 801-1834) were kindly provided by Agata Smogorzewska (Rockefeller University, USA)[187]. The pcDNA3.1 vector for expression of HA-PIN1 wt, W34A and C113A used in this study have been described previously[135].
Advantage HD polymerase (Clontech) was used to alter single S/T-P sites in SLX4 or to generate truncated SLX4 expression constructs by side-directed mutagenesis (SDM). In brief, 50 ng DNA template was mixed with 1x HD buffer, 5 mM dNTPs (Roche), 1.25 µM combined forward and reverse primers and 0.625 Units Advantage HD polymerase in a final volume of 25 µl. All DNA oligos used as primers are listed in table 3.2. Sequences of all constructs were confirmed by sequencing (Microsynth).

Immunofluorescence microscopy

In order to screen the generated clones for YFP-SLX4 expression, cells were grown on coverslips and fixed directly in formaldehyde. Alternatively, cells were permeabilized or pre-extracted for 5 min on ice before fixation in 4% formaldehyde (w/v in PBS) for 15 min as described previously[37]. After incubation with indicated primary and Alexa Fluor-488, -594 and -647 conjugated secondary antibodies (1:000) (Life Technologies) coverslips were mounted with Vectashield® (Vector Laboratories) containing DAPI and imaged either using a Leica DMI6000 widefield fluorescence or a confocal Leica CLSM SP5 Mid UV-VIS microscope at 63X magnification.

Name	Sequence in 5' to 3'
SLX4_T500A_for	GTGGAATTGTCTAGCGCGCCACCACTTCC
SLX4_T500A_rev	CAGGAAGTGGTGGCGCGCTAGACAATTCC
SLX4_S1028A_for	CTCCCTGGCAGGCAGCTCCACCGCACCC
SLX4_S1028A_rev	GGGTGCGGTGGAGCTGCCTGCCAGGGAG
SLX4_S1044A_for	AGGGCGGGGCTCCCCGCGGGTCTCATCAC
SLX4_S1044A_rev	GTGATGAGACCCGCGGGGAGCCCCGCCCT
SLX4_S1070A_S1075A_for	AGGTGGGCGCCCCAACCTTGCTGGCTCCAGCTGTG
SLX4_S1070A_S1075A_rev	CACAGCTGGAGCCAGCAAGGTTGGGGCGCCCACCT
SLX4_S1206A_for	GATCAGGAACCTTCCCAGGCCCCACCAAGAAGCGAAGC
SLX4_S1206A_rev	GCTTCGCTTCTTGGTGGGGCCTGGGAAGGTTCCTGATC
SLX4_T1315A_for	GTCATCAGGCCCCAGGCACCACCGCCC
SLX4_T1315A_rev	GTCTGGGGCGGTGGTGCCTGGGGCCTG
SLX4_T1320A_for	CACCGCCCCAGGCACCGTCCTCATG
SLX4_T1320A_rev	CATGAGGACGGTGCCTGGGGCGGTGG
SLX4_T1326A_S1329A_for	TCCTCATGCCTCGCTCCCGTCGCTCCAGGAACTTCT
SLX4_T1326A_S1329A_rev	AGAAGTTCCTGGAGCGACGGGAGCGAGGCATGAGGA
SLX4_S1342A_for	AGAAGGCAAGGCCACAGAGCCCCTTCCCGTCCCCAC
SLX4_S1342A_rev	GTGGGGACGGGAAGGGGCTCTGTGGCCTTGCCTTCT
SLX4_S1355A_for	CACCCGCACTCCGCTCCGCTGGCTCCACAT
SLX4_S1355A_rev	ATGTGGAGCCAGCGGAGCGGAGTGCGGGTG
SLX4_S1377A_for	TTCCTGAAACACGCGCCGCCTGGGCCAAGC
SLX4_S1377A_rev	GCTTGGCCCAGGCGGCGCGTGTTTCAGGAA
SLX4_S1434A_for	CACATGGAGCCCCTCGCGCCAATTCCCATTG
SLX4_S1434A_rev	GTCAATGGGAATTGGCGCGAGGGGCTCCATGTG
SLX4_1097stop_for	GTCTAAAGAGCCAGGGCACTAGAAAGGCAAAGAGCG
SLX4_1097stop_rev	GACGCTCTTTGCCTTTCTAGTGCCCTGGCTCTTTAG
SLX4_1296stop_for	CGCCCAGGGCCTCAGTATGAAACAGGGAAG
SLX4_1296stop_rev	GTTCCCTTCCCTGTTTCATACTGAGGCCCTGG
SLX4_1338stop_for	GACGGCAGAAGGCAATGATAGAGAAGCCCTTCCCGTCCCC
SLX4_1338stop_rev	GGACGGGAAGGGCTTCTCTATCATTGCCTTCTGCCGTCAG
SLX4_1383stop_for	GCCTGGGCCAAGCTTCTGAACCAGACCCCAG
SLX4_1383stop_rev	CGCTGGGGTCTGGTTCAGAAGCTTGGCCCAG
SLX4_1536stop_for	CCAAGCGCTGGTGGAGCTTAGAAGCCCGAAGG
SLX4_1536stop_rev	GGTGTCTCTAACCCTTCGGGCTTCTAAGCTCCACCAGCG
SLX4_A1315T_for	GTCATCAGGCCCCAGACACCACCGCCCCAG
SLX4_A1315T_rev	CTGGGGCGGTGGTGTCTGGGGCCTGATG
SLX4_A1320T_for	CACCGCCCCAGACACCGTCCTCATGCCTC
SLX4_A1320T_rev	GAGGCATGAGGACGGTGTCTGGGGCGGTG

Table 3.2: Oligonucleotides used as primer

Coupled Immunofluorescence-FISH

In coupled immunofluorescence-FISH experiments a Cy3-conjugated PNA probe was used to detect telomeres. Proteins were first immunofluorescently labeled as described above, before cells fixed on coverslips were further processed as followed. Coverslips were washed three times with PBS and cells fixed again in 4% formaldehyde (in PBS) for 5 min. After repeated washing with PBS, cells were serially dehydrated in 70%, 95% and 100% EtOH for 5 min each and air-dried. Coverslips were incubated with Cy3-labeled PNA probe (Eurogentec) at a final concentration of 100 nM in hybridizing solution (10 mM Tris pH 7.4, 70% formamide (deionized), 0.5% blocking reagent from a 2% stock (blocking reagent (Roche 11096176001) in 100 mM maleic acid, 150 mM NaCl pH 7.5) for 3 min at 85°C followed by 2 h at room temperature. After hybridization, cells were washed twice with wash buffer 1 (10 mM Tris pH 7.4, 70% formamide) for 15 min each and three times with wash buffer 2 (10 mM Tris pH 7.4, 150 mM NaCl, 0.08% Tween-20) for 5 min each before dehydration in EtOH as described above. Coverslips were mounted with Vectashield® (Vector Laboratories) containing DAPI and imaged using a Leica DMI6000 wide field fluorescence microscope at 63x magnification. Quantitative image analysis was carried out using CellProfiler to assess the number of foci per nucleus and colocalization (Broad Institute[270]).

Flow cytometry

For flow cytometry analysis, cells were harvested by trypsinization, whereby the supernatant of each wash step was collected, preventing loss of rounded-up mitotic cells. Cells were either pre-extracted in 0.3% TritonX-100 (v/v in PBS) for 10 min or directly fixed in 4% formaldehyde (v/v in PBS) for 15 min. For H3pS10 staining, non-preextracted cells were permeabilized after fixation and incubated with 0.5% saponin/1% BSA/PBS containing the primary antibody for 2 h at RT, followed by incubation with Alexa 647 conjugated secondary antibody (1:500) (Life Technologies). After a subsequent wash step with 0.5% saponin/1% BSA/PBS, cells were resuspended in 0.5% saponin/1% BSA/PBS containing 100 µg/ml Rnase A and 1 µg/ml DAPI and incubated for 30 min at room temperature. Flu-

orescence intensity was measure on an Attune NxT flow cytometer (Thermofisher) and analyzed with FlowJo X (Tree Star).

Statistics

Statistics were calculated in Graph Pad Prism (GraphPad Software Inc.). Statistical analyses were performed using unpaired, two-tailed t-test. P values expressed as * ($P<0.05$), ** ($P<0.001$) and *** ($P<0.0001$) were considered significant.

Results

4.1 Investigating the biochemical function of CtIP in DSB repair

4.1.1 Identification of a miniature Sae2/Ctp1/CtIP ortholog from *Paramecium tetraurelia* required for sexual reproduction and DNA double-strand break repair

Manuscript submitted to *DNA Repair*

Authors:

Julia Godau[*], Lorenza P. Ferretti[*], Christine von Aesch, Raphaël Guérois, Antoine Marmignon, Lauriane Simon, Emeline Dubois, Aurélie Kapusta, Mireille Bétermier and Alessandro A. Sartori (* equal contribution)

Contribution:

For this study, I have cloned, expressed and purified recombinant PtCtIP wild-type and RHR mutant proteins from insect cells and performed all gel shift assays (Figure 4). Moreover, I have generated U2OS-TLR cells stably expressing FLAG-CtIP RHR mutant used in the HR reporter assay and contributed to other experiments performed in U2OS cells expressing GFP-CtIP (Figure 5). I have drafted the first version of the manuscript together with L.P.F, including preparation of figures.

Identification of a miniature Sae2/Ctp1/CtIP ortholog from *Paramecium tetraurelia* reveals a conserved DNA-binding motif required for DNA-end resection

Julia Godau[1¶] , Lorenza P. Ferretti[1¶,#a], Christine von Aesch[1], Raphaël Guérois[2], Antoine Marmignon[2], Lauriane Simon[2], Emeline Dubois[2], Aurélie Kapusta[2,#b], Mireille Bétermier[2*] and Alessandro A. Sartori[1*]

[1]Institute of Molecular Cancer Research, University of Zurich, Zurich, Switzerland

[2]Institute for Integrative Biology of the Cell (I2BC), CEA, CNRS, Univ. Paris-Sud, Université Paris-Saclay, Gif-sur-Yvette, France

[#a]Current Address: Department of Molecular Mechanisms of Disease, University of Zurich, Zurich, Switzerland

[#b]Current Address: Department of Human Genetics, University of Utah School of Medicine, Salt Lake City, United States of America

*Corresponding authors
E-mails: sartori@imcr.uzh.ch (AAS), mireille.betermier@i2bc.paris-saclay.fr (MB)

[¶]These authors contributed equally to this work.

Abstract

DNA double-strand breaks (DSBs) induced by clastogens can cause cell death or contribute to genomic instability, a major driving force of cancer. By contrast, Spo11-dependent DSBs formed during meiosis are aimed at generating genetic diversity. In eukaryotes, CtIP and the Mre11 nuclease complex are essential for accurate processing and repair of both unscheduled and programmed DSBs by homologous recombination (HR). Here, we applied bioinformatics and genetic analysis to identify *Paramecium tetraurelia* CtIP (PtCtIP), the smallest known Sae2/Ctp1/CtIP ortholog, as a key factor for the completion of meiosis and the recovery of viable sexual progeny. Using *in vitro* assays, we find that purified recombinant PtCtIP preferentially binds to branched, double-stranded DNA substrates. Moreover, mutation of the evolutionarily conserved RHR motif abrogates DNA binding of recombinant PtCtIP but not its ability to physically interact with Mre11. Translating our findings into human cells, we provide evidence that the RHR motif is important for efficient loading of CtIP at DSBs. Consequently, cells expressing a CtIP-RHR mutant are defective in DSB resection and HR. Collectively, our work highlights minimal structural requirements for CtIP protein family members to facilitate the processing of DSBs, thereby maintaining genome stability as well as enabling sexual reproduction.

Author summary

In all living organisms, DNA repair by homologous recombination (HR) is crucial for achieving genetic diversity during meiosis and for maintaining genome stability in response to DNA double-strand breaks (DSBs). DNA-end resection is a prerequisite for the initiation of HR and involves the collaborative action of two protein factors: CtIP and the Mre11 nuclease complex. However, the mechanistic contribution of CtIP to DNA-end resection is still rather poorly understood. Biochemical studies have demonstrated that CtIP plays an important, but as-yet undefined, structural role in promoting DNA cleavage by Mre11. Here, we identify two miniature paralogs of the Sae2/Ctp1/CtIP protein family in *Paramecium tetraurelia* required for efficient repair of meiotic DSBs. Simultaneous loss of both *PtCtIP* genes results in impaired zygotic

nucleus formation and reduced viability of the sexual progeny. In addition, we show that PtCtIP utilizes a highly conserved RHR motif for DNA substrate binding. Mutation of the RHR motif in human CtIP abrogates its localization to damaged chromatin, resulting in reduced HR events. Our work thus establishes PtCtIP as a model minimal protein to gain structural insights into meiotic recombination and emphasizes DNA-binding as an essential feature of CtIP proteins to promote DNA-end resection.

Introduction

DNA double-strand breaks (DSBs) are the most lethal type of DNA damage, and, if incorrectly repaired, can drive tumorigenesis[1]. On the other hand, induction of DSBs by ionizing radiation (IR) or DNA topoisomerase poisons like camptothecin (CPT) represents a common therapeutic strategy to effectively eliminate cancer cells[2]. Cells have evolved two major pathways for the repair of DSBs: Non-homologous end-joining (NHEJ), which ligates broken ends without the need of extensive processing, and homologous recombination (HR), which requires an intact homologous DNA template for repair[3,4]. The first step of HR is termed DNA-end resection and involves nucleolytic processing of DSB ends to generate 3' single-stranded DNA (ssDNA) overhangs that are immediately covered by the replication protein A (RPA). RPA subsequently gets replaced by the Rad51 recombinase, which initiates homology search and strand invasion[5]. In eukaryotes, DNA-end resection is initiated by the concerted action of the Mre11-Rad50-Xrs2/Nbs1 (MRX/N) nuclease complex in association with Sae2/Ctp1/CtIP[5].

At the protein level, human CtIP and its counterparts in other species are predicted to be largely intrinsically disordered, with the exception of a conserved N-terminal coiled-coil domain that assembles into a tetrameric 'dimer-of-dimers' complex[6,7]. In addition, a short C-terminal stretch showing the highest degree of amino acid sequence similarity within CtIP protein members is commonly referred to as the 'Sae2-like' domain[7]. Human CtIP and its functional counterparts in *S. pombe* (Ctp1), *A. thaliana* and *C. elegans* have been identified as homologs of *S. cerevisiae* Sae2 (for Sporulation in the Absence of Spo Eleven), a protein that is required for the initiation of DNA-end resection in meiotic and mitotic yeast cells[8–13].

The biochemical properties of recombinant Sae2/Ctp1/CtIP proteins have been extensively studied in recent years, significantly contributing to our mechanistic understanding of DNA-end resection[7]. First, both Sae2 and CtIP were shown to directly associate with the MRX and MRN complex, respectively, and to stimulate Mre11's weak endonuclease activity in cleaving the 5' strand[13–19]. In a second step, DNA is processed in 3' to 5' direction from the nick towards the DSB end by Mre11's intrinsic exonuclease activity, meanwhile 5' to 3' exonucleases such as Exo1 and Dna2

progressively resect the 5' DNA strand, ultimately generating a 3' single-stranded DNA (ssDNA) overhang compatible for Rad51 binding[20–23].

In the germline, the formation of programmed DSBs, generated by the topoisomerase-like Spo11 protein, is required for genetic recombination during meiosis[24]. Throughout evolution, CtIP and the Mre11 nuclease complex are strictly required for meiotic recombination by removing covalently attached Spo11 from DSB ends and, thereby, allowing DNA-end resection to start[25–29].

Paramecium tetraurelia, like all ciliates, is a unicellular eukaryote that contains two functionally distinct types of nuclei: a large somatic macronucleus (MAC, 800*n*) responsible for gene expression, but not transmitted to sexual progeny, and two identical diploid germline micronuclei (MIC) that undergo meiosis during the sexual cycle (34). In *P. tetraurelia*, correct assembly of newly developing MACs requires the elimination of 25-30% of MIC DNA, including the precise excision of thousands of ~45'000 short internal eliminated sequences (IES). DNA elimination is mediated through the sequential action of PiggyMac, a domesticated piggyBac transposase essential for cleaving DNA at IES ends, and the NHEJ pathway[30–34]. With regards to recombinatorial repair, a recent inventory of meiosis-specific genes in ciliates revealed the presence of two gene copies each for *PtMRE11* and *PtCtIP*, consistent with multiple whole-genome duplication events in the early stages of *P. tetraurelia* evolution[35,36]. Remarkably, with a length of only 198 amino acids, PtCtIP paralogs would constitute the smallest Sae2/Ctp1/CtIP protein family members that have been identified so far.

In the present study, we sought to characterize the function of PtCtIP *in vivo* and *in vitro*. Comparative sequence analysis reveals that PtCtIPa and PtCtIPb, collectively termed as PtCtIP, share the minimal domain architecture present in all Sae2/Ctp1/CtIP proteins. *PtCtIP* expression is required for the processing of Spo11-dependent meiotic DSBs, an essential prerequisite to the production of gametic nuclei and subsequent development of a new somatic MAC in sexual progeny. Purified recombinant PtCtIP binds with high affinity to double-stranded branched DNA molecules but lacks detectable intrinsic nuclease activity. Moreover, PtCtIP-DNA interaction, but not PtCtIP-Mre11 interaction, strongly depends on a highly conserved RHR motif located in the C-terminus. Finally, we provide evidence that the RHR motif mediates efficient

recruitment of human CtIP to sites of DNA damage ensuring efficient DSB resection and repair by HR.

Results

The *Paramecium tetraurelia* genome encodes two protein copies with a domain organization shared by CtIP homologs

CtIP protein sequences are poorly conserved across the eukaryote phylogeny and vary greatly in their molecular size, particularly between yeast and mammalian homologs (Fig 1A). *Schizosaccharomyces pombe* Ctp1 (294 amino acids, aa) represents the smallest CtIP homolog that has been characterized so far[10]. To screen for additional members of the Sae2/Ctp1/CtIP protein family in other species, we ran iterative PSI-BLAST searches using as query the amino acid sequence of the conserved C-terminal domain of human CtIP (~75 aa). Interestingly, we retrieved two putative CtIP-like polypeptides in *Paramecium tetraurelia* comprised of only 198 aa sharing more than 80% sequence identity (Figs 1A and S1A). Closer examination of the *P. tetraurelia* predicted proteome indeed revealed the existence of two closely related CtIP paralogs, PtCtIPa and PtCtIPb (ParameciumDB accession numbers GSPATP00020534001 and GSPATP00027328001)[37]. *PtCtIPa* and *PtCtIPb* gene copies resulted from the most recent whole genome duplication (WGD) that took place before the evolutionary split of the *Paramecium aurelia* genus into 15 sibling species including *P. tetraurelia* [36].

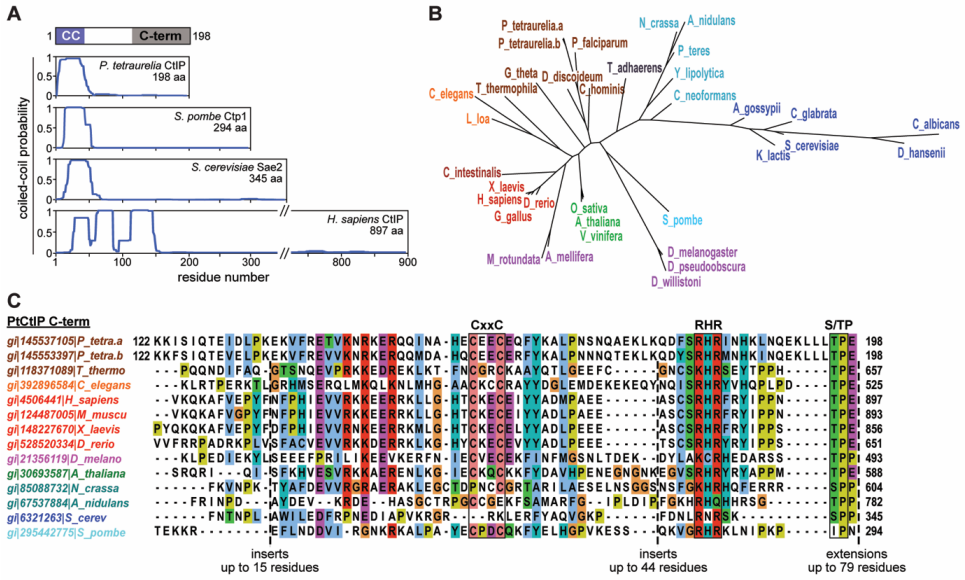

Fig 1. Comparative protein sequence analysis of PtCtIP.

(A) Upper panel, predicted protein scheme of *Paramecium tetraurelia* CtIP (PtCtIP), with putative coiled-coil (CC) and C-terminal regions indicated in coloured boxes. Lower panel, coiled-coil-forming probabilities predicted by the PCOILS program (window length of 21 residues) for the indicated CtIP proteins. **(B)** Phylogenetic tree obtained from the sequence analysis of the CtIP C-terminal region from 35 species using PhyML algorithm. **(C)** Sequence alignment of the C-terminal region of PtCtIPa and PtCtIPb with 12 CtIP proteins from different species. Gene accession numbers (gi) and species names are color-coded according to the phylogenetic tree shown in **(B)**. Insertions and extensions were trimmed and marked by dashed lines with the number of residues indicated below. Evolutionarily conserved CxxC, RHR and S/TP motifs are indicated in black boxes.

To gain further insight into the protein sequence and domain architecture of PtCtIP, we adopted a hierarchical alignment procedure allowing us to align different evolutionarily conserved regions of CtIP homologs. The N-terminus of PtCtIP features five repeating heptad sequences, which are predicted to assemble into a coiled-coil structure typically present in Sae2/Ctp1/CtIP proteins (Figs 1A and S1B). Moreover, upstream of the heptad repeats, a short α-helical region previously reported to mediate CtIP tetramerization can be distinguished with high confidence in PtCtIP (Fig S1B)[6,7]. The phylogenetic tree built from a multiple sequence alignment restricted to the conserved C-terminal domain demonstrates that PtCtIP cluster together with protozoan sequences, as expected, while strong sequence divergences are primarily

observed between ascomycetes, including *S. cerevisiae* Sae2 (Figs 1B and 1C). Closer examination of the PtCtIP C-terminal region revealed the presence of two conserved, closely spaced, short linear sequence motifs: CxxC and RHR (Fig 1C). The RHR motif, located at aa positions 181-183 of PtCtIP, was shown to promote DNA-bridging activity of Ctp1 *in vitro*[7]. We further noted that PtCtIP is the only family member lacking a C-terminal amino-acid extension after the cyclin-dependent kinase (CDK) consensus sequence motif (S/TP) required for DNA-end resection in yeast and human cells (Fig 1C)[38,39]. In fact, PtCtIP is devoid of any additional CDK phosphorylation sites, some of which were reported to promote the interaction of human CtIP with Nbs1 FHA/BRCT domains[40]. Consistent with this observation, no apparent homolog of Nbs1 exists in *P. tetraurelia*. In conclusion, our *in silico* bioinformatic analysis predicts that PtCtIP is mainly composed of the conserved N- and C-terminal regions of the Sae2/Ctp1/CtIP family, making it the smallest CtIP protein known to date.

***Paramecium CtIP* genes are required for the recovery of viable progeny during autogamy**

Autogamy is a self-fertilization process encountered in the *Paramecium aurelia* group of species. Upon starvation, mature *P. tetraurelia* cells that have undergone at least 20 vegetative fissions can start MIC meiosis in the absence of a sexual partner. A fully homozygous zygotic nucleus is formed through the fusion of two identical gametic nuclei. Following two successive nuclear divisions that take place in the absence of cell division, two mitotic copies of the zygotic nucleus give rise to the new MICs while new MACs differentiate from the other two copies. We surveyed the expression of *PtCtIP* compared to *PtSPO11* in *P. tetraurelia* cells at different autogamy stages. Northern blot analysis revealed an early transcription induction peak during MIC meiosis for both *PtCtIP* genes simultaneously to *PtSPO11* (Fig S2A). This result was confirmed by deep sequencing of mRNAs (Fig 2A)[41]. As expected from the conservation of the meiosis process in *Paramecium*, the genome of *P. tetraurelia* carries two recently duplicated *PtMRE11* genes. Northern blot hybridization and deep sequencing of mRNAs revealed that *PtMRE11* genes have quite different patterns of expression: *PtMRE11a* (ParameciumDB accession number GSPATG00020413001)

exhibits a constitutively low level of expression at all stages of the sexual cycle, while *PtMRE11b* (ParameciumDB accession number GSPATG00023641001) is strongly induced during meiosis (Figs 2A and S2A)[37]. Notably, *PtMRE11b* levels peak at the same time during meiosis as both *PtCtIP* and *PtSPO11* mRNAs (Figs 2A and S2A).

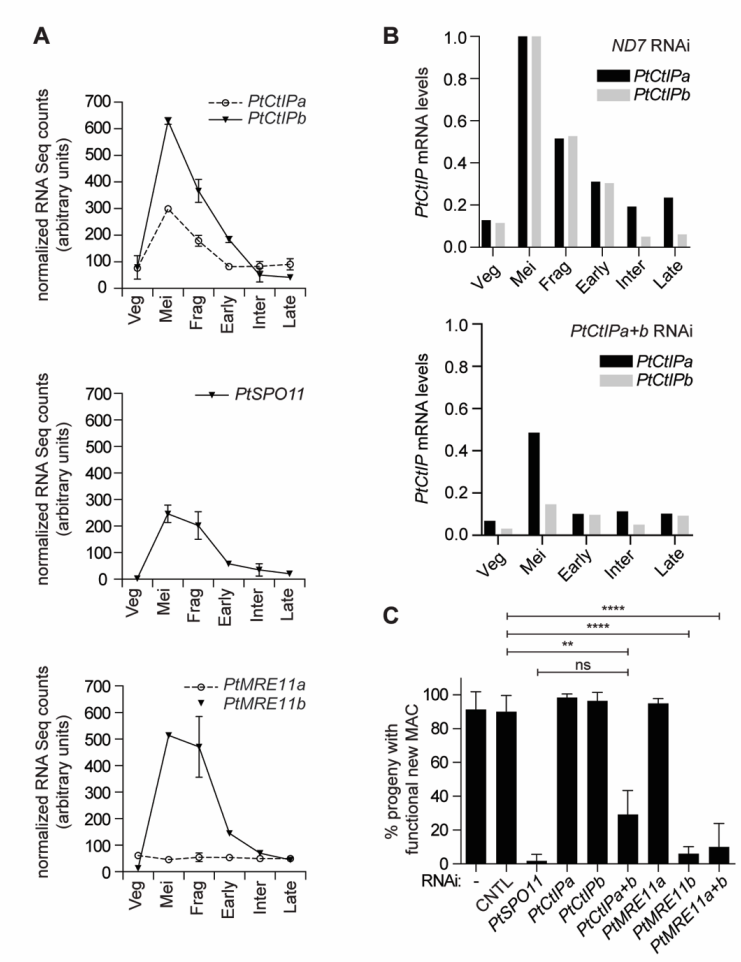

Fig 2. *PtCtIP* genes are required for recovery of viable sexual progeny.

(A) Steady-state levels for *PtCtIP*, *PtSPO11* and *PtMRE11* mRNA at different developmental stages. Curves show the average normalized values calculated for each autogamy stage ($n \geq 2$). RNA-Seq data extracted from[41]. Veg: vegetative cells; Mei: starved cells with meiotic stages; Frg: fragmented old MAC but no visible developing new MACs; Early: early stages of MAC development; Inter: intermediate stages of MAC development; Late: late stages of MAC development. **(B)** Quantification of *PtCtIPa* and *PtCtIPb* mRNA levels during autogamy. *P. tetraurelia* 51 cells were submitted to control (*ND7*) RNAi (upper panel) or to RNAi against both *PtCtIPa* and *PtCtIPb* (lower panel). Autogamy stages were

defined as in (A) following DAPI staining of nuclei (Fig S2B). Northern blots of total RNAs extracted at indicated time-points for each RNAi condition were hybridized with *PtCtIPa*- or *PtCtIPb*-specific labeled probes A2 or B2, respectively (Fig S2B and Table S1). Viable post-autogamous progeny yields in this experiment: 97%, control RNAi; 23%, *PtCtIPa+b* RNAi. 17S rRNA signal was used for normalization. Y-axes are in arbitrary units, with mRNA signals normalized to 1 at the Mei stage for both genes. **(C)** Combined depletion of *PtCtIPa* and *PtCtIPb* impairs new MAC development in *Paramecium* sexual progeny. Histograms show the fraction of sexual progeny harboring functional new MACs after silencing of the respective genes by RNAi. Data are presented as the mean ± SD with n between 2 and 15 for each condition. Statistical differences were determined by paired t-test. ns, non-significant; **P < 0.005; ****P < 0.0001. CNTL: RNAi-mediated targeting of either *ND7* or *ICL7* non-essential genes. For simultaneous silencing of both *PtMRE11* genes, different constructs were used (cross-reacting a2 and b2 constructs, either alone or together; gene-specific a1 and b1 constructs, together; see Table S1).

To gain insight into the function of CtIP in *P. tetraurelia*, we used an RNAi strategy to silence the expression of *PtCtIP* genes during autogamy, individually or altogether. Because both genes are actively transcribed during meiosis (Figs 2A and S2A), vegetative growing cells were fed on dsRNA-producing bacteria and left to starve in the feeding medium until autogamy started. Quantitative analysis of mRNA levels using northern blot hybridization demonstrated an efficient RNAi-mediated downregulation of *PtCtIPa* and *b* (up to ~10 fold) relative to control RNAi (Figs 2B and S2B). During autogamy of cells silenced for the expression of both *PtCtIPa* and *b* genes, the development of new MACs in the sexual progeny was monitored after DAPI staining. Strikingly, in all *PtCtIP* knockdowns, a large fraction of autogamous cells harboured only fragments from the old MAC, but did not develop new MACs (Figs S2B and S2C). No MICs could be detected in these cells either, suggesting that depletion of PtCtIP triggers an early defect during the sexual cycle and prevents the formation of a functional zygotic nucleus. At later stages, cells with two MICs and a single large nucleus surrounded by several smaller fragments started to appear in *PtCtIP* knockdowns (orange population in Fig S2B). These could result from the overgrowth of a minority of viable post-autogamous progeny that succeeded in making their new MACs, throughout the long incubation time of each experiment (3 to 4 days).

To check whether knockdown of *PtCtIP* or *PtMRE11* genes has a debilitating effect on the ability of sexual progeny to resume vegetative growth, we measured the percentage of post-autogamous survivors with functional new MACs. Knockdown of

individual *PtCtIPa* or *b* genes did not cause any reduction of viable progeny, suggesting that *PtCtIP* genes can compensate each other (Fig 2C). However, the concomitant inactivation of both *PtCtIPa* and *b* expression resulted in ~30% lethality in the sexual progeny (Fig 2C). In contrast, silencing of *PtSPO11* or *PtMRE11b* alone was sufficient to induce strong lethality in the post-autogamous progeny, consistent with their respective meiosis-specific expression profiles (Figs 2A and S2A). These results indicate that, despite its short size, PtCtIP, like PtMre11, is fully functional and essential for DSB repair during meiosis in *P. tetraurelia*.

Abnormal meiosis and lack of new developing MACs in cells depleted for *PtCtIP* genes

The complete absence of new MICs and MACs in *PtCtIP* knockdowns likely reflects an early defect in the formation of a functional zygotic nucleus. In the ciliate *T. thermophila*, *SAE2/COM1* knockout was shown to block the progression of MIC meiosis at the meiosis I stage, as a result of defective repair of meiotic DSBs and inefficient pairing of homologous chromosomes, eventually leading to chromosome "disintegration" and MIC degeneration[42]. Because autogamy is poorly synchronous in *P. tetraurelia*, we switched to conjugation in order to synchronize MIC meiosis and zygotic nucleus formation in the population[43]. We used anti-γ-tubulin antibodies to specifically label the MICs, the zygotic nucleus and its mitotic division products[44] in conjugating cells co-silenced for both *PtCtIP* genes (Fig 3A). This experiment confirmed that MIC meiosis proceeded normally at the cytological level, until the 4-MIC stage (*i.e.* meiosis I) in a large majority of cells. Abnormal patterns started to appear at meiosis II, with partial or complete loss of MIC meiotic products and complete absence of a zygotic nucleus in a majority of mating pairs, while normal fragmentation of the old MAC was still observed, suggesting that no fragmentation checkpoint exists in *P. tetraurelia*. Therefore, CtIP depletion in *P. tetraurelia* does not allow the formation of a zygotic nucleus, because it triggers an arrest right after meiosis I.

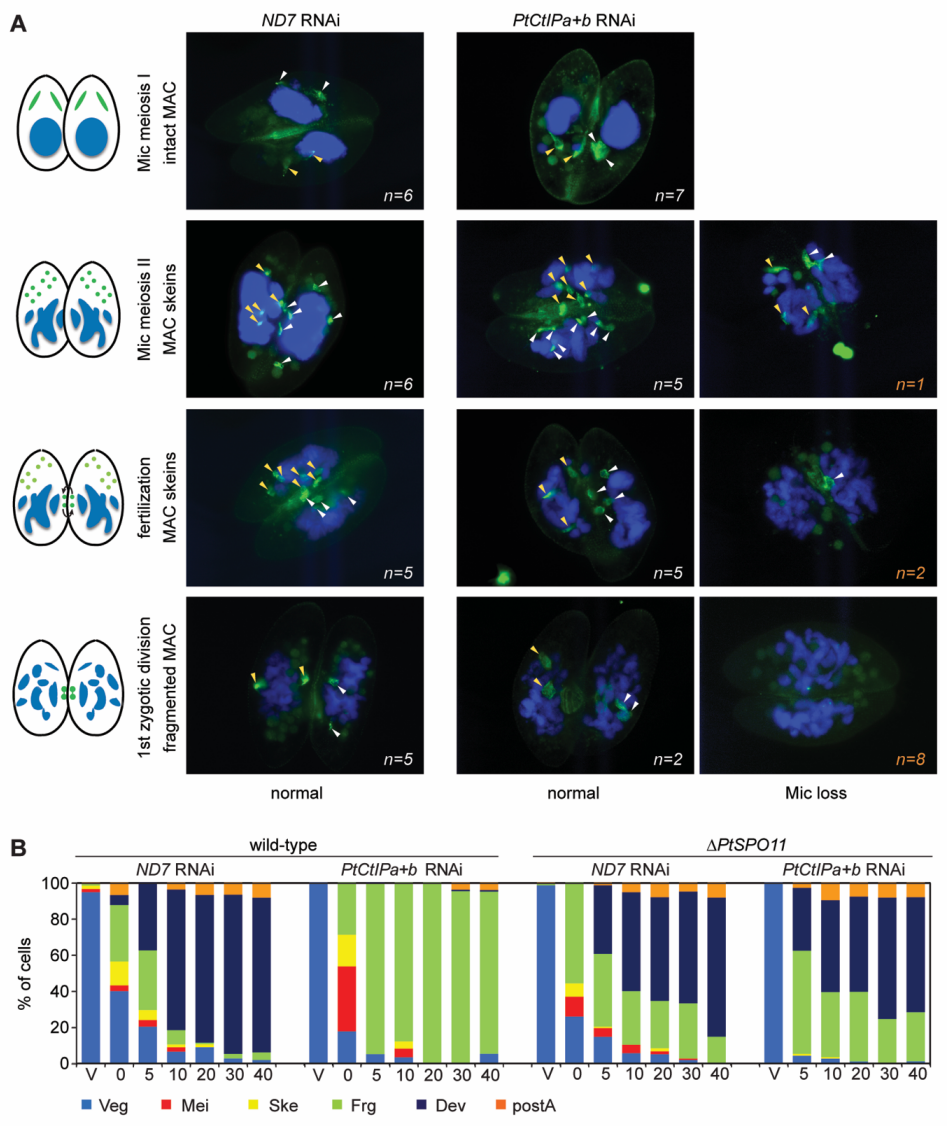

Fig 3. *PtCtIP* silencing impairs new MAC development due to abortive meiosis.

(A) *PtCtIP* RNAi during conjugation triggers a meiotic defect and impairs zygotic nucleus formation. Reactive cells prepared in control (*ND7*) or *PtCtIPa+b* RNAi medium were crossed at T0 and mating pairs were permeabilized and fixed 4.5, 6 and 7.5 hours following the start of conjugation. Fixed cells were pooled before proceeding to immunofluorescence staining using anti-γ-tubulin antibodies (green) and DAPI staining of nuclei. The progression of conjugation was monitored according to the state of the old MAC. Arrowheads (yellow in one partner, white in the other) point to meiotic micronuclei, or to zygotic nuclei and their mitotic products. 22 and 30 mating pairs were analysed for the control (*ND7*) and for *PtCtIP* RNAi, respectively. Numbers in orange refer to pairs in which loss of micronuclei ('Mic

loss') was detected in one or both partners. In the experiment shown here, 37% of mating pairs yielded viable progeny in the *PtCtIP* RNAi (100% in the control RNAi). **(B)** MAC development is inhibited following *PtCtIPa+b* RNAi in wild-type cells and restored at the cytological level in a *SPO11* knockout *Paramecium* strain submitted to *PtCtIPa+b* RNAi. Cultures of isogenic wild-type and Δ*PtSPO11* cells were allowed to undergo autogamy in control (*ND7*) or *PtCtIP* RNAi-inducing medium. The histograms show the progression of autogamy in the four cultures, as monitored by DAPI staining of cells at indicated time-points (hours), with the different cellular stages indicated below. Veg: vegetative cells; Mei: meiotic cells; Ske: cells with MAC skeins; Frg: cells with old MAC fragments but no visible new developing MACs; Dev: cells with two developing MACs; postA: post-autogamous cells with one new MAC and remaining old MAC fragments. Viable post-autogamous progeny yields in this experiment: 93%, wild-type cells, control RNAi; 10%, wild-type cells, *PtCtIP* RNAi, 7%, *ΔPtSPO11* cells, control RNAi; 0% *ΔPtSPO11* cells, *PtCtIP* RNAi.

In other organisms, the absence of CtIP also results in abortive meiosis, due to the accumulation of unrepaired Spo11-dependent DSBs. In *S. pombe*, *ctp1* C-terminal mutations severely reduce the yield of viable spores[26]. In budding yeast, *sae2*Δ mutant cells do not form tetrads, but sporulation is restored in the *sae2*Δ*spo11*Δ double mutant background, even though the resulting spores are not viable[11,45]. To get further insight into the meiotic function of the *P. tetraurelia* CtIP homologs, we knocked down *PtSPO11* by inducing a Δ*SPO11* somatic deletion (Δ$SPO11_{MAC}$) in strain 51 new (see Methods). We then submitted wild-type and Δ$SPO11_{MAC}$ cells to RNAi against *PtCtIP* genes and to a control RNAi against *ND7*. As expected, Δ$SPO11_{MAC}$ cells did not yield viable progeny in either condition (*PtCtIP* or control RNAi, Fig S3A). During the progression of autogamy, significant differences were observed between Δ$SPO11_{MAC}$ and wild-type cells (Fig 3B). In wild-type cells, *PtCtIP* silencing strongly impaired the formation of developing new MACs, as already observed. In the Δ$SPO11_{MAC}$ mutant submitted to a control RNAi, new developing MACs were detected, although not quite with the same efficiency as in the wild-type background. However, as indicated by the low survival rate in the progeny of Δ$SPO11_{MAC}$ cells (Fig S3A), these new MACs were not functional, suggesting that in *P. tetraurelia*, similar to other organisms, Spo11-dependent DSBs are essential for the successful segregation of homologs during meiosis. A dramatic difference was observed between wild-type and Δ$SPO11_{MAC}$ cells upon the silencing of *PtCtIP*. Indeed, the development of new MACs, strongly impaired in a *PtCtIP* knockdown, was partially restored in the double *PtSPO11* + *PtCtIP*

knockdown, indicative of a role for the *Paramecium* CtIP homologs in the repair of Spo11-dependent meiotic DSBs. Likewise, a double RNAi experiment revealed that MAC development is restored following *PtMRE11b* RNAi if cells are simultaneously submitted to RNAi against *PtSPO11* (Figs S3B and S3C). Taken together, these results demonstrate a key function of PtCtIPa+b and PtMRE11b in repairing Spo11-induced DSBs during meiosis and indicate that PtCtIP, despite its short size, is fully functional for promoting HR in *P. tetraurelia*.

PtCtIP DNA-binding depends on a conserved C-terminal RHR motif

Our genetic analyses underscored an essential role for *CtIP* during autogamy and conjugation in *P. tetraurelia*. In order to investigate how PtCtIP contributes to DNA-end resection at the molecular level, we purified full-length recombinant PtCtIPa protein from insect cells (Figs S4A and S4B). First, we aimed to characterize its DNA-binding properties by *in vitro* gel shift assays using 5'-end radiolabelled 50-mer oligonucleotide substrates (Table S1). At a fixed protein/DNA molar ratio, we observed that PtCtIPa specifically interacts with double-stranded, but not single-stranded nucleic acids (Fig 4A). Further protein titration experiments revealed that PtCtIPa exhibits higher binding affinity for forked compared to blunt-ended DNA (Fig 4B). We noted that PtCtIPa-DNA complexes migrated near the top of the gel, indicative of the formation of rather large multimeric assemblies, in particular when considering the low molecular weight of *Paramecium* CtIP (Figs 4A, 4B and S4B). Interestingly, however, recent studies demonstrated that both Ctp1 and human CtIP N-terminal domains can form stable tetramers consisting of two coiled-coil dimers[6,7]. Thus, given that both structural motifs mediating Ctp1/CtIP tetramerization are conserved in PtCtIP (Fig S1B), it is conceivable to predict that recombinant PtCtIPa also exists as a tetramer in solution resulting in the formation of high molecular weight complexes upon DNA binding. Indeed, we observed a similar mobility shift behavior of Ctp1-DNA and PtCtIPa-DNA complexes (Fig 4B). Moreover, the fact that we were unable to effectively cleave off the MBP-tag from all PtCtIPa protein molecules (Fig S4B) might explain why the mobility shift observed for PtCtIPa is even slightly bigger compared with Ctp1 (Fig 4B).

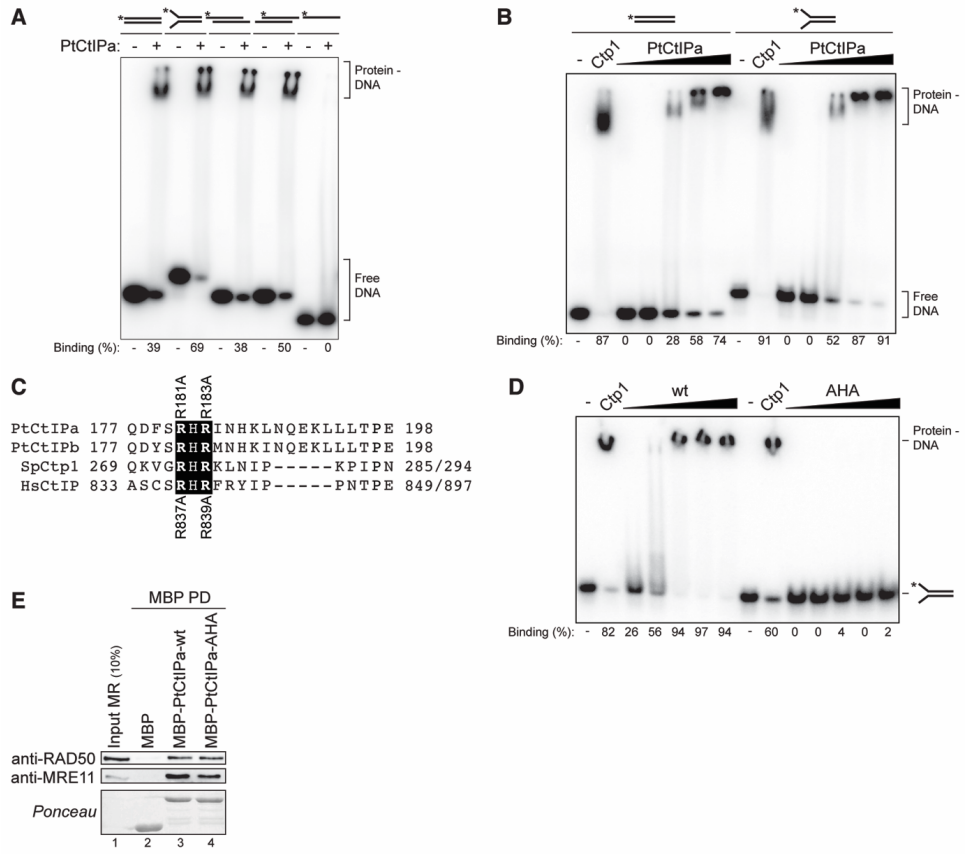

Fig 4. PtCtIP binding to DNA requires a highly conserved RHR motif.

(A) PtCtIP binds double-stranded DNA. Electrophoretic mobility shift assay (EMSA) was carried out with 10 nM of various 5'-labelled DNA substrates and 600 nM of PtCtIPa. **(B)** PtCtIP preferentially binds to forked DNA. EMSA was carried out with 10 nM of the indicated 5'-labeled DNA substrates and Ctp1 (380 nM) or increasing concentrations of PtCtIPa (100 nM, 200 nM, 400 nM, 700 nM and 1 μM). **(C)** Alignment of the amino acid sequences adjoining the conserved RHR motif in CtIP homologs from *P. tetraurelia* (Pt), *S. pombe* (Sp) and *H. sapiens* (Hs). The R181A/R183A and R837A/R839A (AHA) mutations in PtCtIP and HsCtIP are indicated, respectively, above and below the alignment. **(D)** Mutation of the RxR motif in PtCtIP abolishes DNA binding. EMSA was carried out with 10 nM of 5'-labeled forked DNA substrates and increasing concentrations of PtCtIPa wild-type (wt) or AHA mutant (200 nM, 400 nM, 600 nM, 800 nM and 1 μM). Ctp1 (380 nM) was used as positive control in lanes 2 and 9. **(E)** MBP or MBP-tagged PtCtIPa was coupled to amylose beads and incubated with purified recombinant human Mre11-Rad50 (MR) complex. Mre11 and Rad50 proteins in input and pull-down fractions were detected by immunoblotting using the indicated antibodies. MBP and MBP-CtIP proteins were detected by Ponceau staining. In **(A, B and D)**, DNA binding was calculated based on

disappearance of the substrate band and indicated as percentages (%) below the respective gels. ^{32}P-labeled strands are indicated with asterisks.

Notably, employing the same radiolabeled forked-DNA substrates, we could not detect any DNA cleavage activity associated with recombinant PtCtIPa (Figs S4C and S4D).

In addition to the N-terminal multimerization domain, Andres *et al.* reported a 'RHR' DNA-interaction motif located at the Ctp1 C-terminus[7]. As the 'RHR' motif is evolutionarily highly conserved among CtIP homologs from different species including *P. tetraurelia* (Fig 1C), we expressed and purified recombinant PtCtIPa-AHA with R181 and R183 mutated to alanine residues (Figs 4C and S4B). Gel shift assays showed that the PtCtIP-AHA mutant was completely defective in binding to the forked-DNA substrate, confirming the C-terminal RHR motif as a critical determinant of DNA-binding by CtIP proteins (Fig 4D). Remarkably, MBP-pulldown assays revealed that both wild-type PtCtIPa and PtCtIP-AHA mutant are able to interact with recombinant human Mre11-Rad50 (MR) complex, suggesting an evolutionarily conserved mode of interaction between the two factors (Fig 4E). Taken together, our combined genetic and biochemical analysis of PtCtIP strongly supports its key role in DSB repair-related processes.

The RHR motif in CtIP is required for DNA-end resection and HR

The significance of the contribution of CtIP's DNA-binding ability to DNA-end resection and HR in human cells has so far not been investigated. Williams and coworkers demonstrated that *S. pombe* strains expressing Ctp1 RHR mutant versions exhibited intermediate sensitivity to various genotoxic agents and failed to reconstitute full-length chromosomes following IR treatment, indicating a DSB repair defect[7].

To determine whether disruption of the RHR motif in human CtIP confers cellular phenotypes in response to DNA damage, we generated stable U2OS Flp-In T-REx clones expressing doxycycline (Dox)-inducible siRNA-resistant GFP-tagged wild-type (wt) CtIP or a DNA binding-defective CtIP-AHA mutant (R837A/R839A; Fig 4C). Importantly, flow cytometry and immunofluorescence microscopy analysis revealed that the two cell lines display similar cell cycle profiles and GFP-CtIP nuclear

localisation patterns (Figs S5A and S5B). Given that recombinant PtCtIP-AHA was defective in DNA binding, we first examined the assembly of GFP-CtIP at DNA lesions induced by laser micro-irradiation. Importantly, previous studies have shown that Sae2/CtIP and Mre11 are independently recruited to sites of DSBs[46–48]. Remarkably, we observed that the GFP-CtIP fluorescent intensity at DSB-containing tracks marked with γH2AX was significantly reduced in the AHA mutant compared with the wt, suggesting that DNA binding is a critical determinant for CtIP retention at damaged chromatin (Figs 5A and S5C). CtIP is required for CPT-induced hyperphosphorylation of RPA2 at serines 4/8, a surrogate marker for DSB resection revealed by western blotting (Fig 5B, lanes 1-3)[13,49]. We observed that re-expression of CtIP-wt fully restored RPA2 hyperphosphorylation in CtIP-depleted cells, whereas the rescue with CtIP-AHA was only partial (Fig 5B). Of note, GFP-CtIP expression as well as ATM phosphorylation levels were comparable between the two cell lines, indicating proficient upstream DSB signalling (Fig 5B). Consistently, using a flow cytometry-based approach to measure DNA-end resection[50,51], we found that RPA retention on damaged chromatin is strongly reduced in AHA mutant compared to wt expressing cells (Fig 5C). To further evaluate the impact of CtIP DNA binding on the processing of replication-associated DSBs formed at collapsed replication forks, we depleted endogenous CtIP from our U2OS clones and measured their viability following chronic exposure to CPT. In agreement with previous data[51], activation of CtIP-wt expression by Dox administration efficiently rescued CPT hypersensitivity of CtIP-depleted cells (Fig 5D). By contrast, cells expressing the CtIP-AHA mutant remained sensitive to CPT, indicative of an HR defect (Fig 5D). Finally, to directly measure HR efficiency, we made use of the traffic-light reporter (TLR) assay system[6] and engineered U2OS-TLR clones stably expressing siRNA-resistant FLAG-tagged CtIP-wt and -AHA (Fig 5E). Strikingly, whereas HR and DNA-end resection were largely restored in CtIP-depleted cells expressing CtIP-wt, they were still significantly compromised in both RHR-mutant expressing clones (Figs 5E and S5D), indicating that the DNA-binding ability of CtIP is a critical determinant of resection-dependent DSB repair by HR. Collectively, these findings establish that CtIP-DNA interaction via the 'RHR' motif promotes efficient recruitment of CtIP to DSBs, thereby facilitating DNA-end resection and HR in human cells.

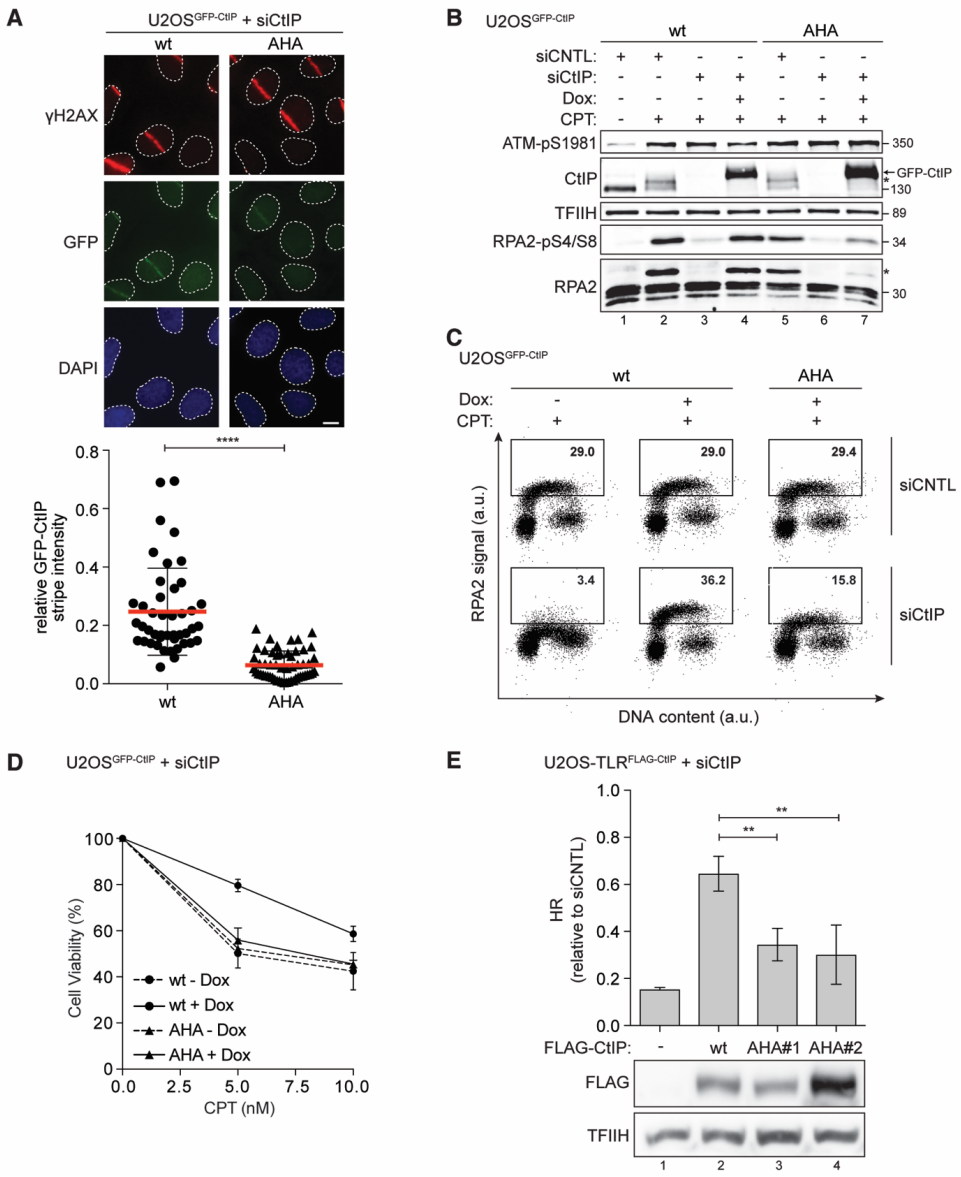

Fig 5. Mutation of the RHR motif impairs CtIP accrual at DSBs, DNA-end resection and HR. (A) U2OS clones harbouring inducible wt and AHA mutant GFP-CtIP were transfected with siCtIP for 48 h. 24 h later, cells were grown on coverslips in the presence of doxycycline (Dox) and BrdU for 24 h prior to laser micro-irradiation. 20 min post-irradiation, cells were fixed, immunostained for γH2AX and counterstained with DAPI for DNA and analysed by fluorescence microscopy. Upper panel: representative images. Scale bar, 10 μM. Lower panel: Scatter plot of relative fluorescent intensities of GFP-CtIP laser stripes normalized to γH2AX stripe intensity (see Fig S5C). Data are presented as the

mean (indicated by red bars) ± SD. Statistical difference was determined by Mann-Whitney test; **** ($P < 0.0001$). For each condition, more than 20 cells from two independent experiments were quantified. **(B)** The same cells as described in **(A)** transfected with control (CNTL) or CtIP siRNA were cultivated for 24 hr in absence (-) or presence (+) of Dox. 48 h post siRNA-transfection, cells were mock-treated (lane 1) or treated with CPT (1 μM) for 1 h and whole cell lysates were analysed by immunoblotting using the indicated antibodies. Asterisks indicate hyperphosphorylated forms of endogenous CtIP and RPA2, respectively. **(C)** The same cells as described in **(B)** were treated with with CPT (1 μM) for 1 h and harvested for FACS analysis. Dot plots show fluorescent intensities (a.u., arbitrary units) of RPA2 signals (y-axis) against the DNA content (x-axis). Quantification gates were established in untreated samples and the percentages of cells within the gates are indicated. One representative out of three experiments with similar results is shown. **(D)** The same cells as described in **(A)** were treated with indicated doses of CPT and survival was determined after 4 days using the CellTiter-Blue® cell viability assay. Data are represented as the mean ± SD (n = 3). **(E)** HR events were quantified in stable U2OS-TLR clones expressing siRNA resistant FLAG-CtIP-wt or -AHA (two different clones). Cells were transfected with siCtIP and 8 h later co-transfected with IFP-I-SceI nuclease and BFP-Donor expression plasmids. 72 h post-siRNA transfection, cells were harvested for flow cytometry and immunoblot analysis. Data are represented as the mean ± SD (n = 3). Statistical differences were determined by ordinary one-way ANOVA test; ** ($P < 0.005$).

Discussion

Spontaneous or damage-induced DSBs need to be accurately repaired to maintain genome integrity and suppress tumorigenesis. During meiosis, however, hundreds of DBSs are deliberately induced by Spo11-dependent cleavage and subsequently repaired by homologous recombination to generate genetic diversity. In mammalian cells, faithful processing of both accidental and programmed DSBs requires the concerted action of the MRN complex and CtIP. Remarkably, while Mre11 and Rad50 are highly conserved and present throughout evolution, CtIP-related proteins have so far only been identified in eukaryotes[52,53]. Moreover, CtIP homologs have rapidly diverged in primary sequence and size ranging from 294 aa (*S. pombe* Ctp1) to 897 aa (human CtIP). In this study, we have characterized the genetic and biochemical activities of *P. tetraurelia* CtIP (PtCtIP), with only 198 aa in size, representing the smallest member of the Sae2/Ctp1/CtIP protein family known to date. Our primary sequence analysis revealed that PtCtIP is basically composed of the two hallmark structural elements common to all CtIP proteins: an N-terminal coiled-coil

domain critical for dimer/tetramer assembly and a highly conserved C-terminus harboring a short linear motif implicated in DNA binding (Figs 1 and S1). In contrast, the large, intrinsically disordered middle region in human CtIP, shown to coordinate multiple protein-protein interactions and to harbor nuclease motifs[54,55], is strongly contracted in PtCtIP, comprising less than 50 amino acids (Figs 1 and S1). Nonetheless, the miniature PtCtIP is fully functional for HR-mediated repair of meiotic DSBs, emphasizing the interest of this homolog as a model to disentangle the core function of the CtIP-MR machinery from other regulatory functions.

P. tetraurelia contains two paralogous *CtIP* genes required for completion of meiotic recombination

An essential role for CtIP-related proteins in DSB repair was first described in *S. cerevisiae*, where Sae2 acts in concert with MRX to remove Spo11-oligonucleotide complexes from DSB ends during meiosis[11,45]. Consequently, Mre11 nuclease-deficient and *sae2*Δ mutant yeast strains fail to sporulate. Similar meiotic recombination defects were later observed for CtIP mutants in *S. pombe*, *A. thaliana*, *C. elegans*, and *T. thermophila*[10,42,56,57]. Furthermore, spore viability of 'CtIP' mutant cells could be partially rescued in a Spo11-deficient background in most species, indicating that it functions downstream of Spo11 in the repair of meiotic DSBs[29].

Due to a recent whole genome duplication event[36], two closely related CtIP gene copies, *PtCtIPa* and *PtCtIPb*, were identified in the model ciliate *P. tetraurelia*[37]. Interestingly, we found that *PtCtIPa* and *PtCtIPb* gene expression profiles are comparable to that of *PtSPO11* and *PtMRE11a*, displaying highest mRNA transcript levels in early meiosis (Figs 2A and 2B). Simultaneous silencing of both PtCtIP genes impaired the recovery of functional new MACs in sexual progeny to a similar extent as Mre11b or Spo11 knockdowns (Fig 2C), indicative of an essential function of PtCtIP during meiotic recombination. Specifically, we show that PtCtIP knockdown cells exhibit a defect in the progression of meiosis I with complete absence of new developing MACs at late stages of the sexual cycle (Fig 3). Strikingly, *PtCtIP* disruption in a Spo11-deleted strain partially restored the physical development of new, yet non-viable MACs (Fig 3B), establishing that PtCtIP is a *bona fide* ortholog of Sae2/Ctp1/CtIP.

RHR motif is critical for PtCtIP DNA-binding and DSB resection in human cells

We demonstrated that purified recombinant PtCtIP preferentially recognizes branched (or flap) DNA substrates through a highly conserved RHR motif located at the C-terminus in all CtIP homologs (Fig 4)[7]. Our gel shift assays further suggested that PtCtIP binds to DNA in a multimeric state, giving rise to a high molecular weight complex. These results are in line with structural studies establishing an N-terminal tetrameric oligomerization scaffold in Ctp1 and CtIP[6,7], core residues of which are conserved in the PtCtIP protein sequence. Remarkably, while being unable to cleave DNA on its own, PtCtIP interacts with recombinant human MR complex, indicative of an evolutionary conserved protein-protein interaction module.

It has been reported that mutations of the RHR motif in Ctp1 resulted in an intermediate level of DNA damage sensitivity in *S. pombe* strains, suggesting that additional factors can partially compensate for DNA-binding defects[7]. Here, we provided evidence that mutation of the RHR motif in human CtIP abrogates its spatial redistribution in response to DNA damage, supporting the importance of the DNA-binding activity across different species (Fig 5A). In addition, we observed that human cells expressing a CtIP-AHA DNA-binding mutant display DNA-end resection and HR defects, ultimately resulting in profound hypersensitivity to CPT treatment (Figs 5B-E). Notably, however, PtCtIP-AHA mutant is proficient for MR interaction *in vitro* (Fig 4E), potentially suggesting that DNA-binding function of CtIP proteins is mechanistically separable from MR activation in DSB repair processes. Similarly, it was reported that DNA-binding of Sae2 is not necessary for the stimulation of the MRX endonuclease[58].

In conclusion, our study provides converging evidence that the minimal *Paramecium* CtIP ortholog, being deprived of most of the regulatory motifs found in other CtIP protein species, has retained the ability to repair Spo11-induced meiotic DSBs. Our combined biochemical and functional analyses further imply that the DNA-binding activity of CtIP-related proteins is critical for the maintenance of genomic stability. Clearly, further investigations are required to elucidate how CtIP structurally integrate with the MR complex to promote efficient repair of DSBs. We propose that the contracted PtCtIP might provide an ideal source for high resolution structural analyses aiming to answer this question.

Methods

Bioinformatics analysis of protein sequences

Due to the high sequence divergence among eukaryotic CtIP orthologs, a hierarchical approach was used to build the global alignment. First, six sequence profiles were independently generated from the full sequences of CtIP proteins in vertebrates (35 sequences), nematodes (10 sequences), plants (16 sequences), arthropods (19 sequences), protozoa (15 sequences) and fungi (63 sequences) using the MAFFT v7.0 algorithm with the E-INS-i iterative refinement method[59]. Next, using the HHsearch algorithm[60], these profiles were hierarchically aligned together resulting in a large multiple sequence alignment of 158 protein sequences. From this alignment, 35 sequences from model organisms were extracted and trimmed so that only the most conserved C-terminal domain was considered for the phylogenetic tree reconstruction. Phylogenetic tree was calculated using the PhyML algorithm[61] focusing on the C-terminal domain spanning residues 122-198 of PtCtIP with standard parameters (LG model of amino acids substitution, discrete gamma model with 6 categories and gamma shape factor of 1.729). Representation of the tree was performed using Dendroscope 3[62]. Coiled-coil predictions were performed using PCOILS[63].

P. tetraurelia strains, cultivation, and gene silencing

Autogamy and conjugation experiments were carried out at 27°C with strain 51new[64]. Cells were grown in a wheat grass powder (WGP, Pines International Inc.) infusion medium bacterized the day before use with *Klebsiella pneumoniae* and supplemented with 0.8 µg/ml β-sitosterol. Somatic *SPO11* knockout strain was generated as described previously[65]. In brief, following conjugation of reactive 51new cells from mating types 7 (mt7) and 8 (mt8), stable mating pairs were transferred to WGP medium inoculated with *Escherichia coli* HT115 bacteria harbouring plasmid PtSPO11-1 and induced for dsRNA production[31].

For RNAi-mediated gene silencing experiments during autogamy, cells were grown for 20 to 25 vegetative divisions under standard conditions, before transfer to WGP medium inoculated with HT115 bacteria harbouring the appropriate dsRNA-producing

plasmids[66]. To monitor the progression of autogamy, cells were permeabilized and fixed prior to DAPI staining as described[33]. Nuclear developmental stages were observed using a Zeiss Axioplan 2 Imaging epifluorescence microscope with 63x/1.4 Plan-Apochromate or 40x/1.3 Plan-Neofluar oil objectives. The capability of sexual progeny to develop a functional new MAC was monitored following individual transfer of 30 autogamous cells to standard culture medium[30].

RNAi experiments during conjugation were performed as described[31]. In brief, reactive 51new mt7 and mt8 cells were prepared in each RNAi medium and mixed to start conjugation. Following 1.75 h incubation at 27°C, freshly induced RNAi medium was added to the mix to synchronize conjugation. Mating pairs were transferred manually to each RNAi medium and incubated at 27°C to complete MAC development and resume vegetative growth. To monitor sexual processes, conjugating cells were permeabilized, fixed and processed for immunostaining as described[32]. To reveal micronuclei and the zygotic nucleus during conjugation, cells were incubated for 1 h with primary anti-γ-tubulin antibodies (1:400[44]), then washed with TBST (10 mM Tris-HCl pH 7.4, 0.15 M NaCl, 0.1% Tween) + 3% BSA prior to 15 min incubation with secondary Alexa Fluor 488-conjugated anti-rabbit antibodies (1:300, ThermoFisher Scientific), followed by DAPI staining. Imaging was performed using a Zeiss Axioplan 2 Imaging epifluorescence microscope with a 63x/1.4 Plan-Apochromate oil objective.

dsRNA-producing plasmids for silencing *P. tetraurelia* genes

All RNAi plasmids are derivatives of vector L4440[67] and carry a target gene fragment between two convergent T7 promoters. Each insert was chosen in order to minimize the risk of cross-silencing by using the "RNAi off-target" tool of ParameciumDB[37]. Plasmids p0ND7c[68], pICL7a[69] and pL4440-SPO11-1[31] were used to target *Paramecium ND7*, *ICL7a* and *SPO11* genes, respectively. RNAi plasmids targeting *PtCtIP* and *PtMRE11* genes were constructed as follows: pL4440-PtCtIPa: a 354-bp fragment from *PtCtIPa* (nt 266-619) was amplified by PCR from total genomic DNA from *P. tetraurelia*, using primers PtCtIPa-SpeI-F and PtCtIPa-SpeI-R (Table S1) and the Phusion High-Fidelity DNA polymerase (New England Biolabs). Following SpeI-restriction, the PCR fragment was inserted into the unique XbaI site of vector L4440. pL4440-PtCtIPb: same cloning procedure for a 354-bp fragment from *PtCtIPb*

(nt 266-619) amplified using primers PtCtIPb-SpeI-F and PtCtIPb-SpeI-R. pL4440-PtMRE11a1: same cloning procedure for a 492-bp fragment from *PtMRE11a* (IF2: nt 1422-1913) amplified using primers PtMRE11a1-SpeI-F and PtMRE11a1-SpeI-R. pL4440-PtMRE11b1: same cloning procedure for a 510-bp fragment from *PtMRE11b* (IF2: nt 1420-1929) amplified using primers PtMRE11b1-SpeI-F and PtMRE11b1-SpeI-R. pL4440-PtMRE11a2: same cloning procedure for a 507-bp fragment from *PtMRE11a* (IF1: nt 24-530) amplified using primers PtMRE11a2-SpeI-F and PtMRE11a2-SpeI-R. The IF1 sequence from *PtMRE11a* cross-reacts with *PtMRE11b*. pL4440-PtMRE11b2: same cloning procedure for a 508-bp fragment from *PtMRE11b* (IF1: nt 24-531) amplified using primers PtMRE11b2-SpeI-F and PtMRE11b2-SpeI-R. The IF1 sequence from *PtMRE11b* cross-reacts with *PtMRE11a*.

Northern blot analysis

Total RNA was extracted from ~400,000 cells for each indicated time point during autogamy of 51new cells grown in standard *K. pneumoniae* medium and processed for northern blot hybridization using ^{32}P-labeled probes as described[31]. Unless otherwise stated, PCR fragments of *PtSPO11*, *PtCtIPa*, *PtCtIPb, PtMRE11a* and *PtMRE11b* RNAi-targeting plasmids were used as gene-specific double-stranded probes (Table S1). The sequence of the 17S rRNA oligonucleotide probe is shown in Table S1. Hybridization signals were collected using a Typhoon TRIO Variable Mode Phosphorimager (GE Healthcare). Quantification was performed using the ImageJ software and mRNA levels were normalized relative to 17S rRNA hybridization signals.

Cloning, expression and purification of recombinant PtCtIPa

The *PtCtIPa* open reading frame (NCBI database GI accession number 145537105) was synthesized, cloned into pUC57 and verified by sequencing (GeneScript, Piscataway, NJ, USA). *PtCtIPa* was PCR-amplified using the primers listed in Table S1 and cloned into the pFastBac(FB)-MBP-His vector. PtCtIPa-R181A/R183A amino acids substitutions were generated by site-directed mutagenesis using PfuTurbo DNA polymerase (Agilent Technologies) and appropriate primers (Table S1). Recombinant PtCtIPa proteins were expressed using the pFB-MBP-PtCtIP-His vectors and the Bac-to-Bac baculovirus expression system (Invitrogen) in insect cells as described previously[70]. In brief, Sf9 cells (1x10^6 cells/ml) cultured in

HyClone SFX-Insect cell culture medium (GE Healthcare) were transduced with high-titer viruses and grown for 52 h at 27°C. All subsequent steps were performed at 4°C. Pellets of 200 ml cultures were resuspended in lysis buffer (50 mM Tris-HCl, pH 7.5, 1 mM EDTA, 1 mM DTT, 1 x Halt Protease Inhibitor Cocktail (Thermo Scientific), 1 mM PMSF, 30 μg/ml leupeptin) and incubated stirring for 20 min before adding 0.5 volumes of 50% glycerol. 5 M NaCl was added dropwise to the sample, to reach a final concentration of 300 mM NaCl, and the solution was incubated 30 min before centrifugation at 38,000 g for 30 min. Soluble extracts were bound to pre-equilibrated amylose resin (New England Biolabs, UK) for 1 h and the resin was washed with wash buffer (50 mM Tris-HCl, pH 7.5, 1 M NaCl, 10% Glycerol, 1 mM PMSF, 2 mM β-mercaptoethanol, 10 μg/ml leupeptin). Proteins were eluted with wash buffer containing 10 mM maltose. To cleave the MBP tag, samples were incubated for 3 h with recombinant prescission protease (PP) expressed in *E. coli* and purified using standard procedures {Anand:2018kn}. Next, imidazole was added to a final concentration of 20 mM before adding 0.5 ml Ni-NTA-agarose (Qiagen). The resin was extensively washed with NTA buffer (50 mM Tris-HCl, pH 7.5, 150 mM NaCl, 10% glycerol, 0.5 mM PMSF, 2 mM β-mercaptoethanol, 10 mM imidazole) and proteins eluted with NTA buffer supplemented with 400 mM imidazole. Peak fractions containing PtCtIPa-His were incubated with amylose resin to remove the remaining uncleaved MBP-tagged PtCtIPa, pooled, and dialyzed against dialysis buffer (50 mM Tris-HCl, pH 7.5, 300 mM NaCl, 10% glycerol, 0.5 mM PMSF and 5 mM β-mercaptoethanol). Small aliquots of the purified PtCtIPa proteins were snap frozen and stored at -80°C. Recombinant Mre11-Rad50 (MR) complex was expressed and purified as described previously[71].

DNA substrates

The sequences of 50mer oligonucleotides used in DNA binding and nuclease assays are listed in Table S1. Where indicated, the 5′ end was labeled with T4 polynucleotide kinase (PNK; New England Biolabs) in the presence of [γ-^{32}P]-ATP, while 3′ end labeling was performed with terminal deoxynucleotidyl transferase (TdT; New England Biolabs) in the presence of [α-^{32}P]-cordycepin-5′-triphosphate. Unincorporated nucleotides were removed using MicroSpin G25 columns (GE

Healthcare). The double-stranded oligo substrates were annealed by heating the oligonucleotides at 95°C and slow gradual cooling to room temperature in either 1x TdT or PNK buffer.

DNA binding assay

All steps were performed at 4°C under native conditions. Recombinant proteins were incubated with 10 nM of the indicated radiolabeled DNA substrates for 20 min at 20°C in 20 µl binding buffer (20 mM Tris-HCl, pH 7.5, 10 mM NaCl, 0.5 mM DTT, 10 µg/ml BSA, 4% glycerol). Protein-DNA complexes were separated on a 4-20% TBE precast gel (Novex) for 120 min at 100 V, respectively, dried and exposed to a phosphor screen before imaging using a Typhon FLA 9500 scanner (GE Healthcare). Data were quantified with ImageQuant TL software (GE Healthcare).

DNA cleavage assays

Recombinant proteins were incubated with 10 nM of 5' or 3' radiolabelled DNA substrates for 60 min at 37°C in 10 µl reaction buffer (20 mM Tris-HCl, pH 7.5, 10 mM NaCl, 0.5 mM DTT, 10 µg/ml BSA, 4% glycerol) supplemented with either 5 mM $MgCl_2$ or 1 mM $MnCl_2$. 10 nM of purified recombinant human DNA2 was used as a control. Nuclease reactions were stopped by adding an equal volume of 80% formamide loading dye. Samples were boiled for 5 min and products were separated on a 20% polyacrylamide gel containing 7 M urea. Gels were fixed in 1x TBE buffer containing 10% acetic acid, 50% EtOH and 10% glycerol for 20 min, dried and exposed to a phosphor screen before imaging on a Typhoon FLA 9500 scanner (GE Healthcare).

MBP pull-down assay

Soluble protein extracts of Sf9 cells expressing MBP alone or MBP-PtCtIPa-His were incubated with amylose resin for 1 h at 4°C. Resin was washed three times with NTEN buffer (20 mM Tris-HCl, pH 7.4, 0.1 mM EDTA, 0.5% NP-40) containing 300 mM NaCl and once with TEN100 buffer (20 mM Tris-HCl, pH 7.4, 0.1 mM EDTA, 100 mM NaCl). MBP proteins coupled to amylose beads were mixed with 0.5 µg of recombinant human Mre11-Rad50 (MR) complex for 2 h at 4°C. Beads were washed with NTEN buffer containing 500 mM NaCl and proteins were eluted in TEN100 buffer

containing 20 mM maltose. Samples were analysed by SDS-PAGE followed by immunoblotting.

Plasmids, antibodies and siRNA

The pcDNA5/FRT/TO-GFP-CtIP-wild type (wt) and 3x Flag-CtIP-wt expression vectors were described previously[6,51]. CtIP-R837A/R839A amino acids substitutions were generated by site-directed mutagenesis using PfuTurbo DNA polymerase and appropriate primers (Table S1). All CtIP constructs are siRNA-resistant[13]. Antibodies for immunoblotting were: anti-FLAG M2 (Sigma F3165, 1:1000), anti-GFP (Santa Cruz B-2, 1:1000), anti-Mre11 (GeneTex 12D7, 1:1000), anti-Rad50 (GeneTex 13B3, 1:1000), anti-TFIIH p89 (Santa Cruz S-19, 1:1000), anti-RPA2 (Calbiochem NA19L, 1:1000), anti-phospho RPA2 (S4/S8) (Bethyl A300-245A, 1:5000), anti-phospho ATM (S1981) (Abcam ab81292, 1:5000). Control siRNA (luciferase 5′-CGUACGCGGAAUACUUCGA-3′) and CtIP siRNA (5′-GCUAAAACAGGAACGAAUC-3′)[13] were purchased from Microsynth.

Cell lines, cell culture, transfections and treatments

U2OS cells were maintained in Dulbecco's modified Eagle's medium (DMEM) supplemented with 10% fetal calf serum (FCS), 100 U/ml penicillin and 100 mg/ml streptomycin. The Flp-In T-REx system (Invitrogen Life Technologies) was used to generate U2OS cells stably expressing siRNA-resistant GFP-tagged CtIP-wt or CtIP-R837A/R839A under the control of a doxycycline-inducible promoter. In brief, pcDNA5/FRT/TO-GFP-CtIP and the Flp recombinase expression plasmid, pOG44, were mixed in a 1:9 ratio and transfected into U2OS Flp-In T-REx cells. 24 h later, cells were plated at different dilutions and 48 h post-transfection the medium was supplemented with 250 mg/ml hygromycin B and 12.5 mg/ml blasticidin S. The medium was replaced every 2–3 days and cells were selected for approximately 14 days. Resistant colonies were picked and single-cell clones analysed for GFP expression by immunoblotting and immunofluorescence microscopy after 24 h induction of protein expression with 1 µg/ml doxycycline (Dox, Sigma-Aldrich). The CtIP-R837A/R839A mutation in stable U2OS cells was verified by genomic sequencing. U2OS-TLR cells[6] stably transfected with Flag-tagged versions of CtIP

were grown in in the presence of 0.5 µg/ml puromycin and 0.5 mg/ml geneticin. Plasmid transfections were performed using the Fugene 6 transfection reagent (Promega) according to the manufacturer's instructions. siRNA transfections were performed using Lipofectamine RNAiMax (Life Technologies) according to the manufacturer's instructions. Camptothecin (CPT) was purchased from Sigma. Laser micro-irradiation was performed as described previously[51]. In brief, cells were grown in medium supplemented with 10 μM BrdU for 24 h. Cells were microirradiated using a MMI CELLCUT system containing a UVA laser of 355 nM (Molecular Machines and Industries). The laser intensity was set to 50% energy output and each cell was exposed to the laser beam for 300 ms.

Immunofluorescence microscopy

Cells grown on coverslips were fixed directly in formaldehyde (4%, w/v in PBS) for 15 min and permeabilized for 5 min in 0.5% Triton X-100 in PBS. Cells were incubated for 1 h with primary anti-H2AX-pS139 antibody (Cell Signalling 20E3, 1:500), followed by 1 h incubation with secondary Alexa Fluor 594-conjugated anti-rabbit antibody (Life Technologies, 1:1000). Coverslips were mounted with Vectrashield® (Vector Laboratories) containing DAPI and imaged using a Leica DM6B fluorescence microscope at 63X magnification.

DNA-end resection assay

Flow cytometry-based resection assay was performed as described previously[51]. Briefly, U2OS cells were transfected with CtIP siRNA. Where indicated, 24 h post-transfection, doxycycline was added to the cells to induce the expression of GFP-CtIP. 48 h post-transfection, cells were either mock-treated or treated for 1 h with 1 µM CPT. Cells were harvested, pre-extracted with 0.3% Triton-X100 in PBS for 15 min on ice and fixed with 4% formaldehyde (w/v) for 10 min at room temperature. Cells were incubated for 1 h with anti-RPA2 antibody (Calbiochem NA19L, 1:100) or anti-H2AX-pS139 antibody (Cell Signalling 20E3, 1:200), followed by 30 min incubation with Alexa Fluor 647- or 488-conjugated secondary antibody (Life Technologies, 1:250) and counterstained with DAPI/RNase. Samples were analysed by flow cytometry on a

CyAn ADP 9 (Dako). Data analysis was performed using FlowJo X software (Tree Star).

CellTiter-Blue® Cell viability assay

Cell viability was measured as previously described[51]. Briefly, U2OS clones stably expressing doxycycline-inducible siRNA-resistant forms of GFP-CtIP were transfected with indicated siRNAs. 24 h post-transfection, cells were seeded in triplicates at a density of 500 cells/well in a 96-well plate in medium supplemented with 1 µg/ml doxycycline. 24 h later, cells were continuously treated with indicated doses of CPT and grown for 4 days at 37°C. To measure viability, CellTiter-Blue® reagent (Promega) was added on the last day and incubated for 4 h at 37°C before fluorescence was measured at 560/590 nm using a microplate reader (Molecular Devices).

Homologous recombination reporter assay

Homologous recombination (HR) was measured using the TLR assay as described[6]. In brief, U2OS-TLR cells stably expressing siRNA-resistant forms of 3xFLAG-CtIP were seeded at a density of 500'000 cells per 6-cm dish. 6 h after siRNA transfection, cells were co-transfected with 2 µg of BFP donor and 3 µg of IFP-*I-SceI* endonuclease plasmids. 3 days after siRNA transfection, cells were harvested, fixed in 2% paraformaldehyde/PBS for 20 min at room temperature, washed and resuspended in 300 ul of PBS supplemented with 1 mg/ml BSA. Flow cytometry analysis was performed using the LSR-Fortessa Cell Analyzer (BD Biosciences). A minimum of 10,000 BFP/IFP double-positive cells were scored for GFP signal representing HR. Data analysis was performed using FlowJo X software (Tree Star).

Acknowledgements

We thank Pavel Janscak (University of Zurich, Switzerland) for providing purified recombinant human Mre11-Rad50 complex and for experimental advice. We thank Petr Cejka (Institute for Research in Biomedicine, Bellinzona, Switzerland) for

providing pFastBac-MBP-His vector, pGEX-1T-GST-PP expression construct and purified recombinant human DNA2. Purified recombinant *S. pombe* Ctp1 protein was a kind gift of Scott Williams (National Institute of Environmental Health Sciences, US National Institutes of Health, Research Triangle Park USA). Anti-γ-tubulin antibodies were kindly provided by Janine Beisson and Anne-Marie Tassin (I2BC, Gif-sur-Yvette, France). We acknowledge Stephen P. Jackson (Wellcome Trust Cancer Research UK Gurdon Institute, University of Cambridge, UK) for providing U2OS-TLR cells and FLAG-CtIP expression plasmid and Daniel Durocher (University of Toronto, Canada) for sharing U2OS Flp-In T-REx cells.

References

1. Hanahan, D. & Weinberg, R. A. Hallmarks of Cancer: The Next Generation. *Cell* **144,** 646–674 (2011).

2. Pommier, Y., Sun, Y., Huang, S. N. & Nitiss, J. L. Roles of eukaryotic topoisomerases in transcription, replication and genomic stability. *Nat. Rev. Mol. Cell Biol.* **17,** 703–721 (2016).

3. Chang, H. H. Y., Pannunzio, N. R., Adachi, N. & Lieber, M. R. Non-homologous DNA end joining and alternative pathways to double-strand break repair. *Nat. Rev. Mol. Cell Biol.* **18,** 495–506 (2017).

4. Jasin, M. & Rothstein, R. Repair of strand breaks by homologous recombination. *Cold Spring Harb. Perspect. Biol.* **5,** a012740 (2013).

5. Symington, L. S. Mechanism and regulation of DNA end resection in eukaryotes. *Crit. Rev. Biochem. Mol. Biol.* **51,** 195–212 (2016).

6. Davies, O. R. *et al.* CtIP tetramer assembly is required for DNA-end resection and repair. *Nat. Struct. {&} Mol. Biol.* **22,** 150–157 (2015).

7. Andres, S. N. *et al.* Tetrameric Ctp1 coordinates DNA binding and DNA bridging in DNA double-strand-break repair. *Nat. Struct. {&} Mol. Biol.* **22,** 158–166 (2015).

8. Penkner, A. *et al.* A conserved function for a Caenorhabditis elegans Com1/Sae2/CtIP protein homolog in meiotic recombination. *EMBO J.* **26,** 5071–5082 (2007).

9. Uanschou, C. *et al.* A novel plant gene essential for meiosis is related to the human CtIP and the yeast COM1/SAE2 gene. *EMBO J.* **26,** 5061–5070 (2007).

10. Limbo, O. *et al.* Ctp1 is a cell-cycle-regulated protein that functions with Mre11 complex to control double-strand break repair by homologous recombination. *Mol. Cell* **28,** 134–46 (2007).

11. McKee, A. H. & Kleckner, N. A general method for identifying recessive diploid-specific mutations in Saccharomyces cerevisiae, its application to the isolation of mutants blocked at intermediate stages of meiotic prophase and characterization of a new gene SAE2. *Genetics* **146,** 797–816 (1997).

12. Prinz, S., Amon, A. & Klein, F. Isolation of COM1, a new gene required to complete meiotic double-strand break-induced recombination in Saccharomyces cerevisiae. *Genetics* **146,** 781–795 (1997).

13. Sartori, A. A. *et al.* Human CtIP promotes DNA end resection. *Nature* **450,** 509–514 (2007).

14. Cannavo, E. & Cejka, P. Sae2 promotes dsDNA endonuclease activity within Mre11-Rad50-Xrs2 to resect DNA breaks. *Nature* **514,** 122–5 (2014).

15. Paull, T. T. & Gellert, M. The 3′ to 5′ Exonuclease Activity of Mre11 Facilitates Repair of DNA Double-Strand Breaks. *Mol. Cell* **1,** 969–979 (1998).

16. Paull, T. T. & Gellert, M. Nbs1 potentiates ATP-driven DNA unwinding and endonuclease cleavage by the Mre11/Rad50 complex. *Genes Dev.* **13,** 1276–88 (1999).

17. Anand, R., Ranjha, L., Cannavo, E. & Cejka, P. Phosphorylated CtIP Functions as a Co-factor of the MRE11-RAD50-NBS1 Endonuclease in DNA End Resection. *Mol. Cell* **64,** 940–950 (2016).

18. Garcia, V., Phelps, S. E. L., Gray, S. & Neale, M. J. Bidirectional resection of DNA double-strand breaks by Mre11 and Exo1. *Nature* **479,** 241–244 (2011).

19. Paudyal, S. C., Li, S., Yan, H., Hunter, T. & You, Z. Dna2 initiates resection at clean DNA double-strand breaks. *Nucleic Acids Res.* **45,** 11766–11781 (2017).

20. Mimitou, E. P. & Symington, L. S. Sae2, Exo1 and Sgs1 collaborate in DNA double-strand break processing. *Nature* **455,** 770–774 (2008).

21. Zhu, Z., Chung, W.-H., Shim, E. Y., Lee, S. E. & Ira, G. Sgs1 Helicase and Two Nucleases Dna2 and Exo1 Resect DNA Double-Strand Break Ends. *Cell* **134,** 981–994 (2008).

22. Nicolette, M. L. *et al.* Mre11-Rad50-Xrs2 and Sae2 promote 5' strand resection of DNA double-strand breaks. *Nat. Struct. Mol. Biol.* **17,** 1478–85 (2010).

23. Niu, H. *et al.* Mechanism of the ATP-dependent DNA end-resection machinery from Saccharomyces cerevisiae. *Nature* **467,** 108–111 (2010).

24. Lam, I. & Keeney, S. Mechanism and regulation of meiotic recombination initiation. *Cold Spring Harb. Perspect. Biol.* **7,** a016634 (2014).

25. Arora, S. *et al.* Genetic Separation of Sae2 Nuclease Activity from Mre11 Nuclease Functions in Budding Yeast. *Mol. Cell. Biol.* **37,** (2017).

26. Ma, L., Milman, N., Nambiar, M. & Smith, G. R. Two separable functions of Ctp1 in the early steps of meiotic DNA double-strand break repair. *Nucleic Acids Res.* **43,** 7349–7359 (2015).

27. Lemmens, B. B. L. G., Johnson, N. M. & Tijsterman, M. COM-1 Promotes Homologous Recombination during Caenorhabditis elegans Meiosis by Antagonizing Ku-Mediated Non-Homologous End Joining. *PLoS Genet.* **9,** e1003276 (2013).

28. Hartsuiker, E. *et al.* Ctp1CtIP and Rad32Mre11 nuclease activity are required for Rec12Spo11

removal, but Rec12Spo11 removal is dispensable for other MRN-dependent meiotic functions. *Mol. Cell. Biol.* **29,** 1671–81 (2009).

29. Hartsuiker, E., Neale, M. J. & Carr, A. M. Distinct Requirements for the Rad32Mre11 Nuclease and Ctp1CtIP in the Removal of Covalently Bound Topoisomerase I and II from DNA. *Mol. Cell* **33,** 117–123 (2009).

30. Kapusta, A. *et al.* Highly Precise and Developmentally Programmed Genome Assembly in Paramecium Requires Ligase IV–Dependent End Joining. *PLoS Genet.* **7,** e1002049 (2011).

31. Baudry, C. *et al.* PiggyMac, a domesticated piggyBac transposase involved in programmed genome rearrangements in the ciliate Paramecium tetraurelia. *Genes {&} Dev.* **23,** 2478–2483 (2009).

32. Dubois, E. *et al.* Multimerization properties of PiggyMac, a domesticated piggyBac transposase involved in programmed genome rearrangements. *Nucleic Acids Res.* **45,** 3204–3216 (2017).

33. Marmignon, A. *et al.* Ku-Mediated Coupling of DNA Cleavage and Repair during Programmed Genome Rearrangements in the Ciliate Paramecium tetraurelia. *PLoS Genet.* **10,** e1004552 (2014).

34. Arnaiz, O. *et al.* The Paramecium Germline Genome Provides a Niche for Intragenic Parasitic DNA: Evolutionary Dynamics of Internal Eliminated Sequences. *PLoS Genet.* **8,** e1002984 (2012).

35. Chi, J., Mahé, F., Loidl, J., Logsdon, J. & Dunthorn, M. Meiosis Gene Inventory of Four Ciliates Reveals the Prevalence of a Synaptonemal Complex-Independent Crossover Pathway. *Mol. Biol. Evol.* **31,** 660–672 (2014).

36. Aury, J.-M. *et al.* Global trends of whole-genome duplications revealed by the ciliate Paramecium tetraurelia. *Nature* **444,** 171–178 (2006).

37. Arnaiz, O. & Sperling, L. ParameciumDB in 2011: new tools and new data for functional and comparative genomics of the model ciliate Paramecium tetraurelia. *Nucleic Acids Res.* **39,** D632–D636 (2011).

38. Huertas, P., Cortés-Ledesma, F., Sartori, A. A., Aguilera, A. & Jackson, S. P. CDK targets Sae2 to control DNA-end resection and homologous recombination. *Nature* **455,** 689–692 (2008).

39. Huertas, P. & Jackson, S. P. Human CtIP mediates cell cycle control of DNA end resection and double strand break repair. *J. Biol. Chem.* **284,** 9558–65 (2009).

40. Wang, H. *et al.* The Interaction of CtIP and Nbs1 Connects CDK and ATM to Regulate HR–Mediated Double-Strand Break Repair. *PLoS Genet.* **9,** e1003277 (2013).

41. Arnaiz, O. *et al.* Improved methods and resources for paramecium genomics: transcription units, gene annotation and gene expression. *BMC Genomics* **18,** 483 (2017).

42. Lukaszewicz, A., Howard-Till, R. A., Novatchkova, M., Mochizuki, K. & Loidl, J. MRE11 and COM1/SAE2 are required for double-strand break repair and efficient chromosome pairing during meiosis of the protist Tetrahymena. *Chromosoma* **119,** 505–518 (2010).

43. Bétermier, M., Duharcourt, S., Seitz, H. & Meyer, E. Timing of developmentally programmed excision and circularization of Paramecium internal eliminated sequences. *Mol. Cell. Biol.* **20,** 1553–61 (2000).

44. Klotz, C. *et al.* Gamma-tubulin and MTOCs in Paramecium. *Protist* **154,** 193–209 (2003).

45. Prinz, S., Amon, A. & Klein, F. Isolation of COM1, a new gene required to complete meiotic double-strand break-induced recombination in Saccharomyces cerevisiae. *Genetics* **146,** 781–95 (1997).

46. Lisby, M., Barlow, J. H., Burgess, R. C. & Rothstein, R. Choreography of the DNA Damage Response. *Cell* **118,** 699–713 (2004).

47. Chen, L., Nievera, C. J., Lee, A. Y.-L. & Wu, X. Cell Cycle-dependent Complex Formation of BRCA1·CtIP·MRN Is Important for DNA Double-strand Break Repair. *J. Biol. Chem.* **283,** 7713–7720 (2008).

48. Eid, W. *et al.* DNA end resection by CtIP and exonuclease 1 prevents genomic instability. *EMBO Rep.* **11,** 962–8 (2010).

49. Kousholt, A. N. *et al.* CtIP-dependent DNA resection is required for DNA damage checkpoint maintenance but not initiation. *J. Cell Biol.* **197,** 869–876 (2012).

50. Forment, J. V, Jackson, S. P. & Pellegrini, L. When two is not enough: a CtIP tetramer is required for DNA repair by Homologous Recombination. *Nucleus* (2015). doi:10.1080/19491034.2015.1086050

51. Ferretti, L. P. *et al.* Cullin3-KLHL15 ubiquitin ligase mediates CtIP protein turnover to fine-tune DNA-end resection. *Nat. Commun.* **7,** (2016).

52. Stracker, T. H. & Petrini, J. H. J. The MRE11 complex: starting from the ends. *Nat. Rev. Mol. Cell Biol.* **12,** 90–103 (2011).

53. Lim, C. T., Lai, P. J., Leach, D. R. F., Maki, H. & Furukohri, A. A novel mode of nuclease

action is revealed by the bacterial Mre11/Rad50 complex. *Nucleic Acids Res.* **43,** gkv855 (2015).

54. Andres, S. N. & Williams, R. S. CtIP/Ctp1/Sae2, molecular form fit for function. *DNA Repair (Amst).* **56,** 109–117 (2017).

55. Makharashvili, N. & Paull, T. T. CtIP: A DNA damage response protein at the intersection of DNA metabolism. *DNA Repair (Amst).* **32,** 75–81 (2015).

56. Uanschou, C. *et al.* A novel plant gene essential for meiosis is related to the human CtIP and the yeast COM1/SAE2 gene. *EMBO J.* **26,** 5061–5070 (2007).

57. Penkner, A. *et al.* A conserved function for a Caenorhabditis elegans Com1/Sae2/CtIP protein homolog in meiotic recombination. *EMBO J.* **26,** 5071–5082 (2007).

58. Cannavo, E. & Cejka, P. Sae2 promotes dsDNA endonuclease activity within Mre11–Rad50–Xrs2 to resect DNA breaks. *Nature* **514,** 122–125 (2014).

59. Katoh, K. & Standley, D. M. MAFFT Multiple Sequence Alignment Software Version 7: Improvements in Performance and Usability. *Mol. Biol. Evol.* **30,** 772–780 (2013).

60. Soding, J. Protein homology detection by HMM-HMM comparison. *Bioinformatics* **21,** 951–960 (2005).

61. Guindon, S. *et al.* New Algorithms and Methods to Estimate Maximum-Likelihood Phylogenies: Assessing the Performance of PhyML 3.0. *Syst. Biol.* **59,** 307–321 (2010).

62. Huson, D. H. & Scornavacca, C. Dendroscope 3: An Interactive Tool for Rooted Phylogenetic Trees and Networks. *Syst. Biol.* **61,** 1061–1067 (2012).

63. Lupas, A., Van Dyke, M. & Stock, J. Predicting coiled coils from protein sequences. *Science (80-.).* **252,** 1162–1164 (1991).

64. Gratias, A. & Bétermier, M. Processing of double-strand breaks is involved in the precise excision of paramecium internal eliminated sequences. *Mol. Cell. Biol.* **23,** 7152–62 (2003).

65. Saudemont, B. *et al.* The fitness cost of mis-splicing is the main determinant of alternative splicing patterns. *Genome Biol.* **18,** 208 (2017).

66. Galvani, A. & Sperling, L. RNA interference by feeding in Paramecium. *Trends Genet.* **18,** 11–2 (2002).

67. Kamath, R. S., Martinez-Campos, M., Zipperlen, P., Fraser, A. G. & Ahringer, J. Effectiveness of specific RNA-mediated interference through ingested double-stranded RNA in Caenorhabditis elegans. *Genome Biol.* **2,** research0002.1 (2000).

68. Garnier, O., Serrano, V., Duharcourt, S. & Meyer, E. RNA-Mediated Programming of Developmental Genome Rearrangements in Paramecium tetraurelia. *Mol. Cell. Biol.* **24,** 7370–7379 (2004).

69. Gogendeau, D. *et al.* Functional diversification of centrins and cell morphological complexity. *J. Cell Sci.* **121,** 65–74 (2008).

70. Cejka, P. & Kowalczykowski, S. C. The Full-length Saccharomyces cerevisiae Sgs1 Protein Is a Vigorous DNA Helicase That Preferentially Unwinds Holliday Junctions. *J. Biol. Chem.* **285,** 8290–8301 (2010).

71. Zheng, L. *et al.* MRE11 complex links RECQ5 helicase to sites of DNA damage. *Nucleic Acids Res.* **37,** 2645–2657 (2009).

Supporting information

- **Fig S1. PtCtIPa and PtCtIPb protein sequence analysis.**
- **Fig S2. Analysis of PtCtIP, PtMRE11 and PtSPO11 expression and PtCtIP RNAi efficiency during autogamy.**
- **Fig S3. MAC development is restored in cells silenced for both PtMRE11b and PtSPO11**.
- **Fig S4. Recombinant PtCtIPa is devoid of intrinsic nuclease activity.**
- **Fig S5. Characterization of U2OS clones stably expressing CtIP-wt and -AHA.**

Supplementary Figures

Table S1. Oligonucleotides used in this study

Name	Sequence (5' to 3')	Use
Spo11-02-SpeI	ggactagtATGAACTTACCATTATTGCATGAAGAATG	PtSPO11-1 feeding insert and gene-specific probe on Northern blot
Spo11-08-SpeI	ggactagtGCATTTCATTTATCAAGTGAAAATACACAG	
PtCtIPa-SpeI-F	ggactagtCTTCTTGATAATCAACCAAAATCAACCAAG	PtCtIPa feeding insert and gene-specific probe A1 on Northern blot
PtCtIPa-SpeI-R	ggactagtCATTCTGGAGTTAATAGTAATTTTTCTTG	
PtCtIPa-1USpeI	ggactagtATGTTTTTCTCACCTTAATTTTAAGAATTT	Gene-specific probe A2 on Northern blot (does not hybridize with feeding insert)
PtCtIPa probe 3’	AAGTACTTCACTTATTGTTGTctatttatttt attc	
PtCtIPb-SpeI-F	ggactagtCTTATCGATAATCAACCAAAATCAGCTAAA	PtCtIPb feeding insert and gene-specific probe B1 on Northern blot
PtCtIPb-SpeI-R	ggactagtCATTCTGGAGTTAATAATAATTTTTCTTG	
PtCtIPb-1USpeI	ggactagtATGTTTTTCGCTCCTCAATTTCAAGAGTTC	Gene-specific probe B2 on Northern blot (does not hybridize with feeding insert)
PtCtIPb probe 3’	AAGTAAATCATTAAGTTTTTACTATTTATTTTATTC	
PtMRE11a1-SpeI-F	ggactagtCTATCGACTAAGTTGTATCAATA	PtMRE11a1 feeding insert and gene-specific probe (IF2 fragment) on Northern blot
PtMRE11a1-SpeI-R	ggactagtATTCTTAGGCAAAGAGTCATC	
PtMRE11b1-SpeI-F	ggactagtCTATCACAAAAGTTGTTTCAG	PtMRE11b1 feeding insert and gene-specific probe (IF2 fragment) on Northern blot
PtMRE11b1-SpeI-R	ggactagtCTAGCCATATCTAGGAAAA	
PtMRE11a2-SpeI-F	ggactagtCATCAAAGTATTTGACTTTCACAAT	PtMRE11a2 feeding insert (crossreacting with PtMRE11b)
PtMRE11a2-SpeI-R	ggactagtGGTTTTATACAAACATTTGATTAATCAG	
PtMRE11b2-SpeI-F	ggactagtCATTAAAGTATTTGACTTTCAAAT	PtMRE11b2 feeding insert (crossreacting with PtMRE11a)
PtMRE11b2-SpeI-R	ggactagtGGTTTAATAGAAACAAAGGATTAATC	
17Sext_NcoI	ACCCGTGACTGCCATGGTAGTCCAATACA	17S oligo probe on Northern blot

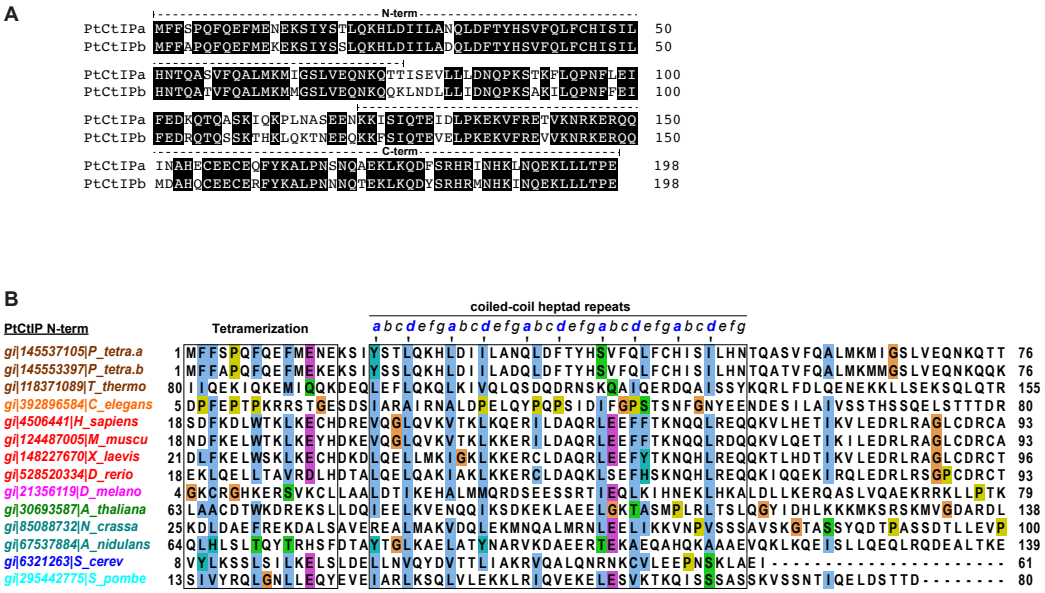

S1 Fig. PtCtIPa and PtCtIPb protein sequence analysis.
(A) Amino acid (aa) sequence alignment of full-length *Paramecium tetraurelia* (Pt) CtIPa and CtIPb. N-terminal and C-terminal regions (76 aa residues each) are indicated by dashed lines.
(B) Sequence alignment of the N-terminal region of PtCtIPa and PtCtIPb with 12 CtIP proteins from different species. Gene accession numbers (gi) and species names are color-coded according to the phylogenetic tree shown in Figure 1B. Insertions and extensions were trimmed and marked by dashed lines with the number of residues indicated below. Conserved structural elements implicated in CtIP tetramerization and dimerization (positions 'a' and 'd' of the coiled-coil 'a-g' heptad repeat are highlighted in blue) are indicated in black boxes.

Figure S2

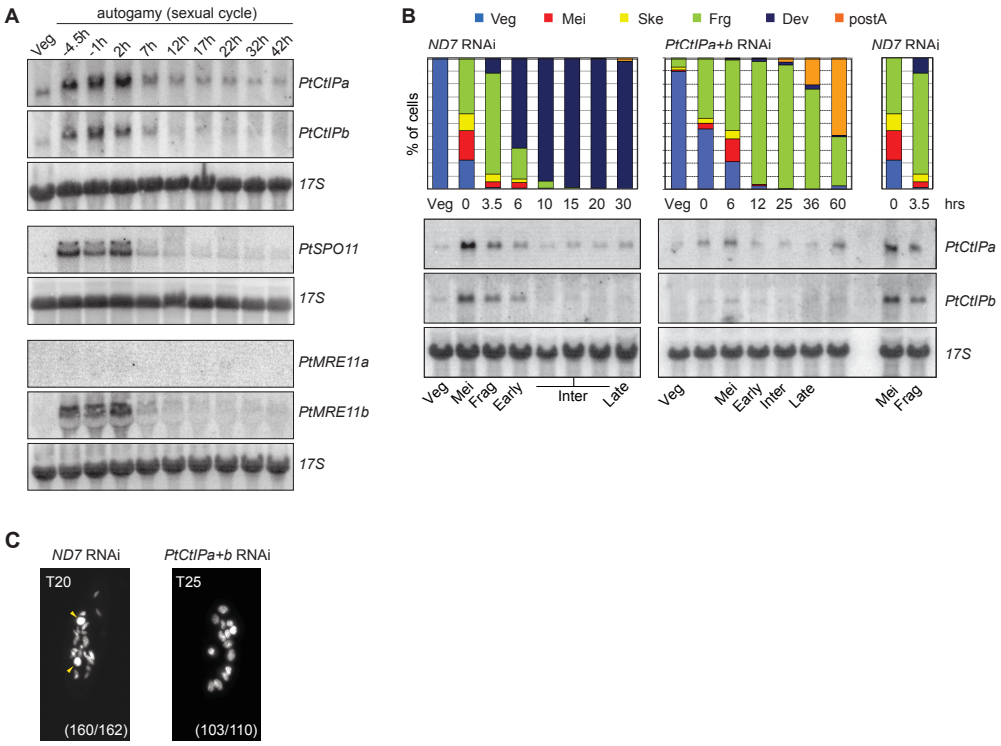

Figure S2: Analysis of *PtCtIP*, *PtMRE11* and *PtSPO11* expression and *PtCtIP* RNAi efficiency during autogamy.
(A) Northern blot analysis of *PtCtIP*, *PtSPO11* and *PtMRE11* mRNAs during autogamy. 17S rRNA is used as loading control for each sample. Veg: vegetative cells. Samples were taken at the indicated time-points with respect to a reference time 0, when 50% of the cells display a fragmented old MAC. *PtCtIP* probes were A1 and B1 for *PtCtIPa* and *PtCtIPb*, respectively (Supplementary Table S1).
(B) Northern blot analysis of *PtCtIPa* and *PtCtIPb* mRNA in RNAi experiments. *P. tetraurelia* 51 cells were submitted to control (ND7) RNAi or to RNAi against both *PtCtIPa* and *PtCtIPb*. Upper panel, the histograms show the progression of autogamy, monitored by microscopic imaging of DAPI-stained nuclei, with the different cellular stages indicated on top. Veg: vegetative cells; Mei: meiotic cells; Ske: cells with MAC skeins; Frg: cells with old MAC fragments but no visible new developing MACs; Dev: cells with two developing MACs; postA: post-autogamous cells with one new MAC and remaining old MAC fragments. Lower panel, Northern blots of total RNAs extracted at indicated time-points for each RNAi condition were hybridized with *PtCtIPa*- or *PtCtIPb*-specific labeled probes A2 and B2, respectively (Supplementary Table S1). Relevant autogamy stages are indicated at the bottom: for ND7 RNAi, the T15 time-point was selected for further quantification of PtCtIP mRNA at the “inter” stage (Figure 2C). Viable post-autogamous progeny yields in this experiment: 97%, control RNAi; 23%, *PtCtIPa+b* RNAi.
(C) Representative images of DAPI-stained nuclei of cells at T20 (control ND7 RNAi) and T25 (*PtCtIPa+b* RNAi) during autogamy progression as described in (B). Yellow arrowheads in control-depleted cells indicate developing new MACs. Numbers in parentheses indicate the number of cells at the corresponding stage shown in the picture relative to the total number of cells that were observed on the microscope slide.

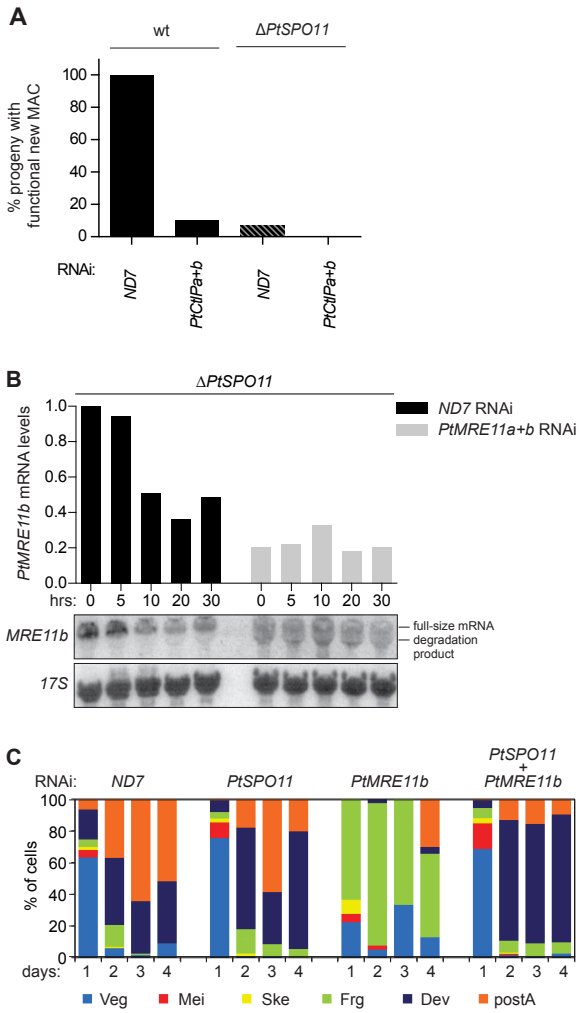

S3 Fig. MAC development is restored in cells silenced for both *PtMRE11b* and *PtSPO11*.
(A) Analysis of the progeny of wild-type and *ΔSPO11*$_{MAC}$ cells submitted to RNAi against *PtCtlPa+b*. Each histogram shows the percentage of progeny with a functional new MAC obtained for each condition (same experiment as in Figure 3B).
(B) Quantification of *PtMRE11b* mRNA levels in cells submitted to control ND7 or *PtMRE11a+b* RNAi (here a *ΔSPO11* clone was used). For simultaneous silencing of both *PtMRE11* genes, a combination of gene-specific a1 and b1 constructs was used (see Supplementary Table S1). The *PtMRE11b*-specific IF2 fragment was used as a probe for northern blot hybridizations. 17S rRNA signal was used for normalization. Y-axes are in arbitrary units.
(C) Progression of MAC development upon single and combined *PtMRE11* and *PtSPO11* gene silencing. For simultaneous silencing of both *PtMRE11* genes, the cross-reacting b2 construct was used (see Supplementary Table S1). Monitoring of MAC development was performed following DAPI staining. Veg: Vegetative cells; Mei: mic meiotic stages; Ske: MAC skeins; Frg: fragmented old MAC with no visible new MACs; Dev: cells with two developing new MACs; postA: post-autogamous cells with one new MAC and fragments of the old MAC. Viable post-autogamous progeny yields in this experiment: 93%, control RNAi; 3%, *PtSPO11* RNAi, 37%, *PtMRE11* RNAi, 37%; 0%, *PtSPO11+PtMRE11* RNAi.

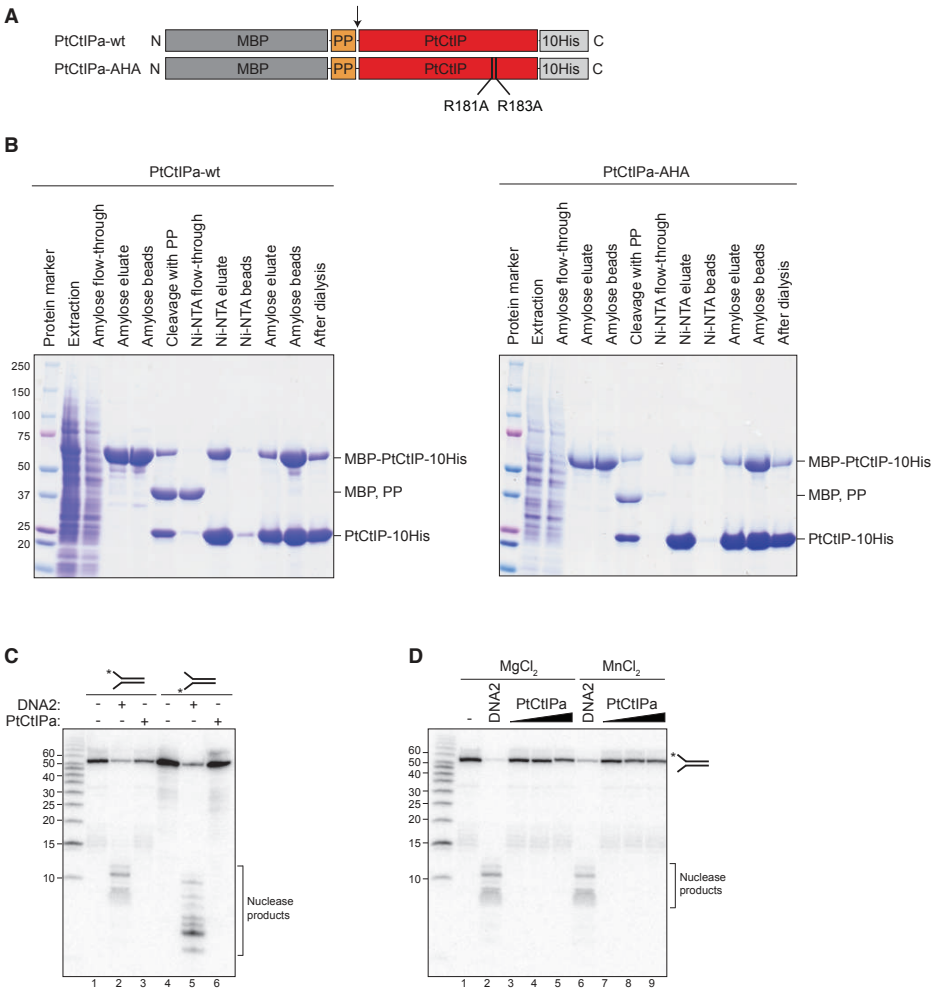

S4 Fig. Recombinant PtCtIPa is devoid of intrinsic nuclease activity.
(A) Schematic of the PtCtIPa-wt and PtCtIP-AHA mutant expression constructs. 'MBP' denotes maltose-binding protein. Arrow indicates the PreScission Protease (PP) cleavage site.
(B) Recombinant PtCtIPa-wt (left panel) and PtCtIPa-AHA mutant (right panel) were expressed and purified from Sf9 insect cells. Fractions of the subsequent purification steps were analyzed by SDS-PAGE and stained with Coomassie Brilliant Blue. The molecular weight (kDa) of the size markers are indicated on the left panel.
(C) Purified recombinant PtCtIPa (1 μM) or human DNA2 (10 nM) were incubated with 10 nM of 5'- or 3' end-labeled forked DNA substrates in presence of 5 mM $MgCl_2$ for 60 min at 37°C.
(D) PtCtIPa (400 nM, 700 nM and 1 μM) or human DNA2 (10 nM) DNA were incubated with 10 nM of 5' end-labeled forked DNA substrates in presence of 5 mM $MgCl_2$ or 1 mM $MnCl_2$ for 60 min at 37°C.
(C and D) DNA substrate and cleavage products were resolved on a 20% denaturing polyacrylamide gel containing 7 M urea. ^{32}P-labeled DNA strands are indicated with asterisks.

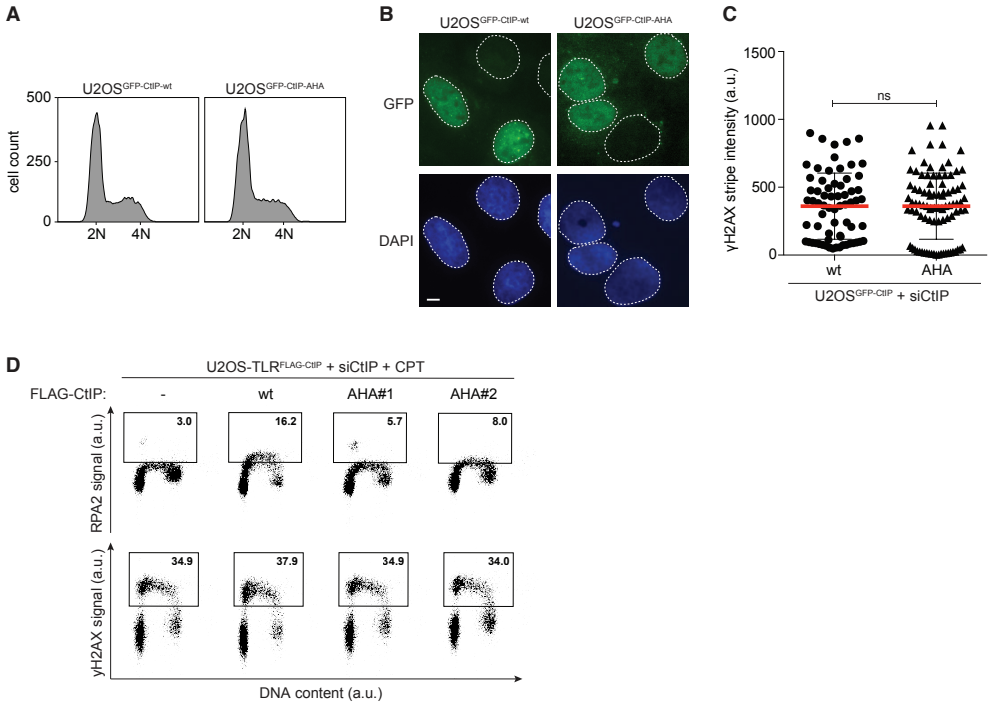

S5 Fig. Characterization of U2OS clones stably expressing CtIP-wt and -AHA.
(A) U2OS clones harbouring inducible wt and AHA mutant GFP-CtIP were transfected with CtIP siRNA for 48 h. GFP-CtIP expression was induced by Dox for the last 24 h and cells were analysed by FACS.
(B) The same cells as described in (A) were analysed by immunofluorescence microscopy. Scale bar, 10 μm.
(C) The same cells as described in (A) were transfected with siCtIP. 24 h later, cells were grown on coverslips in the presence of doxycycline (Dox) and BrdU for 24 h prior to laser micro-irradiation. 20 min post-irradiation, cells were fixed, immunostained for γH2AX and counterstained with DAPI for DNA and analysed by fluorescence microscopy (see Figure 7A). Scatter plot shows the fluorescence intensity (a.u., arbitrary units) of γH2AX in the micro-irradiated area. Data are presented as the mean (indicated by red bars) ± SD. Statistical difference was determined by Mann-Whitney test; ns, non-significant. For each condition more than 20 cells from two independent experiments were measured.
(D) U2OS-TLR clones stably expressing siRNA resistant FLAG-CtIP-wt or -AHA (two different clones) were transfected with siCtIP. 48 h later cells were treated with CPT (1 μM) for 1 h and harvested for FACS analysis. Dot plots show fluorescent intensities (a.u., arbitrary units) of RPA2 signals or γH2AX respectively (y-axis) against the DNA content (x-axis). Quantification gates were established in untreated samples and the percentages of cells within the gates are indicated.

4.1.2 *Paramecium* CtIP stimulates MRE11 nuclease activity

As summarized in the manuscript, we could show that PtCtIP binds preferentially to 5' flap DNA substrates via its RHR motif but lacks intrinsic nuclease activity. It has been reported that Sae2 and human CtIP associates with and stimulates MRE11's endonuclease activity[37,40,41,57,136]. To investigate whether the same applies to PtCtIP, we performed pulldown experiments with MBP-tagged PtCtIPa and recombinant human MRE11-RAD50 (MR) complex. As shown in the manuscript, both wild-type (wt) and the AHA DNA-binding mutant of PtCtIPa were proficient in binding to MR, confirming an evolutionarily conserved mode of interaction between the two factors (Figure 4.1A).

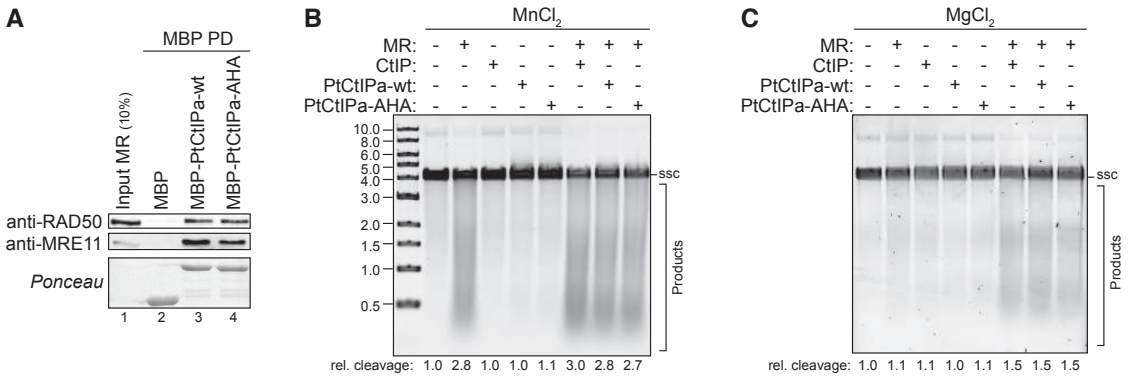

Figure 4.1: PtCtIP binds to and stimulates human MR endonuclease activity. (**A**) MBP or MBP-tagged PtCtIPa was coupled to amylose beads and incubated with purified recombinant human Mre11-Rad50 (MR) complex. Mre11 and Rad50 proteins in input and pulldown fractions were detected by immunoblotting using the indicated antibodies. MBP and MBP-CtIP proteins were detected by Ponceau staining. (**B**) PhiX174 substrate was incubated with human MR (50 nM), human CtIP (200 nM) or PtCtIPa (wt and AHA, 200 nM) in presence of 5 mM $MnCl_2$ for 2 h at 37C. DNA was separated on an agarose gel and stained with SYBR Gold. Size markers (in kb) are shown on the left site. ssc = single-stranded circular DNA. Relative DNA cleavage (normalized to buffer alone) is indicated below the gel. (**C**) PhiX174 cleavage assay as described in (B) but in presence of 5 mM $MgCl_2$.

Using closed-circular single-stranded PhiX174 virion DNA as a substrate, human CtIP was found to stimulate MR-dependent endonuclease activity in the presence of magnesium but not manganese[37]. Remarkably, under the exact same assay conditions, we observed that PtCtIPa is able to specifically enhance MR-mediated cleavage (Figures 4.1B and 4.1C). Interestingly, PtCtIP-AHA promoted MR activity to the same extent as PtCtIPa-wt, suggesting that DNA-binding function of PtCtIP is dispensable for stimu-

lating MR endonuclease activity. Taken together, our combined genetic and biochemical analysis of PtCtIP support its role in DSB repair.

4.2 Deciphering the potential regulation of SLX4 by PIN1-mediated isomerization

4.2.1 Validation of the PIN1-SLX4 interaction

Regulation of the DDR by phosphorylation-dependent signalling is essential to maintain genome integrity and prevent tumorigenesis[271]. Our lab has recently published a study about the contribution of PIN1-mediated isomerization of CtIP in the regulation of DSB repair[135,254]. We demonstrated that upon CDK-mediated phosphorylation of CtIP at S276 and T315, PIN1 catalyses a conformational change in CtIP, thereby controlling its DNA-end resection function in DSB repair[135]. However, besides CtIP, our proteomic analysis revealed other DDR proteins as putative PIN1 substrates, including the multidomain scaffold protein SLX4. Importantly, using GST pulldown and co-immunoprecipitation assays we could corroborate the interaction between PIN1 and SLX4 (Figure 4.2A and 4.2B). Moreover, we observed that PIN1 binding to SLX4 is abrogated in a WW domain mutant of PIN1 (W34A), indicating that the interaction is most likely mediated through specific S/T-P phosphorylation sites within SLX4 (Figure 4.2A and 4.2B)[272]. Similarly, treating cell lysates with lambda phosphatase (PPase) abolished the interaction between PIN1 and SLX4, further substantiating the assumption that the interaction is phosphorylation-dependent (Figure 4.2C). Additionally, co-immunoprecipitation experiments from HeLa nuclear extracts using anti-PIN1 antibody confirmed a robust interaction between endogenous PIN1 and SLX4 (Figure 4.2D).

4.2.2 Identification of the PIN1-interaction motif in SLX4

PIN1 binding occurs within the central part of SLX4

PIN1-mediated conformational changes regulate the activities of numerous proteins, thereby affecting diverse cellular processes, including cell cycle progression, cell growth and various stress responses[213]. Therefore, in order to determine the significance of PIN1-mediated isomerization for any given PIN1 target, it is critically important to define sub-

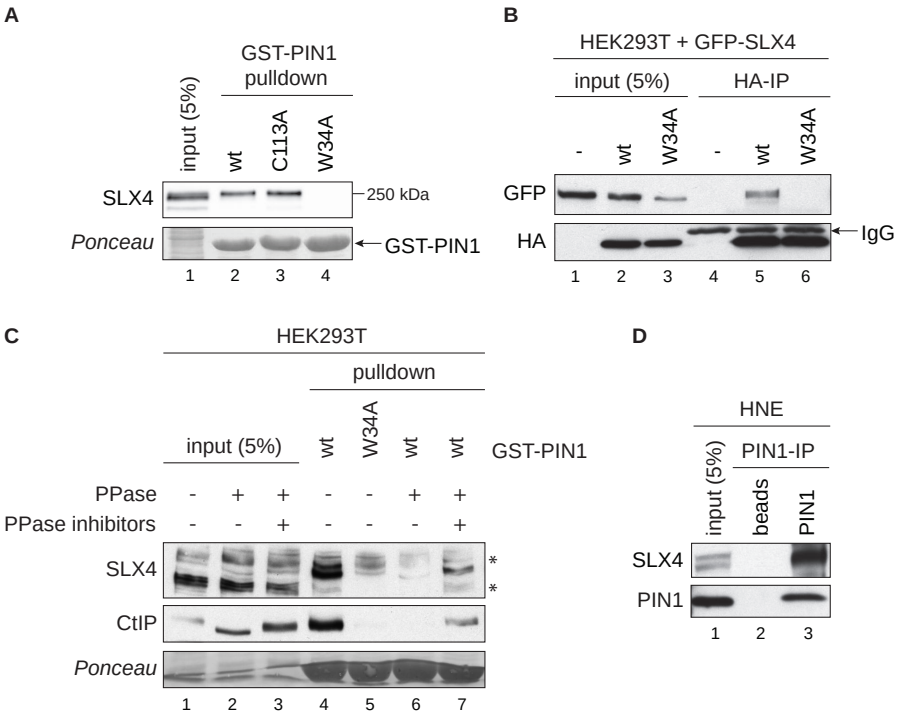

Figure 4.2: SLX4 interacts with PIN1 isomerase. (**A**) Extracts from untreated HEK293T cells (1 mg) were subjected to GST pulldown experiments using recombinant PIN1 wild type (wt), the catalytic dead mutant (C113A) or the phosphobinding-deficient mutant (W34A) as baits. Isolated proteins were separated by SDS-PAGE and analyzed by immunoblotting. Equal amounts of recombinant GST-PIN1 were confirmed by Ponceau staining. (**B**) HEK293T cells were co-transfected with plasmids encoding GFP-tagged SLX4 and HA-tagged PIN1. Cell extracts (1 mg) were subjected to immunoprecipitation (IP) using HA-antibodies. Precipitated immunocomplexes were separated by SDS-PAGE and analyzed by immunoblotting. (**C**) HEK293T lysates were pre-treated with lambda-phosphatase (PPase) or solvent control and subjected to GST pulldown assays. PPase activity was inhibited by the addition of 50 mM NaF and EDTA. Asterisks indicate unspecific bands. (**D**) Immunoprecipitation was performed with 1 mg of HeLa nuclear extracts (HNE) using either protein A beads alone or beads coupled with anti-PIN1 antibodies. Immunocomplexes were analyzed by Western blotting. Blots (B-D) were kindly provided by Dr. Lorenzo Lafranchi, a former colleague in the lab.

strate-specific PIN1 binding site(s). According to publicly available high-throughput mass spectrometry data, human SLX4 (1834 aa) is phosphorylated at 30 out of 41 minimal CDK consensus sites (S/T-P) scattered throughout the entire protein (source: http://www.phosphosite.org). Thus, to narrow down the region in SLX4 critical for PIN1 binding, we first screened different FLAG-tagged SLX4 truncation mutants for their ability to interact with PIN1 (provided by Dr. Agata Smogorzewska, Rockefeller University, US)[273]. GST-PIN1 pulldown experiments revealed that the first 800 amino acids in SLX4 are dispensable for PIN1 binding (Figure 4.3A).

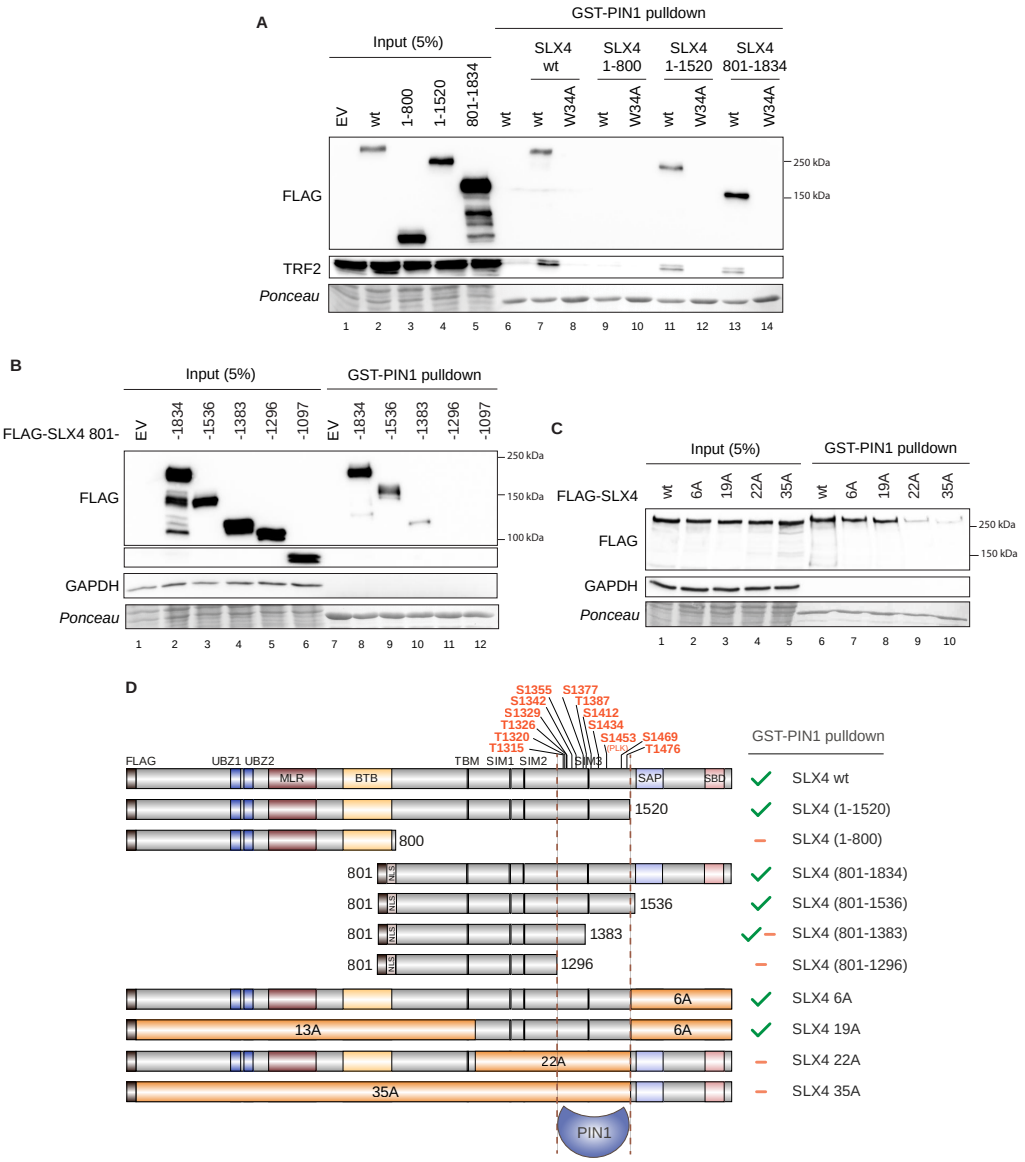

Figure 4.3: PIN1-SLX4 interaction motif lies within the low complexity region of SLX4. (**A**) HEK293T cells were transfected with FLAG-tagged SLX4 constructs covering different stretches of the protein sequence. Cell extracts were subjected to GST-PIN1 pulldown assays using either PIN1 wt or W34A mutant and bound proteins were analyzed by immunoblotting. (**B**) Truncated protein variants derived from the FLAG-SLX4 801-1834 construct were tested in a GST-PIN1 wt pulldown applying the same experimental procedure as in (A). (**C**) The binding ability of SLX4 S/T-P cluster mutants to GST-PIN1 wt was analyzed by GST-PIN1 pulldown. Same experimental approach as in (A). (**D**) Summary of the results of GST-PIN1 pulldown experiments shown in A-C.

To further map the interacting region, we generated several C-terminal deletion mutants by introducing Stop-codons into FLAG-SLX4_801-1834. We found that SLX4_801-1296 failed to interact with PIN1, whereas longer fragments were proficient in PIN1 binding, albeit with quite variable efficiency (Figure 4.3B). To more specifically focus on SLX4 phosphorylation sites, we applied SLX4 S/T-P cluster mutants in which multiple serines or threonines adjacent to proline residues were mutated to alanines (6A, 19A, 22A and 35A; provided by Dr. Joao Matos, ETH Zurich)[192]. In large agreement with our previous mapping analysis, we found that PIN1 is proficient in binding to the 6A and 19A mutant but severely impaired in binding to the SLX4-22A and -35A mutant (Figure 4.3C and 4.3D). Collectively, these findings indicate that PIN1-SLX4 interaction is mediated by one or multiple phosphorylated S/T-P sites located within a 200 aa long stretch between residues 1300-1500 (Figure 4.3D).

Analysis of single S/T-P motifs within SLX4 potentially required for PIN1 binding

The region in SLX4 responsible for mediating PIN1 interaction is overall poorly conserved and contains 13 potential S/T-P phosphorylation sites (Figure 4.3D). Therefore, we next took an unbiased approach and generated YFP-tagged full-length SLX4 expression constructs harboring individual single S/T to A substitution mutations. Unfortunately, using GST-PIN1 pulldown assays, we found that none of the mutants exhibited reduced PIN1 binding, indicating that PIN1 most likely binds to several S/T-P motifs in this region (Figures 4.4A-C). Of note, we observed reduced amounts of PLK1, a known SLX4 interactor (Figure 1.6), when the pulldown was performed with SLX4-S1452A/S1453A, encompassing the mutated 'SSP' polo-box domain binding motif (Figure 4.4C, lane 9)[46]. This finding suggests that PIN1 binds to the SLX4-PLK1 complex but, at the same time, that PLK1-dependent SLX4 phosphorylation is dispensable for PIN1-SLX4 interaction.

T1315 and T1320 are sufficient for binding of PIN1 to SLX4

It has been proposed that substrate binding of PIN1 occurs via the WW domain and isomerization is mediated by the PPIase domain[217,274]. If these steps happen in a sequential manner or simultaneously is still unclear[214]. However, it is likely that multiple S/T-P sites

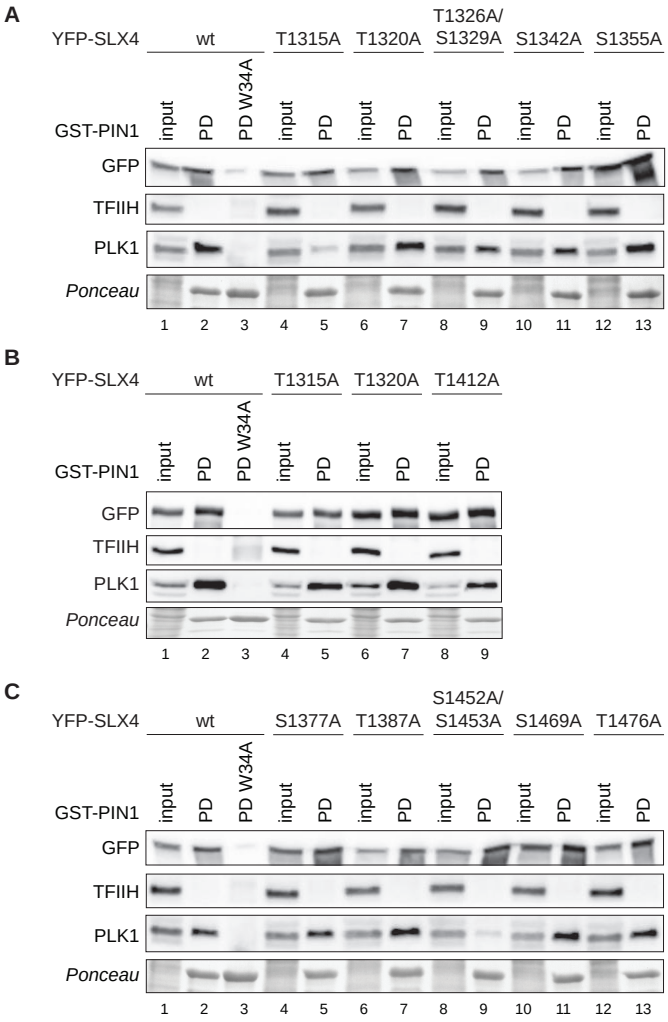

Figure 4.4: PIN1-SLX4 interaction does not depend on a single phosphorylated S/T-P motif. (**A-C**) Whole cell lysates of HEK293T cells transfected with the indicated YFP-tagged SLX4 single S/T to A mutant constructs were subjected to GST-PIN1 pulldown (PD) experiments. Bound proteins were separated by SDS-PAGE and analyzed by immunoblotting.

are required for efficient PIN1-mediated isomerization[214,272]. For instance, CtIP phosphorylation at two neighboring sites are responsible for PIN1 binding[135]. Therefore, we assessed whether combined mutation of closely spaced S/T-P sites in SLX4 abrogate PIN1 interaction. Unfortunately, none of the tested double and triple S/T-P motif mutants displayed reduced PIN1 binding (Figure 4.5A and 4.5B).

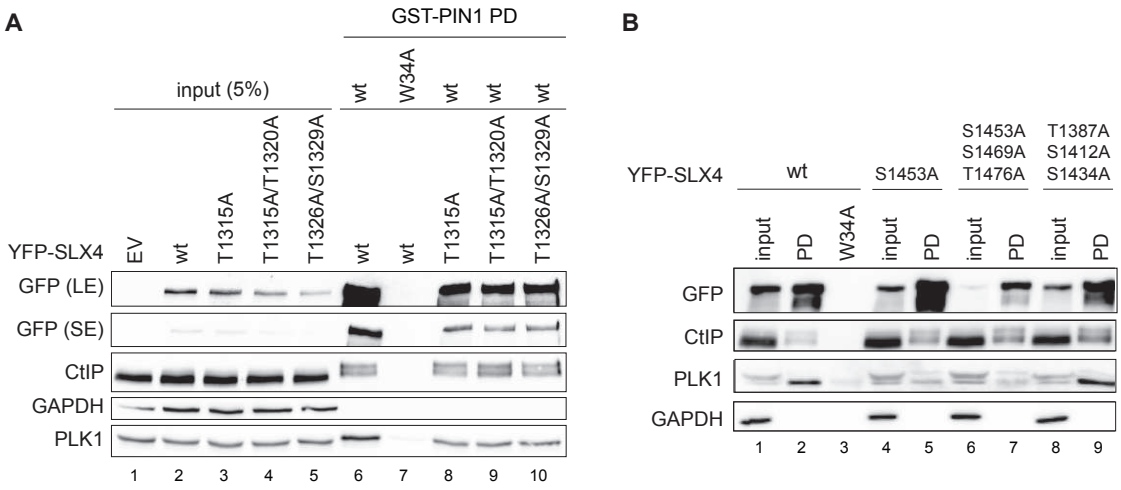

Figure 4.5: Double and triple S/T-P mutations do not abolish PIN1-SLX4 interaction. (**A**) and (**B**) HEK293T cells were transfected with indicated YFP-tagged SLX4 constructs harboring either single or combined mutations. Cell extracts were subjected to GST-PIN1 pulldown (PD) assays and bound proteins analyzed by Western blot.

Intriguingly, high-throughput proteomics analysis revealed that T1315 and S1329 are by far the most predominant phosphorylation sites in human SLX4, repeatedly scoring in independent mass spectrometry screens (Figure 4.6).

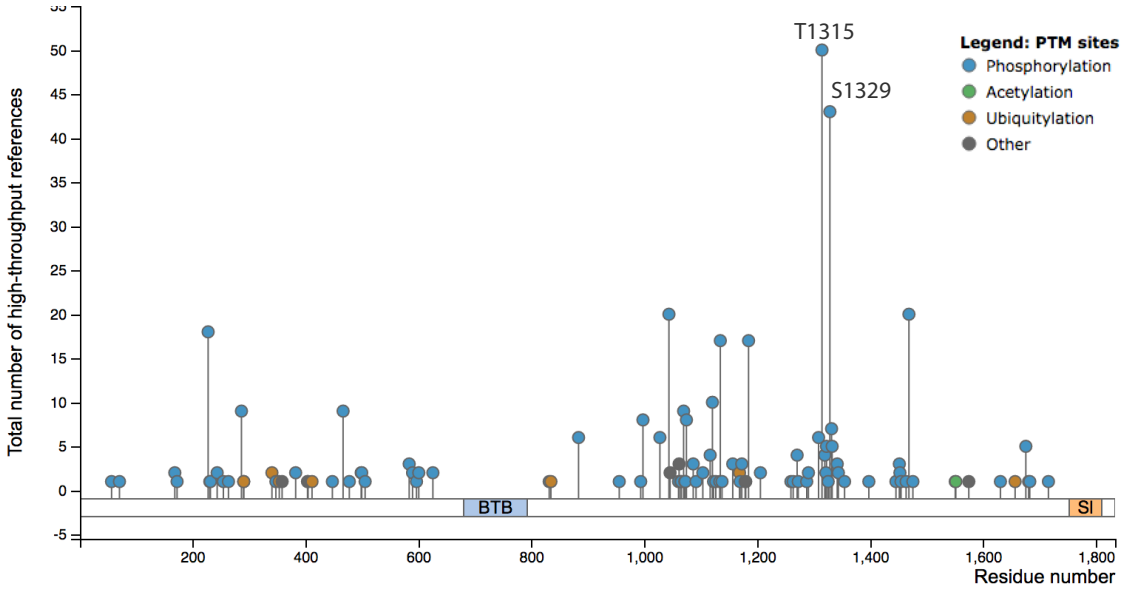

Figure 4.6: Schematic SLX4 protein with illustrated scorings of PTM from mass spectrometry screens. Number of records in which the indicated PTMs were determined using proteomic discovery mass spectrometry. Adapted from phosphosite.org.

We further noticed that most of the SLX4 phosphorylation sites potentially implicated in PIN1 interaction (including T1315 and S1329) are not conserved in mouse or frog SLX4 but appear rather primate-specific (Figure 4.7).

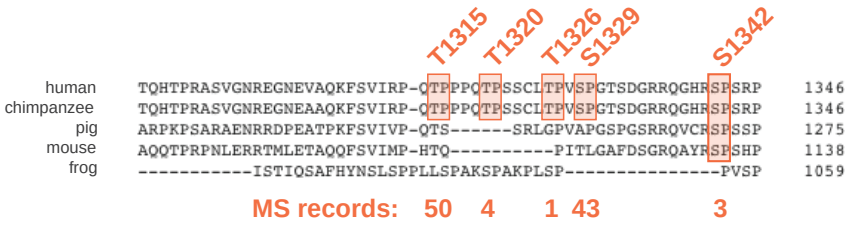

Figure 4.7: Alignment of SLX4 orthologs arising from BLAST searches with human SLX4 1288-1346. Red boxes indicate S/T-P motifs. Numbers indicate records in which the corresponding site was assigned by phosphoproteomics to be phosphorylated.

At first glance, this is somewhat surprising. However, a similar scenario has been reported for the TRF2 binding motif in SLX4, which is conserved in primates but not in other mammalian species including mouse[197]. As we were unable to identify SLX4 S/T-P mutants abrogating PIN1 interaction, we changed our approach and reconstituted functional S/T-P motifs at T1315 and T1320 into the SLX4-22A cluster mutant defective in PIN1 binding (see Figure 4.3C). Strikingly, incorporating functional S/T-P motifs at T1315 and at T1315/T1320 in SLX4-22A, resulting in SLX4-21A and 20A, respectively, restored SLX4 binding to PIN1 (Figure 4.8), indicating that these two phosphorylation sites are sufficient for PIN1 interaction.

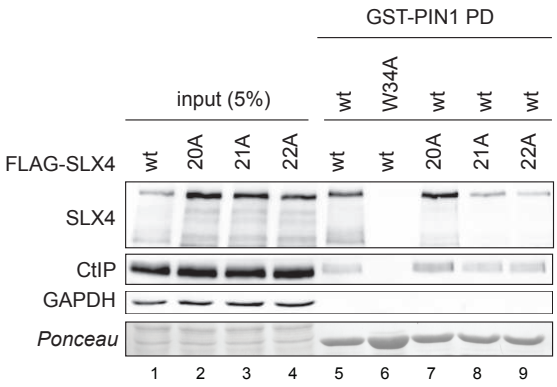

Figure 4.8: S/T-P motifs T1315 and T1320 are sufficient for PIN1 interaction. Reconstituting wild-type T1315 (21A) or T1315/T1320 (20A) into the compound SLX4-22A mutant restored PIN1 binding in GST-pulldown assays.

PIN1-SLX4 interaction is direct and dependent on phosphorylation

Next, we aimed to investigate whether PIN1-SLX4 interaction is indeed direct or potentially mediated through an unknown accessory protein. To this end, immunoprecipitated FLAG-SLX4 was subjected to far-western blotting using recombinant GST-PIN1. Interestingly, PIN1 was efficiently binding to SLX4-wt but not to SLX4-22A, indicative of a direct physical link between SLX4 and PIN1 mediated by S/T-P phosphorylation motifs (Figure 4.9A). Prompted by this promising result, we tested the binding ability of GST-PIN1 to FLAG-SLX4 harboring the minimal PIN1-interaction region (aa 801-1383, see Figure 4.3B) using far-western blotting. In line with our pulldown experiments, PIN1 associated with SLX4 801-1383 but not with SLX4 801-1296, (Figure 4.9B). Importantly, the binding was abrogated following treatment of SLX4 with lambda phosphatase but rescued in presence of phosphatase inhibitors (Figure 4.9B), further substantiating that phosphorylation of multiple S/T-P motifs located within residues 1296-1383 (including T1315, T1320, T1326, S1329 and S1342, see Figure 4.3D) is critical for SLX4-PIN1 interaction.

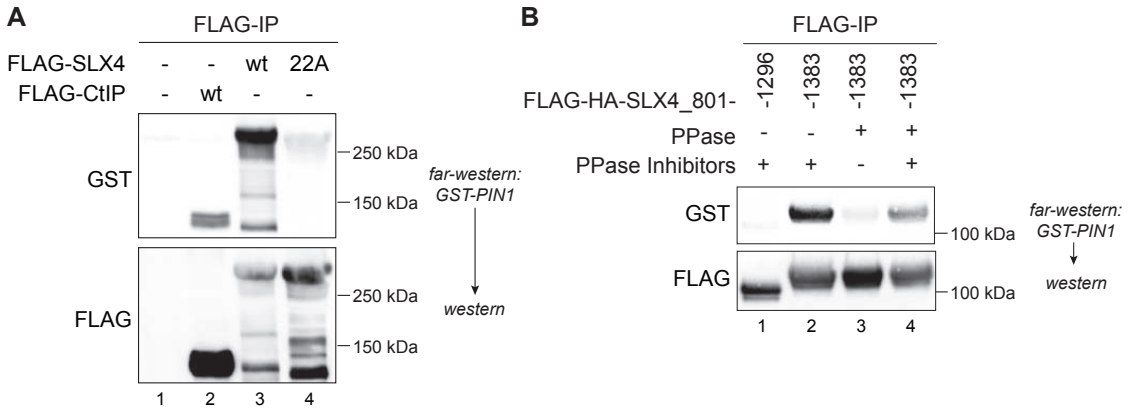

Figure 4.9: PIN1-SLX4 interaction is direct and phosphorylation-dependent. (**A**) Anti-FLAG immunoprecipitates from HEK293T cells transfected with FLAG-tagged CtIP and SLX4 variants were subjected to far-western analysis using purified GST-PIN1 as a probe followed by anti-GST immunoblotting. After stripping, the same membrane was reprobed using anti-FLAG antibody. 22A is the SLX4 phosphorylation cluster mutant (kind gift of Dr. Joao Matos, ETH Zurich). (**B**) Same experimental procedure as in (A) after transfection of FLAG-tagged SLX4 truncation mutants. SLX4 truncation constructs bound to FLAG-beads were either incubated in the presence of phosphatase-inhibitors or treated with lambda-phosphatase before eluted and subjected to far-western analysis.

In conclusion, our results suggest that SLX4 and PIN1 physically interact in a phosphorylation-dependent-manner and that SLX4-T1315 is a critical residue supporting PIN1 binding.

4.2.3 Establishing a phospho-SLX4 (T1315) antibody

The S/T-P site comprising T1315A is the phosphorylation site scoring highest in independent mass spectrometry screens (Figure 4.6). In order to test whether T1315 is indeed phosphorylated *in vivo* we ordered customized phospho-specific antibodies. To this end, Creative Biolabs immunized rabbits with a phospho-epitope (CSVIRPQ(p-T)PPPQT-NH2) and we subsequently tested the specificity of the obtained antibodies using whole cell extracts or YFP-SLX4 enriched protein fractions. The antibody raised against pT1315 specifically recognized YFP-SLX4-wt but not the SLX4-2A protein, harboring the T1315A/T1320A mutation, indicating that T1315 is most likely phosphorylated *in vivo* (Figure 4.10).

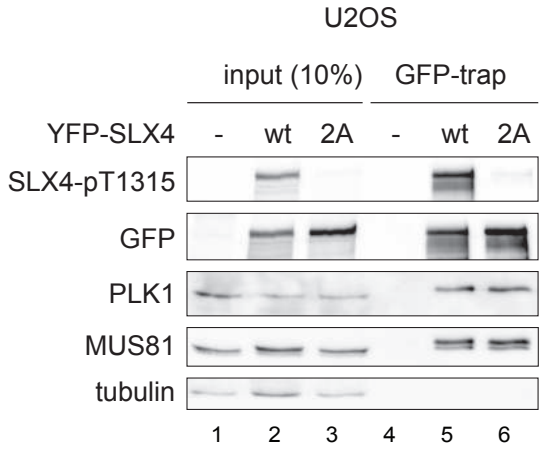

Figure 4.10: Phospho-specific antibody recognizes SLX4 when phosphorylated at T1315A. Extracts (1 mg) from HEK293T cells transfected with YFP-tagged SLX4 -wt or -T1315A/T1320A (2A) for 48 h were subjected to a GFP-trap with subsequent immunoblotting.

4.2.4 Investigating the potential role of PIN1 in regulating SLX4 function

PIN1 is not regulating known SLX4 protein-protein interactions

PIN1 provides a molecular timer to regulate the function of many phosphoproteins by altering protein-protein interactions[275]. SLX4 is known to be a scaffold protein for various nucleases engaged in multiple protein-protein interactions with some of them being regulated by phosphorylation[185,276]. For instance, the assembly of SLX4 with MUS81-EME1 occurs at the entry of M phase mediated by CDK phosphorylation of EME1[47]. Furthermore, phosphorylation of SLX4 at S/T-P sites within its SAP motif (residues 1540-1623) are important for MUS81 binding during mitosis[192,277]. The interaction with the kinase PLK1 is suggested to be dependent on S1453[46]. Moreover, it was shown that SLX4 interacts via S1260 with TOPBP1 in a CDK-dependent manner constituting a crucial step to recruit SLX4 to chromatin[278].

Thus, we wanted to interrogate whether the binding of specific partners of SLX4 are controlled by PIN1. To this end, we performed anti-FLAG co-immunoprecipitations from cells transiently transfected with FLAG-SLX4 and HA-tagged PIN1 expression constructs (wt, W34A: binding-deficient mutant, C113A: isomerase-dead mutant). However, PIN1 overexpression did not alter SLX4 interactions with PLK1, MUS81, TRF2 (Figure 4.11A), XPF or SLX1 (Figure 4.11B). Similar results were obtained when endogenous SLX4 interactions were analyzed following knockdown of PIN1 (Figure 4.11C). Of note, PIN1 could not be retrieved in any of the anti-SLX4 co-immunoprecipitates tested, suggesting a very transient interaction between the two proteins (Figures 4.11A-C). Interestingly, however, we observed that overexpression of PIN1 mutants caused a reduction in FLAG-SLX4 protein levels (Figures 4.11A and 4.11B).

Given that PIN1 was shown to regulate the stability of many of its substrate proteins, we investigated whether PIN1 regulates SLX4 protein turnover. Our preliminary analysis revealed that knockdown of PIN1 accelerates SLX4 degradation in presence of the translation inhibitor cycloheximide, suggesting that PIN1 may protect SLX4 from proteasomal degradation (Figure 4.12). Clearly, further experiments are required to verify a potential role for PIN1 in stabilizing SLX4 molecules.

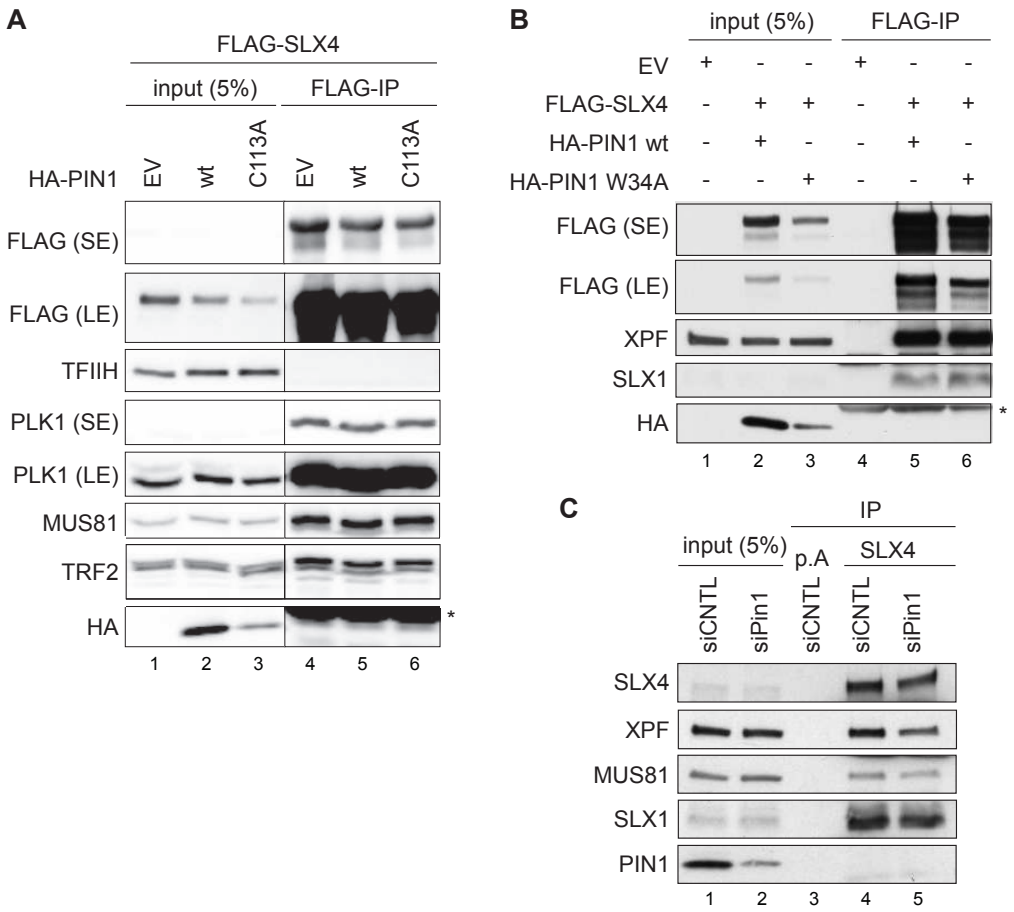

Figure 4.11: PIN1 status has no major effect on the interaction between SLX4 and PLK1, MUS81, TRF2, XPF and SLX1. (**A**) HEK293T cells were co-transfected with plasmids encoding FLAG-SLX4 wt and HA-tagged PIN1 variants or empty vector (EV) instead. Cell extracts were subjected to immunoprecipitation (IP) using FLAG-antibodies. Precipitated immunocomplexes were separated by SDS-PAGE and analyzed by immunoblotting. SE= short exposure, LE= long exposure. (**B**) Same experimental approach as in (A) but immunoblotting was performed for different proteins. (**C**) HEK293T were transfected with siluc (control) or siPIN1. 48h later, immunoprecipitation was performed with 1 mg of cell extracts using either protein A beads (p. A) alone or beads coupled with anti-SLX4 antibodies. Immunocomplexes were analyzed by Western blotting. Experiments shown in (B) and (C) were performed by Dr. Lorenzo Lafranchi (Sartori Lab).

PIN1 is not regulating SLX4 localization to telomeres

Chromosome ends are protected by DNA structures called telomeres to ensure genetic stability and to counteract replication-dependent degradation of genetic information. Telomeres consist of short tandem DNA repeats ending in a single-stranded 3' overhang, which are covered by the shelterin complex[279]. The shelterin complex promotes the formation of a telomeric loop structure (called the T-loop) thus protecting

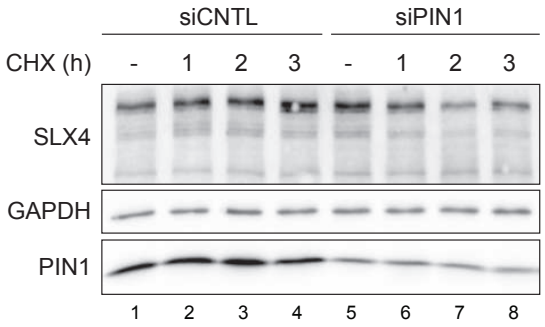

Figure 4.12: Knockdown of PIN1 affects SLX4 protein stability. HEK293T cells transfected with siluc (control) or siPIN1 were treated with 50 µg/ml cycloheximide (CHX) for the indicated times (in hours) and whole cell lysates were analyzed by immunoblotting using the indicated antibodies.

the telomeres from being misidentified as DNA breaks. In addition, the complex facilitates telomere maintenance. Especially in telomerase-negative cancer, cells counteract telomere attrition by alternative lengthening of telomeres (ALT), a mechanism dependent on homologous recombination[280]. These cells aim to achieve homeostasis of HR-dependent synthesis of new telomeric DNA versus 'telomere trimming', to not risk generation of too long or too short telomeres. The shelterin complex consists of several DNA-binding proteins, most prominently TRF2, which prevent chromosome end-to-end fusions[279]. Via its TRFH domain, TRF2 recruits also non-shelterin proteins important for telomere maintenance[281,282]. It was reported that SLX4-SLX1 complex interacts and colocalizes with TRF2 at telomeres, mediating the resolution of certain DNA structures (D-loops)[197,283], leading to a cleave-off the T-loop and by that playing a role in telomere trimming[46,197,199,200,276]. It is suggested that disruption of the SLX4-TRF2 interaction causes telomere fragility, as cells from SLX4$^{-/-}$ mice exhibit very long and fragile telomeres[197,199].

Thus, we wondered if SLX4 function at telomeres is regulated by phosphorylation-dependent isomerization. To examine whether PIN1 regulates context-dependent subnuclear localization of SLX4, we generated U2OS cells inducibly expressing siRNA-resistant YFP-SXL4 (kindly provided by Dr. Pierre-Henri Gaillard, Centre National de la Recherche Scientifique, France)[196]. Importantly, we were able to confirm telomeric localization of SLX4 by indirect immunofluorescence microscopy using either anti-TRF2 antibodies or FISH analysis with a Cy3-labeled telomeric probe (Figures 4.13A and 4.14A).

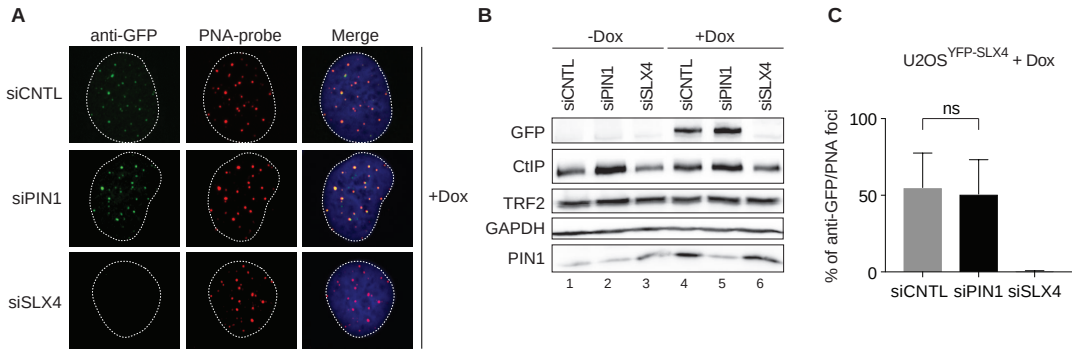

Figure 4.13: Knockdown of PIN1 does not affect SLX4 telomeric localization. (**A**) Representative immunofluorescence microscopy images of U2OS Flp-In T-REx cells stably expressing Dox-inducible YFP-SLX4, transfected with indicated siRNA oligos. A Cy3-labeled PNA-probe was used for fluorescent *in-situ* hybridization to visualize telomeres. Simultaneously, the YFP-labeled SLX4 was detected using anti-GFP antibody. (**B**) Same cells as in (A) were subjected to immunoblotting. (**C**) Quantification of YFP-SLX4 foci visualized using anti-GFP staining colocalizing with the telomeric probe (as in A) was performed using a customized CellProfiler[270] pipeline as described in Figure 4.15 and statistics calculated in Graphpad Prism. Data are presented as mean ± s.d. Numbers of cells analyzed: siluc = 100, siPIN1 = 135, siSLX4 = 37.

Acquired microscopic images were analyzed using CellProfiler, an open-source software tool for quantitative analysis of biological images, to extract the number of colocalizing foci[270].

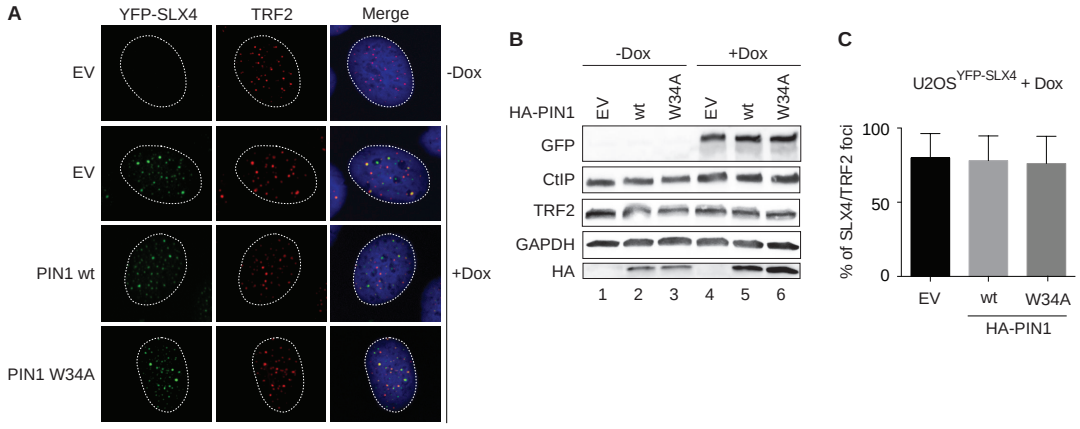

Figure 4.14: Overexpression of PIN1 does not affect localization of SLX4 to TRF2. (**A**) Representative immunofluorescence microscopy images of U2OS Flp-In T-REx cells stably expressing Dox-inducible YFP-SLX4, transfected with plasmids encoding for HA-PIN1-wt or W34A. Cells were stained with anti-TRF2 antibodies. (**B**) Same cells as in (A) were subjected to immunoblotting. (**C**) Same cells as in (A) were analyzed by immunofluorescence microscopy and YFP-SLX4 foci colocalizing with TRF2 foci were assessed using CellProfiler automated foci counting. Data are presented as mean ± s.d. Numbers of cells analyzed: EV = 76, HA-PIN1 wt = 156, HA-PIN1 W34A = 95.

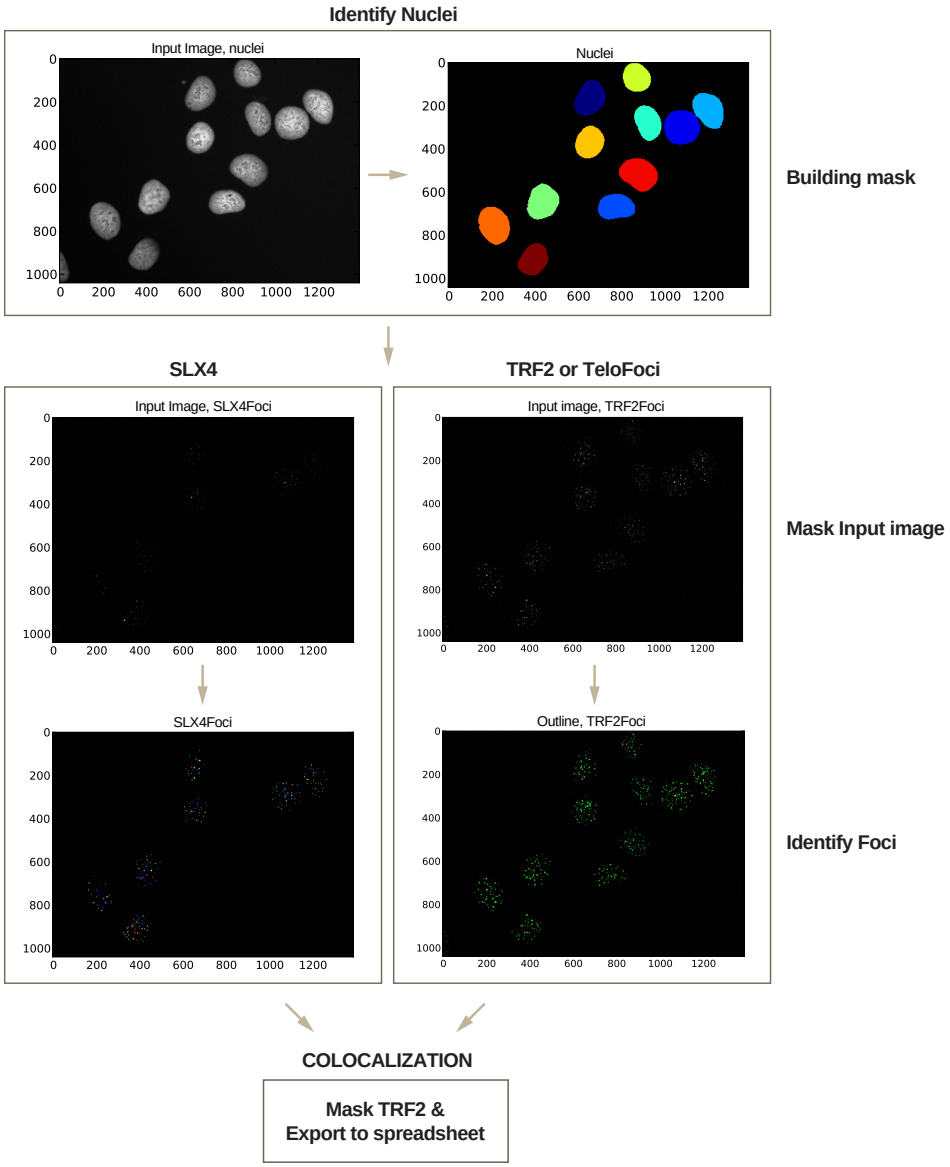

Figure 4.15: Customized CellProfiler pipeline setup. Single nuclei were identified and used to mask the pictures from channels of SLX4 and TRF2 (or the telomeric probe). Subsequently, SLX4 foci were identified and outlines of TRF2 foci determined in each single nucleus. As a last step, SLX4 foci were used as a mask to detect SLX4 foci positive for TRF2 and the information extracted.

To identify nuclei (DAPI channel) and the number of YFP-SLX4 foci colocalizing with either TRF2 foci or the telomeric PNA-probe we generated a customized analysis pipeline as illustrated in Figure 4.15.

However, neither PIN1 depletion (Figures 4.13A-C) nor PIN1 overexpression (Figures 4.14A-C) caused any significant change in telomeric localization of SLX4. Conclusively, our re-

sults suggest that PIN1 in general, but most likely also its interaction with SLX4, is not critical for telomere maintenance. This data is also consistent with our previous finding that overexpression of PIN1 (wt or catalytic dead) is not affecting SLX4-TRF2 interaction (see Figure 4.11A). To completely rule out a role for PIN1 in affecting SLX4 function at telomeres, further analyses have to be performed measuring telomere length, such as Telomere Restriction Fragment analysis and Telomere Repeat Amplification[284].

HeLa cells overexpressing SLX4-T1315A/T1320A undergo increased mitosis

Although not strictly required for PIN1 binding, we have identified T1315 and T1320 as potential PIN1 interaction motifs in SLX4. It has been shown that the interplay SLX4 with its nucleases differ between cell cycle stages, suggesting cell cycle-specific functions[45,285,286]. In yeast, association with Dpb11 (TOPBP1), Rtt107 and the nuclease SLX1 is S-phase specific and is proposed to have a role in dampening the DNA damage checkpoint, while the assembling with Mus81 is promoted in M phase to resolve DNA joint molecules[285]. Indeed, SLX4 has a prominent role in resolving under-replicated regions and joint molecules in mitosis to ensure chromosome segregation and preservation of genome integrity[47,286,287]. Moreover, cells lacking SLX4-MUS81 were shown to exhibit defects in chromosome segregation and concomitant micronucleus formation[278]. At the onset of mitosis, the SLX4-MUS81 complex is brought to chromatin via TOPBP1 in a CDK1-regulated fashion[278,288]. In addition, PLK1- and CDK-dependent phosphorylation controls complex formation of SLX4 with MUS81 in G2/M, an important step which is normally suppressed by Wee1 during S phase to prevent unscheduled processing of replication intermediates[192]. These reports clearly showed that SLX4 functions are governed by cell-cycle-dependent phosphorylation events. Because PIN1 is a known driver of mitotic progression and depletion of PIN1 promotes premature entry into mitosis[233,234], we aimed to investigate whether PIN1-mediated isomerization might add another layer of complexity to SLX4 regulation during G2/M transition and mitosis.

To this end, we created stable HeLa clones inducibly expressing siRNA-resistant YFP-SLX4-wt and T1315A/T1320A (2A) double mutant (Figure 4.16A). First, screening of clones expressing SLX4-T1315A/T1320A by immunofluorescence microscopy analysis

did not reveal any change in SLX4 localization and foci formation compared to SLX4-wt cells (Figure 4.16A).

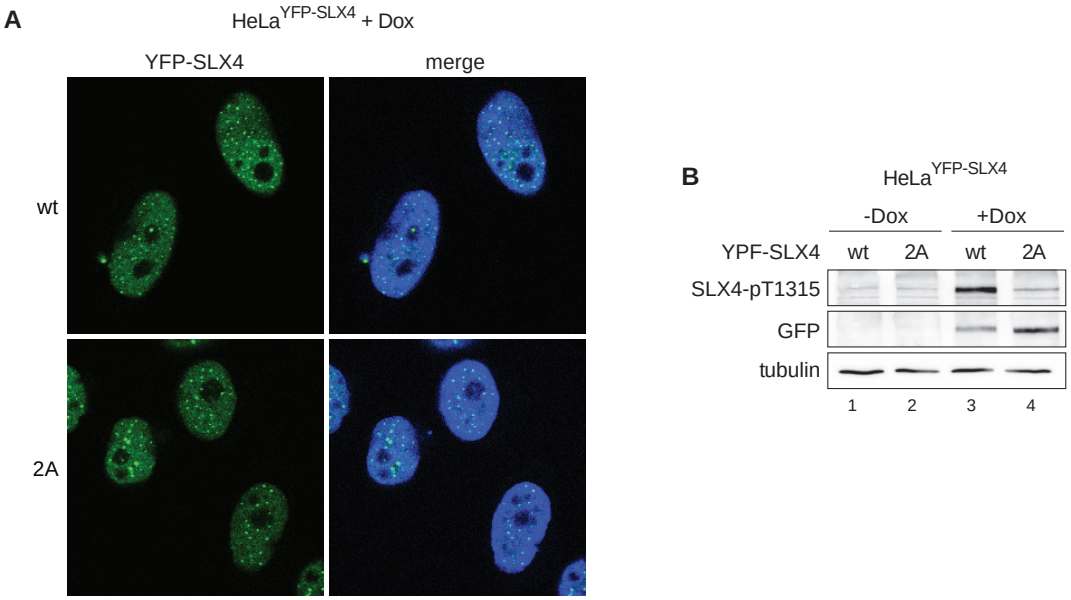

Figure 4.16: (**A**) Representative immunofluorescence microscopy images of HeLa Flp-In T-REx cells stably expressing YFP-SLX4-wt and T1315A/T1320A (2A) mutant (clone 7) grown in the presence of Dox for 24 h hours before fixation. (**B**) Extracts from same cells as in (A) were subjected to immunoblotting using the indicated antibodies.

To confirm that SLX4 is phosphorylated in our HeLa clones, we made use of the phospho-specific antibody raised against pT1315 (Figure 4.10). Indeed, our results indicate that YFP-SLX4-wt is phosphorylated, whereas the YFP-SLX4 T1315A/T1320A mutant (2A) is not (Figure 4.16B).

Remarkably, in the course of our microscopic inspection, we noticed that HeLa cells expressing YFP-SLX4-2A revealed a higher frequency of cells displaying condensed metaphase chromosomes compared to wild-type cells (Figure 4.17).

To substantiate these findings, we monitored the level of histone H3 phosphorylation at S10, a surrogate marker of cells undergoing mitosis, using immunoblotting. Consistent with our immunofluorescence data, overexpression of SLX4-2A resulted in increased H3-pS10 levels compared to YFP-SLX4-wt (Figure 4.18A). To assess whether the increase in H3-pS10 levels is dependent on SLX4-2A expression levels, we titrated the Dox concen-

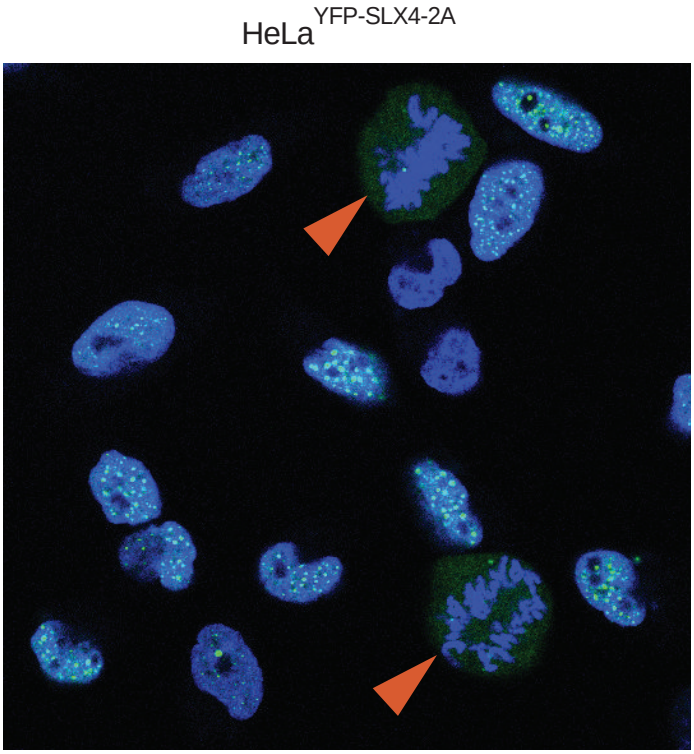

Figure 4.17: HeLa cells overexpressing YFP-SLX4-T1315A/T1320A (2A) display elevated number of mitotic cells. Immunofluorescence microscopy of HeLa Flp-In T-REx cell clones stably expressing doxycycline (Dox)-inducible YFP-SLX4-2A mutant. Cells were cultivated in the presence of 1 μg/ml Dox for 24 h before being fixed, permeabilized and imaged. Merged image is shown.

trations in the culturing media (Figure 4.18B). Interestingly, we observed that H3-pS10 induction correlated with higher amounts of SLX4-2A mutant but not of SLX4-wt.

To further corroborate these findings, we applied flow cytometry analysis of HeLa clones expressing similar levels of SLX4-wt and -2A (clone 7) (Figure 4.18A) and also displayed similar percentage of YFP-positive cells (Figure 4.19A). Upon gating for YFP/H3-pS10 double-positive cells, we observed a two-fold increase of the mitotic fraction in cells expressing SLX4-2A (Figure 4.19B). Of note, as endogenous SLX4 is still present in both cell lines, we speculated that SLX4-2A is acting in a dominant-negative manner to block cells in mitosis. However, as the 2A mutant is still proficient in interacting with PIN1, it remains to be established whether this phenotype is linked to dysregulation of SLX4 by PIN1. During mitosis, SLX4 is homogenously distributed among the nucleus in contrast to its foci-formation in interphase (Figure 4.17). Investigating mitotic cells means to focus

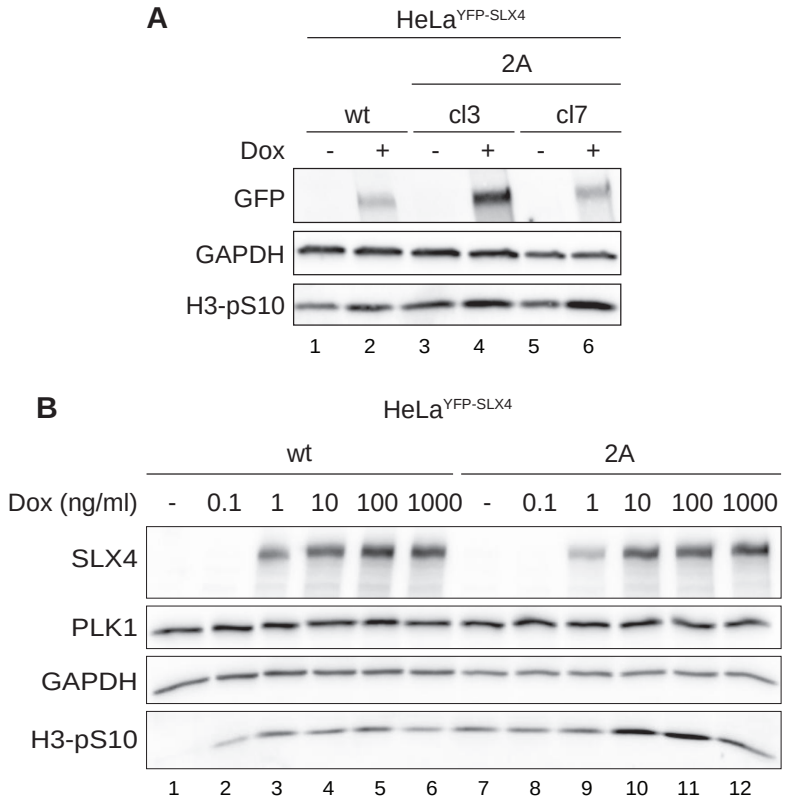

Figure 4.18: Expression of YFP-SLX4 T1315A/T1320A but not wt did result in increase in H3-pS10 level. (**A**) U2OS Flp-In T-REx or HeLa Flp-In T-REx cells inducibly expressing YFP-SLX4 wt or T1315A/T1320A were cultivated in the presence or absence of 1 μg/ml Dox for 24 h. Lysates were subjected to immunoblotting using the indicated antibodies. SE = short exposure time, LE = long exposure. (**B**) wt and clone 7 of YFP-SLX4 T1315/T1320A cells were cultivated in the absence or presence of increased Dox (0 – 1000 ng/ml) concentrations. 24 h later, cells were lysed and subjected to immunoblotting using the indicated antibodies.

on a small population, thus more experiments are needed to analyze SLX4 localization patterns between mitotic from interphase cells. Therefore, we are currently establishing a method combining flow cytometry analysis with immunofluorescence microscopy. This would equip us with the ability to analyze highly heterogeneous samples and rare subpopulations in a flow cytometry format and to simultaneously determine cell cycle distribution, signal intensity and subnuclear localization patterns.

In conclusion, our observation that expression of YFP-SLX4-2A mutant triggers increased mitosis, suggest that T1315 phosphorylation of SLX4, involved in promoting PIN1 binding, is required to ensure proper mitosis.

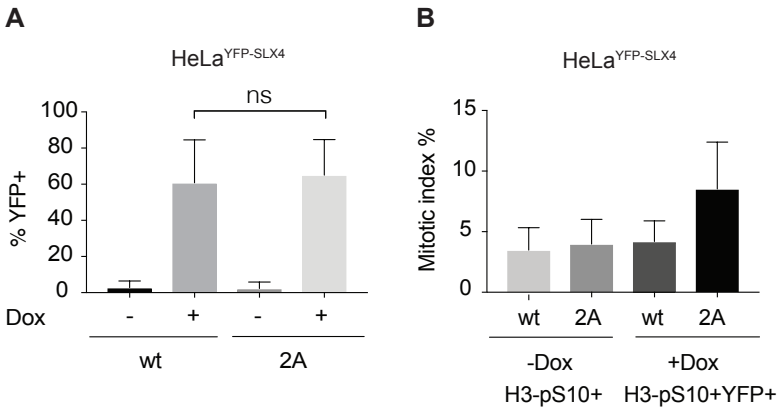

Figure 4.19: HeLa clones expressing YFP-SLX4-wt and -2A mutant (clone 7) were cultivated in the presence or absence of 1 μg/ml Dox for 24 h. Cells were permeabilized, fixed, immunostained with anti-H3-pS10 antibodies and analyzed by flow cytometry analysis. Quantification gates were established in untreated samples. Data are presented as mean HeLa ± s.d (n=4). (**A**) Percentage of YFP-positive cells. (**B**) Mitotic index of YFP-positive cells. To illustrate equal amount of mitotic cell before YFP-SLX4 induction, cells cultivated in the absence of Dox were gated for H3-pS10. After induction of protein expression gating was set to double-positive YFP/H3-pS10 cells.

Discussion and Outlook

5.1 Investigating the biochemical function of CtIP in DSB repair

In the first part of my Ph.D. thesis, we characterized *Paramecium tetraurelia* CtIP (PtCtIP), representing the shortest known CtIP ortholog in evolution. Remarkably, multiple sequence alignments revealed that PtCtIP largely consists of the conserved N- and C-terminal domains but lacks most of the internal, intrinsically disordered region containing multiple PTMs and short linear motifs mediating protein-protein interactions. In collaboration with the group of Dr. Mireille Bétermier (Institut de Biologie Intégrative de la Cellule, France), our goal was to validate PtCtIP as a true CtIP ortholog and examine its physiological role *in vivo*. Moreover, we aimed to investigate the biochemical properties of PtCtIP *in vitro* and address whether a highly conserved C-terminal RHR motif is required for the repair of DSBs by HR.

P. tetraurelia encodes two PtCtIP paralogs (*PtCtIPa* and *PtCtIPb*) that have emerged from the most recent whole genome duplication event. We found that both *PtCtIP* genes are induced during autogamy. During the sexual cycle of *P. tetraurelia*, meiotic processes take place during the formation of the zygote, giving rise to the MICs and a new MAC. Microarray analyses revealed early transcription of both *PtCtIPa* and *PtCtIPb* during MIC meiosis, which we confirmed by deep sequencing of mRNA and northern blot analysis. To get insights into the function of the *PtCtIP* genes, we used an RNAi strategy to silence their expression during autogamy. The simultaneous inactivation of *PtCtIPa* and *PtCtIPb* resulted in a significant decrease in viability of sexual progeny, meanwhile individual gene silencing did not show any effect. Consequently, we concluded that the paralogs are functionally redundant during meiosis.

Microscopic monitoring of *P. tetraurelia* autogamy stages demonstrated a pronounced meiotic defect upon co-silencing of *PtCtIPa* and *PtCtIPb*. Autogamous cells depleted for PtCtIP displayed old MAC fragmentation and a defect in new MAC development. Additionally, MIC generation was also impaired. The complete absence of new MICs and MACs likely reflected an early defect in the formation of the zygotic nucleus.

In large agreement with our findings, *COM-1* knockout in *Tetrahymena thermophila* was shown to block the progression of MIC meiosis as a result of defective meiotic break repair and inefficient pairing of homologous chromosomes[289]. In budding yeast, *Sae2*Δ and *Mre11* nuclease-defective mutants were unable to resect meiotic DSBs with SPO11 covalently attached to the break site[290,291]. Furthermore, mutant strains displayed sensitivity towards DSB-inducing agents[292]. However, sporulation could be restored in a *Sae2*Δ*/SPO11*Δ double mutant background, even though the resulting spores were not viable[101,102]. Taking advantage of a Δ*SPO11* somatic strain subjected to RNAi silencing of *PtCtIP* genes, we could show that new MACs developed, although these MACs were not functional indicated by the low survival rate in the progeny. This demonstrated the importance of the CtIP-mediated cleavage ability to initiate resection at Spo11-induced DSB ends that are otherwise inaccessible for subsequent repair steps. These results coincided with previous findings of CtIP counterparts in other organisms and corroborated the assumption of PtCtIP being a functional ortholog of CtIP in *P. tetraurelia* with important implications in the repair of Spo11-dependent meiotic DSBs[37,104–106]. Nevertheless, it would be important to determine if PtCtIP is also required for cell survival upon induction of DSBs *in vivo*. For instance, a pilot experiment could be performed to examine hypersensitivity of *P. tetraurelia* wild-type and PtCtIP knockdown cells following exposure to DSB-inducing agents, such as CPT or MMC.

Our study further highlighted *P. tetraurelia* as a model organism to study DNA repair processes, particularly considering its unique separation of MAC and MIC genome and the enormous genome rearrangements during each sexual cycle. The development of a MAC is a complex process in which the 2n MIC genome is amplified to approximately 800n and internal eliminated sequences (IES), which are transposon-like sequences, are removed prior to chromosome fragmentation and telomere addition[260,293]. IES excision

is facilitated by cleavage on each site of the sequence and was shown to generate DSBs with 4 nts 5' overhangs[294]. It was demonstrated that the broken DNA ends align and undergo limited processing before being repaired by employing a cut-and-close mechanism similar to NHEJ to ensure functional somatic chromosomes. Until now, several essential factors have been identified in *P. tetraurelia* to process DNA ends during IES excision, many of them known for their DNA repair functions in other organisms such as Ku70/80[10,260]. Thus, it would be interesting to investigate whether CtIP plays a role in the 5' end processing of the DNA or is implied in bridging of IES ends.

In the context of this project, we aimed to investigate DNA binding and cleavage properties of recombinant PtCtIP as well as its interaction with the MR complex *in vitro*. Previous attempts to express PtCtIP in bacteria yielded low amounts of soluble protein. We therefore switched to a baculovirus-insect cell expression system with the capacity to produce high levels of recombinant proteins with PTMs approaching that of mammalian cells. Based on the functional redundancy of the two PtCtIP paralogs *in vivo*, we decided to focus our biochemical studies on PtCtIPa. However, as PtCtIPa and PtCtIPb only share 80% sequence identity, it could be worth exploring whether PtCtIPb behaves identical to PtCtIPa in terms of DNA binding. Our tandem affinity purification strategy, utilizing N-terminal MBP- and C-terminal His-tags, provided good yields of pure recombinant PtCtIPa-wt and PtCtIPa-AHA, harboring a mutated RHR motif. Employing mobility-shift assays, we showed that PtCtIPa, presumably in a multimeric state, efficiently binds to double-stranded DNA substrates with a slight preference towards flap-structures. In large agreement with this, a C-terminal region of human CtIP (aa 769 to 897) containing the RHR motif was previously reported to possess DNA-binding ability *in vitro*[108]. In contrast, the PtCtIP-AHA mutant failed to produce shifted bands, emphasizing that the evolutionarily highly conserved RHR motif is required for DNA binding. These findings are in line with a recent study in fission yeast, identifying a 'RHR' DNA binding motif[104,107].
Sae2/CtIP collaborates with MRX/N in DSB processing. In the proposed bidirectional DNA-end resection model, CtIP stimulates the endonucleolytic activity of MRN to generate a nick in the 5' strand. Then, MRE11 continues to exonucleolytically degrade the DNA towards the break. As a second step, exonucleases such as EXO1 and DNA2-BLM start

at the generated nick to resect the same strand in a 5' to 3' direction[40,41,136]. Whether CtIP has intrinsic nuclease activity has been debated extensively. Interestingly, it has been reported earlier that CtIP and Sae2 exhibit endonuclease activity *in vitro*[139,140,295]. However, an increasing number of publications provide strong evidence arguing against CtIP being an endonuclease[57,107,126,136]. In fact, we could not detect any nuclease activity associated with recombinant PtCtIPa. The different findings might, at least partially, be explained by the different protein purification protocols used. However, Daley *et al.* did not observe nuclease activity in recombinant human CtIP despite using same expression construct and purification protocol as described by Makharashvili *et al.*[126,139].

Remarkably, in cross-species experiments, we found that PtCtIP functionally interacts with recombinant human MR complex and moderately stimulates its endonuclease activity *in vitro*. It was recently reported that MR endonuclease activity is greatly enhanced by NBS1 and by CtIP phosphorylation at T847[57]. To our great surprise, we could not identify an open reading frame encoding for an NBS1 ortholog in *P. tetraurelia*, suggesting that NBS1 is dispensable for MR and CtIP-dependent DSB processing in this organism. Along that line, a recent study in *C. elegans* showed that NBS-1 is not essential for Spo11 removal from DSBs, suggesting an MR-independent function during meiotic recombination[121]. With regards to the potential role of CtIP phosphorylation in facilitating DSB processing, alignment of the PtCtIP amino acid sequence revealed the presence of T196 located at the very C-terminal end, potentially corresponding to the T847 in human CtIP (Figure 5.1).

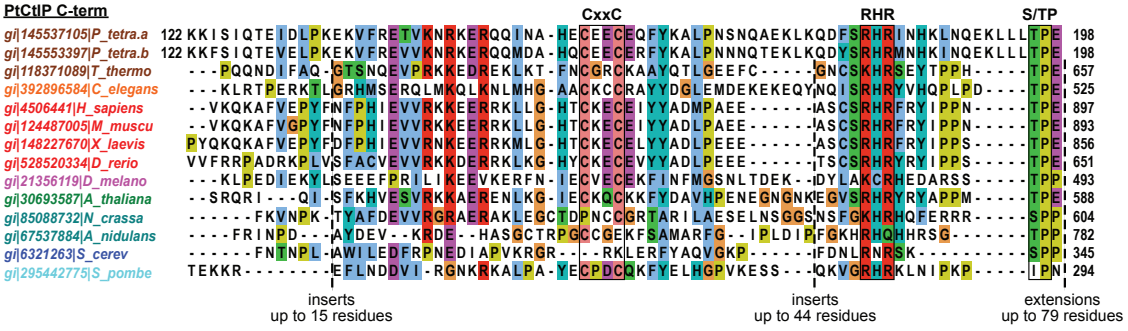

Figure 5.1: Sequence alignment of the C-terminal region of PtCtIPa and PtCtIPb with 12 CtIP proteins from different species.

Consequently, phosphorylation of T196 in PtCtIP may be required for efficient stimulation of MR. However, as protein expression in insect cells should increase the chance of intact PTMs, we speculate that PtCtIP-T196 is either not phosphorylated or that our purification scheme is incompatible with retaining phosphorylated residues.

An important goal of our study was to translate our findings from *P. tetraurelia* to human cells. Previously, it has been reported that mutation of the RHR motif in *S. pombe* Ctp1 leads to cellular hypersensitivity to DNA-damaging agents[107]. Consistently, CtIP-AHA expressing human cells demonstrated reduced capability for DNA-end resection and HR repair and displayed hypersensitivity to CPT treatment. Interestingly, disruption of the RHR motif in human CtIP resulted in its defective localization to sites of DNA damage, indicating that DNA binding is a critical determinant for efficient localization of CtIP to DSBs. To distinguish in more detail whether initial recruitment of CtIP to DSBs or rather retention of CtIP at damaged chromatin is affected in the RHR mutant, we consider applying live cell imaging analysis of GFP-tagged CtIP (wt vs. AHA) in combination with UV laser-induced DSB damage.
Intriguingly, the PtCtIP-AHA mutant is proficient in MRN binding and stimulation *in vitro*, despite its inability to bind DNA. These findings suggest that the DNA-binding function of CtIP most likely serves another purpose in DSB repair than to simply enhance MRN endonuclease activity. However, as our *in vitro* assays were performed with recombinant proteins using naked DNA substrates, we cannot exclude the possibility that DNA-binding of CtIP acts cooperatively with MR to promote DSB processing in the context of damaged chromatin in live cells. Indeed, we found that human CtIP-AHA mutant is largely defective in accumulating at DSBs generated by micro-laser irradiation. In addition, we observed that disruption of the RHR motif in human cells does not fully abrogate DSB resection and HR repair, suggesting that additional DNA binding sites in CtIP may compensate.

There is increasing biochemical evidence suggesting that DNA tethering function of CtIP and MRN is critical for HR. For example, CtIP/Ctp1 were found to form tetramers in solution able to bridge DBS ends *in vitro*[107,108,296]. Crystallographic analyses revealed the formation of dimer-to-dimer tetrads mediated by the coiled-coil segments located in the N-terminal part of the protein[107,296]. Andres *et. al* further reported that the tetramerization

domain and the length of the internally disordered region are crucial for Ctp1 bridging activity *in vitro*[107]. Our gel mobility shift assays indicated that PtCtIP binds to DNA in an oligomeric state, further corroborating the assumption that protein tetramerization is an important and evolutionary conserved feature of CtIP proteins. The MRN complex promotes DSB repair by tethering of the DSB strands holding them in close proximity for subsequent processing[113,114,297,298]. Recently, MRN was found to bridge DSBs on a broken chromatid with its intact sister chromatid, thereby assisting chromatid recombination[147].

Taking into consideration the bidirectional model of DNA-end resection, many questions arise as to how DSB tethering by CtIP, MRN or CtIP-MRN together guides DSB processing to promote efficient HR. For instance: Does MRN-CtIP-mediated DNA bridging causes the formation of a certain DSB structure/configuration (e.g. a loop) that is favouring further processing and HR repair? Does CtIP remain at the nick, that is generated by the MRN endo activity, in order to bridge DNA molecules while MRN leaves the nick to exonucleolytically degrades the DNA? Alternatively, CtIP's DNA binding ability might coordinate the second step, which is called long-range resection. Interestingly, CtIP was shown to directly interact with proteins involved in long-range resection, such as BLM helicase and EXO1. Interestingly, while binding of CtIP to BLM increases BLM helicase activity and simultaneously stimulates DNA2 nuclease activity, CtIP restrains EXO1 exonuclease activity[126,127]. Taken together, elucidating mechanistic details of the CtIP-MRN interaction and its interconnection with DNA binding and cleavage is extremely challenging and, to our opinion, would ultimately require the availability of high-resolution structures of MRN-CtIP complexed to DNA.

As PtCtIP comprises a stripped-down version of the human CtIP protein, consisting of only 198 amino acids, it might facilitate in-depth structural and biochemical analysis. Hence, to gain insights into structural conformation and considering the feasibility to obtain high yields of soluble PtCtIP protein from insect cells, solving the three-dimensional structure of purified recombinant PtCtIP alongside with MR complex or/and DNA substrates would lead to a better understanding of the function of CtIP in DNA bridging and interaction with MR.

5.2 Deciphering the potential regulation of SLX4 by PIN1-mediated isomerization

In the second part of my PhD thesis, we aimed to uncover how SLX4 functions in genome stability maintenance are controlled by combined site-specific phosphorylation and subsequent PIN1-mediated isomerization. The peptidyl-prolyl isomerase (PPIase) PIN1 belongs to a class of enzymes that catalyse *cis/trans* isomerization, thereby controlling a broad range of protein functions. Interestingly, PIN1 was shown to regulate diverse biological processes, including cell cycle progression, cell growth and various stress responses[213,225]. Further studies associated PIN1 overexpression and its regulatory isomerization activity with tumorigenesis[244,250–253]. However, our knowledge of the implications of PIN1-mediated isomerization in the DDR is very limited[299]. Interestingly, a current study found PIN1 to control anti-apoptotic activity of ATR at mitochondria upon UV exposure[255]. Furthermore, PIN1 inhibits phosphatase activity of PP2A during DNA damage repair in S-phase[256]. Additionally, our lab demonstrated that PIN1-mediated isomerization promotes CtIP ubiquitination and subsequent proteasomal degradation, thereby controlling DSB repair pathway choice[135]. The former study was launched following an unbiased mass spectrometry-based approach to identify novel PIN1 interactors, of which CtIP and SLX4 were ranked among the top candidate hits[135].

SLX4 is a multi-domain scaffold protein for several structure-specific nucleases involved in the cleavage of ICLs, resolution of HJs as well as in the trimming of telomeric loops[106,186,200,276]. Consistent with our mass spectrometry screen, we found a robust and direct phosphorylation-dependent interaction between PIN1 and SLX4. As PIN1 exclusively binds to and isomerizes phosphorylated S/T-P motifs in its target proteins, a major goal of this project was to identify PIN1 binding site(s) in SLX4. Unfortunately, the fact that SLX4 contains 41 potential S/T-P phosphorylation sites made it a rather tedious process to unveil the responsible PIN1 binding motif(s). Using SLX4 S/T-P cluster mutants and truncation mutants enabled us to narrow-down the PIN1 interacting region to a 200 aa stretch of SLX4 encompassing 13 S/T-P sites. However, none of our single or double S/T-P mutants displayed decreased PIN1 interaction, suggesting that a spe-

cific combination of multiple phosphorylated S/T-P sites in this region is responsible for PIN1 binding. In line with that, CtIP-pT315 serves as a docking site for PIN1, meanwhile CtIP-pS276 is the major isomerization site[135]. These and other findings reported in the literature implied a scenario in which PIN1 binds pS/T-P motifs via its WW domain to facilitate isomerization of one or several pS/T-P motifs in close proximity[214]. In fact, we still have to proof that PIN1 can indeed isomerize SLX4 molecules, which we plan to do using partial proteolysis assays[135,300].

Interestingly, by reintroducing intact phosphorylation sites into a SLX4-22A S/T-P cluster mutant defective in PIN1 binding, we could show that T1315 and, to a lesser extent, T1320 are sufficient for PIN1 interaction. Moreover, we have developed a phospho-specific antibody specifically detecting SLX4-wt but not SLX4-T1315A/T1320A (2A), providing us with a powerful tool to investigate the signalling mechanisms regulating SLX4-T1315 phosphorylation, and, consequently, SLX4 isomerization. In detail, we plan to follow SLX4-T1315 phosphorylation levels during cell cycle progression and identify the protein kinase responsible for SLX4-T1315 phosphorylation.

Analyses of HeLa cells stably expressing inducible YFP-SLX4-2A revealed a roughly two-fold increase in the mitotic index compared to cells expressing YFP-SLX4-wt, suggesting that these sites are important for cells to properly undergo mitosis and cytokinesis. To corroborate our findings, we will conduct time-lapse microscopy experiments in order to monitor spatial distribution of YFP-SLX4 during the cell cycle. Additionally, we plan to make use of the ImageStreamX (Amnis) to analyze the mitotic fraction in a more elaborate way. It would be interesting to investigate whether this mitotic arrest is caused by aberrant chromosome segregation as it was reported that SLX4 promotes resolution of underreplicated regions and joint molecules in mitosis to ensure mitotic progression and cell division[47,192,286]. To do so, SLX4 associates with MUS81 with kinases CDK1 and PLK1 acting as a timer for MUS81-SLX4 assembly to promote cleavage of persisting replication intermediates at the onset of mitosis[192]. Although our findings indicate that PIN1 does not affect interaction of SLX4 with MUS81, the question arises to whether PIN1 is implicated in controlling SLX4's function during mitosis.

Besides serving as a scaffold for structure-specific nucleases, SLX4 interacts and is re-

cruited to telomeres via TRF2, a member of the shelterin complex, important for telomere maintenance[198,283]. Surprisingly, also the TRF2 motif in SLX4 located in the central region of the protein is primate-specific, and so are the phosphorylated S/T-P motifs scoring the highest in high-throughput mass spectrometry data. That prompted us to investigate if the telomeric localization of SLX4 is regulated by phosphorylation-dependent isomerization. However, neither PIN1 overexpression nor knockdown altered the telomeric localization pattern of SLX4, suggesting that PIN1 is not governing SLX4 function in telomere maintenance.

Upon replication fork stalling, ATR is activated and promotes fork repair[301]. However, when ATR is inhibited, stalled forks collapse due to SLX4/MUS81-dependent nucleolytic cleavage, resulting in an increased number of DSBs and resection-dependent nascent-strand ss-DNA formation[201,302]. Noteworthy, the versatile functions of the SLX4 complex at damaged DNA, stalled forks and telomeres are controlled through its interaction with ubiquitinated or SUMOylated proteins via UBZ or SIM motifs. Furthermore, SLX4 was shown to contain SUMO E3 ligase activity that SUMOylates itself and XPF-ERCC1[194,196]. Interestingly, SLX4 SIMs are located close to the region important for PIN1 interaction, suggesting a potential crosstalk between SLX4 isomerization and sumoylation. The SUMO-related functions of SLX4 are not essential for ICL repair but are responsible for the accumulation of DSBs after replication fork stalling. In addition, PLK1 was also shown to lead to replication fork collapse in ATR-deficient cells upon replication stress, suggesting that PLK1 enhances activity of SLX4 or makes DNA replication fork structures more accessible for subsequent cleavage[201]. Therefore, it could be interesting to investigate the effect of PIN1 on the SUMOylation function of SLX4 and to test the effect of PIN1 depletion or overexpression in replication fork restart or collapse by fiber analysis and BrdU/EdU pulse labeling. Interestingly, our interaction studies revealed the co-existence of a PIN1-SLX4-PLK1 tripartite complex, indicating that PIN1 and PLK1 may act in conjunction to regulate SLX4 function(s) in a phosphorylation- and cell cycle-dependent manner, most likely during G2/M transition and in mitosis.

Mutations of SLX4/FANCP are associated with Fanconi Anemia (FA), a rare recessive genetic disease characterized by predisposition to cancer and bone marrow failure[84].

Consequently, cells lacking SLX4 are hypersensitive to ICL-inducing agents and display increased chromosomal instability, cellular hallmarks of FA[276,303]. Whether SLX4 phosphorylation at T1315 and other residues critical for PIN1 binding is critical for the repair of ICLs remains another key open question. To address this issue, we consider employing clonogenic survival assays and metaphase spread analysis upon MMC treatment in cells expressing S/T-P mutants. However, first and foremost, it will be of utmost importance to generate an SLX4 mutant clearly defective in PIN1 binding. To this end, we are currently in the process of making an SLX4-5A mutant, with residues T1315, T1320, T1326, S1329 and S1342 simultaneously substituted with alanine residues. If this mutant fails to interact with PIN1, cell lines will be generated stably expressing SLX4-5A and phenotypically analysed (e.g. SLX4 PPIs, SLX4 stability, telomere fragility, ICL repair, etc.)

In summary, the second Ph.D thesis project highlights prolyl isomerization as potential mechanism for controlling SLX4 activity, We believe that a detailed investigation of the PIN1-SLX4 regulatory axis will be important for evaluating the therapeutic potential of PIN1 inhibitors in cancer.

Bibliography

[1] F. H. C. Crick and J. D. Watson. The Complementary Structure of Deoxyribonucleic Acid. *Proc. R. Soc. A Math. Phys. Eng. Sci.*, 223(1152):80–96, apr 1954. ISSN 1364-5021. doi: 10.1098/rspa.1954.0101.

[2] Michael R. Stratton, Peter J. Campbell, and P. Andrew Futreal. The cancer genome. *Nature*, 458(7239): 719–724, apr 2009. ISSN 0028-0836. doi: 10.1038/nature07943. URL http://www.ncbi.nlm.nih.gov/pubmed/19360079http://www.pubmedcentral.nih.gov/articlerender.fcgi?artid=PMC2821689http://www.nature.com/articles/nature07943.

[3] Lucy R. Yates and Peter J. Campbell. Evolution of the cancer genome. *Nat. Rev. Genet.*, 13(11):795–806, nov 2012. ISSN 1471-0056. doi: 10.1038/nrg3317. URL http://www.ncbi.nlm.nih.gov/pubmed/23044827http://www.pubmedcentral.nih.gov/articlerender.fcgi?artid=PMC3666082http://www.nature.com/articles/nrg3317.

[4] Ivana Bozic, Tibor Antal, Hisashi Ohtsuki, Hannah Carter, Dewey Kim, Sining Chen, Rachel Karchin, Kenneth W Kinzler, Bert Vogelstein, and Martin A Nowak. Accumulation of driver and passenger mutations during tumor progression. *Proc. Natl. Acad. Sci. U. S. A.*, 107(43):18545–50, oct 2010. ISSN 1091-6490. doi: 10.1073/pnas.1010978107. URL http://www.ncbi.nlm.nih.gov/pubmed/20876136http://www.pubmedcentral.nih.gov/articlerender.fcgi?artid=PMC2972991.

[5] ROBERT A. WEINBERG. The Molecular Basis of Oncogenes and Tumor Suppressor Genes. *Ann. N. Y. Acad. Sci.*, 758(1 DNA):331–338, jun 1995. ISSN 0077-8923. doi: 10.1111/j.1749-6632.1995.tb24838.x. URL http://doi.wiley.com/10.1111/j.1749-6632.1995.tb24838.x.

[6] Simona Negrini, Vassilis G. Gorgoulis, and Thanos D. Halazonetis. Genomic instability — an evolving hallmark of cancer. *Nat. Rev. Mol. Cell Biol.*, 11(3):220–228, mar 2010. ISSN 1471-0072. doi: 10.1038/nrm2858. URL http://www.ncbi.nlm.nih.gov/pubmed/20177397http://www.nature.com/articles/nrm2858.

[7] Johan P. de Winter and Hans Joenje. The genetic and molecular basis of Fanconi anemia. *Mutat. Res. Mol. Mech. Mutagen.*, 668(1-2):11–19, jul 2009. ISSN 00275107. doi: 10.1016/j.mrfmmm.2008.11.004. URL http://www.ncbi.nlm.nih.gov/pubmed/19061902http://linkinghub.elsevier.com/retrieve/pii/S0027510708002820.

[8] Y Miki, J Swensen, D Shattuck-Eidens, P A Futreal, K Harshman, S Tavtigian, Q Liu, C Cochran, L M Bennett, and W Ding. A strong candidate for the breast and ovarian cancer susceptibility gene BRCA1. *Science*, 266(5182): 66–71, oct 1994. ISSN 0036-8075. URL http://www.ncbi.nlm.nih.gov/pubmed/7545954.

[9] M.-C. King, Joan H Marks, Jessica B Mandell, and New York Breast Cancer Study Group. Breast and Ovarian Cancer Risks Due to Inherited Mutations in BRCA1 and BRCA2. *Science (80-.).*, 302(5645):643–646, oct 2003. ISSN 0036-8075. doi: 10.1126/science.1088759. URL http://www.ncbi.nlm.nih.gov/pubmed/14576434http://www.sciencemag.org/cgi/doi/10.1126/science.1088759.

[10] Antoine Marmignon, Julien Bischerour, Aude Silve, Clémentine Fojcik, Emeline Dubois, Olivier Arnaiz, Aurélie Kapusta, Sophie Malinsky, and Mireille Bétermier. Ku-Mediated Coupling of DNA Cleavage and Repair during Programmed Genome Rearrangements in the Ciliate Paramecium tetraurelia. *PLoS Genet.*, 10(8):e1004552, aug 2014. ISSN 1553-7404. doi: 10.1371/journal.pgen.1004552.

URL http://www.ncbi.nlm.nih.gov/pubmed/25166013http://www.pubmedcentral.nih.gov/articlerender.fcgi?artid=PMC4148214http://dx.plos.org/10.1371/journal.pgen.1004552.

[11] Douglas Hanahan and Robert A Weinberg. The Hallmarks of Cancer. *Cell*, 100(1):57–70, jan 2000. ISSN 0092-8674. doi: 10.1016/S0092-8674(00)81683-9. URL https://www.sciencedirect.com/science/article/pii/S0092867400816839?via{%}3Dihub.

[12] Douglas Hanahan and Robert A Weinberg. Hallmarks of Cancer: The Next Generation. *Cell*, 144(5):646–674, 2011.

[13] Jan H.J. Hoeijmakers. DNA Damage, Aging, and Cancer. *N. Engl. J. Med.*, 361(15):1475–1485, oct 2009. ISSN 0028-4793. doi: 10.1056/NEJMra0804615. URL http://www.nejm.org/doi/abs/10.1056/NEJMra0804615.

[14] Anthony Tubbs and André Nussenzweig. Endogenous DNA Damage as a Source of Genomic Instability in Cancer. *Cell*, 168(4):644–656, feb 2017. ISSN 0092-8674. doi: 10.1016/J.CELL.2017.01.002. URL https://www.sciencedirect.com/science/article/pii/S0092867417300053?via{%}3Dihub.

[15] Nancy Maizels. Immunoglobulin Gene Diversification. *Annu. Rev. Genet.*, 39(1):23–46, dec 2005. ISSN 0066-4197. doi: 10.1146/annurev.genet.39.073003.110544. URL http://www.annualreviews.org/doi/10.1146/annurev.genet.39.073003.110544.

[16] Indra A Shaltiel, Lenno Krenning, Wytse Bruinsma, and René H Medema. The same, only different - DNA damage checkpoints and their reversal throughout the cell cycle. *J. Cell Sci.*, 128(4):607–20, feb 2015. ISSN 1477-9137. doi: 10.1242/jcs.163766. URL http://www.ncbi.nlm.nih.gov/pubmed/25609713.

[17] Stephen P Jackson and Jiri Bartek. The DNA-damage response in human biology and disease. *Nature*, 461(7267):1071–1078, oct 2009.

[18] Jacob Falck, Julia Coates, and Stephen P. Jackson. Conserved modes of recruitment of ATM, ATR and DNA-PKcs to sites of DNA damage. *Nature*, 434(7033):605–611, mar 2005. ISSN 0028-0836. doi: 10.1038/nature03442. URL http://www.nature.com/articles/nature03442.

[19] Alexandre Maréchal and Lee Zou. DNA damage sensing by the ATM and ATR kinases. *Cold Spring Harb. Perspect. Biol.*, 5(9), sep 2013. ISSN 1943-0264. doi: 10.1101/cshperspect.a012716. URL http://www.ncbi.nlm.nih.gov/pubmed/24003211http://www.pubmedcentral.nih.gov/articlerender.fcgi?artid=PMC3753707.

[20] Joanne Smith, Lye Mun Tho, Naihan Xu, and David A. Gillespie. The ATM–Chk2 and ATR–Chk1 Pathways in DNA Damage Signaling and Cancer. *Adv. Cancer Res.*, 108:73–112, jan 2010. ISSN 0065-230X. doi: 10.1016/B978-0-12-380888-2.00003-0. URL https://www.sciencedirect.com/science/article/pii/B9780123808882000030?via{%}3Dihub.

[21] Aziz Sancar, Laura A. Lindsey-Boltz, Keziban Ünsal-Kaçmaz, and Stuart Linn. Molecular Mechanisms of Mammalian DNA Repair and the DNA Damage Checkpoints. *Annu. Rev. Biochem.*, 73(1):39–85, jun 2004. ISSN 0066-4154. doi: 10.1146/annurev.biochem.73.011303.073723. URL http://www.ncbi.nlm.nih.gov/pubmed/15189136http://www.annualreviews.org/doi/10.1146/annurev.biochem.73.011303.073723.

[22] Lorenza P Ferretti, Lorenzo Lafranchi, and Alessandro A Sartori. Controlling DNA-end resection: a new task for CDKs. *Front. Genet.*, 4:99, dec 2012.

[23] Lara Wohlbold and Robert P. Fisher. Behind the wheel and under the hood: Functions of cyclin-dependent kinases in response to DNA damage. *DNA Repair (Amst).*, 8(9):1018–1024, sep 2009. ISSN 15687864. doi: 10.1016/j.dnarep.2009.04.009. URL http://www.ncbi.nlm.nih.gov/pubmed/19464967http://www.pubmedcentral.nih.gov/articlerender.fcgi?artid=PMC2725215http://linkinghub.elsevier.com/retrieve/pii/S1568786409001037.

[24] Michael B. Kastan and Jiri Bartek. Cell-cycle checkpoints and cancer. *Nature*, 432(7015):316–323, nov 2004. ISSN 0028-0836. doi: 10.1038/nature03097. URL http://www.ncbi.nlm.nih.gov/pubmed/15549093http://www.nature.com/articles/nature03097.

[25] Hans E Krokan and Magnar Bjørås. Base excision repair. *Cold Spring Harb. Perspect. Biol.*, 5(4):a012583, apr 2013. ISSN 1943-0264. doi: 10.1101/cshperspect.a012583. URL http://www.ncbi.nlm.nih.gov/pubmed/23545420http://www.pubmedcentral.nih.gov/articlerender.fcgi?artid=PMC3683898.

[26] Orlando D Schärer. Nucleotide excision repair in eukaryotes. *Cold Spring Harb. Perspect. Biol.*, 5(10):a012609, oct 2013. ISSN 1943-0264. doi: 10.1101/cshperspect.a012609. URL http://www.ncbi.nlm.nih.gov/pubmed/24086042http://www.pubmedcentral.nih.gov/articlerender.fcgi?artid=PMC3783044.

[27] J. Jiricny. Postreplicative Mismatch Repair. *Cold Spring Harb. Perspect. Biol.*, 5(4):a012633–a012633, apr 2013. ISSN 1943-0264. doi: 10.1101/cshperspect.a012633. URL http://www.ncbi.nlm.nih.gov/pubmed/23545421http://www.pubmedcentral.nih.gov/articlerender.fcgi?artid=PMC3683899http://cshperspectives.cshlp.org/lookup/doi/10.1101/cshperspect.a012633.

[28] Paul Modrich. Mechanisms in Eukaryotic Mismatch Repair. *J. Biol. Chem.*, 281(41):30305–30309, oct 2006. ISSN 0021-9258. doi: 10.1074/jbc.R600022200. URL http://www.ncbi.nlm.nih.gov/pubmed/16905530http://www.pubmedcentral.nih.gov/articlerender.fcgi?artid=PMC2234602http://www.jbc.org/lookup/doi/10.1074/jbc.R600022200.

[29] M. F. Goodman and R. Woodgate. Translesion DNA Polymerases. *Cold Spring Harb. Perspect. Biol.*, 5(10):a010363–a010363, oct 2013. ISSN 1943-0264. doi: 10.1101/cshperspect.a010363. URL http://www.ncbi.nlm.nih.gov/pubmed/23838442http://www.pubmedcentral.nih.gov/articlerender.fcgi?artid=PMC3783050http://cshperspectives.cshlp.org/lookup/doi/10.1101/cshperspect.a010363.

[30] Maria Jasin and Rodney Rothstein. Repair of strand breaks by homologous recombination. *Cold Spring Harb. Perspect. Biol.*, 5(11):a012740, nov 2013. ISSN 1943-0264. doi: 10.1101/cshperspect.a012740. URL http://www.ncbi.nlm.nih.gov/pubmed/24097900http://www.pubmedcentral.nih.gov/articlerender.fcgi?artid=PMC3809576.

[31] Raphael Ceccaldi, Beatrice Rondinelli, and Alan D D'Andrea. Repair Pathway Choices and Consequences at the Double-Strand Break. *Trends Cell Biol.*, 26(1):52–64, jan 2016. ISSN 1879-3088. doi: 10.1016/j.tcb.2015.07.009. URL http://www.ncbi.nlm.nih.gov/pubmed/26437586http://www.pubmedcentral.nih.gov/articlerender.fcgi?artid=PMC4862604.

[32] Mark J. O'Connor. Targeting the DNA Damage Response in Cancer. *Mol. Cell*, 60(4):547–560, nov 2015. ISSN 1097-2765. doi: 10.1016/J.MOLCEL.2015.10.040. URL https://www.sciencedirect.com/science/article/pii/S109727651500831X.

[33] Laurence H. Pearl, Amanda C. Schierz, Simon E. Ward, Bissan Al-Lazikani, and Frances M. G. Pearl. Therapeutic opportunities within the DNA damage response. *Nat. Rev. Cancer*, 15(3):166–180, mar 2015. ISSN 1474-175X. doi: 10.1038/nrc3891. URL http://www.nature.com/articles/nrc3891.

[34] Peter Ahnesorg, Philippa Smith, and Stephen P. Jackson. XLF Interacts with the XRCC4-DNA Ligase IV Complex to Promote DNA Nonhomologous End-Joining. *Cell*, 124(2):301–313, jan 2006. ISSN 00928674. doi: 10.1016/j.cell.2005.12.031. URL http://www.ncbi.nlm.nih.gov/pubmed/16439205http://linkinghub.elsevier.com/retrieve/pii/S0092867406000031.

[35] Michael R Lieber. The mechanism of double-strand DNA break repair by the nonhomologous DNA end-joining pathway. *Annu. Rev. Biochem.*, 79:181–211, 2010. ISSN 1545-4509. doi: 10.1146/annurev.biochem.052308.093131. URL http://www.ncbi.nlm.nih.gov/pubmed/20192759http://www.pubmedcentral.nih.gov/articlerender.fcgi?artid=PMC3079308.

[36] Elisa Gobbini, Corinne Cassani, Matteo Villa, Diego Bonetti, and Maria Longhese. Functions and regulation of the MRX complex at DNA double-strand breaks. *Microb. Cell*, 3(8):329–337, aug 2016. ISSN 23112638. doi: 10.15698/mic2016.08.517. URL http://microbialcell.com/researcharticles/functions-and-regulation-of-the-mrx-complex-at-dna-double-strand-breaks/.

[37] Alessandro A Sartori, Claudia Lukas, Julia Coates, Martin Mistrik, Shuang Fu, Jiri Bartek, Richard Baer, Jiri Lukas, and Stephen P Jackson. Human CtIP promotes DNA end resection. *Nature*, 450(7169):509–514, nov 2007.

[38] Lorraine S Symington. End resection at double-strand breaks: mechanism and regulation. *Cold Spring Harb. Perspect. Biol.*, 6(8):a016436, aug 2014. ISSN 1943-0264. doi: 10.1101/cshperspect.a016436. URL http://www.ncbi.nlm.nih.gov/pubmed/25085909http://www.pubmedcentral.nih.gov/articlerender.fcgi?artid=PMC4107989.

[39] Elda Cannavo and Petr Cejka. Sae2 promotes dsDNA endonuclease activity within Mre11–Rad50–Xrs2 to resect DNA breaks. *Nature*, 514(7520):122–125, oct 2014. ISSN 0028-0836. doi: 10.1038/nature13771. URL http://www.nature.com/articles/nature13771.

[40] Valerie Garcia, Sarah E. L. Phelps, Stephen Gray, and Matthew J. Neale. Bidirectional resection of DNA double-strand breaks by Mre11 and Exo1. *Nature*, 479(7372):241–244, nov 2011. ISSN 0028-0836. doi: 10.1038/nature10515. URL http://www.nature.com/articles/nature10515.

[41] Sharad C. Paudyal, Shan Li, Hong Yan, Tony Hunter, and Zhongsheng You. Dna2 initiates resection at clean DNA double-strand breaks. *Nucleic Acids Res.*, 45(20):11766–11781, nov 2017. ISSN 0305-1048. doi: 10.1093/nar/gkx830. URL http://www.ncbi.nlm.nih.gov/pubmed/28981724http://www.pubmedcentral.nih.gov/articlerender.fcgi?artid=PMC5714177http://academic.oup.com/nar/article/45/20/11766/4157875.

[42] J. Ross Chapman, Martin R.G. Taylor, and Simon J. Boulton. Playing the End Game: DNA Double-Strand Break Repair Pathway Choice. *Mol. Cell*, 47(4):497–510, aug 2012. ISSN 1097-2765. doi: 10.1016/J.MOLCEL.2012.07.029. URL https://www.sciencedirect.com/science/article/pii/S1097276512006569?via{%}3Dihub.

[43] A. H. Bizard and I. D. Hickson. The Dissolution of Double Holliday Junctions. *Cold Spring Harb. Perspect. Biol.*, 6(7):a016477–a016477, jul 2014. ISSN 1943-0264. doi: 10.1101/cshperspect.a016477. URL http://www.ncbi.nlm.nih.gov/pubmed/24984776http://www.pubmedcentral.nih.gov/articlerender.fcgi?artid=PMC4067992http://cshperspectives.cshlp.org/lookup/doi/10.1101/cshperspect.a016477.

[44] Haley D M Wyatt and Stephen C West. Holliday junction resolvases. *Cold Spring Harb. Perspect. Biol.*, 6(9):a023192, sep 2014. ISSN 1943-0264. doi: 10.1101/cshperspect.a023192. URL http://www.ncbi.nlm.nih.gov/pubmed/25183833http://www.pubmedcentral.nih.gov/articlerender.fcgi?artid=PMC4142969.

[45] Joao Matos and Stephen C. West. Holliday junction resolution: Regulation in space and time. *DNA Repair (Amst).*, 19:176–181, jul 2014. ISSN 15687864. doi: 10.1016/j.dnarep.2014.03.013. URL http://www.ncbi.nlm.nih.gov/pubmed/24767945http://www.pubmedcentral.nih.gov/articlerender.fcgi?artid=PMC4065333http://linkinghub.elsevier.com/retrieve/pii/S1568786414000846.

[46] Jennifer M Svendsen, Agata Smogorzewska, Mathew E Sowa, Brenda C O'Connell, Steven P Gygi, Stephen J Elledge, and J Wade Harper. Mammalian BTBD12/SLX4 Assembles A Holliday Junction Resolvase and Is Required for DNA Repair. *Cell*, 138(1):63–77, jul 2009.

[47] Haley D M Wyatt, Shriparna Sarbajna, Joao Matos, and Stephen C. West. Coordinated actions of SLX1-SLX4 and MUS81-EME1 for holliday junction resolution in human cells. *Mol. Cell*, 52(2):234–247, 2013. ISSN 10972765. doi: 10.1016/j.molcel.2013.08.035.

[48] Scott Keeney, Julian Lange, and Neeman Mohibullah. Self-Organization of Meiotic Recombination Initiation: General Principles and Molecular Pathways. *Annu. Rev. Genet.*, 48(1):187–214, nov 2014. ISSN 0066-4197. doi: 10.1146/annurev-genet-120213-092304. URL http://www.ncbi.nlm.nih.gov/pubmed/25421598http://www.pubmedcentral.nih.gov/articlerender.fcgi?artid=PMC4291115http://www.annualreviews.org/doi/10.1146/annurev-genet-120213-092304.

[49] Scott L. Page and R. Scott Hawley. THE GENETICS AND MOLECULAR BIOLOGY OF THE SYNAPTONEMAL COMPLEX. *Annu. Rev. Cell Dev. Biol.*, 20(1):525–558, nov 2004. ISSN 1081-0706. doi: 10.1146/annurev.cellbio.19.111301.155141. URL http://www.ncbi.nlm.nih.gov/pubmed/15473851http://www.annualreviews.org/doi/10.1146/annurev.cellbio.19.111301.155141.

[50] Jan-Michael Peters, Antonio Tedeschi, and Julia Schmitz. The cohesin complex and its roles in chromosome biology. *Genes Dev.*, 22(22):3089–114, nov 2008. ISSN 0890-9369. doi: 10.1101/gad.1724308. URL http://www.ncbi.nlm.nih.gov/pubmed/19056890.

[51] Neil Hunter. Meiotic Recombination: The Essence of Heredity. *Cold Spring Harb. Perspect. Biol.*, 7(12): a016618, oct 2015. ISSN 1943-0264. doi: 10.1101/cshperspect.a016618. URL http://www.ncbi.nlm.nih.gov/pubmed/26511629http://www.pubmedcentral.nih.gov/articlerender.fcgi?artid=PMC4665078http://cshperspectives.cshlp.org/lookup/doi/10.1101/cshperspect.a016618.

[52] Hong Sun, Douglas Treco, Neil P. Schultes, and Jack W. Szostak. Double-strand breaks at an initiation site for meiotic gene conversion. *Nature*, 338(6210):87–90, mar 1989. ISSN 0028-0836. doi: 10.1038/338087a0. URL http://www.ncbi.nlm.nih.gov/pubmed/2645528http://www.nature.com/doifinder/10.1038/338087a0.

[53] Agnès Bergerat, Bernard de Massy, Danielle Gadelle, Paul-Christophe Varoutas, Alain Nicolas, and Patrick Forterre. An atypical topoisomerase II from archaea with implications for meiotic recombination. *Nature*, 386 (6623):414–417, mar 1997. ISSN 0028-0836. doi: 10.1038/386414a0. URL http://www.nature.com/doifinder/10.1038/386414a0.

[54] S Keeney, C N Giroux, and N Kleckner. Meiosis-specific DNA double-strand breaks are catalyzed by Spo11, a member of a widely conserved protein family. *Cell*, 88(3):375–84, feb 1997. ISSN 0092-8674. URL http://www.ncbi.nlm.nih.gov/pubmed/9039264.

[55] Scott Keeney. Spo11 and the Formation of DNA Double-Strand Breaks in Meiosis. *Genome Dyn. Stab.*, 2:81–123, jan 2008. ISSN 1861-3373. doi: 10.1007/7050_2007_026. URL http://www.ncbi.nlm.nih.gov/pubmed/21927624http://www.pubmedcentral.nih.gov/articlerender.fcgi?artid=PMC3172816.

[56] Matthew J. Neale, Jing Pan, and Scott Keeney. Endonucleolytic processing of covalent protein-linked DNA double-strand breaks. *Nature*, 436(7053):1053–1057, aug 2005. ISSN 0028-0836. doi: 10.1038/nature03872. URL http://www.ncbi.nlm.nih.gov/pubmed/16107854http://www.pubmedcentral.nih.gov/articlerender.fcgi?artid=PMC1262668http://www.nature.com/articles/nature03872.

[57] Roopesh Anand, Lepakshi Ranjha, Elda Cannavo, and Petr Cejka. Phosphorylated CtIP Functions as a Co-factor of the MRE11-RAD50-NBS1 Endonuclease in DNA End Resection. *Mol. Cell*, 64(5):940–950, dec 2016. ISSN 1097-2765. doi: 10.1016/J.MOLCEL.2016.10.017. URL https://www.sciencedirect.com/science/article/pii/S1097276516306621?via{%}3Dihub.

[58] Kristi L. Jensen and Paul Russell. Ctp1-dependent clipping and resection of DNA double-strand breaks by Mre11 endonuclease complex are not genetically separable. *Nucleic Acids Res.*, 44(17):8241–8249, 2016. ISSN 13624962. doi: 10.1093/nar/gkw557.

[59] Lijuan Ma, Neta Milman, Mridula Nambiar, and Gerald R. Smith. Two separable functions of Ctp1 in the early steps of meiotic DNA double-strand break repair. *Nucleic Acids Res.*, 43(15):7349–7359, 2015. ISSN 13624962. doi: 10.1093/nar/gkv644.

[60] Douglas K Bishop. Rad51, the lead in mitotic recombinational DNA repair, plays a supporting role in budding yeast meiosis. *Cell Cycle*, 11(22):4105–6, nov 2012. ISSN 1551-4005. doi: 10.4161/cc.22396. URL http://www.ncbi.nlm.nih.gov/pubmed/23075494http://www.pubmedcentral.nih.gov/articlerender.fcgi?artid=PMC3524198.

[61] Veronica Cloud, Yuen-Ling Chan, Jennifer Grubb, Brian Budke, and Douglas K Bishop. Rad51 is an accessory factor for Dmc1-mediated joint molecule formation during meiosis. *Science*, 337(6099):1222–5, sep 2012. ISSN 1095-9203. doi: 10.1126/science.1219379. URL http://www.ncbi.nlm.nih.gov/pubmed/22955832http://www.pubmedcentral.nih.gov/articlerender.fcgi?artid=PMC4056682.

[62] Ulrich Rass, Sarah A Compton, Joao Matos, Martin R Singleton, Stephen C Y Ip, Miguel G Blanco, Jack D Griffith, and Stephen C West. Mechanism of Holliday junction resolution by the human GEN1 protein. *Genes Dev.*, 24(14): 1559–69, jul 2010. ISSN 1549-5477. doi: 10.1101/gad.585310. URL http://www.ncbi.nlm.nih.gov/pubmed/20634321http://www.pubmedcentral.nih.gov/articlerender.fcgi?artid=PMC2904945.

[63] Andrew J Deans and Stephen C West. DNA interstrand crosslink repair and cancer. *Nat. Rev. Cancer*, 11 (7):467–80, jun 2011. ISSN 1474-1768. doi: 10.1038/nrc3088. URL http://www.ncbi.nlm.nih.gov/pubmed/21701511http://www.pubmedcentral.nih.gov/articlerender.fcgi?artid=PMC3560328.

[64] Maria Tomasz. Mitomycin C: small, fast and deadly (but very selective). *Chem. Biol.*, 2(9):575–579, sep 1995. ISSN 1074-5521. doi: 10.1016/1074-5521(95)90120-5. URL https://www.sciencedirect.com/science/article/pii/1074552195901205?via{%}3Dihub.

[65] Elizabeth R. Jamieson And and Stephen J. Lippard*. Structure, Recognition, and Processing of CisplatinDNA Adducts. 1999. doi: 10.1021/CR980421N. URL https://pubs.acs.org/doi/abs/10.1021/cr980421n.

[66] Philip J. Brooks and Samir Zakhari. Acetaldehyde and the genome: Beyond nuclear DNA adducts and carcinogenesis. *Environ. Mol. Mutagen.*, 55(2):77–91, mar 2014. ISSN 08936692. doi: 10.1002/em.21824. URL http://www.ncbi.nlm.nih.gov/pubmed/24282063http://doi.wiley.com/10.1002/em.21824.

[67] Michael P. Stone, Young-Jin Cho, Hai Huang, Hye-Young Kim, Ivan D. Kozekov, Albena Kozekova, Hao Wang, Irina G. Minko, R. Stephen Lloyd, Thomas M. Harris, and Carmelo J. Rizzo. Interstrand DNA Cross-Links Induced by α,β-Unsaturated Aldehydes Derived from Lipid Peroxidation and Environmental Sources. *Acc. Chem. Res.*, 41(7):793–804, jul 2008. ISSN 0001-4842. doi: 10.1021/ar700246x. URL http://www.ncbi.nlm.nih.gov/pubmed/18500830http://www.pubmedcentral.nih.gov/articlerender.fcgi?artid=PMC2785109http://pubs.acs.org/doi/abs/10.1021/ar700246x.

[68] Y M Akkari, R L Bateman, C A Reifsteck, S B Olson, and M Grompe. DNA replication is required To elicit cellular responses to psoralen-induced DNA interstrand cross-links. *Mol. Cell. Biol.*, 20(21):8283–9, nov 2000. ISSN 0270-7306. URL http://www.ncbi.nlm.nih.gov/pubmed/11027296http://www.pubmedcentral.nih.gov/articlerender.fcgi?artid=PMC86436.

[69] George-Lucian Moldovan and Alan D D'Andrea. How the fanconi anemia pathway guards the genome. *Annu. Rev. Genet.*, 43:223–49, 2009. ISSN 1545-2948. doi: 10.1146/annurev-genet-102108-134222. URL http://www.ncbi.nlm.nih.gov/pubmed/19686080http://www.pubmedcentral.nih.gov/articlerender.fcgi?artid=PMC2830711.

[70] Alberto Ciccia, Chen Ling, Rachel Coulthard, Zhijiang Yan, Yutong Xue, Amom Ruhikanta Meetei, El Houari Laghmani, Hans Joenje, Neil McDonald, Johan P. de Winter, Weidong Wang, and Stephen C. West. Identification of FAAP24, a Fanconi Anemia Core Complex Protein that Interacts with FANCM. *Mol. Cell*, 25(3):331–343, feb 2007. ISSN 1097-2765. doi: 10.1016/J.MOLCEL.2007.01.003. URL https://www.sciencedirect.com/science/article/pii/S109727650700007X.

[71] Min Huang, Jung Min Kim, Bunsyo Shiotani, Kailin Yang, Lee Zou, and Alan D. D'Andrea. The FANCM/FAAP24 Complex Is Required for the DNA Interstrand Crosslink-Induced Checkpoint Response. *Mol. Cell*, 39(2):259–268, jul 2010. ISSN 1097-2765. doi: 10.1016/J.MOLCEL.2010.07.005. URL https://www.sciencedirect.com/science/article/pii/S1097276510005277.

[72] Thiyam Ramsing Singh, Dorina Saro, Abdullah Mahmood Ali, Xiao-Feng Zheng, Chang-hu Du, Michael W. Killen, Aristidis Sachpatzidis, Kebola Wahengbam, Andrew J. Pierce, Yong Xiong, Patrick Sung, and Amom Ruhikanta Meetei. MHF1-MHF2, a Histone-Fold-Containing Protein Complex, Participates in the Fanconi Anemia Pathway via FANCM. *Mol. Cell*, 37(6):879–886, mar 2010. ISSN 10972765. doi: 10.1016/j.molcel.2010.01.036. URL http://www.ncbi.nlm.nih.gov/pubmed/20347429http://www.pubmedcentral.nih.gov/articlerender.fcgi?artid=PMC2848122http://linkinghub.elsevier.com/retrieve/pii/S1097276510001553.

[73] Nobuko Matsushita, Hiroyuki Kitao, Masamichi Ishiai, Naoki Nagashima, Seiki Hirano, Katsuya Okawa, Tomohiko Ohta, David S. Yu, Peter J. McHugh, Ian D. Hickson, Ashok R. Venkitaraman, Hitoshi Kurumizaka, and Minoru Takata. A FancD2-Monoubiquitin Fusion Reveals Hidden Functions of Fanconi Anemia Core Complex in DNA Repair. *Mol. Cell*, 19(6):841–847, sep 2005. ISSN 10972765. doi: 10.1016/j.molcel.2005.08.018. URL http://www.ncbi.nlm.nih.gov/pubmed/16168378http://linkinghub.elsevier.com/retrieve/pii/S1097276505015601.

[74] Ashley E Sims, Elizabeth Spiteri, Robert J Sims, Adriana G Arita, Francis P Lach, Thomas Landers, Melanie Wurm, Marcel Freund, Kornelia Neveling, Helmut Hanenberg, Arleen D Auerbach, and Tony T Huang. FANCI is a second monoubiquitinated member of the Fanconi anemia pathway. *Nat. Struct. Mol. Biol.*, 14(6):564–567, jun 2007. ISSN 1545-9993. doi: 10.1038/nsmb1252. URL http://www.ncbi.nlm.nih.gov/pubmed/17460694http://www.nature.com/articles/nsmb1252.

[75] Agata Smogorzewska, Shuhei Matsuoka, Patrizia Vinciguerra, E. Robert McDonald, Kristen E. Hurov, Ji Luo, Bryan A. Ballif, Steven P. Gygi, Kay Hofmann, Alan D. D'Andrea, and Stephen J. Elledge. Identification of the FANCI Protein, a Monoubiquitinated FANCD2 Paralog Required for DNA Repair. *Cell*, 129(2):289–301, apr 2007. ISSN 00928674. doi: 10.1016/j.cell.2007.03.009. URL http://www.ncbi.nlm.nih.gov/pubmed/17412408http://www.pubmedcentral.nih.gov/articlerender.fcgi?artid=PMC2175179http://linkinghub.elsevier.com/retrieve/pii/S0092867407003200.

[76] Kelly E. Cybulski and Niall G. Howlett. FANCP/SLX4. *Cell Cycle*, 10(11):1757–1763, jun 2011. ISSN 1538-4101. doi: 10.4161/cc.10.11.15818. URL http://www.ncbi.nlm.nih.gov/pubmed/21527828http://www.pubmedcentral.nih.gov/articlerender.fcgi?artid=PMC3142459http://www.tandfonline.com/doi/abs/10.4161/cc.10.11.15818.

[77] K. N. Yamamoto, S. Kobayashi, M. Tsuda, H. Kurumizaka, M. Takata, K. Kono, J. Jiricny, S. Takeda, and K. Hirota. Involvement of SLX4 in interstrand cross-link repair is regulated by the Fanconi anemia pathway. *Proc. Natl. Acad. Sci.*, 108(16):6492–6496, 2011. ISSN 0027-8424. doi: 10.1073/pnas.1018487108. URL http://www.pnas.org/cgi/doi/10.1073/pnas.1018487108.

[78] Daisy Klein Douwel, Rick A C M Boonen, David T Long, Anna A Szypowska, Markus Räschle, Johannes C Walter, and Puck Knipscheer. XPF-ERCC1 acts in Unhooking DNA interstrand crosslinks in cooperation with FANCD2 and FANCP/SLX4. *Mol. Cell*, 54(3):460–71, may 2014. ISSN 1097-4164. doi: 10.1016/j.molcel.2014.03.015. URL http://www.ncbi.nlm.nih.gov/pubmed/24726325http://www.pubmedcentral.nih.gov/articlerender.fcgi?artid=PMC5067070.

[79] Hyungjin Kim and Alan D D'Andrea. Regulation of DNA cross-link repair by the Fanconi anemia/BRCA pathway. *Genes Dev.*, 26(13):1393–408, jul 2012. ISSN 1549-5477. doi: 10.1101/gad.195248.112. URL http://www.ncbi.nlm.nih.gov/pubmed/22751496http://www.pubmedcentral.nih.gov/articlerender.fcgi?artid=PMC3403008.

[80] Juan I Garaycoechea, K J Patel, I Arvidsson, B Jacobsson, E Hellström-Lindberg, R Hast, and S E Jacobsen. Why does the bone marrow fail in Fanconi anemia? *Blood*, 123(1):26–34, jan 2014. ISSN 1528-0020. doi: 10.1182/blood-2013-09-427740. URL http://www.ncbi.nlm.nih.gov/pubmed/10979941http://www.ncbi.nlm.nih.gov/pubmed/24200684.

[81] Helen Walden and Andrew J. Deans. The Fanconi Anemia DNA Repair Pathway: Structural and Functional Insights into a Complex Disorder. *Annu. Rev. Biophys.*, 43(1):257–278, may 2014. ISSN 1936-122X. doi: 10.1146/annurev-biophys-051013-022737. URL http://www.annualreviews.org/doi/10.1146/annurev-biophys-051013-022737.

[82] Hongbin Dong, Daniel W Nebert, Elspeth A Bruford, David C Thompson, Hans Joenje, and Vasilis Vasiliou. Update of the human and mouse Fanconi anemia genes. *Hum. Genomics*, 9:32, nov 2015. ISSN 1479-7364. doi: 10.1186/s40246-015-0054-y. URL http://www.ncbi.nlm.nih.gov/pubmed/26596371http://www.pubmedcentral.nih.gov/articlerender.fcgi?artid=PMC4657327.

[83] Philip S. Rosenberg, Hannah Tamary, and Blanche P. Alter. How high are carrier frequencies of rare recessive syndromes? Contemporary estimates for Fanconi Anemia in the United States and Israel. *Am. J. Med. Genet. Part A*, 155(8):1877–1883, aug 2011. ISSN 15524825. doi: 10.1002/ajmg.a.34087. URL http://www.ncbi.nlm.nih.gov/pubmed/21739583http://www.pubmedcentral.nih.gov/articlerender.fcgi?artid=PMC3140593http://doi.wiley.com/10.1002/ajmg.a.34087.

[84] Alan D. D'Andrea. Susceptibility Pathways in Fanconi's Anemia and Breast Cancer. *N. Engl. J. Med.*, 362(20):1909–1919, may 2010. ISSN 0028-4793. doi: 10.1056/NEJMra0809889. URL http://www.ncbi.nlm.nih.gov/pubmed/20484397http://www.pubmedcentral.nih.gov/articlerender.fcgi?artid=PMC3069698http://www.nejm.org/doi/10.1056/NEJMra0809889.

[85] Christopher. Walsh. *Posttranslational modification of proteins : expanding nature's inventory*. Roberts and Co. Publishers, 2006. ISBN 0974707732. URL https://books.google.ch/books?hl=de{&}lr={&}id=JGBfQXIzdwgC{&}oi=fnd{&}pg=PR15{&}dq=protein+isomerization+posttranslational+modification{&}ots=v8SCA-{_}qRP{&}sig=ess18FGGxP98OpA1cb6qSIDbBTI{#}v=onepage{&}q=proteinisomerizationposttranslationalmodification{&}f=false.

[86] George A. Khoury, Richard C. Baliban, and Christodoulos A. Floudas. Proteome-wide post-translational modification statistics: frequency analysis and curation of the swiss-prot database. *Sci. Rep.*, 1(1):90, dec 2011. ISSN 2045-2322. doi: 10.1038/srep00090. URL http://www.nature.com/articles/srep00090.

[87] Sudhakaran Prabakaran, Guy Lippens, Hanno Steen, and Jeremy Gunawardena. Post-translational modification: nature's escape from genetic imprisonment and the basis for dynamic information encoding. *Wiley Interdiscip. Rev. Syst. Biol. Med.*, 4(6):565–583, nov 2012. ISSN 19395094. doi: 10.1002/wsbm.1185. URL http://www.ncbi.nlm.nih.gov/pubmed/22899623http://www.pubmedcentral.nih.gov/articlerender.fcgi?artid=PMC3473174http://doi.wiley.com/10.1002/wsbm.1185.

[88] Ivo A. Hendriks and Alfred C. O. Vertegaal. A comprehensive compilation of SUMO proteomics. *Nat. Rev. Mol. Cell Biol.*, 17(9):581–595, sep 2016. ISSN 1471-0072. doi: 10.1038/nrm.2016.81. URL http://www.nature.com/articles/nrm.2016.81.

[89] Michael Rape. Ubiquitylation at the crossroads of development and disease. *Nat. Rev. Mol. Cell Biol.*, 19(1):59–70, sep 2017. ISSN 1471-0072. doi: 10.1038/nrm.2017.83. URL http://www.nature.com/doifinder/10.1038/nrm.2017.83.

[90] X Z Zhou, P J Lu, G Wulf, and K P Lu. Phosphorylation-dependent prolyl isomerization: a novel signaling regulatory mechanism. *Cell. Mol. Life Sci.*, 56(9-10):788–806, nov 1999. ISSN 1420-682X. URL http://www.ncbi.nlm.nih.gov/pubmed/11212339.

[91] Philip Cohen. The origins of protein phosphorylation. *Nat. Cell Biol.*, 4(5):E127–E130, may 2002. ISSN 1465-7392. doi: 10.1038/ncb0502-e127. URL http://www.ncbi.nlm.nih.gov/pubmed/11988757http://www.nature.com/articles/ncb0502-e127.

[92] Matthias Mann, Shao-En Ong, Mads Grønborg, Hanno Steen, Ole N. Jensen, and Akhilesh Pandey. Analysis of protein phosphorylation using mass spectrometry: deciphering the phosphoproteome. *Trends Biotechnol.*, 20(6):261–268, jun 2002. ISSN 0167-7799. doi: 10.1016/S0167-7799(02)01944-3. URL https://www.sciencedirect.com/science/article/pii/S0167779902019443?via{%}3Dihub.

[93] Louise N. Johnson* And and Richard J. Lewis. Structural Basis for Control by Phosphorylation. 2001. doi: 10.1021/CR000225S. URL https://pubs.acs.org/doi/abs/10.1021/cr000225s.

[94] S. Arena, S. Benvenuti, and A. Bardelli. Genetic analysis of the kinome and phosphatome in cancer. *Cell. Mol. Life Sci.*, 62(18):2092–2099, sep 2005. ISSN 1420-682X. doi: 10.1007/s00018-005-5205-1. URL http://www.ncbi.nlm.nih.gov/pubmed/16132230http://link.springer.com/10.1007/s00018-005-5205-1.

[95] G. Manning, D B Whyte, R Martinez, T Hunter, and S Sudarsanam. The Protein Kinase Complement of the Human Genome. *Science (80-.).*, 298(5600):1912–1934, dec 2002. ISSN 00368075. doi: 10.1126/science.1075762. URL http://www.ncbi.nlm.nih.gov/pubmed/12471243http://www.sciencemag.org/cgi/doi/10.1126/science.1075762.

[96] Alberto Ciccia and Stephen J. Elledge. The DNA Damage Response: Making It Safe to Play with Knives. *Mol. Cell*, 40(2):179–204, oct 2010. ISSN 1097-2765. doi: 10.1016/J.MOLCEL.2010.09.019. URL https://www.sciencedirect.com/science/article/pii/S1097276510007471?via{%}3Dihub.

[97] Yingying Guo, Wanjuan Feng, Shirley M H Sy, and Michael S Y Huen. ATM-dependent Phosphorylation of the Fanconi Anemia Protein PALB2 Promotes the DNA Damage Response. *J. Biol. Chem.*, 290(46):27545–56, nov 2015. ISSN 1083-351X. doi: 10.1074/jbc.M115.672626. URL http://www.ncbi.nlm.nih.gov/pubmed/26420486http://www.pubmedcentral.nih.gov/articlerender.fcgi?artid=PMC4646007.

[98] Tomoko Shigechi, Junya Tomida, Koichi Sato, Masahiko Kobayashi, John K Eykelenboom, Fabio Pessina, Yanbin Zhang, Emi Uchida, Masamichi Ishiai, Noel F Lowndes, Kenichi Yamamoto, Hitoshi Kurumizaka, Yoshihiko Maehara, and Minoru Takata. ATR-ATRIP kinase complex triggers activation of the Fanconi anemia DNA repair pathway. *Cancer Res.*, 72(5):1149–56, mar 2012. ISSN 1538-7445. doi: 10.1158/0008-5472.CAN-11-2904. URL http://www.ncbi.nlm.nih.gov/pubmed/22258451.

[99] Toshiyasu Taniguchi, Irene Garcia-Higuera, Bo Xu, Paul R. Andreassen, Richard C. Gregory, Seong-Tae Kim, William S. Lane, Michael B. Kastan, and Alan D. D'Andrea. Convergence of the Fanconi Anemia and Ataxia Telangiectasia Signaling Pathways. *Cell*, 109(4):459–472, may 2002. ISSN 0092-8674. doi: 10.1016/S0092-8674(02)00747-X. URL https://www.sciencedirect.com/science/article/pii/S009286740200747X.

[100] Kun Ping Lu and Xiao Zhen Zhou. The prolyl isomerase PIN1: a pivotal new twist in phosphorylation signalling and disease. *Nat. Rev. Mol. Cell Biol.*, 8(11):904–916, nov 2007. ISSN 1471-0072. doi: 10.1038/nrm2261. URL http://www.nature.com/articles/nrm2261.

[101] A H McKee and N Kleckner. A general method for identifying recessive diploid-specific mutations in Saccharomyces cerevisiae, its application to the isolation of mutants blocked at intermediate stages of meiotic prophase and characterization of a new gene SAE2. *Genetics*, 146(3):797–816, jul 1997. ISSN 0016-6731. URL http://www.ncbi.nlm.nih.gov/pubmed/9215888http://www.pubmedcentral.nih.gov/articlerender.fcgi?artid=PMC1208052.

[102] S Prinz, A Amon, and F Klein. Isolation of COM1, a new gene required to complete meiotic double-strand break-induced recombination in Saccharomyces cerevisiae. *Genetics*, 146(3):781–95, jul 1997. ISSN 0016-6731. URL http://www.ncbi.nlm.nih.gov/pubmed/9215887http://www.pubmedcentral.nih.gov/articlerender.fcgi?artid=PMC1208051.

[103] Phang-Lang Chen, Feng Liu, Suna Cai, Xiaoqin Lin, Aihua Li, Yumay Chen, Bingnan Gu, Eva Y-H P Lee, and Wen-Hwa Lee. Inactivation of CtIP leads to early embryonic lethality mediated by G1 restraint and to tumorigenesis by haploid insufficiency. *Mol. Cell. Biol.*, 25(9):3535–42, may 2005. ISSN 0270-7306. doi: 10.1128/MCB.25.9.3535-3542.2005. URL http://mcb.asm.org/cgi/doi/10.1128/MCB.25.9.3535-3542.2005http://www.ncbi.nlm.nih.gov/pubmed/15831459http://www.pubmedcentral.nih.gov/articlerender.fcgi?artid=PMC1084307.

[104] Oliver Limbo, Charly Chahwan, Yoshiki Yamada, Robertus A M de Bruin, Curt Wittenberg, and Paul Russell. Ctp1 is a cell-cycle-regulated protein that functions with Mre11 complex to control double-strand break repair by homologous recombination. *Mol. Cell*, 28(1):134–46, oct 2007. ISSN 1097-2765. doi: 10.1016/j.molcel.2007.09.009. URL http://www.ncbi.nlm.nih.gov/pubmed/17936710http://www.pubmedcentral.nih.gov/articlerender.fcgi?artid=PMC2066204.

[105] Alexandra Penkner, Zsuzsanna Portik-Dobos, Lois Tang, Ralf Schnabel, Maria Novatchkova, Verena Jantsch, and Josef Loidl. A conserved function for a Caenorhabditis elegans Com1/Sae2/CtIP protein homolog in meiotic recombination. *EMBO J.*, 26(24):5071–5082, dec 2007. ISSN 0261-4189. doi: 10.1038/sj.emboj.7601916. URL http://www.ncbi.nlm.nih.gov/pubmed/18007596http://www.pubmedcentral.nih.gov/articlerender.fcgi?artid=PMC2140103http://emboj.embopress.org/cgi/doi/10.1038/sj.emboj.7601916.

[106] Clemens Uanschou, Tanja Siwiec, Andrea Pedrosa-Harand, Claudia Kerzendorfer, Eugenio Sanchez-Moran, Maria Novatchkova, Svetlana Akimcheva, Alexander Woglar, Franz Klein, and Peter Schlögelhofer. A novel plant gene essential for meiosis is related to the human CtIP and the yeast COM1/SAE2 gene. *EMBO J.*, 26(24):5061–5070, dec 2007. ISSN 0261-4189. doi: 10.1038/sj.emboj.7601913. URL http://www.ncbi.nlm.nih.gov/pubmed/18007598http://www.pubmedcentral.nih.gov/articlerender.fcgi?artid=PMC2140101http://emboj.embopress.org/cgi/doi/10.1038/sj.emboj.7601913.

[107] Sara N Andres, C Denise Appel, James W Westmoreland, Jessica S Williams, Yvonne Nguyen, Patrick D Robertson, Michael A Resnick, and R Scott Williams. Tetrameric Ctp1 coordinates DNA binding and DNA bridging in DNA double-strand-break repair. *Nat. Struct. {&} Mol. Biol.*, 22(2):158–166, feb 2015.

[108] Owen R Davies, Josep V Forment, Meidai Sun, Rimma Belotserkovskaya, Julia Coates, Yaron Galanty, Mukerrem Demir, Christopher R Morton, Neil J Rzechorzek, Stephen P Jackson, and Luca Pellegrini. CtIP tetramer assembly is required for DNA-end resection and repair. *Nat. Struct. {&} Mol. Biol.*, 22(2):150–157, feb 2015.

[109] Hailong Wang, Zhengping Shao, Linda Z. Shi, Patty Yi-Hwa Hwang, Lan N. Truong, Michael W. Berns, David J. Chen, and Xiaohua Wu. CtIP Protein Dimerization Is Critical for Its Recruitment to Chromosomal DNA Double-stranded Breaks. *J. Biol. Chem.*, 287(25):21471–21480, jun 2012. ISSN 0021-9258. doi: 10.1074/jbc.M112.355354. URL http://www.ncbi.nlm.nih.gov/pubmed/22544744http://www.pubmedcentral.nih.gov/articlerender.fcgi?artid=PMC3375568http://www.jbc.org/lookup/doi/10.1074/jbc.M112.355354.

[110] Hailong Wang, Linda Z. Shi, Catherine C. L. Wong, Xuemei Han, Patty Yi-Hwa Hwang, Lan N. Truong, Qingyuan Zhu, Zhengping Shao, David J. Chen, Michael W. Berns, John R. Yates, Longchuan Chen, and Xiaohua Wu. The Interaction of CtIP and Nbs1 Connects CDK and ATM to Regulate HR–Mediated Double-Strand Break Repair. *PLoS Genet.*, 9(2):e1003277, feb 2013. ISSN 1553-7404. doi: 10.1371/journal.pgen.1003277. URL http://www.ncbi.nlm.nih.gov/pubmed/23468639http://www.pubmedcentral.nih.gov/articlerender.fcgi?artid=PMC3585124http://dx.plos.org/10.1371/journal.pgen.1003277.

[111] K P Hopfner, A Karcher, L Craig, T T Woo, J P Carney, and J A Tainer. Structural biochemistry and interaction architecture of the DNA double-strand break repair Mre11 nuclease and Rad50-ATPase. *Cell*, 105(4):473–85, may 2001. ISSN 0092-8674. URL http://www.ncbi.nlm.nih.gov/pubmed/11371344.

[112] J.-H. Lee and Tanya T Paull. ATM Activation by DNA Double-Strand Breaks Through the Mre11-Rad50-Nbs1 Complex. *Science (80-.).*, 308(5721):551–554, apr 2005. ISSN 0036-8075. doi: 10.1126/science.1108297. URL http://www.ncbi.nlm.nih.gov/pubmed/15790808http://www.sciencemag.org/cgi/doi/10.1126/science.1108297.

[113] R. Scott Williams, Gabriel Moncalian, Jessica S. Williams, Yoshiki Yamada, Oliver Limbo, David S. Shin, Lynda M. Groocock, Dana Cahill, Chiharu Hitomi, Grant Guenther, Davide Moiani, James P. Carney, Paul Russell, and John A. Tainer. Mre11 Dimers Coordinate DNA End Bridging and Nuclease Processing in Double-Strand-Break Repair. *Cell*, 135(1):97–109, oct 2008. ISSN 00928674. doi: 10.1016/j.cell.2008.08.017. URL http://www.ncbi.nlm.nih.gov/pubmed/18854158http://www.pubmedcentral.nih.gov/articlerender.fcgi?artid=PMC2681233http://linkinghub.elsevier.com/retrieve/pii/S0092867408010623.

[114] Julien Lafrance-Vanasse, Gareth J. Williams, and John A. Tainer. Envisioning the dynamics and flexibility of Mre11-Rad50-Nbs1 complex to decipher its roles in DNA replication and repair. *Prog. Biophys. Mol. Biol.*, 117(2-3):182–193, mar 2015. ISSN 0079-6107. doi: 10.1016/J.PBIOMOLBIO.2014.12.004. URL https://www.sciencedirect.com/science/article/pii/S0079610714001898.

[115] R Scott Williams, Gerald E Dodson, Oliver Limbo, Yoshiki Yamada, Jessica S Williams, Grant Guenther, Scott Classen, J N Mark Glover, Hiroshi Iwasaki, Paul Russell, and John A Tainer. Nbs1 flexibly tethers Ctp1 and Mre11-Rad50 to coordinate DNA double-strand break processing and repair. *Cell*, 139(1):87–99, oct 2009. ISSN 1097-4172. doi: 10.1016/j.cell.2009.07.033. URL http://www.ncbi.nlm.nih.gov/pubmed/19804755http://www.pubmedcentral.nih.gov/articlerender.fcgi?artid=PMC2762657.

[116] Zhongsheng You, Linda Z. Shi, Quan Zhu, Peng Wu, You-Wei Zhang, Andrew Basilio, Nina Tonnu, Inder M. Verma, Michael W. Berns, and Tony Hunter. CtIP Links DNA Double-Strand Break Sensing to Resection. *Mol. Cell*, 36(6):954–969, dec 2009. ISSN 10972765. doi: 10.1016/j.molcel.2009.12.002. URL http://www.ncbi.nlm.nih.gov/pubmed/20064462http://www.pubmedcentral.nih.gov/articlerender.fcgi?artid=PMC2807415http://linkinghub.elsevier.com/retrieve/pii/S1097276509009058.

[117] R. Scott Williams, Jessica S. Williams, and John A. Tainer. Mre11–Rad50–Nbs1 is a keystone complex connecting DNA repair machinery, double-strand break signaling, and the chromatin templateThis paper is one of a selection of papers published in this Special Issue, entitled 28th International West Coast Chromatin a. *Biochem. Cell Biol.*, 85(4):509–520, aug 2007. ISSN 0829-8211. doi: 10.1139/O07-069. URL http://www.nrcresearchpress.com/doi/10.1139/O07-069.

[118] G Luo, M S Yao, C F Bender, M Mills, A R Bladl, A Bradley, and J H Petrini. Disruption of mRad50 causes embryonic stem cell lethality, abnormal embryonic development, and sensitivity to ionizing radiation. *Proc. Natl. Acad. Sci. U. S. A.*, 96(13):7376–81, jun 1999. ISSN 0027-8424. doi: 10.1073/PNAS.96.13.7376. URL http://www.ncbi.nlm.nih.gov/pubmed/10377422http://www.pubmedcentral.nih.gov/articlerender.fcgi?artid=PMC22093.

[119] Y Xiao and D T Weaver. Conditional gene targeted deletion by Cre recombinase demonstrates the requirement for the double-strand break repair Mre11 protein in murine embryonic stem cells. *Nucleic Acids Res.*, 25(15):2985–91, aug 1997. ISSN 0305-1048. URL http://www.ncbi.nlm.nih.gov/pubmed/9224597http://www.pubmedcentral.nih.gov/articlerender.fcgi?artid=PMC146850.

[120] Jie Zhu, Simone Petersen, Lino Tessarollo, and André Nussenzweig. Targeted disruption of the Nijmegen breakage syndrome gene NBS1 leads to early embryonic lethality in mice. *Curr. Biol.*, 11(2):105–109, jan 2001. ISSN 0960-9822. doi: 10.1016/S0960-9822(01)00019-7. URL https://www.sciencedirect.com/science/article/pii/S0960982201000197.

[121] Chloe Girard, Baptiste Roelens, Karl A Zawadzki, and Anne M Villeneuve. Interdependent and separable functions of Caenorhabditis elegans MRN-C complex members couple formation and repair of meiotic DSBs. *Proc. Natl. Acad. Sci. U. S. A.*, 115(19):E4443–E4452, may 2018. ISSN 1091-6490. doi: 10.1073/pnas.1719029115. URL http://www.ncbi.nlm.nih.gov/pubmed/29686104http://www.pubmedcentral.nih.gov/articlerender.fcgi?artid=PMC5948970.

[122] Jeffrey Buis, Yipin Wu, Yibin Deng, Jennifer Leddon, Gerwin Westfield, Mark Eckersdorff, JoAnn M. Sekiguchi, Sandy Chang, and David O. Ferguson. Mre11 Nuclease Activity Has Essential Roles in DNA Repair and Genomic Stability Distinct from ATM Activation. *Cell*, 135(1):85–96, oct 2008. ISSN 0092-8674. doi: 10.1016/J.CELL.2008.08.015. URL https://www.sciencedirect.com/science/article/pii/S0092867408010234.

[123] Huan Chen, Roberto A Donnianni, Naofumi Handa, Sarah K Deng, Julyun Oh, Leonid A Timashev, Stephen C Kowalczykowski, and Lorraine S Symington. Sae2 promotes DNA damage resistance by removing the Mre11-Rad50-Xrs2 complex from DNA and attenuating Rad53 signaling. *Proc. Natl. Acad. Sci. U. S. A.*, 112(15):E1880–7, apr 2015. ISSN 1091-6490. doi: 10.1073/pnas.1503331112. URL http://www.ncbi.nlm.nih.gov/pubmed/25831494http://www.pubmedcentral.nih.gov/articlerender.fcgi?artid=PMC4403154.

[124] Eleni P Mimitou and Lorraine S Symington. Ku prevents Exo1 and Sgs1-dependent resection of DNA ends in the absence of a functional MRX complex or Sae2. *EMBO J.*, 29(19):3358–69, oct 2010. ISSN 1460-2075. doi: 10.1038/emboj.2010.193. URL http://www.ncbi.nlm.nih.gov/pubmed/20729809http://www.pubmedcentral.nih.gov/articlerender.fcgi?artid=PMC2957202.

[125] Federica Polato, Elsa Callen, Nancy Wong, Robert Faryabi, Samuel Bunting, Hua-Tang Chen, Marina Kozak, Michael J Kruhlak, Colleen R Reczek, Wen-Hwa Lee, Thomas Ludwig, Richard Baer, Lionel Feigenbaum, Stephen Jackson, and André Nussenzweig. CtIP-mediated resection is essential for viability and can operate independently of BRCA1. *J. Exp. Med.*, 211(6):1027–36, jun 2014. ISSN 1540-9538. doi: 10.1084/jem.20131939. URL http://www.ncbi.nlm.nih.gov/pubmed/24842372http://www.pubmedcentral.nih.gov/articlerender.fcgi?artid=PMC4042650.

[126] James M. Daley, Judit Jimenez-Sainz, Weibin Wang, Adam S. Miller, Xiaoyu Xue, Kevin A. Nguyen, Ryan B. Jensen, and Patrick Sung. Enhancement of BLM-DNA2-Mediated Long-Range DNA End Resection by CtIP. *Cell Rep.*, 21(2):324–332, oct 2017. ISSN 2211-1247. doi: 10.1016/J.CELREP.2017.09.048. URL https://www.sciencedirect.com/science/article/pii/S2211124717313384?via{%}3Dihub.

[127] Wassim Eid, Martin Steger, Mahmoud El-Shemerly, Lorenza P Ferretti, Javier Peña-Diaz, Christiane König, Emanuele Valtorta, Alessandro A Sartori, and Stefano Ferrari. DNA end resection by CtIP and exonuclease 1 prevents genomic instability. *EMBO Rep.*, 11(12):962–8, dec 2010. ISSN 1469-3178. doi: 10.1038/embor.2010.157. URL http://www.ncbi.nlm.nih.gov/pubmed/21052091http://www.pubmedcentral.nih.gov/articlerender.fcgi?artid=PMC2999859.

[128] Hailong Wang, Zhengping Shao, Linda Z. Shi, Patty Yi-Hwa Hwang, Lan N. Truong, Michael W. Berns, David J. Chen, and Xiaohua Wu. CtIP Protein Dimerization Is Critical for Its Recruitment to Chromosomal DNA Double-stranded Breaks. *J. Biol. Chem.*, 287(25):21471–21480, jun 2012. ISSN 0021-9258. doi: 10.1074/jbc.M112.355354. URL http://www.jbc.org/lookup/doi/10.1074/jbc.M112.355354.

[129] Manu J Dubin, Philippa H Stokes, Eleanor Y M Sum, R Scott Williams, Valentina A Valova, Phillip J Robinson, Geoffrey J Lindeman, J N Mark Glover, Jane E Visvader, and Jacqueline M Matthews. Dimerization of CtIP, a BRCA1- and CtBP-interacting protein, is mediated by an N-terminal coiled-coil motif. *J. Biol. Chem.*, 279(26):26932–8, jun 2004. ISSN 0021-9258. doi: 10.1074/jbc.M313974200. URL http://www.ncbi.nlm.nih.gov/pubmed/15084581.

[130] M Charpentier, A H Y Khedher, S Menoret, A Brion, K Lamribet, E Dardillac, C Boix, L Perrouault, L Tesson, S Geny, A De Cian, J M Itier, I Anegon, B Lopez, C Giovannangeli, and J P Concordet. CtIP fusion to Cas9 enhances transgene integration by homology-dependent repair. *Nat. Commun.*, 9(1):1133, mar 2018. doi: 10.1038/s41467-018-03475-7. URL http://www.ncbi.nlm.nih.gov/pubmed/29556040.

[131] Eleni P Mimitou and Lorraine S Symington. Nucleases and helicases take center stage in homologous recombination. *Trends Biochem. Sci.*, 34(5):264–272, may 2009.

[132] Per Qvist, Pablo Huertas, Sonia Jimeno, Mette Nyegaard, Muhammad J. Hassan, Stephen P. Jackson, and Anders D. Børglum. CtIP Mutations Cause Seckel and Jawad Syndromes. *PLoS Genet.*, 7(10):e1002310, oct 2011. ISSN 1553-7404. doi: 10.1371/journal.pgen.1002310. URL http://www.ncbi.nlm.nih.gov/pubmed/21998596http://www.pubmedcentral.nih.gov/articlerender.fcgi?artid=PMC3188555http://dx.plos.org/10.1371/journal.pgen.1002310.

[133] Pablo Huertas, Felipe Cortés-Ledesma, Alessandro A. Sartori, Andrés Aguilera, and Stephen P. Jackson. CDK targets Sae2 to control DNA-end resection and homologous recombination. *Nature*, 455(7213):689–692, oct 2008. ISSN 0028-0836. doi: 10.1038/nature07215. URL http://www.nature.com/doifinder/10.1038/nature07215.

[134] Pablo Huertas and Stephen P Jackson. Human CtIP mediates cell cycle control of DNA end resection and double strand break repair. *J. Biol. Chem.*, 284(14):9558–65, apr 2009. ISSN 0021-9258. doi: 10.1074/jbc.M808906200. URL http://www.jbc.org/lookup/doi/10.1074/jbc.M808906200http://www.ncbi.nlm.nih.gov/pubmed/19202191http://www.pubmedcentral.nih.gov/articlerender.fcgi?artid=PMC2666608.

[135] Martin Steger, Olga Murina, Daniela Hühn, Lorenza P Ferretti, Reto Walser, Kay Hänggi, Lorenzo Lafranchi, Christine Neugebauer, Shreya Paliwal, Pavel Janscak, Bertran Gerrits, Giannino Del Sal, Oliver Zerbe, and Alessandro A Sartori. Prolyl isomerase PIN1 regulates DNA double-strand break repair by counteracting DNA end resection. *Mol. Cell*, 50(3):333–343, may 2013.

[136] Elda Cannavo and Petr Cejka. Sae2 promotes dsDNA endonuclease activity within Mre11-Rad50-Xrs2 to resect DNA breaks. *Nature*, 514(7520):122–5, oct 2014. ISSN 1476-4687. doi: 10.1038/nature13771. URL http://dx.doi.org/10.1038/nature13771.

[137] Edgar Hartsuiker, Matthew J. Neale, and Antony M. Carr. Distinct Requirements for the Rad32Mre11 Nuclease and Ctp1CtIP in the Removal of Covalently Bound Topoisomerase I and II from DNA. *Mol. Cell*, 33(1):

117–123, jan 2009. ISSN 10972765. doi: 10.1016/j.molcel.2008.11.021. URL http://www.ncbi.nlm.nih.gov/pubmed/19150433http://www.pubmedcentral.nih.gov/articlerender.fcgi?artid=PMC2675033http://linkinghub.elsevier.com/retrieve/pii/S109727650800854X.

[138] Bettina M Lengsfeld, Alison J Rattray, Venugopal Bhaskara, Rodolfo Ghirlando, and Tanya T Paull. Sae2 is an endonuclease that processes hairpin DNA cooperatively with the Mre11/Rad50/Xrs2 complex. *Mol. Cell*, 28(4): 638–651, nov 2007.

[139] Nodar Makharashvili, Anthony T. Tubbs, Soo-Hyun Yang, Hailong Wang, Olivia Barton, Yi Zhou, Rajashree A. Deshpande, Ji-Hoon Lee, Markus Lobrich, Barry P. Sleckman, Xiaohua Wu, and Tanya T. Paull. Catalytic and Noncatalytic Roles of the CtIP Endonuclease in Double-Strand Break End Resection. *Mol. Cell*, 54(6):1022–1033, jun 2014. ISSN 10972765. doi: 10.1016/j.molcel.2014.04.011. URL http://www.ncbi.nlm.nih.gov/pubmed/24837676http://www.pubmedcentral.nih.gov/articlerender.fcgi?artid=PMC4079050http://linkinghub.elsevier.com/retrieve/pii/S1097276514003220.

[140] Hailong Wang, Yongjiang Li, Lan N. Truong, Linda Z. Shi, Patty Yi-Hwa Hwang, Jing He, Johnny Do, Michael Jeffrey Cho, Hongzhi Li, Alejandro Negrete, Joseph Shiloach, Michael W. Berns, Binghui Shen, Longchuan Chen, and Xiaohua Wu. CtIP Maintains Stability at Common Fragile Sites and Inverted Repeats by End Resection-Independent Endonuclease Activity. *Mol. Cell*, 54(6):1012–1021, jun 2014. ISSN 10972765. doi: 10.1016/j.molcel.2014.04.012. URL http://www.ncbi.nlm.nih.gov/pubmed/24837675http://www.pubmedcentral.nih.gov/articlerender.fcgi?artid=PMC4105207http://linkinghub.elsevier.com/retrieve/pii/S1097276514003232.

[141] Nodar Makharashvili and Tanya T Paull. CtIP: A DNA damage response protein at the intersection of DNA metabolism. *DNA Repair (Amst).*, 32:75–81, jul 2015.

[142] Steven Raynard, Hengyao Niu, and Patrick Sung. DNA double-strand break processing: the beginning of the end. *Genes Dev.*, 22(21):2903–7, nov 2008. ISSN 0890-9369. doi: 10.1101/gad.1742408. URL http://www.ncbi.nlm.nih.gov/pubmed/18981468http://www.pubmedcentral.nih.gov/articlerender.fcgi?artid=PMC2751443.

[143] Michael Lisby, Jacqueline H. Barlow, Rebecca C. Burgess, and Rodney Rothstein. Choreography of the DNA Damage Response. *Cell*, 118(6):699–713, sep 2004. ISSN 00928674. doi: 10.1016/j.cell.2004.08.015. URL http://www.ncbi.nlm.nih.gov/pubmed/15369670http://linkinghub.elsevier.com/retrieve/pii/S0092867404007974.

[144] Fabio Puddu, Tobias Oelschlaegel, Ilaria Guerini, Nicola J Geisler, Hengyao Niu, Mareike Herzog, Israel Salguero, Bernardo Ochoa-Montaño, Emmanuelle Viré, Patrick Sung, David J Adams, Thomas M Keane, and Stephen P Jackson. Synthetic viability genomic screening defines Sae2 function in DNA repair. *EMBO J.*, 34(11):1509–22, jun 2015. ISSN 1460-2075. doi: 10.15252/embj.201590973. URL http://www.ncbi.nlm.nih.gov/pubmed/25899817http://www.pubmedcentral.nih.gov/articlerender.fcgi?artid=PMC4474527.

[145] Michela Clerici, Davide Mantiero, Giovanna Lucchini, and Maria Pia Longhese. The Saccharomyces cerevisiae Sae2 Protein Promotes Resection and Bridging of Double Strand Break Ends. *J. Biol. Chem.*, 280(46):38631–38638, nov 2005. ISSN 0021-9258. doi: 10.1074/jbc.M508339200. URL http://www.ncbi.nlm.nih.gov/pubmed/16162495http://www.jbc.org/lookup/doi/10.1074/jbc.M508339200.

[146] R. A. Deshpande, G. J. Williams, O. Limbo, R. S. Williams, J. Kuhnlein, J.-H. Lee, S. Classen, G. Guenther, P. Russell, J. A. Tainer, and T. T. Paull. ATP-driven Rad50 conformations regulate DNA tethering, end resection, and ATM checkpoint signaling. *EMBO J.*, 33(5):482–500, mar 2014. ISSN 0261-4189. doi: 10.1002/embj.201386100. URL http://www.ncbi.nlm.nih.gov/pubmed/24493214http://www.pubmedcentral.nih.gov/articlerender.fcgi?artid=PMC3989629http://emboj.embopress.org/cgi/doi/10.1002/embj.201386100.

[147] Min Zhu, Hongchang Zhao, Oliver Limbo, and Paul Russell. Mre11 complex links sister chromatids to promote repair of a collapsed replication fork. *Proc. Natl. Acad. Sci.*, page 201808189, aug 2018. ISSN 0027-8424. doi: 10.1073/pnas.1808189115. URL http://www.ncbi.nlm.nih.gov/pubmed/30104346http://www.pnas.org/lookup/doi/10.1073/pnas.1808189115.

[148] Janette Lloyd, J. Ross Chapman, Julie A. Clapperton, Lesley F. Haire, Edgar Hartsuiker, Jiejin Li, Antony M. Carr, Stephen P. Jackson, and Stephen J. Smerdon. A Supramodular FHA/BRCT-Repeat Architecture Mediates Nbs1 Adaptor Function in Response to DNA Damage. *Cell*, 139(1):100–111, oct 2009. ISSN 0092-8674. doi: 10.1016/J.CELL.2009.07.043. URL https://www.sciencedirect.com/science/article/pii/S0092867409009805.

[149] U Schaeper, T Subramanian, L Lim, J M Boyd, and G Chinnadurai. Interaction between a cellular protein that binds to the C-terminal region of adenovirus E1A (CtBP) and a novel cellular protein is disrupted by E1A through a conserved PLDLS motif. *J. Biol. Chem.*, 273(15):8549–52, apr 1998. ISSN 0021-9258. URL http://www.ncbi.nlm.nih.gov/pubmed/9535825.

[150] Carlo Fusco, Alexandre Reymond, and Antonis S Zervos. Molecular Cloning and Characterization of a Novel Retinoblastoma-Binding Protein. *Genomics*, 51(3):351–358, aug 1998. ISSN 08887543. doi: 10.1006/geno.1998.5368. URL http://www.ncbi.nlm.nih.gov/pubmed/9721205http://linkinghub.elsevier.com/retrieve/pii/S088875439895368X.

[151] P.-L. Chen, F. Liu, S. Cai, X. Lin, A. Li, Y. Chen, B. Gu, E. Y.-H. P. Lee, and W.-H. Lee. Inactivation of CtIP Leads to Early Embryonic Lethality Mediated by G1 Restraint and to Tumorigenesis by Haploid Insufficiency. *Mol. Cell. Biol.*, 25(9):3535–3542, may 2005. ISSN 0270-7306. doi: 10.1128/MCB.25.9.3535-3542.2005. URL http://www.ncbi.nlm.nih.gov/pubmed/15831459http://www.pubmedcentral.nih.gov/articlerender.fcgi?artid=PMC1084307http://mcb.asm.org/cgi/doi/10.1128/MCB.25.9.3535-3542.2005.

[152] F. Liu and W.-H. Lee. CtIP Activates Its Own and Cyclin D1 Promoters via the E2F/RB Pathway during G1/S Progression. *Mol. Cell. Biol.*, 26(8):3124–3134, apr 2006. ISSN 0270-7306. doi: 10.1128/MCB.26.8.3124-3134.2006. URL http://www.ncbi.nlm.nih.gov/pubmed/16581787http://www.pubmedcentral.nih.gov/articlerender.fcgi?artid=PMC1446954http://mcb.asm.org/cgi/doi/10.1128/MCB.26.8.3124-3134.2006.

[153] M. Wu, D. R. Soler, M. C. Abba, M. I. Nunez, R. Baer, C. Hatzis, A. Llombart-Cussac, A. Llombart-Bosch, and C. M. Aldaz. CtIP Silencing as a Novel Mechanism of Tamoxifen Resistance in Breast Cancer. *Mol. Cancer Res.*, 5(12):1285–1295, dec 2007. ISSN 1541-7786. doi: 10.1158/1541-7786.MCR-07-0126. URL http://www.ncbi.nlm.nih.gov/pubmed/18171986http://mcr.aacrjournals.org/cgi/doi/10.1158/1541-7786.MCR-07-0126.

[154] Shaun E. Peterson, Yinyin Li, Foon Wu-Baer, Brian T. Chait, Richard Baer, Hong Yan, Max E. Gottesman, and Jean Gautier. Activation of DSB Processing Requires Phosphorylation of CtIP by ATR. *Mol. Cell*, 49(4):657–667, feb 2013. ISSN 10972765. doi: 10.1016/j.molcel.2012.11.020. URL http://www.ncbi.nlm.nih.gov/pubmed/23273981http://www.pubmedcentral.nih.gov/articlerender.fcgi?artid=PMC3582837http://linkinghub.elsevier.com/retrieve/pii/S109727651200977X.

[155] Shaun E. Peterson, Yinyin Li, Foon Wu-Baer, Brian T. Chait, Richard Baer, Hong Yan, Max E. Gottesman, and Jean Gautier. Activation of DSB Processing Requires Phosphorylation of CtIP by ATR. *Mol. Cell*, 49(4):657–667, feb 2013. ISSN 10972765. doi: 10.1016/j.molcel.2012.11.020. URL http://www.ncbi.nlm.nih.gov/pubmed/23273981http://www.pubmedcentral.nih.gov/articlerender.fcgi?artid=PMC3582837http://linkinghub.elsevier.com/retrieve/pii/S109727651200977X.

[156] Pablo Huertas and Stephen P Jackson. Human CtIP mediates cell cycle control of DNA end resection and double strand break repair. *J. Biol. Chem.*, 284(14):9558–65, apr 2009. ISSN 0021-9258. doi: 10.1074/jbc.M808906200. URL http://www.ncbi.nlm.nih.gov/pubmed/19202191http://www.pubmedcentral.nih.gov/articlerender.fcgi?artid=PMC2666608.

[157] Yucai Wang, Justin W Leung, Yingjun Jiang, Megan G Lowery, Huong Do, Karen M Vasquez, Junjie Chen, Weidong Wang, and Lei Li. FANCM and FAAP24 maintain genome stability via cooperative as well as unique functions. *Mol. Cell*, 49(5):997–1009, mar 2013. ISSN 1097-4164. doi: 10.1016/j.molcel.2012.12.010. URL http://www.ncbi.nlm.nih.gov/pubmed/23333308http://www.pubmedcentral.nih.gov/articlerender.fcgi?artid=PMC3595374.

[158] Isabel Soria-Bretones, Cristina Cepeda-García, Cintia Checa-Rodriguez, Vincent Heyer, Bernardo Reina-San-Martin, Evi Soutoglou, and Pablo Huertas. DNA end resection requires constitutive sumoylation of CtIP by CBX4.

Nat. Commun., 8(1):113, 2017. ISSN 2041-1723. doi: 10.1038/s41467-017-00183-6. URL http://www.ncbi.nlm.nih.gov/pubmed/28740167http://www.pubmedcentral.nih.gov/articlerender.fcgi?artid=PMC5524638.

[159] Isabel Soria-Bretones, Cristina Cepeda-García, Cintia Checa-Rodriguez, Vincent Heyer, Bernardo Reina-San-Martin, Evi Soutoglou, and Pablo Huertas. DNA end resection requires constitutive sumoylation of CtIP by CBX4. *Nat. Commun.*, 8(1):113, dec 2017. ISSN 2041-1723. doi: 10.1038/s41467-017-00183-6. URL http://www.nature.com/articles/s41467-017-00183-6.

[160] Lorenza P. Ferretti, Sarah Felicitas Himmels, Anika Trenner, Christina Walker, Christine Von Aesch, Aline Eggenschwiler, Olga Murina, Radoslav I. Enchev, Matthias Peter, Raimundo Freire, Antonio Porro, and Alessandro A. Sartori. Cullin3-KLHL15 ubiquitin ligase mediates CtIP protein turnover to fine-tune DNA-end resection. *Nat. Commun.*, 7, 2016. ISSN 20411723. doi: 10.1038/ncomms12628.

[161] Xiaochun Yu and Junjie Chen. DNA damage-induced cell cycle checkpoint control requires CtIP, a phosphorylation-dependent binding partner of BRCA1 C-terminal domains. *Mol. Cell. Biol.*, 24(21):9478–86, nov 2004. ISSN 0270-7306. doi: 10.1128/MCB.24.21.9478-9486.2004. URL http://www.ncbi.nlm.nih.gov/pubmed/15485915http://www.pubmedcentral.nih.gov/articlerender.fcgi?artid=PMC522253.

[162] Maximina H. Yun and Kevin Hiom. CtIP-BRCA1 modulates the choice of DNA double-strand-break repair pathway throughout the cell cycle. *Nature*, 459(7245):460–463, may 2009. ISSN 0028-0836. doi: 10.1038/nature07955. URL http://www.ncbi.nlm.nih.gov/pubmed/19357644http://www.pubmedcentral.nih.gov/articlerender.fcgi?artid=PMC2857324http://www.nature.com/articles/nature07955.

[163] Tomas Aparicio and Jean Gautier. BRCA1-CtIP interaction in the repair of DNA double-strand breaks. *Mol. Cell. Oncol.*, 3(4):e1169343, jul 2016. ISSN 2372-3556. doi: 10.1080/23723556.2016.1169343. URL http://www.ncbi.nlm.nih.gov/pubmed/27652321http://www.pubmedcentral.nih.gov/articlerender.fcgi?artid=PMC4972120.

[164] Colleen R Reczek, Matthias Szabolcs, Jeremy M Stark, Thomas Ludwig, and Richard Baer. The interaction between CtIP and BRCA1 is not essential for resection-mediated DNA repair or tumor suppression. *J. Cell Biol.*, 201(5):693–707, may 2013. ISSN 1540-8140. doi: 10.1083/jcb.201302145. URL http://www.ncbi.nlm.nih.gov/pubmed/23712259http://www.pubmedcentral.nih.gov/articlerender.fcgi?artid=PMC3664708.

[165] Cristina Escribano-Díaz, Alexandre Orthwein, Amélie Fradet-Turcotte, Mengtan Xing, Jordan T.F. Young, Ján Tkáč, Michael A. Cook, Adam P. Rosebrock, Meagan Munro, Marella D. Canny, Dongyi Xu, and Daniel Durocher. A Cell Cycle-Dependent Regulatory Circuit Composed of 53BP1-RIF1 and BRCA1-CtIP Controls DNA Repair Pathway Choice. *Mol. Cell*, 49(5):872–883, mar 2013. ISSN 10972765. doi: 10.1016/j.molcel.2013.01.001. URL http://www.ncbi.nlm.nih.gov/pubmed/23333306http://linkinghub.elsevier.com/retrieve/pii/S1097276513000026.

[166] Andrés Cruz-García, Ana López-Saavedra, and Pablo Huertas. BRCA1 Accelerates CtIP-Mediated DNA-End Resection. *Cell Rep.*, 9(2):451–459, oct 2014. ISSN 22111247. doi: 10.1016/j.celrep.2014.08.076. URL http://www.ncbi.nlm.nih.gov/pubmed/25310973http://linkinghub.elsevier.com/retrieve/pii/S2211124714007682.

[167] Olivia Barton, Steffen C. Naumann, Ronja Diemer-Biehs, Julia Künzel, Monika Steinlage, Sandro Conrad, Nodar Makharashvili, Jiadong Wang, Lin Feng, Bernard S. Lopez, Tanya T. Paull, Junjie Chen, Penny A. Jeggo, and Markus Löbrich. Polo-like kinase 3 regulates CtIP during DNA double-strand break repair in G1. *J. Cell Biol.*, 206(7):877–894, sep 2014. ISSN 0021-9525. doi: 10.1083/jcb.201401146. URL http://www.ncbi.nlm.nih.gov/pubmed/25267294http://www.pubmedcentral.nih.gov/articlerender.fcgi?artid=PMC4178966http://www.jcb.org/lookup/doi/10.1083/jcb.201401146.

[168] Abderrahmane Kaidi, Brian T Weinert, Chunaram Choudhary, and Stephen P Jackson. Human SIRT6 promotes DNA end resection through CtIP deacetylation. *Science*, 329(5997):1348–53, sep 2010. ISSN 1095-9203. doi: 10.1126/science.1192049. URL http://www.ncbi.nlm.nih.gov/pubmed/20829486http://www.pubmedcentral.nih.gov/articlerender.fcgi?artid=PMC3276839.

[169] Lorenzo Lafranchi, Harmen R de Boer, Elisabeth GE de Vries, Shao-En Ong, Alessandro A Sartori, and Marcel ATM van Vugt. APC/C C dh1 controls CtIP stability during the cell cycle and in response to DNA damage. *EMBO J.*, 33(23):2860–2879, dec 2014. ISSN 0261-4189. doi: 10.15252/embj.201489017. URL http://www.ncbi.nlm.nih.gov/pubmed/25349192http://www.pubmedcentral.nih.gov/articlerender.fcgi?artid=PMC4282561http://emboj.embopress.org/lookup/doi/10.15252/embj.201489017.

[170] Antonia Germani, Audrey Prabel, Samia Mourah, Marie-Pierre Podgorniak, Anna Di Carlo, Ricardo Ehrlich, Sylvie Gisselbrecht, Nadine Varin-Blank, Fabien Calvo, and Heriberto Bruzzoni-Giovanelli. SIAH-1 interacts with CtIP and promotes its degradation by the proteasome pathway. *Oncogene*, 22(55):8845–8851, dec 2003. ISSN 0950-9232. doi: 10.1038/sj.onc.1206994. URL http://www.ncbi.nlm.nih.gov/pubmed/14654780http://www.nature.com/articles/1206994.

[171] Alexander KC Wong, Patricia A Ormonde, Ralph Pero, Yuan Chen, Lubing Lian, Grant Salada, Simin Berry, Quentin Lawrence, Priya Dayananth, Phuong Ha, Sean V Tavtigian, David H-F Teng, and Paul L Bartel. Characterization of a carboxy-terminal BRCA1 interacting protein. *Oncogene*, 17(18):2279–2285, nov 1998. ISSN 0950-9232. doi: 10.1038/sj.onc.1202150. URL http://www.ncbi.nlm.nih.gov/pubmed/9811458http://www.nature.com/articles/1202150.

[172] Rahul Arya and Craig H. Bassing. V(D)J Recombination Exploits DNA Damage Responses to Promote Immunity. *Trends Genet.*, 33(7):479–489, jul 2017. ISSN 01689525. doi: 10.1016/j.tig.2017.04.006. URL http://www.ncbi.nlm.nih.gov/pubmed/28532625http://www.pubmedcentral.nih.gov/articlerender.fcgi?artid=PMC5499712http://linkinghub.elsevier.com/retrieve/pii/S0168952517300719.

[173] Cristina Bilbao, Raquel Ramírez, Germán Rodríguez, Orlando Falcón, Laureano León, Nicolás Díaz-Chico, Manuel Perucho, and Juan Carlos Díaz-Chico. Double strand break repair components are frequent targets of microsatellite instability in endometrial cancer. *Eur. J. Cancer*, 46(15):2821–2827, oct 2010. ISSN 09598049. doi: 10.1016/j.ejca.2010.06.116. URL http://www.ncbi.nlm.nih.gov/pubmed/20638839http://linkinghub.elsevier.com/retrieve/pii/S0959804910006325.

[174] S Vilkki, V Launonen, A Karhu, P Sistonen, I Västrik, and L A Aaltonen. Screening for microsatellite instability target genes in colorectal cancers. *J. Med. Genet.*, 39(11):785–9, nov 2002. ISSN 1468-6244. URL http://www.ncbi.nlm.nih.gov/pubmed/12414815http://www.pubmedcentral.nih.gov/articlerender.fcgi?artid=PMC1735006.

[175] Isabel Soria-Bretones, Carmen Sáez, Manuel Ruíz-Borrego, Miguel A Japón, and Pablo Huertas. Prognostic value of CtIP/RBBP8 expression in breast cancer. *Cancer Med.*, 2(6):774–83, dec 2013. ISSN 2045-7634. doi: 10.1002/cam4.141. URL http://www.ncbi.nlm.nih.gov/pubmed/24403251http://www.pubmedcentral.nih.gov/articlerender.fcgi?artid=PMC3892382.

[176] Colleen R. Reczek, Reena Shakya, Yana Miteva, Matthias Szabolcs, Thomas Ludwig, and Richard Baer. The DNA resection protein CtIP promotes mammary tumorigenesis. *Oncotarget*, 7(22):32172–83, may 2016. ISSN 1949-2553. doi: 10.18632/oncotarget.8605. URL http://www.ncbi.nlm.nih.gov/pubmed/27058754http://www.pubmedcentral.nih.gov/articlerender.fcgi?artid=PMC5078005http://www.oncotarget.com/fulltext/8605.

[177] Z Ping Lin, Elena S Ratner, Margaret E Whicker, Yashang Lee, and Alan C Sartorelli. Triapine disrupts CtIP-mediated homologous recombination repair and sensitizes ovarian cancer cells to PARP and topoisomerase inhibitors. *Mol. Cancer Res.*, 12(3):381–393, mar 2014. ISSN 1557-3125. doi: 10.1158/1541-7786.MCR-13-0480. URL http://www.ncbi.nlm.nih.gov/pubmed/24413181http://www.pubmedcentral.nih.gov/articlerender.fcgi?artid=PMC3962722.

[178] Begoña Cánovas, Ana Igea, Alessandro A. Sartori, Roger R. Gomis, Tanya T. Paull, Michitaka Isoda, Héctor Pérez-Montoyo, Violeta Serra, Eva González-Suárez, Travis H. Stracker, and Angel R. Nebreda. Targeting p38α Increases DNA Damage, Chromosome Instability, and the Anti-tumoral Response to Taxanes in Breast Cancer Cells. *Cancer Cell*, 33(6):1094–1110.e8, jun 2018. ISSN 1535-6108. doi: 10.1016/J.CCELL.2018.04.010. URL https://www.sciencedirect.com/science/article/pii/S1535610818301818?via{%}3Dihub.

[179] Francesca Menghi, Floris P Barthel, Vinod Yadav, Ming Tang, Bo Ji, Zhonghui Tang, Gregory W Carter, Yijun Ruan, Ralph Scully, Roel G W Verhaak, Jos Jonkers, and Edison T Liu. The Tandem Duplicator Phenotype Is a Prevalent Genome-Wide Cancer Configuration Driven by Distinct Gene Mutations. *Cancer Cell*, 34(2):197–210.e5, aug 2018. ISSN 1878-3686. doi: 10.1016/j.ccell.2018.06.008. URL http://www.ncbi.nlm.nih.gov/pubmed/30017478.

[180] J R Mullen, V Kaliraman, S S Ibrahim, and S J Brill. Requirement for three novel protein complexes in the absence of the Sgs1 DNA helicase in Saccharomyces cerevisiae. *Genetics*, 157(1):103–18, jan 2001. ISSN 0016-6731. URL http://www.ncbi.nlm.nih.gov/pubmed/11139495http://www.pubmedcentral.nih.gov/articlerender.fcgi?artid=PMC1461486.

[181] Gerry P Crossan and Ketan J Patel. The Fanconi anaemia pathway orchestrates incisions at sites of crosslinked DNA. *J. Pathol.*, 226(2):326–337, jan 2012. ISSN 00223417. doi: 10.1002/path.3002. URL http://doi.wiley.com/10.1002/path.3002.

[182] Yonghwan Kim, Francis P Lach, Rohini Desetty, Helmut Hanenberg, Arleen D Auerbach, and Agata Smogorzewska. Mutations of the SLX4 gene in Fanconi anemia. *Nat. Genet.*, 43(2):142–146, feb 2011.

[183] Sohela Shah, Yonghwan Kim, Irina Ostrovnaya, Rajmohan Murali, Kasmintan A. Schrader, Francis P. Lach, Kara Sarrel, Rohini Rau-Murthy, Nichole Hansen, Liyng Zhang, Tomas Kirchhoff, Zsofia Stadler, Mark Robson, Joseph Vijai, Kenneth Offit, and Agata Smogorzewska. Assessment of SLX4 Mutations in Hereditary Breast Cancers. *PLoS One*, 8(6):e66961, jun 2013. ISSN 1932-6203. doi: 10.1371/journal.pone.0066961. URL http://www.ncbi.nlm.nih.gov/pubmed/23840564http://www.pubmedcentral.nih.gov/articlerender.fcgi?artid=PMC3694110http://dx.plos.org/10.1371/journal.pone.0066961.

[184] Irene Catucci, Mara Colombo, Paolo Verderio, Loris Bernard, Filomena Ficarazzi, Frederique Mariette, Monica Barile, Bernard Peissel, Elisa Cattaneo, Siranoush Manoukian, Paolo Radice, and Paolo Peterlongo. Sequencing Analysis of SLX4/FANCP Gene in Italian Familial Breast Cancer Cases. *PLoS One*, 7(2):e31038, feb 2012. ISSN 1932-6203. doi: 10.1371/journal.pone.0031038. URL http://www.ncbi.nlm.nih.gov/pubmed/22383991http://www.pubmedcentral.nih.gov/articlerender.fcgi?artid=PMC3285620http://dx.plos.org/10.1371/journal.pone.0031038.

[185] Samira Fekairi, Sarah Scaglione, Charly Chahwan, Ewan R Taylor, Agnès Tissier, Stéphane Coulon, Meng-Qiu Dong, Cristian Ruse, John R Yates, Paul Russell, Robert P Fuchs, Clare H McGowan, and Pierre-Henri L Gaillard. Human SLX4 is a Holliday junction resolvase subunit that binds multiple DNA repair/recombination endonucleases. *Cell*, 138(1):78–89, jul 2009.

[186] Ivan M Muñoz, Karolina Hain, Anne-Cécile Déclais, Mary Gardiner, Geraldine W Toh, Luis Sanchez-Pulido, Johannes M Heuckmann, Rachel Toth, Thomas Macartney, Berina Eppink, Roland Kanaar, Chris P Ponting, David M J Lilley, and John Rouse. Coordination of structure-specific nucleases by human SLX4/BTBD12 is required for DNA repair. *Mol. Cell*, 35(1):116–127, jul 2009.

[187] Yonghwan Kim, Gabriella S Spitz, Uma Veturi, Francis P Lach, Arleen D Auerbach, and Agata Smogorzewska. Regulation of multiple DNA repair pathways by the Fanconi anemia protein SLX4. *Blood*, 121(1):54–63, jan 2013.

[188] Dennis Castor, Nidhi Nair, Anne-Cécile Déclais, Christophe Lachaud, Rachel Toth, Thomas J. Macartney, David M.J. Lilley, J.Simon C. Arthur, and John Rouse. Cooperative Control of Holliday Junction Resolution and DNA Repair by the SLX1 and MUS81-EME1 Nucleases. *Mol. Cell*, 52(2):221–233, oct 2013. ISSN 10972765. doi: 10.1016/j.molcel.2013.08.036. URL http://www.ncbi.nlm.nih.gov/pubmed/24076219http://www.pubmedcentral.nih.gov/articlerender.fcgi?artid=PMC3808987http://linkinghub.elsevier.com/retrieve/pii/S1097276513006369.

[189] Elizabeth Garner, Yonghwan Kim, Francis P. Lach, Molly C. Kottemann, and Agata Smogorzewska. Human GEN1 and the SLX4-Associated Nucleases MUS81 and SLX1 Are Essential for the Resolution of Replication-Induced Holliday Junctions. *Cell Rep.*, 5(1):207–215, oct 2013. ISSN 22111247. doi: 10.1016/j.celrep.2013.08.041. URL http://www.ncbi.nlm.nih.gov/pubmed/24080495http://www.pubmedcentral.nih.gov/articlerender.fcgi?artid=PMC3844290http://linkinghub.elsevier.com/retrieve/pii/S2211124713004981.

[190] Meret Arter, Vanesa Hurtado-Nieves, Ashwini Oke, Tangna Zhuge, Rahel Wettstein, Jennifer C. Fung, Miguel G. Blanco, and Joao Matos. Regulated Crossing-Over Requires Inactivation of Yen1/GEN1 Resolvase during Meiotic Prophase I. *Dev. Cell*, 45(6):785–800.e6, jun 2018. ISSN 1534-5807. doi: 10.1016/J.DEVCEL.2018.05.020. URL https://www.sciencedirect.com/science/article/pii/S1534580718304131?via{%}3Dihub.

[191] Joao Matos, Miguel G. Blanco, Sarah Maslen, J. Mark Skehel, and Stephen C. West. Regulatory Control of the Resolution of DNA Recombination Intermediates during Meiosis and Mitosis. *Cell*, 147(1):158–172, sep 2011. ISSN 00928674. doi: 10.1016/j.cell.2011.08.032. URL http://www.ncbi.nlm.nih.gov/pubmed/21962513http://www.pubmedcentral.nih.gov/articlerender.fcgi?artid=PMC3560330http://linkinghub.elsevier.com/retrieve/pii/S0092867411010026.

[192] Heike Duda, Meret Arter, Jiradet Gloggnitzer, Federico Teloni, Philipp Wild, Miguel G. Blanco, Matthias Altmeyer, and Joao Matos. A Mechanism for Controlled Breakage of Under-replicated Chromosomes during Mitosis. *Dev. Cell*, 39(6):740–755, dec 2016. ISSN 15345807. doi: 10.1016/j.devcel.2016.11.017. URL http://www.ncbi.nlm.nih.gov/pubmed/27997828http://linkinghub.elsevier.com/retrieve/pii/S1534580716308292.

[193] C. Lachaud, D. Castor, K. Hain, I. Munoz, J. Wilson, T. J. MacArtney, D. Schindler, and J. Rouse. Distinct functional roles for the two SLX4 ubiquitin-binding UBZ domains mutated in Fanconi anemia. *J. Cell Sci.*, 127(13):2811–2817, 2014. ISSN 0021-9533. doi: 10.1242/jcs.146167. URL http://jcs.biologists.org/cgi/doi/10.1242/jcs.146167.

[194] Jian Ouyang, Elizabeth Garner, Alexander Hallet, Hai Dang Nguyen, Kimberly A Rickman, Grace Gill, Agata Smogorzewska, and Lee Zou. Noncovalent Interactions with SUMO and Ubiquitin Orchestrate Distinct Functions of the SLX4 Complex in Genome Maintenance. *Mol. Cell*, 57(1):108–122, jan 2015.

[195] Román González Prieto, Sabine A G Cuijpers, Martijn S Luijsterburg, Haico van Attikum, and Alfred C O Vertegaal. SUMOylation and PARylation cooperate to recruit and stabilize SLX4 at DNA damage sites. *EMBO Rep.*, 16(4):e201440017—-519, feb 2015.

[196] Jean-Hugues Guervilly, Arato Takedachi, Valeria Naim, Sarah Scaglione, Charly Chawhan, Yoann Lovera, Emmanuelle Despras, Isao Kuraoka, Patricia Kannouche, Filippo Rosselli, and Pierre-Henri L. Gaillard. The SLX4 Complex Is a SUMO E3 Ligase that Impacts on Replication Stress Outcome and Genome Stability. *Mol. Cell*, 57(1):123–137, jan 2015. ISSN 1097-2765. doi: 10.1016/J.MOLCEL.2014.11.014. URL https://www.sciencedirect.com/science/article/pii/S1097276514009095?via{%}3Dihub{#}fig3.

[197] Jamie S J Wilson, Agueda M Tejera, Dennis Castor, Rachel Toth, Maria A Blasco, and John Rouse. Localization-dependent and -independent roles of SLX4 in regulating telomeres. *Cell Rep.*, 4(5):853–860, sep 2013.

[198] Rekha Rai, Yong Chen, Ming Lei, and Sandy Chang. TRF2-RAP1 is required to protect telomeres from engaging in homologous recombination-mediated deletions and fusions. *Nat. Commun.*, 7:10881, mar 2016. ISSN 2041-1723. doi: 10.1038/ncomms10881. URL http://www.ncbi.nlm.nih.gov/pubmed/26941064http://www.pubmedcentral.nih.gov/articlerender.fcgi?artid=PMC4785230http://www.nature.com/doifinder/10.1038/ncomms10881.

[199] Jaya Sarkar, Bingbing Wan, Jinhu Yin, Haritha Vallabhaneni, Kent Horvath, Tomasz Kulikowicz, Vilhelm A Bohr, Yanbin Zhang, Ming Lei, and Yie Liu. SLX4 contributes to telomere preservation and regulated processing of telomeric joint molecule intermediates. *Nucleic Acids Res.*, 43(12):5912–5923, jul 2015.

[200] Jinhu Yin, Bingbing Wan, Jaya Sarkar, Kent Horvath, Jian Wu, Yong Chen, Guangjuan Cheng, Ke Wan, Peiju Chin, Ming Lei, and Yie Liu. Dimerization of SLX4 contributes to functioning of the SLX4-nuclease complex. *Nucleic Acids Res.*, 44(10):4871–4880, jun 2016. ISSN 0305-1048. doi: 10.1093/nar/gkw354. URL https://academic.oup.com/nar/article-lookup/doi/10.1093/nar/gkw354.

[201] Ryan L. Ragland, Sima Patel, Rebecca S. Rivard, Kevin Smith, Ashley A. Peters, Anja Katrin Bielinsky, and Eric J. Brown. RNF4 and PLK1 are required for replication fork collapse in ATR-deficient cells. *Genes Dev.*, 27(20):2259–2273, 2013. ISSN 08909369. doi: 10.1101/gad.223180.113.

[202] Tania M. Roberts, Michael S. Kobor, Suzanne A. Bastin-Shanower, Miki Ii, Sonja A. Horte, Jennifer W. Gin, Andrew Emili, Jasper Rine, Steven J. Brill, and Grant W. Brown. Slx4 Regulates DNA Damage Checkpoint-dependent Phosphorylation of the BRCT Domain Protein Rtt107/Esc4. *Mol. Biol. Cell*, 17(1):539–548, jan 2006. ISSN 1059-1524. doi: 10.1091/mbc.e05-08-0785. URL http://www.ncbi.nlm.nih.gov/pubmed/16267268http://www.pubmedcentral.nih.gov/articlerender.fcgi?artid=PMC1345688http://www.molbiolcell.org/doi/10.1091/mbc.e05-08-0785.

[203] Lisa E Hang, Jie Peng, Wei Tan, Barnabas Szakal, Demis Menolfi, Ziwei Sheng, Kirill Lobachev, Dana Branzei, Wenyi Feng, and Xiaolan Zhao. Rtt107 Is a Multi-functional Scaffold Supporting Replication Progression with Partner SUMO and Ubiquitin Ligases. *Mol. Cell*, 60(2):268–79, oct 2015. ISSN 1097-4164. doi: 10.1016/j.molcel.2015.08.023. URL http://www.ncbi.nlm.nih.gov/pubmed/26439300http://www.pubmedcentral.nih.gov/articlerender.fcgi?artid=PMC4609303.

[204] Patrice Y. Ohouo, Francisco M. Bastos de Oliveira, Beatriz S. Almeida, and Marcus B. Smolka. DNA Damage Signaling Recruits the Rtt107-Slx4 Scaffolds via Dpb11 to Mediate Replication Stress Response. *Mol. Cell*, 39(2): 300–306, jul 2010. ISSN 10972765. doi: 10.1016/j.molcel.2010.06.019. URL http://www.ncbi.nlm.nih.gov/pubmed/20670896http://linkinghub.elsevier.com/retrieve/pii/S1097276510004600.

[205] Achille Pellicioli and Marco Foiani. Signal Transduction: How Rad53 Kinase Is Activated. *Curr. Biol.*, 15(18):R769–R771, sep 2005. ISSN 09609822. doi: 10.1016/j.cub.2005.08.057. URL http://www.ncbi.nlm.nih.gov/pubmed/16169479http://linkinghub.elsevier.com/retrieve/pii/S096098220501016X.

[206] José R Cussiol, Carolyn M Jablonowski, Askar Yimit, Grant W Brown, and Marcus B Smolka. Dampening DNA damage checkpoint signalling via coordinated BRCT domain interactions. *EMBO J.*, 34(12):1704–17, jun 2015. ISSN 1460-2075. doi: 10.15252/embj.201490834. URL http://www.ncbi.nlm.nih.gov/pubmed/25896509http://www.pubmedcentral.nih.gov/articlerender.fcgi?artid=PMC4475403.

[207] Patrice Y. Ohouo, Francisco M. Bastos de Oliveira, Yi Liu, Chu Jian Ma, and Marcus B. Smolka. DNA-repair scaffolds dampen checkpoint signalling by counteracting the adaptor Rad9. *Nature*, 493(7430): 120–124, nov 2012. ISSN 0028-0836. doi: 10.1038/nature11658. URL http://www.ncbi.nlm.nih.gov/pubmed/23160493http://www.pubmedcentral.nih.gov/articlerender.fcgi?artid=PMC3536934http://www.nature.com/doifinder/10.1038/nature11658.

[208] William J Wedemeyer, Ervin Welker, and Harold A Scheraga. Proline cis-trans isomerization and protein folding. *Biochemistry*, 41(50):14637–44, dec 2002. ISSN 0006-2960. URL http://www.ncbi.nlm.nih.gov/pubmed/12475212.

[209] David E. Stewart, Atom Sarkar, and John E. Wampler. Occurrence and role ofcis peptide bonds in protein structures. *J. Mol. Biol.*, 214(1):253–260, jul 1990. ISSN 00222836. doi: 10.1016/0022-2836(90)90159-J. URL http://www.ncbi.nlm.nih.gov/pubmed/2370664http://linkinghub.elsevier.com/retrieve/pii/002228369090159J.

[210] Chi-Wai Cheng, Ka-Wai Leong, Yiu-Ming Ng, Yok-Lam Kwong, and Eric Tse. The peptidyl-prolyl isomerase PIN1 relieves cyclin-dependent kinase 2 (CDK2) inhibition by the CDK inhibitor p27. *J. Biol. Chem.*, 292(52):21431–21441, dec 2017. ISSN 1083-351X. doi: 10.1074/jbc.M117.801373. URL http://www.ncbi.nlm.nih.gov/pubmed/29118189http://www.pubmedcentral.nih.gov/articlerender.fcgi?artid=PMC5766953.

[211] Goethel S Marahiel M. Peptidyl-prolyl cis-trans isomerases, a superfamily of ubiquitous folding catalysts. *Cell. Mol. Life Sci.*, 55(3):423–436, 1999.

[212] Kun Ping Lu, Steven D. Hanes, and Tony Hunter. A human peptidyl–prolyl isomerase essential for regulation of mitosis. *Nature*, 380(6574):544–547, apr 1996. ISSN 0028-0836. doi: 10.1038/380544a0. URL http://www.nature.com/doifinder/10.1038/380544a0.

[213] Yih-Cherng Liou, Xiao Zhen Zhou, and Kun Ping Lu. Prolyl isomerase Pin1 as a molecular switch to determine the fate of phosphoproteins. *Trends Biochem. Sci.*, 36(10):501–514, oct 2011. ISSN 09680004. doi: 10.1016/j.tibs.2011.07.001. URL http://www.ncbi.nlm.nih.gov/pubmed/21852138http:

//www.pubmedcentral.nih.gov/articlerender.fcgi?artid=PMC3185210http://linkinghub.elsevier.com/retrieve/pii/S0968000411001125.

[214] Brendan T Innes, Melanie L Bailey, Christopher J Brandl, Brian H Shilton, and David W Litchfield. Non-catalytic participation of the Pin1 peptidyl-prolyl isomerase domain in target binding. *Front. Physiol.*, 4:18, 2013. ISSN 1664-042X. doi: 10.3389/fphys.2013.00018. URL http://www.ncbi.nlm.nih.gov/pubmed/23407864http://www.pubmedcentral.nih.gov/articlerender.fcgi?artid=PMC3571201.

[215] C.D. Behrsin, M.L. Bailey, K.S. Bateman, K.S. Hamilton, L.M. Wahl, C.J. Brandl, B.H. Shilton, and D.W. Litchfield. Functionally Important Residues in the Peptidyl-prolyl Isomerase Pin1 Revealed by Unigenic Evolution. *J. Mol. Biol.*, 365(4):1143–1162, jan 2007. ISSN 00222836. doi: 10.1016/j.jmb.2006.10.078. URL http://www.ncbi.nlm.nih.gov/pubmed/17113106http://linkinghub.elsevier.com/retrieve/pii/S0022283606015038.

[216] P J Lu, X Z Zhou, M Shen, and K P Lu. Function of WW domains as phosphoserine- or phosphothreonine-binding modules. *Science*, 283(5406):1325–8, feb 1999. ISSN 0036-8075. URL http://www.ncbi.nlm.nih.gov/pubmed/10037602.

[217] R Ranganathan, K P Lu, T Hunter, and J P Noel. Structural and functional analysis of the mitotic rotamase Pin1 suggests substrate recognition is phosphorylation dependent. *Cell*, 89(6):875–86, jun 1997. ISSN 0092-8674. URL http://www.ncbi.nlm.nih.gov/pubmed/9200606.

[218] M B Yaffe, M Schutkowski, M Shen, X Z Zhou, P T Stukenberg, J U Rahfeld, J Xu, J Kuang, M W Kirschner, G Fischer, L C Cantley, and K P Lu. Sequence-specific and phosphorylation-dependent proline isomerization: a potential mitotic regulatory mechanism. *Science*, 278(5345):1957–60, dec 1997. ISSN 0036-8075. URL http://www.ncbi.nlm.nih.gov/pubmed/9395400.

[219] Isakov Nath. Regulation of Immune Cell Functions by Pin1. *Int. Trends Immun.*, 2, 2014.

[220] Akihide Ryo, Yih-Cherng Liou, Kun Ping Lu, and Gerburg Wulf. Prolyl isomerase Pin1: a catalyst for oncogenesis and a potential therapeutic target in cancer. *J. Cell Sci.*, 116(Pt 5):773–83, mar 2003. ISSN 0021-9533. URL http://www.ncbi.nlm.nih.gov/pubmed/12571275.

[221] Elizabeth S. Yeh and Anthony R. Means. PIN1, the cell cycle and cancer. *Nat. Rev. Cancer*, 7(5):381–388, may 2007. ISSN 1474-175X. doi: 10.1038/nrc2107. URL http://www.nature.com/articles/nrc2107.

[222] Xiao Zhen Zhou and Kun Ping Lu. The isomerase PIN1 controls numerous cancer-driving pathways and is a unique drug target. *Nat. Rev. Cancer*, 16(7):463–478, jul 2016. ISSN 1474-175X. doi: 10.1038/nrc.2016.49. URL http://www.ncbi.nlm.nih.gov/pubmed/27256007http://www.nature.com/articles/nrc.2016.49.

[223] Eunice H. Y. Chan, Anna Santamaria, Herman H. W. Silljé, and Erich A. Nigg. Plk1 regulates mitotic Aurora A function through βTrCP-dependent degradation of hBora. *Chromosoma*, 117(5):457–469, oct 2008. ISSN 0009-5915. doi: 10.1007/s00412-008-0165-5. URL http://www.ncbi.nlm.nih.gov/pubmed/18521620http://www.pubmedcentral.nih.gov/articlerender.fcgi?artid=PMC2921497http://link.springer.com/10.1007/s00412-008-0165-5.

[224] Y.-C. Lee, J. Que, Y.-C. Chen, J.-T. Lin, Y.-C. Liou, P.-C. Liao, Y.-P. Liu, K.-H. Lee, L.-C. Lin, M. Hsiao, L.-Y. Hung, C.-Y. Huang, and P.-J. Lu. Pin1 acts as a negative regulator of the G2/M transition by interacting with the Aurora-A-Bora complex. *J. Cell Sci.*, 126(21):4862–4872, nov 2013. ISSN 0021-9533. doi: 10.1242/jcs.121368. URL http://www.ncbi.nlm.nih.gov/pubmed/23970419http://jcs.biologists.org/cgi/doi/10.1242/jcs.121368.

[225] Cheng-Han Lin, Hao-Yi Li, Yu-Cheng Lee, Marcus J Calkins, Kuen-Haur Lee, Chia-Ning Yang, and Pei-Jung Lu. Landscape of Pin1 in the cell cycle. *Exp. Biol. Med. (Maywood).*, 240(3):403–8, mar 2015. ISSN 1535-3699. doi: 10.1177/1535370215570829. URL http://www.ncbi.nlm.nih.gov/pubmed/25662955http://www.pubmedcentral.nih.gov/articlerender.fcgi?artid=PMC4935233.

[226] P H O'Farrell. Triggering the all-or-nothing switch into mitosis. *Trends Cell Biol.*, 11(12):512–9, dec 2001. ISSN 0962-8924. URL http://www.ncbi.nlm.nih.gov/pubmed/11719058http://www.pubmedcentral.nih.gov/articlerender.fcgi?artid=PMC2765372.

[227] K. Okamoto and N. Sagata. Mechanism for inactivation of the mitotic inhibitory kinase Wee1 at M phase. *Proc. Natl. Acad. Sci.*, 104(10):3753–3758, mar 2007. ISSN 0027-8424. doi: 10.1073/pnas.0607357104. URL http://www.ncbi.nlm.nih.gov/pubmed/17360425http://www.pubmedcentral.nih.gov/articlerender.fcgi?artid=PMC1820656http://www.pnas.org/cgi/doi/10.1073/pnas.0607357104.

[228] Steven D. Hanes, Peter R. Shank, and Keith A. Bostian. Sequence and mutational analysis ofESS1, a gene essential for growth inSaccharomyces cerevisiae. *Yeast*, 5(1):55–72, jan 1989. ISSN 0749-503X. doi: 10.1002/yea.320050108. URL http://www.ncbi.nlm.nih.gov/pubmed/2648698http://doi.wiley.com/10.1002/yea.320050108.

[229] Yih-Cherng Liou, Akihide Ryo, Han-Kuei Huang, Pei-Jung Lu, Roderick Bronson, Fumihiro Fujimori, Takafumi Uchida, Tony Hunter, and Kun Ping Lu. Loss of Pin1 function in the mouse causes phenotypes resembling cyclin D1-null phenotypes. *Proc. Natl. Acad. Sci.*, 99(3):1335–1340, feb 2002.

[230] Fumihiro Fujimori, Katsuhiko Takahashi, Chiyoko Uchida, and Takafumi Uchida. Mice Lacking Pin1 Develop Normally, but Are Defective in Entering Cell Cycle from G0 Arrest. *Biochem. Biophys. Res. Commun.*, 265(3):658–663, nov 1999. ISSN 0006-291X. doi: 10.1006/BBRC.1999.1736. URL https://www.sciencedirect.com/science/article/pii/S0006291X99917369.

[231] Han You, Hongwu Zheng, Steven A Murray, Qiang Yu, Takafumi Uchida, Daiming Fan, and Zhi-Xiong Jim Xiao. IGF-1 induces Pin1 expression in promoting cell cycle S-phase entry. *J. Cell. Biochem.*, 84(2):211–6, 2002. ISSN 0730-2312. URL http://www.ncbi.nlm.nih.gov/pubmed/11787050.

[232] D. G. Crenshaw, J Yang, A R Means, and S Kornbluth. The mitotic peptidyl-prolyl isomerase, Pin1, interacts with Cdc25 and Plx1. *EMBO J.*, 17(5):1315–1327, mar 1998. ISSN 14602075. doi: 10.1093/emboj/17.5.1315. URL http://www.ncbi.nlm.nih.gov/pubmed/9482729http://www.pubmedcentral.nih.gov/articlerender.fcgi?artid=PMC1170480http://emboj.embopress.org/cgi/doi/10.1093/emboj/17.5.1315.

[233] K E Winkler, K I Swenson, S Kornbluth, and A R Means. Requirement of the prolyl isomerase Pin1 for the replication checkpoint. *Science*, 287(5458):1644–7, mar 2000. ISSN 0036-8075. URL http://www.ncbi.nlm.nih.gov/pubmed/10698738.

[234] Minhui Shen, P. Todd Stukenberg, Marc W. Kirschner, and Kun Ping Lu. The essential mitotic peptidyl-prolyl isomerase Pin1 binds and regulates mitosis-specific phosphoproteins. *Genes Dev.*, 12(5):706–720, 1998. ISSN 08909369. doi: 10.1101/gad.12.5.706.

[235] F. Suizu, A. Ryo, G. Wulf, J. Lim, and K. P. Lu. Pin1 Regulates Centrosome Duplication, and Its Overexpression Induces Centrosome Amplification, Chromosome Instability, and Oncogenesis. *Mol. Cell. Biol.*, 26(4):1463–1479, feb 2006. ISSN 0270-7306. doi: 10.1128/MCB.26.4.1463-1479.2006. URL http://www.ncbi.nlm.nih.gov/pubmed/16449657http://www.pubmedcentral.nih.gov/articlerender.fcgi?artid=PMC1367188http://mcb.asm.org/cgi/doi/10.1128/MCB.26.4.1463-1479.2006.

[236] Frank Eckerdt, Juping Yuan, Krishna Saxena, Bernd Martin, Sven Kappel, Christine Lindenau, Andrea Kramer, Steffen Neumann, Sebastian Daum, Gunter Fischer, Ivan Dikic, Manfred Kaufmann, and Klaus Strebhardt. Polo-like kinase 1-mediated phosphorylation stabilizes Pin1 by inhibiting its ubiquitination in human cells. *J. Biol. Chem.*, 280(44):36575–36583, 2005. ISSN 00219258. doi: 10.1074/jbc.M504548200.

[237] Tae Ho Lee, Lucia Pastorino, and Kun Ping Lu. Peptidyl-prolyl cis-trans isomerase Pin1 in ageing, cancer and Alzheimer disease. *Expert Rev. Mol. Med.*, 13:e21, 2011.

[238] Akihide Ryo, Yih-Cherng Liou, Gerburg Wulf, Masafumi Nakamura, Sam W Lee, and Kun Ping Lu. PIN1 is an E2F target gene essential for Neu/Ras-induced transformation of mammary epithelial cells. *Mol. Cell. Biol.*, 22 (15):5281–95, aug 2002. ISSN 0270-7306. URL http://www.ncbi.nlm.nih.gov/pubmed/12101225http://www.pubmedcentral.nih.gov/articlerender.fcgi?artid=PMC133940.

[239] G. M. Wulf, A Ryo, G G Wulf, S W Lee, T Niu, V Petkova, and K P Lu. Pin1 is overexpressed in breast cancer and cooperates with Ras signaling in increasing the transcriptional activity of c-Jun towards cyclin D1. *EMBO J.*, 20(13):3459–3472, jul 2001. ISSN 14602075. doi: 10.1093/emboj/20.13.3459. URL http://www.ncbi.nlm.nih.gov/pubmed/11432833http://www.pubmedcentral.nih.gov/articlerender.fcgi?artid=PMC125530http://emboj.embopress.org/cgi/doi/10.1093/emboj/20.13.3459.

[240] Kun Ping Lu, Greg Finn, Tae Ho Lee, and Linda K Nicholson. Prolyl cis-trans isomerization as a molecular timer. *Nat. Chem. Biol.*, 3(10):619–629, oct 2007.

[241] G Sorrentino, M Mioni, C Giorgi, N Ruggeri, P Pinton, U Moll, F Mantovani, and G Del Sal. The prolyl-isomerase Pin1 activates the mitochondrial death program of p53. *Cell Death Differ.*, 20(2):198–208, feb 2013. ISSN 1476-5403. doi: 10.1038/cdd.2012.112. URL http://www.ncbi.nlm.nih.gov/pubmed/22935610http://www.pubmedcentral.nih.gov/articlerender.fcgi?artid=PMC3554345.

[242] Gerburg M. Wulf, Yih-Cherng Liou, Akihide Ryo, Sam W. Lee, and Kun Ping Lu. Role of Pin1 in the Regulation of p53 Stability and p21 Transactivation, and Cell Cycle Checkpoints in Response to DNA Damage. *J. Biol. Chem.*, 277(50):47976–47979, dec 2002. ISSN 0021-9258. doi: 10.1074/jbc.C200538200. URL http://www.ncbi.nlm.nih.gov/pubmed/12388558http://www.jbc.org/lookup/doi/10.1074/jbc.C200538200.

[243] Hongwu Zheng, Han You, Xiao Zhen Zhou, Stephen A. Murray, Takafumi Uchida, Gerburg Wulf, Ling Gu, Xiaoren Tang, Kun Ping Lu, and Zhi-Xiong Jim Xiao. The prolyl isomerase Pin1 is a regulator of p53 in genotoxic response. *Nature*, 419(6909):849–853, oct 2002. ISSN 0028-0836. doi: 10.1038/nature01116. URL http://www.ncbi.nlm.nih.gov/pubmed/12397361http://www.nature.com/articles/nature01116.

[244] Peng Liao, Shelya X. Zeng, Xiang Zhou, Tianjian Chen, Fen Zhou, Bo Cao, Ji Hoon Jung, Giannino Del Sal, Shiwen Luo, and Hua Lu. Mutant p53 Gains Its Function via c-Myc Activation upon CDK4 Phosphorylation at Serine 249 and Consequent PIN1 Binding. *Mol. Cell*, 68(6):1134–1146.e6, dec 2017. ISSN 1097-2765. doi: 10.1016/J.MOLCEL.2017.11.006. URL https://www.sciencedirect.com/science/article/pii/S1097276517308419?via{%}3Dihub.

[245] Gustavo Ayala, Dagong Wang, Gerburg Wulf, Anna Frolov, Rile Li, Janusz Sowadski, Thomas M Wheeler, Kun Ping Lu, and Lere Bao. The Prolyl Isomerase Pin1 Is a Novel Prognostic Marker in Human Prostate Cancer. *Cancer Res.*, 63(19):6244–6251, oct 2003.

[246] Lere Bao, Amy Kimzey, Guido Sauter, Janusz M. Sowadski, Kun Ping Lu, and Da-Gong Wang. Prevalent Overexpression of Prolyl Isomerase Pin1 in Human Cancers. *Am. J. Pathol.*, 164(5):1727–1737, may 2004. ISSN 00029440. doi: 10.1016/S0002-9440(10)63731-5. URL http://www.ncbi.nlm.nih.gov/pubmed/15111319http://www.pubmedcentral.nih.gov/articlerender.fcgi?artid=PMC1615639http://linkinghub.elsevier.com/retrieve/pii/S0002944010637315.

[247] Takeshi Sasaki, Akihide Ryo, Hiroji Uemura, Hitoshi Ishiguro, Yoshiaki Inayama, Shoji Yamanaka, Yoshinobu Kubota, Yoji Nagashima, Masaoki Harada, and Ichiro Aoki. An immunohistochemical scoring system of prolyl isomerase Pin1 for predicting relapse of prostate carcinoma after radical prostatectomy. *Pathol. - Res. Pract.*, 202(5):357–364, may 2006. ISSN 03440338. doi: 10.1016/j.prp.2005.12.007. URL http://www.ncbi.nlm.nih.gov/pubmed/16516405http://linkinghub.elsevier.com/retrieve/pii/S0344033806000136.

[248] Alessandra Rustighi, Alessandro Zannini, Elena Campaner, Yari Ciani, Silvano Piazza, and Giannino Del Sal. PIN1 in breast development and cancer: a clinical perspective. *Cell Death Differ.*, 24(2):200–211, feb 2017. ISSN 1350-9047. doi: 10.1038/cdd.2016.122. URL http://www.nature.com/articles/cdd2016122.

[249] Zhimin Lu and Tony Hunter. Prolyl isomerase Pin1 in cancer. *Cell Res.*, 24(9):1033–1049, sep 2014.

[250] Alessandra Rustighi, Alessandro Zannini, Luca Tiberi, Roberta Sommaggio, Silvano Piazza, Giovanni Sorrentino, Simona Nuzzo, Antonella Tuscano, Vincenzo Eterno, Federica Benvenuti, Libero Santarpia, Iannis Aifantis, Antonio Rosato, Silvio Bicciato, Alberto Zambelli, and Giannino Del Sal. Prolyl-isomerase Pin1 controls normal and cancer stem cells of the breast. *EMBO Mol. Med.*, 6(1):99–119, jan 2014. ISSN 17574676. doi: 10.1002/emmm.201302909. URL http://www.ncbi.nlm.nih.gov/pubmed/24357640http://www.pubmedcentral.nih.gov/articlerender.fcgi?artid=PMC3936488http://embomolmed.embopress.org/cgi/doi/10.1002/emmm.201302909.

[251] M.-L. Luo, C. Gong, C.-H. Chen, D. Y. Lee, H. Hu, P. Huang, Y. Yao, W. Guo, F. Reinhardt, G. Wulf, J. Lieberman, X. Z. Zhou, E. Song, and K. P. Lu. Prolyl Isomerase Pin1 Acts Downstream of miR200c to Promote Cancer Stem-like Cell Traits in Breast Cancer. *Cancer Res.*, 74(13):3603–3616, jul 2014. ISSN 0008-5472. doi: 10.1158/0008-5472.CAN-13-2785. URL http://www.ncbi.nlm.nih.gov/pubmed/24786790http://www.pubmedcentral.nih.gov/articlerender.fcgi?artid=PMC4079726http://cancerres.aacrjournals.org/cgi/doi/10.1158/0008-5472.CAN-13-2785.

[252] Shingo Kozono, Yu-Min Lin, Hyuk-Soo Seo, Benika Pinch, Xiaolan Lian, Chenxi Qiu, Megan K Herbert, Chun-Hau Chen, Li Tan, Ziang Jeff Gao, Walter Massefski, Zainab M Doctor, Brian P Jackson, Yuanzhong Chen, Sirano Dhe-Paganon, Kun Ping Lu, and Xiao Zhen Zhou. Arsenic targets Pin1 and cooperates with retinoic acid to inhibit cancer-driving pathways and tumor-initiating cells. *Nat. Commun.*, 9(1):3069, aug 2018. ISSN 2041-1723. doi: 10.1038/s41467-018-05402-2. URL http://www.ncbi.nlm.nih.gov/pubmed/30093655http://www.pubmedcentral.nih.gov/articlerender.fcgi?artid=PMC6085299.

[253] Elena Campaner, Alessandra Rustighi, Alessandro Zannini, Alberto Cristiani, Silvano Piazza, Yari Ciani, Ori Kalid, Gali Golan, Erkan Baloglu, Sharon Shacham, Barbara Valsasina, Ulisse Cucchi, Agnese Chiara Pippione, Marco Lucio Lolli, Barbara Giabbai, Paola Storici, Paolo Carloni, Giulia Rossetti, Federica Benvenuti, Ezia Bello, Maurizio D'Incalci, Elisa Cappuzzello, Antonio Rosato, and Giannino Del Sal. A covalent PIN1 inhibitor selectively targets cancer cells by a dual mechanism of action. *Nat. Commun.*, 8:15772, jun 2017. ISSN 2041-1723. doi: 10.1038/ncomms15772. URL http://www.nature.com/doifinder/10.1038/ncomms15772.

[254] Alessandro A Sartori and Martin Steger. Prolyl isomerization: a new PIN code for DSB repair. *Cell Cycle*, 12 (17):2717–8, sep 2013. ISSN 1551-4005. doi: 10.4161/cc.26077. URL http://www.ncbi.nlm.nih.gov/pubmed/23966151http://www.pubmedcentral.nih.gov/articlerender.fcgi?artid=PMC3899182.

[255] Benjamin A. Hilton, Zhengke Li, Phillip R. Musich, Hui Wang, Brian M. Cartwright, Moises Serrano, Xiao Zhen Zhou, Kun Ping Lu, and Yue Zou. ATR Plays a Direct Antiapoptotic Role at Mitochondria, which Is Regulated by Prolyl Isomerase Pin1. *Mol. Cell*, 60(1):35–46, oct 2015. ISSN 1097-2765. doi: 10.1016/J.MOLCEL.2015.08.008. URL https://www.sciencedirect.com/science/article/pii/S1097276515006541?via{%}3Dihub.

[256] Y Tong, H Ying, R Liu, L Li, J Bergholz, and Z-X Xiao. Pin1 inhibits PP2A-mediated Rb dephosphorylation in regulation of cell cycle and S-phase DNA damage. *Cell Death Dis.*, 6(2):e1640, feb 2015. ISSN 2041-4889. doi: 10.1038/cddis.2015.3. URL http://www.nature.com/doifinder/10.1038/cddis.2015.3.

[257] T. M. Sonneborn. Methods in the general biology and genetics of paramecium aurelia. *J. Exp. Zool.*, 113(1): 87–147, feb 1950. ISSN 0022-104X. doi: 10.1002/jez.1401130106. URL http://doi.wiley.com/10.1002/jez.1401130106.

[258] Douglas L Chalker, Eric Meyer, and Kazufumi Mochizuki. Epigenetics of ciliates. *Cold Spring Harb. Perspect. Biol.*, 5(12):a017764, dec 2013. ISSN 1943-0264. doi: 10.1101/cshperspect.a017764. URL http://www.ncbi.nlm.nih.gov/pubmed/24296171http://www.pubmedcentral.nih.gov/articlerender.fcgi?artid=PMC3839606.

[259] Janine Beisson, Mireille Bétermier, Marie-Hélène Bré, Jean Cohen, Sandra Duharcourt, Laurent Duret, Ching Kung, Sophie Malinsky, Eric Meyer, John R Preer, and Linda Sperling. Paramecium tetraurelia: the renaissance of an early unicellular model. *Cold Spring Harb. Protoc.*, 2010(1):pdb.emo140, jan 2010. ISSN 1559-6095. doi: 10.1101/pdb.emo140. URL http://www.ncbi.nlm.nih.gov/pubmed/20150105.

[260] Mireille Betermier and Sandra Duharcourt. Programmed Rearrangement in Ciliates: Paramecium. In *Mob. DNA III*, volume 2, pages 369–388. American Society of Microbiology, dec 2014. doi: 10.1128/microbiolspec.MDNA3-0035-2014. URL http://www.asmscience.org/content/book/10.1128/9781555819217.chap17.

[261] Mireille Bétermier. Large-scale genome remodelling by the developmentally programmed elimination of germ line sequences in the ciliate Paramecium. *Res. Microbiol.*, 155(5):399–408, jun 2004. ISSN 0923-2508. doi: 10.1016/J.RESMIC.2004.01.017. URL https://www.sciencedirect.com/science/article/pii/S0923250804000701.

[262] Céline Baudry, Sophie Malinsky, Matthieu Restituito, Aurélie Kapusta, Sarah Rosa, Eric Meyer, and Mireille Betermier. PiggyMac, a domesticated piggyBac transposase involved in programmed genome rearrangements in the ciliate Paramecium tetraurelia. *Genes {&} Dev.*, 23(21):2478–2483, nov 2009.

[263] Aurélie Kapusta, Atsushi Matsuda, Antoine Marmignon, Michael Ku, Aude Silve, Eric Meyer, James D. Forney, Sophie Malinsky, and Mireille Bétermier. Highly Precise and Developmentally Programmed Genome Assembly in Paramecium Requires Ligase IV–Dependent End Joining. *PLoS Genet.*, 7(4):e1002049, apr 2011. ISSN 1553-7404. doi: 10.1371/journal.pgen.1002049. URL http://dx.plos.org/10.1371/journal.pgen.1002049.

[264] Jean-Marc Aury, Olivier Jaillon, Laurent Duret, Benjamin Noel, Claire Jubin, Betina M. Porcel, Béatrice Ségurens, Vincent Daubin, Véronique Anthouard, Nathalie Aiach, Olivier Arnaiz, Alain Billaut, Janine Beisson, Isabelle Blanc, Khaled Bouhouche, Francisco Câmara, Sandra Duharcourt, Roderic Guigo, Delphine Gogendeau, Michael Katinka, Anne-Marie Keller, Roland Kissmehl, Catherine Klotz, France Koll, Anne Le Mouël, Gersende Lepère, Sophie Malinsky, Mariusz Nowacki, Jacek K. Nowak, Helmut Plattner, Julie Poulain, Françoise Ruiz, Vincent Serrano, Marek Zagulski, Philippe Dessen, Mireille Bétermier, Jean Weissenbach, Claude Scarpelli, Vincent Schächter, Linda Sperling, Eric Meyer, Jean Cohen, and Patrick Wincker. Global trends of whole-genome duplications revealed by the ciliate Paramecium tetraurelia. *Nature*, 444(7116):171–178, nov 2006. ISSN 0028-0836. doi: 10.1038/nature05230. URL http://www.ncbi.nlm.nih.gov/pubmed/17086204http://www.nature.com/articles/nature05230.

[265] Jingyun Chi, Frédéric Mahé, Josef Loidl, John Logsdon, and Micah Dunthorn. Meiosis Gene Inventory of Four Ciliates Reveals the Prevalence of a Synaptonemal Complex-Independent Crossover Pathway. *Mol. Biol. Evol.*, 31 (3):660–672, mar 2014. ISSN 1537-1719. doi: 10.1093/molbev/mst258. URL http://www.ncbi.nlm.nih.gov/pubmed/24336924https://academic.oup.com/mbe/article-lookup/doi/10.1093/molbev/mst258.

[266] Sucheta Arora, Rajashree A Deshpande, Martin Budd, Judy Campbell, America Revere, Xiaoming Zhang, Kristina H Schmidt, and Tanya T Paull. Genetic Separation of Sae2 Nuclease Activity from Mre11 Nuclease Functions in Budding Yeast. *Mol. Cell. Biol.*, 37(24), dec 2017. ISSN 1098-5549. doi: 10.1128/MCB.00156-17. URL http://www.ncbi.nlm.nih.gov/pubmed/28970327http://www.pubmedcentral.nih.gov/articlerender.fcgi?artid=PMC5705816.

[267] Sarah E Allen and Mariusz Nowacki. Necessity Is the Mother of Invention: Ciliates, Transposons, and Transgenerational Inheritance. *Trends Genet.*, 33(3):197–207, mar 2017. ISSN 0168-9525. doi: 10.1016/j.tig.2017.01.005. URL http://www.ncbi.nlm.nih.gov/pubmed/28174020.

[268] Laurent Duret, Jean Cohen, Claire Jubin, Philippe Dessen, Jean-François Goût, Sylvain Mousset, Jean-Marc Aury, Olivier Jaillon, Benjamin Noël, Olivier Arnaiz, Mireille Bétermier, Patrick Wincker, Eric Meyer, and Linda Sperling. *Genome research.* Cold Spring Harbor Laboratory Press. URL https://genome.cshlp.org/content/18/4/585/F1.expansion.html.

[269] Olga Murina, Christine von Aesch, Ufuk Karakus, Lorenza P. Ferretti, Hella A. Bolck, Kay Hänggi, and Alessandro A. Sartori. FANCD2 and CtIP cooperate to repair DNA interstrand crosslinks. *Cell Rep.*, 7(4):1030–1038, 2014. ISSN 22111247. doi: 10.1016/j.celrep.2014.03.069.

[270] Anne E Carpenter, Thouis R Jones, Michael R Lamprecht, Colin Clarke, In Kang, Ola Friman, David A Guertin, Joo Chang, Robert A Lindquist, Jason Moffat, Polina Golland, and David M Sabatini. CellProfiler: image analysis software for identifying and quantifying cell phenotypes. *Genome Biol.*, 7(10): R100, 2006. ISSN 14656906. doi: 10.1186/gb-2006-7-10-r100. URL http://www.ncbi.nlm.nih.gov/pubmed/17076895http://www.pubmedcentral.nih.gov/articlerender.fcgi?artid=PMC1794559http://genomebiology.biomedcentral.com/articles/10.1186/gb-2006-7-10-r100.

[271] Sophie E Polo and Stephen P Jackson. Dynamics of DNA damage response proteins at DNA breaks: a focus on protein modifications. *Genes Dev.*, 25(5):409–33, mar 2011. ISSN 1549-5477. doi: 10.1101/gad.2021311. URL http://www.ncbi.nlm.nih.gov/pubmed/21363960http://www.pubmedcentral.nih.gov/articlerender.fcgi?artid=PMC3049283.

[272] Kun Ping Lu, Yih Cherng Liou, and Xiao Zhen Zhou. Pinning down proline-directed phosphorylation signaling. *Trends Cell Biol.*, 12(4):164–72, apr 2002. ISSN 0962-8924. URL http://www.ncbi.nlm.nih.gov/pubmed/11978535.

[273] Yonghwan Kim. Nuclease delivery: versatile functions of SLX4/FANCP in genome maintenance. *Mol. Cells*, 37(8):569–74, aug 2014. ISSN 0219-1032. doi: 10.14348/molcells.2014.0118. URL http://www.ncbi.nlm.nih.gov/pubmed/24938228http://www.pubmedcentral.nih.gov/articlerender.fcgi?artid=PMC4145367.

[274] Elena Bayer, Sandra Goettsch, Jonathan W Mueller, Bernhard Griewel, Elena Guiberman, Lorenz M Mayr, and Peter Bayer. Structural analysis of the mitotic regulator hPin1 in solution: insights into domain architecture and substrate binding. *J. Biol. Chem.*, 278(28):26183–93, jul 2003. ISSN 0021-9258. doi: 10.1074/jbc.M300721200. URL http://www.ncbi.nlm.nih.gov/pubmed/12721297.

[275] Yih-Cherng Liou, Xiao Zhen Zhou, and Kun Ping Lu. Prolyl isomerase Pin1 as a molecular switch to determine the fate of phosphoproteins. *Trends Biochem. Sci.*, 36(10):501–514, oct 2011.

[276] Yonghwan Kim. Nuclease Delivery: Versatile Functions of SLX4/FANCP in Genome Maintenance. *Mol. Cells*, 37(8):569–574, aug 2014. ISSN 1016-8478. doi: 10.14348/molcells.2014.0118. URL http://www.ncbi.nlm.nih.gov/pubmed/24938228http://www.pubmedcentral.nih.gov/articlerender.fcgi?artid=PMC4145367http://www.molcells.org/journal/view.html?doi=10.14348/molcells.2014.0118.

[277] Boris Pfander and Joao Matos. Control of Mus81 nuclease during the cell cycle. *FEBS Lett.*, 591(14):2048–2056, jul 2017. ISSN 00145793. doi: 10.1002/1873-3468.12727. URL http://www.ncbi.nlm.nih.gov/pubmed/28640495http://doi.wiley.com/10.1002/1873-3468.12727.

[278] Dalia Gritenaite, Lissa N Princz, Barnabas Szakal, Susanne C S Bantele, Lina Wendeler, Sandra Schilbach, Bianca H Habermann, Joao Matos, Michael Lisby, Dana Branzei, and Boris Pfander. A cell cycle-regulated Slx4-Dpb11 complex promotes the resolution of DNA repair intermediates linked to stalled replication. *Genes Dev.*, 28 (14):1604–19, jul 2014. ISSN 1549-5477. doi: 10.1101/gad.240515.114. URL http://www.ncbi.nlm.nih.gov/pubmed/25030699http://www.pubmedcentral.nih.gov/articlerender.fcgi?artid=PMC4102767.

[279] Titia de Lange. Shelterin: the protein complex that shapes and safeguards human telomeres. *Genes Dev.*, 19(18):2100–10, sep 2005. ISSN 0890-9369. doi: 10.1101/gad.1346005. URL http://www.ncbi.nlm.nih.gov/pubmed/16166375.

[280] Anthony J. Cesare and Roger R. Reddel. Alternative lengthening of telomeres: models, mechanisms and implications. *Nat. Rev. Genet.*, 11(5):319–330, may 2010. ISSN 1471-0056. doi: 10.1038/nrg2763. URL http://www.nature.com/articles/nrg2763.

[281] Y. Chen, Y. Yang, M. van Overbeek, J. R. Donigian, P. Baciu, T. de Lange, and M. Lei. A Shared Docking Motif in TRF1 and TRF2 Used for Differential Recruitment of Telomeric Proteins. *Science (80-.).*, 319(5866):1092–1096, feb 2008. ISSN 0036-8075. doi: 10.1126/science.1151804. URL http://www.ncbi.nlm.nih.gov/pubmed/18202258http://www.sciencemag.org/cgi/doi/10.1126/science.1151804.

[282] A Smogorzewska, B van Steensel, A Bianchi, S Oelmann, M R Schaefer, G Schnapp, and T de Lange. Control of human telomere length by TRF1 and TRF2. *Mol. Cell. Biol.*, 20(5):1659–68, mar 2000. ISSN 0270-7306. URL http://www.ncbi.nlm.nih.gov/pubmed/10669743http://www.pubmedcentral.nih.gov/articlerender.fcgi?artid=PMC85349.

[283] Bingbing Wan, Jinhu Yin, Kent Horvath, Jaya Sarkar, Yong Chen, Jian Wu, Ke Wan, Jian Lu, Peili Gu, Eun Young Yu, Neal F. Lue, Sandy Chang, Yie Liu, and Ming Lei. SLX4 Assembles a Telomere Maintenance Toolkit by Bridging Multiple Endonucleases with Telomeres. *Cell Rep.*, 4(5):861–869, sep 2013. ISSN 22111247. doi: 10.1016/j.celrep.2013.08.017. URL http://www.ncbi.nlm.nih.gov/pubmed/24012755http://www.pubmedcentral.nih.gov/articlerender.fcgi?artid=PMC4334113http://linkinghub.elsevier.com/retrieve/pii/S2211124713004580.

[284] Alison J Montpetit, Areej A Alhareeri, Marty Montpetit, Angela R Starkweather, Lynne W Elmore, Kristin Filler, Lathika Mohanraj, Candace W Burton, Victoria S Menzies, Debra E Lyon, Colleen K Jackson-Cook, Joseph M. Teefey, and Colleen K. Jackson-Cook. Telomere length: a review of methods for measurement. *Nurs. Res.*, 63(4): 289–99, 2014. ISSN 1538-9847. doi: 10.1097/NNR.0000000000000037. URL http://www.ncbi.nlm.nih.gov/pubmed/24977726http://www.pubmedcentral.nih.gov/articlerender.fcgi?artid=PMC4292845.

[285] Lissa N Princz, Dalia Gritenaite, and Boris Pfander. The Slx4-Dpb11 scaffold complex: coordinating the response to replication fork stalling in S-phase and the subsequent mitosis. *Cell Cycle*, 14(4):488–94, 2015. ISSN 1551-4005. doi: 10.4161/15384101.2014.989126. URL http://www.ncbi.nlm.nih.gov/pubmed/25496009http://www.pubmedcentral.nih.gov/articlerender.fcgi?artid=PMC4612105.

[286] Haley D M Wyatt, Rob C Laister, Stephen R Martin, Cheryl H Arrowsmith, and Stephen C West. The SMX DNA Repair Tri-nuclease. *Mol. Cell*, 65(5):848–860.e11, mar 2017. ISSN 1097-4164. doi: 10.1016/j.molcel.2017.01.031. URL http://www.ncbi.nlm.nih.gov/pubmed/28257701http://www.pubmedcentral.nih.gov/articlerender.fcgi?artid=PMC5344696.

[287] Irene Gallina, Signe Korbo Christiansen, Rune Troelsgaard Pedersen, Michael Lisby, and Vibe H Oestergaard. TopBP1-mediated DNA processing during mitosis. *Cell Cycle*, 15(2):176–83, 2016. ISSN 1551-4005. doi: 10.1080/15384101.2015.1128595. URL http://www.ncbi.nlm.nih.gov/pubmed/26701150http://www.pubmedcentral.nih.gov/articlerender.fcgi?artid=PMC4825820.

[288] Rune Troelsgaard Pedersen, Thomas Kruse, Jakob Nilsson, Vibe H. Oestergaard, and Michael Lisby. TopBP1 is required at mitosis to reduce transmission of DNA damage to G1 daughter cells. *J. Cell Biol.*, 210(4):565–582, 2015. ISSN 15408140. doi: 10.1083/jcb.201502107.

[289] Agnieszka Lukaszewicz, Rachel A Howard-Till, Maria Novatchkova, Kazufumi Mochizuki, and Josef Loidl. MRE11 and COM1/SAE2 are required for double-strand break repair and efficient chromosome pairing during meiosis of the protist Tetrahymena. *Chromosoma*, 119(5):505–518, oct 2010.

[290] S Keeney and N Kleckner. Covalent protein-DNA complexes at the 5' strand termini of meiosis-specific double-strand breaks in yeast. *Proc. Natl. Acad. Sci. U. S. A.*, 92(24):11274–8, nov 1995. ISSN 0027-8424. URL http://www.ncbi.nlm.nih.gov/pubmed/7479978http://www.pubmedcentral.nih.gov/articlerender.fcgi?artid=PMC40614.

[291] Takehiko Usui, Tsutomu Ohta, Hiroyuki Oshiumi, Jun-ichi Tomizawa, Hideyuki Ogawa, and Tomoko Ogawa. Complex Formation and Functional Versatility of Mre11 of Budding Yeast in Recombination. *Cell*, 95(5):705–716, nov 1998. ISSN 0092-8674. doi: 10.1016/S0092-8674(00)81640-2. URL https://www.sciencedirect.com/science/article/pii/S0092867400816402?via{%}3Dihub.

[292] Changchun Deng, James A. Brown, Dongqing You, and J. Martin Brown. Multiple Endonucleases Function to Repair Covalent Topoisomerase I Complexes in Saccharomyces cerevisiae. *Genetics*, 170(2): 591–600, jun 2005. ISSN 0016-6731. doi: 10.1534/genetics.104.028795. URL http://www.ncbi.nlm.nih.gov/pubmed/15834151http://www.pubmedcentral.nih.gov/articlerender.fcgi?artid=PMC1450417http://www.genetics.org/lookup/doi/10.1534/genetics.104.028795.

[293] M Bétermier, S Duharcourt, H Seitz, and E Meyer. Timing of developmentally programmed excision and circularization of Paramecium internal eliminated sequences. *Mol. Cell. Biol.*, 20(5):1553–61, mar 2000. ISSN 0270-7306. URL http://www.ncbi.nlm.nih.gov/pubmed/10669733http://www.pubmedcentral.nih.gov/articlerender.fcgi?artid=PMC85339.

[294] Ariane Gratias and Mireille Bétermier. Processing of double-strand breaks is involved in the precise excision of paramecium internal eliminated sequences. *Mol. Cell. Biol.*, 23(20):7152–62, oct 2003. ISSN 0270-7306. URL http://www.ncbi.nlm.nih.gov/pubmed/14517286http://www.pubmedcentral.nih.gov/articlerender.fcgi?artid=PMC230320.

[295] Bettina M. Lengsfeld, Alison J. Rattray, Venugopal Bhaskara, Rodolfo Ghirlando, and Tanya T. Paull. Sae2 Is an Endonuclease that Processes Hairpin DNA Cooperatively with the Mre11/Rad50/Xrs2 Complex. *Mol. Cell*, 28(4):638–651, nov 2007. ISSN 10972765. doi: 10.1016/j.molcel.2007.11.001. URL http://www.ncbi.nlm.nih.gov/pubmed/18042458http://www.pubmedcentral.nih.gov/articlerender.fcgi?artid=PMC2194599http://linkinghub.elsevier.com/retrieve/pii/S1097276507007332.

[296] Josep V Forment, Stephen P Jackson, and Luca Pellegrini. When two is not enough: a CtIP tetramer is required for DNA repair by Homologous Recombination. *Nucleus*, aug 2015. ISSN 1949-1042. doi: 10.1080/19491034.2015.1086050. URL http://www.ncbi.nlm.nih.gov/pubmed/26305173.

[297] M de Jager, J van Noort, D C van Gent, C Dekker, R Kanaar, and C Wyman. Human Rad50/Mre11 is a flexible complex that can tether DNA ends. *Mol. Cell*, 8(5):1129–35, nov 2001. ISSN 1097-2765. URL http://www.ncbi.nlm.nih.gov/pubmed/11741547.

[298] Travis H. Stracker and John H. J. Petrini. The MRE11 complex: starting from the ends. *Nat. Rev. Mol. Cell Biol.*, 12(2):90–103, feb 2011. ISSN 1471-0072. doi: 10.1038/nrm3047. URL http://www.ncbi.nlm.nih.gov/pubmed/21252998http://www.pubmedcentral.nih.gov/articlerender.fcgi?artid=PMC3905242http://www.nature.com/articles/nrm3047.

[299] Tilman Polonio-Vallon, Daniel Krüger, and Thomas G Hofmann. ShaPINg Cell Fate Upon DNA Damage: Role of Pin1 Isomerase in DNA Damage-Induced Cell Death and Repair. *Front. Oncol.*, 4:148, 2014. ISSN 2234-943X. doi: 10.3389/fonc.2014.00148. URL http://www.ncbi.nlm.nih.gov/pubmed/24982848http://www.pubmedcentral.nih.gov/articlerender.fcgi?artid=PMC4058901.

[300] Nadja Bitomsky, Elisa Conrad, Christian Moritz, Tilman Polonio-Vallon, Dirk Sombroek, Kathrin Schultheiss, Carolina Glas, Vera Greiner, Christoph Herbel, Fiamma Mantovani, Giannino del Sal, Francesca Peri, and Thomas G Hofmann. Autophosphorylation and Pin1 binding coordinate DNA damage-induced HIPK2 activation and cell death. *Proc. Natl. Acad. Sci. U. S. A.*, 110(45):E4203–12, nov 2013. ISSN 1091-6490. doi: 10.1073/pnas.1310001110. URL http://www.ncbi.nlm.nih.gov/pubmed/24145406http://www.pubmedcentral.nih.gov/articlerender.fcgi?artid=PMC3831444.

[301] Tony S. Byun, Marcin Pacek, Muh Ching Yee, Johannes C. Walter, and Karlene A. Cimprich. Functional uncoupling of MCM helicase and DNA polymerase activities activates the ATR-dependent checkpoint. *Genes Dev.*, 19(9):1040–1052, 2005. ISSN 08909369. doi: 10.1101/gad.1301205.

[302] Frank B. Couch, Carol E. Bansbach, Robert Driscoll, Jessica W. Luzwick, Gloria G. Glick, Rémy Bétous, Clinton M. Carroll, Sung Yun Jung, Jun Qin, Karlene A. Cimprich, and David Cortez. ATR phosphorylates SMARCAL1 to prevent replication fork collapse. *Genes Dev.*, 27(14):1610–1623, 2013. ISSN 08909369. doi: 10.1101/gad.214080.113.

[303] Shriparna Sarbajna, Derek Davies, and Stephen C West. Roles of SLX1-SLX4, MUS81-EME1, and GEN1 in avoiding genome instability and mitotic catastrophe. *Genes Dev.*, 28(10):1124–36, may 2014. ISSN 1549-5477. doi: 10.1101/gad.238303.114. URL http://www.ncbi.nlm.nih.gov/pubmed/24831703http://www.pubmedcentral.nih.gov/articlerender.fcgi?artid=PMC4035540.

Acknowledgments

First, I would like to express my deep gratitude to Prof. Alessandro A. Sartori for giving me the opportunity to do my PhD in his lab and for the believe and support over the past years. I highly appreciate the encouragement and guidance, enthusiastic ideas and useful critiques on these projects.
I would also like to thanks Prof. Matthias Altmeyer, Prof. Joao Matos and PD Dr. Pavel Janscak for critical discussions and insightful comments and for their thoughtful advice.

Moreover, I would like to acknowledge PD. Pavel Janscak and PD. Stefano Ferrari for providing purified proteins, Prof. PH Gaillard, Prof. Joao Matos and Prof. Agata Smogorzewska for sharing plasmid constructs and reagents.
Furthermore, I would like to thank all the past and present members of the Sartori lab, especially Chrigi, Martin, Lorenzo, Lorenza, Anika, Antonio, Christina, Hella, Sara and Sarah for their scientific input but also for their help and positive words during frustrating times and their readiness to celebrate good times. It is a great team spirit and wonderful working atmosphere, I so far never experienced somewhere else.
I consider myself fortunate having had the opportunity to work at the IMCR during my PhD and would like to thank all present and past members for creating such a great working atmosphere and their willingness to share and collaborate. I would like to thank particularly Farah, Odete and the technicians for providing such a great infrastructure, which make it easier for me to focus on my projects.
Special thanks should be given to my friends from the q-club and the affiliates to share so many great moments over the past years. I am grateful for my friends I connected with during the time of my PhD, sometimes by accidently walking into, for giving me such

a good time in Zurich. Furthermore, I want to thank my old friends from Hamburg for reminding me where my heart is.

Finally, I wish to thank my family for their encouragement throughout my study and, although a couple of kilometers away, being there for me. Always.

Appendix

Curriculum Vitae

JULIA EILEEN GODAU
DATE OF BIRTH: 10st MARCH 1986
PLACE OF ORIGIN: HAMBURG

EDUCATION AND WORK EXPERIENCE

11/2014 - present **Ph.D. in Cancer Biology**
Life Science Zurich Graduate School, University of Zurich
PhD thesis research in the laboratory of Prof. A.A. Sartori,
Institute of Molecular Cancer Research
Project: "*Biochemical and regulatory aspects of DNA double-strand break repair"*

03/2014 - 09/2014 **Research Associate**
High-Throughput Binder Selection Platform, University of Zurich

03/2012 - 12/2013 **Ph.D. in Biology**
Charité Berlin, Germany
PhD thesis research in the laboratory of Prof. F. Jundt,
Project: "*Identification and therapeutic targeting of novel Notch interacting pathways in multiple myeloma"*

04/2011 - 02/2012 **Test Analyst**
Roche Diagnostics AG, Rotkreuz

12/2009 - 12/2010 **Master of Science in Molecular and Cell Biology**
Master thesis research in the laboratory of Prof. A.A. Sartori,
Institute of Molecular Cancer Research
Project: "*Towards a structure-function analysis of Paramecium CtIP"*

03/2008 - 08/2008 **Bachelor of Science in Biology**
University of Hamburg
Bachelor thesis research in the laboratory of Prof. T. Dobner at the Heinrich-Pette-Institute for Experimental Virology and Immunology
Project: "*Analysis of the transforming potential of the E1B-55K protein of Adenovirus Serotype 5"*

08/2007 - 03/2008 **Student Research Associate**
DNA-Cloning-Service e. K., Hamburg

06/2004 **Abitur (Matura)**
Gymnasium Lohbrügge, Hamburg

RELATED PROFESSIONAL EXPERIENCE

Since 11/2015 **PhD student representative**
Cancer Biology PhD program, University of Zurich

10/2017 and 11/2017 **Teaching assistant**
Laboratory course "Practical course in Biochemistry", University Zurich

04/2015 and 05/2016 **Teaching assistant**
Practical block course "Genome Instability and Molecular Cancer Research" for Master students, University Zurich

PUBLICATIONS

Submitted PLoS Genetics	**Godau, J.**, Ferretti, L. P., Aesch, v. C., Guérois, R., Marmignon, A., et al. Identification of a miniature Sae2/Ctp1/CtIP ortholog from *Paramecium tetraurelia* reveals a conserved DNA-binding motif required for DNA-end resection.
2018 Molecular Cancer Therapeutics	Trenner, A., **Godau, J.**, Sartori, A. A. A Short BRCA2-Derived Cell-Penetrating Peptide Targets RAD51 Function and Confers Hypersensitivity toward PARP Inhibition.
2014 Blood Cancer	Schwarzer, R.*****, Nickel, N.*****, **Godau, J.***, Willie, B. M., Duda, G. N., et al. Notch pathway inhibition controls myeloma bone disease in the murine MOPC315.BM model. (*contributed equally to this work).

PRESENTATIONS AT CONFERENCES

	LS²/Louis-Jeantet Satellite Meeting "The Genetic Evolution of Cancer"
10/2017	Geneva, Switzerland (Oral presentation)
	7th Cancer Network Zurich Retreat
03/2017	Emmetten, Switzerland (Poster presentation)
	Swiss Meeting on Genome Stability and Chromatin Dynamics
06/2016	Emmetten, Switzerland (Poster presentation)
	6th Cancer Network Zurich Retreat
04/2015	Emmetten, Switzerland (Poster presentation)

A S hort BRCA2-Derived Cell-Penetrating Peptide Targets RAD51 Function and Confers Hypersensitivity toward PARP Inhibition.

Anika Trenner, **Julia Godau** and Alessandro A. Sartori

Article published in Molecular Cancer Therapeutics, 2018.

I examined whether BRC4 CPPs provoke olaparib-induced cell death in cancer cells and noncancerous cell lines. Specifically, I performed colony formation assays and immunoblotting as shown in Figure 6E and S6A. Furthermore, I helped revising the manuscript.

Published OnlineFirst April 13, 2018; DOI: 10.1158/1535-7163.MCT-17-1156

Small Molecule Therapeutics

Molecular Cancer Therapeutics

A Short BRCA2-Derived Cell-Penetrating Peptide Targets RAD51 Function and Confers Hypersensitivity toward PARP Inhibition

Anika Trenner, Julia Godau, and Alessandro A. Sartori

Abstract

Under conditions of genotoxic stress, cancer cells strongly rely on efficient DNA repair to survive and proliferate. The human BRCA2 tumor suppressor protein is indispensable for the repair of DNA double-strand breaks by homologous recombination (HR) by virtue of its ability to promote RAD51 loading onto single-stranded DNA. Therefore, blocking the interaction between BRCA2 and RAD51 could significantly improve the efficacy of conventional anticancer therapies. However, targeting protein–protein interaction (PPI) interfaces has proven challenging because flat and large PPI surfaces generally do not support binding of small-molecule inhibitors. In contrast, peptides are more potent for targeting PPIs but are otherwise difficult to deliver into cells. Here, we report that a synthetic 16-mer peptide derived from the BRC4 repeat motif of BRCA2 is capable of blocking RAD51 binding to BRCA2. Efficient noncytotoxic cellular uptake of a nona-arginine (R9)-conjugated version of the BRC4 peptide interferes with DNA damage–induced RAD51 foci formation and HR. Moreover, transduction of the BRC4 peptide impairs replication fork–protective function of BRCA2 and triggers MRE11-dependent degradation of nascent DNA in response to DNA replication stress. Finally, the BRC4 cell-penetrating peptide (CPP) confers selective hypersensitivity to PARP inhibition in cancer cells but spares noncancerous cells. Taken together, our data highlight an innovative approach to develop novel peptide-based DNA repair inhibitors and establish BRCA2-derived CPPs as promising anticancer agents. *Mol Cancer Ther; 17(7); 1392–404. ©2018 AACR.*

Introduction

Double-strand breaks (DSB) are highly detrimental DNA lesions because, if left unrepaired or misrepaired, they can trigger cell death and genomic instability, ultimately causing cancer (1). To circumvent this threat, cells are equipped with diverse DSB repair mechanisms, including nonhomologous end joining (NHEJ) and homologous recombination (HR) as the two major pathways (2). Furthermore, recent work has established that in response to DNA replication stress, several key HR factors play a crucial role in protecting stalled DNA replication forks from nucleolytic degradation (3). Because rapidly dividing cancer cells rely on efficient DSB repair and fork protection mechanisms for their survival, inhibiting HR represents an attractive strategy for the development of novel therapeutic drugs, in particular when used in combination with DNA-damaging agents (4, 5).

The human BRCA2 protein plays an essential role in HR by promoting homology search and stimulating strand invasion into the sister chromatid (6). Specifically, following DNA-end resection, BRCA2 directs RAD51 filament nucleation onto RPA-coated single-stranded DNA (ssDNA; ref. 7). RAD51 interacts with two distinct regions in BRCA2, the BRC repeat motifs and a C-terminal domain (8–10). Importantly, the eight evolutionarily conserved BRC repeats, each consisting of about 35 amino acids, significantly differ in their capacity to bind RAD51 with BRC4 displaying the highest affinity (11, 12). Consequently, it was proposed that BRC repeats 1–4 facilitate nucleation of RAD51 by binding monomeric RAD51 and reducing its ATPase activity (11, 13). Structural analysis of the BRC4 repeat identified residues 1523-GFHTASG-1529 of BRCA2 to structurally mimic the self-oligomerization motif of RAD51 (14). In addition to the FHTA motif, a second consensus tetrameric module in BRC4, denoted as LFDE motif, was shown to bind to a distinct pocket in RAD51 distant from the oligomerization interface (15). In contrast to the BRC repeats, the C-terminal domain does not bind monomeric RAD51 but instead stabilizes RAD51 nucleoprotein filaments (9, 10). Taken together, compounds that selectively and efficiently block BRCA2–RAD51 interaction could advance into the clinic as bona fide HR inhibitors for both monotherapy and add-on therapy with DNA-damaging agents.

The physical nature of protein–protein interaction (PPI) interfaces often renders them unable to support binding of small-molecule inhibitors (SMI). Instead, peptide therapeutics offer an alternative way to target PPIs with key advantages over SMIs, including their direct similarity to protein fragments and the coverage of extensive PPI interfaces (16). However, poor membrane permeability has previously limited their use to extracellular targets (17). Thus, hydrophilic peptides are reliant on a permeation-enhancing strategy that facilitates targeting of intracellular molecules (18). Recently, cell-penetrating peptides (CPP)

Institute of Molecular Cancer Research, University of Zurich, Zurich, Switzerland.

Note: Supplementary data for this article are available at Molecular Cancer Therapeutics Online (http://mct.aacrjournals.org/).

Corresponding Author: Alessandro A. Sartori, Institute of Molecular Cancer Research, University of Zurich, Winterthurerstrasse 190, Zurich 8057, Switzerland. Phone: 414-4635-3473; Fax: 414-4635-3484; E-mail: sartori@imcr.uzh.ch

doi: 10.1158/1535-7163.MCT-17-1156

Published OnlineFirst April 13, 2018; DOI: 10.1158/1535-7163.MCT-17-1156

have been developed to enhance the cellular uptake and nuclear translocation of membrane-impermeable cargo molecules (19). They comprise a highly diverse class of short, primarily cationic peptides that combine a limited cytotoxicity and the ability to mediate receptor-independent transport of cargoes across cell membranes (20). Notably, the nona-arginine (R9) peptide is one of the most potent CPPs, giving a high transduction efficiency combined with low cytotoxicity (21).

Here, we design a CPP comprised of a 16-amino acid stretch of the BRCA2 BRC4 repeat able to inhibit BRCA2–RAD51 interaction. Our detailed functional analysis reveals that an R9-fused BRC4 CPP prevents RAD51 loading onto ssDNA, resulting in defective homology-mediated repair of DSBs as well as increased MRE11-dependent degradation of stalled DNA replication forks. Consequently, peptide incubation renders cells hypersensitive to the PARP inhibitor olaparib, providing a potential use for BRCA2-derived peptides in the treatment of certain types of cancer.

Materials and Methods

Cell culture

HeLa, U2OS, RPE1, MRC5 (all from ATCC), and HeLa DR-GFP were cultured in DMEM (Gibco) supplemented with 10% FCS (Sigma-Aldrich), 100 U/mL penicillin, and 100 μg/mL streptomycin (Life Technologies). PEO1 and PEO4 cells were purchased from the Health Protection Agency Culture Collections and cultured in RPMI medium (Gibco) supplemented with 10% FCS, 2 mmol/L sodium pyruvate (Gibco), and penicillin/streptomycin. MCF10A cells were purchased from ATCC and cultured in DMEM/F12 (Gibco) containing 5% Horse Serum (Gibco), 20 ng/mL human EGF (Sigma-Aldrich), 0.5 mg/mL hydrocortisone (Sigma-Aldrich), 10 μg/mL insulin, and penicillin/streptomycin. Stable U2OS cells expressing GFP-RAD51 (22) were grown in DMEM supplemented with 10% Tet system approved FCS (GIBCO) and penicillin/streptomycin. To induce GFP-RAD51 expression, cells were treated with 1 μg/mL doxycycline (Sigma-Aldrich) for 24 hours. All cell lines were confirmed to be free of mycoplasma contamination on a regular basis (PCR Mycoplasma Test Kit, AppliChem). Cells were passaged for no longer than 2 months after thawing of early-passage stocks. For cells that have been received from secondary sources, no cell line authentication was performed. Irradiation was performed using a Faxitron X-ray machine.

Chemicals and peptides

Camptothecin, RAD51 inhibitor B02 (23), cycloheximide, hydroxyurea (HU), and mirin (24) were purchased from Sigma-Aldrich. Olaparib (AZD2281) was provided by Selleck Chemicals. Thymidine analogs CIdU, IdU, and EdU were purchased from Sigma-Aldrich and Life Technologies, respectively. Custom-designed peptides were purchased from Bachem AG and, if not specified, synthesized according to standard practice (L-amino acids, N-terminal tag or acetylation, C-terminal amidation). Lyophilized peptides were dissolved in PBS at 1 mg/mL.

Antibodies

A detailed list of all primary and secondary antibodies can be found in Supplementary Tables S1 and S2, respectively.

siRNA

A detailed list of siRNA oligonucleotide sequences used in this study can be found in Supplementary Table S3. siRNA oligos were used at a final concentration of 10 nmol/L and transfected using Lipofectamine RNAiMAX (Invitrogen) according to the manufacturer's instructions.

Recombinant protein expression

BRCA2 GST-fusion plasmids (GST-BRC 1-2, GST-BRC3-5, GST-BRC6-8, GST-C-term) have been described before (25). BRCA2 GST-fusion proteins were expressed in BL21-CodonPlus-RIL *Escherichia coli* (*E. coli*) by growing them overnight at 18°C using 100 μmol/L isopropyl β-D-thiogalactoside. Recombinant full-length RAD51 was prepared as described previously (26).

Immunoblotting

If not specified otherwise, cells were lysed in Laemmli buffer (4% SDS, 20% glycerol, 120 mmol/L Tris-HCl pH 6.8) and resolved by Tris-glycine SDS-PAGE. To probe for BRCA2, 3%–6% NuPAGE Tris-Acetate gels (Thermo Fisher Scientific) were run according to the manufacturer's instructions. After transfer to nitrocellulose membranes, immunoblotting was performed with indicated primary antibodies overnight at 4°C and secondary antibodies for 1 hour at room temperature. Stained proteins were visualized using the Advansta WesternBright ECL reagent and the VilberLourmat Fusion Solo S imaging system.

Pull-down assays

For peptide pull-downs, 30 μL streptavidin-coupled Dynabeads (Life Technologies) were incubated with 5 μg (2.7 nmol) of biotinylated BRC4 peptides or biotin analogue d-desthiobiotin (Sigma-Aldrich) in 1 mL PBS-T (0.1% Triton X-100) for 1 hour at 4°C. Beads were washed three times with PBS-T and blocked for 30 minutes with 0.3% BSA in PBS at 4°C. A total of 50 ng (1.35 pmol) recombinant RAD51 together with 2 μmol/L ATP was added to the beads and incubated for 2 hours in 700 μL PBS-T. The beads were washed four times with NTEN300 (20 mmol/L Tris pH 7.4, 0.1 mmol/L EDTA, 300 mmol/L NaCl, 0.5% NP-40) and once with TEN100 (20 mmol/L Tris pH 7.4, 0.1 mmol/L EDTA, 100 mmol/L NaCl) before complexes were boiled in 2× SDS sample buffer (10 mmol/L Tris pH 6.8, 20% glycerol, 3% SDS, 200 mmol/L DTT, 0.04% bromophenol blue) and subjected to immunoblotting. For GST pull-down assays, glutathione sepharose beads (GE Healthcare) were incubated for 1 hour at 4°C with equalized amounts of BL21 *E. coli* soluble extracts expressing one of the four GST-BRCA2 fusion constructs in TEN100. Beads were washed three times with NTEN300 buffer and once with TEN100 before adding either 1 mg HeLa nuclear extracts (CilBiotech) or 50 ng purified RAD51 supplemented with varying amounts of $BRC4^{wt}$ or $BRC4^{mut}$ peptides filled up to 1 mL with TEN100. After 2 hours of incubation, beads were washed twice with NTEN500 (20 mmol/L Tris pH 7.4, 0.1 mmol/L EDTA, 500 mmol/L NaCl, 0.5% NP-40), twice with NTEN300, and twice with TEN100 buffer before boiling in SDS sample buffer and protein analysis by immunoblotting.

Coimmunoprecipitation

Cell extracts were prepared using NP-40 extraction buffer [50 mmol/L Tris-HCl pH 7.5, 120 mmol/L NaCl, 1 mmol/L EDTA, 6 mmol/L EGTA, 15 mmol/L sodium pyrophosphate and 1% NP-40 supplemented with phosphatase inhibitors

Published OnlineFirst April 13, 2018; DOI: 10.1158/1535-7163.MCT-17-1156

(20 mmol/L NaF, 1 mmol/L sodium orthovanadate), and protease inhibitors (1 mmol/L benzamidine and 0.1 mmol/L PMSF)]. After benzonase (Novagen) digestion for 30 minutes at 4°C, cell extracts were cleared by centrifugation. Lysates (2 mg) were supplemented with increasing amounts of peptides filled up to 1 mL with NP-40 extraction buffer and incubated for 1 hour at 4°C before adding 20 μL GFP-Trap agarose beads (ChromoTek) for 1 hour at 4°C. Beads were subsequently washed three times with GFP-IP buffer (100 mmol/L NaCl, 0.2% NP-40, 1 mmol/L $MgCl_2$, 10% glycerol, 5 mmol/L NaF, 50 mmol/L Tris-HCl pH 7.5) and boiled in SDS sample buffer for analysis by immunoblotting.

Peptide transfection

Cells were seeded either into 8-well chamber imaging slides (μ-Slide 8 Well, ibidi), 24-well plates, 6-well plates, or 6-cm culture dishes (Sarstedt) and grown to around 80% confluence at day of peptide transfection. Cells were washed at least once with PBS to remove residual FCS and incubated with indicated peptide concentrations in appropriate serum-free medium for 1 hour at 37°C. If not specified otherwise, the following incubation volumes were used: 0.3 mL for 8-well chamber imaging slides and 24-well plates, 0.5 mL for 12-well plates and 2 mL for 6-well plates and 6-cm culture dishes.

Confocal microscopy

A total of 4×10^4 cells were seeded into 8-well chamber imaging slides and grown overnight. After 30 minutes of staining with 0.5 μg/mL Hoechst 33342 (Life Technologies), cells were washed twice with PBS and incubated with indicated peptide concentrations. Cells were washed twice with PBS and imaged in Live Cell Imaging solution (Thermo Fisher Scientific). Images were taken with CLSM SP5 Mid UV-VIS Leica with 63× objective at 37°C at ambient CO_2 concentrations.

Flow cytometry

EdU incorporation was analyzed using the Click-it EdU technology (Thermo Fisher Scientific) according to the manufacturer's instructions. For peptide uptake studies, 1×10^5 cells were seeded into 12-well plates. The day after, peptide transfection was performed and cells were harvested by trypsinization to remove membrane-bound peptides. After one wash with PBS, cells were resuspended in PBS and subjected to flow cytometry analysis. To quantify intracellular peptide stability, same cells were released for indicated time points in DMEM + 10% FCS and fixed with 4% formaldehyde (w/v) in PBS for 15 minutes at room temperature. To measure the TAMRA fluorescence intensity, the LSR II Fortessa equipped with a 561 nm laser line and a 586/15 band-pass filter was used. Of note, the fluorescence intensity of TAMRA-labeled R9-$BRC4^{mut}$ peptides was corrected for quenching by multiplying measured TAMRA intensity with a quenching factor. The quenching factor was calculated by loading 10 pmol of freshly solubilized peptides on Tricine SDS-PAGE gel and quantifying TAMRA intensity (see Fig. 2C, lane 5). Fluorescein intensity was measured with Attune Nxt Flow Cytometer equipped with 488 laser and 530/30 band-pass filter. For each condition, 20,000 events were recorded. MACS Quant Calibration Beads (MACS Miltenyi Biotec) were applied for voltage standardization to exclude any machine-dependent variations between measurements.

Tricine SDS-PAGE

To resolve low molecular weight peptides, Tricine SDS-PAGE was performed as described previously (27). For peptide separation, Laemmli lysates were loaded onto 16% Tricine SDS-PAGE gel containing 6 mol/L urea. For peptide detection via fluorescence, gels were scanned using a Typhoon FLA 9500 FluorImager.

HR reporter assay

HR frequency was measured as described previously (28, 29). Briefly, following siRNA transfection, 1×10^5 HeLa cells containing a stably integrated DR-GFP reporter construct were seeded into 12-well plates. The day after, cells were either mock-transfected or transfected with 0.6 μg *I-SceI* expression plasmid (pCBASce) using jetPrime transfection reagent (Polyplus transfection). Four hours later, medium was exchanged and either a 1-hour peptide incubation or second siRNA transfection was performed. Peptide incubations were repeated 24 and 34 hours post–*I-SceI* transfection. After each peptide incubation, 0.5 mL of DMEM + 20% FCS was directly added to the peptide/DMEM mix. Forty-eight hours after *I-SceI* transfection, cells were harvested and directly analyzed for GFP expression by flow cytometry using an Attune Nxt Flow Cytometer.

Immunofluorescence microscopy

Twenty-four hours after siRNA transfection, 8×10^4 cells were seeded on coverslips in 24-well plates. The day after, cells were treated either with 100 nmol/L camptothecin for 1 hour or irradiated and incubated for another hour with the peptides, before releasing them for 3 hours by directly adding 1 mL of DMEM + 14% FCS. Alternatively, cells were transfected with the peptides, followed by 1-hour camptothecin treatment and direct processing. Cells were preextracted for 5 minutes on ice (25 mmol/L HEPES pH 7.4, 50 mmol/L NaCl, 1 mmol/L EDTA, 3 mmol/L $MgCl_2$, 300 mmol/L sucrose, 0.5% Triton X-100), fixed with 4% formaldehyde (w/v) in PBS for 15 minutes at room temperature, before incubating them with indicated primary and appropriate secondary antibodies for 1 hour. Afterwards, coverslips were mounted with Vectashield (Vector Laboratories) containing DAPI and sealed. Images were acquired on Leica DMI6000 widefield fluorescence microscope with a 63× objective.

DNA fiber analysis

DNA fiber analyses were carried out as described previously (30). In brief, U2OS cells were seeded into 6-well plates at a confluence of 40%. Twenty-four hours later, cells were pulse-labeled with 33 μmol/L CIdU for 30 minutes, followed by 340 μmol/L IdU for 30 minutes prior to incubation with 2 mmol/L HU and peptides (10 μmol/L) for 4 hours in serum-free medium. Cells were lysed (200 mmol/L Tris-HCl pH 7.4, 50 mmol/L EDTA, 0.5% SDS) and DNA fibers were stretched onto glass slides before fixation in methanol–acetic acid (3:1, Merck) overnight. Rehydration in PBS was followed by denaturation in 2.5 mol/L HCl for 1 hour, a PBS wash, and blockage (2% BSA (w/v) PBS, 0.1% Tween 20) for 40 minutes. CIdU and IdU staining was performed using anti-BrdU primary and secondary antibodies for 2.5 hours. Coverslips were mounted using Antifade Gold (Invitrogen). Images were acquired on Olympus microscope IX81 with ×60 magnification, and analysis was carried out using ImageJ software.

Published OnlineFirst April 13, 2018; DOI: 10.1158/1535-7163.MCT-17-1156

Colony formation assay

Indicated cell lines were plated in poly-L-lysine (Sigma-Aldrich) coated 24-well plates at low cell dilutions of 200 cells/well in technical triplicates. PEO1 and PEO4 cells were seeded at 500 and 1,000 cells/well, respectively. Twenty-four hours later, cells were washed once with PBS and incubated with olaparib in presence or absence of peptides. After 1 hour, 1 mL of appropriate medium containing 14% FCS with indicated olaparib concentrations was directly added to the cells without removing the peptide solution. For MCF10A cells, FCS concentration of culture medium was increased to 7%. Alternatively, HeLa cells were treated for 1 hour with 1 μmol/L camptothecin, washed twice with PBS, and peptide transfection was carried out for 1 hour before directly adding 1 mL of DMEM + 14% FCS. Cells were grown for 10 days before fixation with crystal violet solution [0.5 % crystal violet, 20% ethanol (w/v)]. For analysis, plates were scanned and analyzed with the ImageJ Plugin ColonyArea using the parameter colony intensity, integrating the percentage of the covered area and staining intensity (31).

Statistical analysis

All results were confirmed in at least two independent experiments. Quantitative data are displayed as mean ± SD, and statistical analyses were performed using GraphPad Prism 7. *P* values <0.05 were considered statistically significant.

Results

BRC4 peptide inhibits BRCA2–RAD51 interaction

It is well established that BRCA2 binds RAD51 through its BRC repeats composed of two highly conserved tetrameric motifs (Supplementary Fig. S1A). Among the eight BRC repeats, BRC4 was reported to display the highest affinity for RAD51, mainly using its FHTA sequence to bind the RAD51 oligomerization motif. To specifically target the BRCA2–RAD51 protein interaction interface, we therefore synthesized a 16-mer peptide mimicking the N-terminal half of BRC4 comprising the FHTA hydrophobic motif (Fig. 1A). In addition to the "wild type" BRC4 peptide ($BRC4^{wt}$), we included a "mutated" BRC4 peptide ($BRC4^{mut}$) harboring an inverted FHTA sequence (Fig. 1A). Employing N-terminally biotinylated peptides, recombinant RAD51 was efficiently pulled down by $BRC4^{wt}$ but to a much lesser extent by $BRC4^{mut}$ (Fig. 1B). In agreement with previous reports (32), we observed that GST-tagged BRCA2 fusion proteins spanning BRC 1-2, BRC 3-5, or the C-terminal (C-term) domain were able to interact with RAD51 (Supplementary

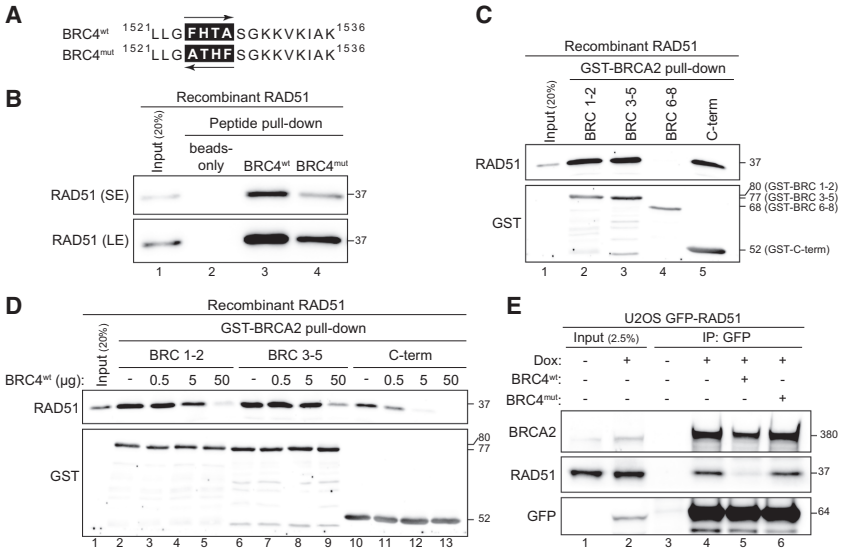

Figure 1.

A short BRC4 peptide inhibits BRCA2–RAD51 interaction. **A,** Amino acid sequences of BRCA2-derived 16-mer peptides used in this study. In addition to the wild-type BRC4 peptide ($BRC4^{wt}$), a mutant version ($BRC4^{mut}$) was included, characterized by an inverted FHTA tetrapeptide motif. **B,** Biotinylated BRC4 peptides coupled to streptavidin beads were used to perform pull-down assays using bacterially expressed and purified human RAD51. Inputs and pulled down protein complexes were analyzed by immunoblotting. SE and LE denote short and long exposure times of the same anti-RAD51 immunoblot. **C,** Different GST-BRCA2 fusion proteins coupled to glutathione–sepharose beads were used to perform pull-down assays using recombinant RAD51. Inputs and pulled down protein complexes were analyzed by immunoblotting. **D,** GST-BRCA2 pull-down assays with recombinant RAD51 in the absence or presence of increasing amounts of $BRC4^{wt}$ peptides. Inputs and pulled down protein complexes were analyzed by immunoblotting. **E,** Lysates of U2OS cells inducibly expressing GFP-RAD51 were supplemented with 50 μg of the indicated BRC4 peptides and subjected to immunoprecipitation (IP) using anti-GFP affinity resin. Inputs and coimmunoprecipitated protein complexes were analyzed by immunoblotting.

Published OnlineFirst April 13, 2018; DOI: 10.1158/1535-7163.MCT-17-1156

Fig. S1B; Fig. 1C). Remarkably, BRC4^{wt} was able to outcompete each of these individual interactions in a concentration-dependent manner (Fig. 1D). Interestingly, the BRC4 peptide was more effective in outcompeting RAD51 binding to the BRCA2 C-term and BRC repeats 1-2 than to BRC repeats 3-5 (Fig. 1D), indicating that the BRC4 repeat of BRCA2 exhibits the highest binding affinity for RAD51. Similar GST pull-down results were obtained using HeLa nuclear extracts as a source for RAD51 (Supplementary Fig. S1C). Given that the BRCA2 C-terminal region exclusively binds to assembled RAD51 oligomers, we reasoned that the BRC4 peptide is able to disrupt RAD51 multimers present in solution, which is in agreement with binding of the FHTA cluster to the RAD51 oligomerization motif (9, 10, 14). Most importantly, coimmunoprecipitation experiments in U2OS cells inducibly expressing GFP-tagged RAD51 demonstrated that BRC4^{wt}, but not BRC4^{mut}, is capable of interfering both with BRCA2 binding to RAD51 and RAD51 oligomerization (Fig. 1E; Supplementary Fig. S1D and S1E). Taken together, our results indicated that a short, synthetic BRC4-derived peptide is proficient in blocking BRCA2–RAD51 protein–protein interaction.

The CPP R9 facilitates intracellular delivery of BRC4

Native peptides do not readily cross cell membranes. To enhance cellular uptake, we decided to conjugate BRC4 peptides with a nona-arginine (R9) CPP. In addition, a red fluorescent dye (TAMRA) was N-terminally attached to R9-BRC4 peptides to analyze cellular uptake. Using confocal microscopy, we observed robust cytoplasmic and nuclear TAMRA signals in HeLa and U2OS cells upon transfection with R9-fused peptides (Fig. 2A). Moreover, we found that the concentration threshold for efficient R9-BRC4 cell penetration was above 10 μmol/L (Supplementary Fig. S2A). Flow cytometry analyses further confirmed that BRC4 peptide delivery reached a transduction efficiency of almost 100% when fused to R9 (Fig. 2B; Supplementary Fig. S2B). Importantly, when replacing the TAMRA label with a green fluorescent dye (Fluorescein), we observed very similar subcellular localization patterns and fluorescent intensities of the R9-BRC4 peptides (Supplementary Fig. S2C and S2D). As peptides are prone to proteolytic degradation upon cellular uptake, we next determined the amount of intact peptides being delivered to the cells. To differentiate between full-length and degraded peptides, whole-cell lysates of HeLa and U2OS cells incubated with fluorescently labeled peptides were subjected to SDS-PAGE designed for resolving very low molecular weight protein species (27). Using this approach, we detected significant amounts of intact TAMRA- and Fluorescein-labeled R9-BRC4 peptides being effectively delivered to HeLa and U2OS cells (Fig. 2C; Supplementary Fig. S2E). Comparing the band intensity of TAMRA signals between 10 pmol of freshly solubilized peptides directly loaded onto the gel and those of peptide-transduced cell lysates, we calculated a delivery rate of approximately 10^7 peptides per cell, yielding an estimated intracellular peptide concentration of around 1 to 10 μmol/L (Fig. 2C).

Next, to more precisely determine the intracellular residence time and stability of our BRC4 CPPs, we modified a previously established method (33) and monitored the Fluorescein signal intensity in HeLa cells over a time course of 24 hours after peptide incubation. SDS-PAGE analysis revealed that BRC4^{wt} as well as BRC4^{mut} cargo peptides were gradually degraded with an approximate half-life of 2 hours (Fig. 3A). Strikingly, using the same experimental setup, flow cytometry analysis of Fluorescein-R9-BRC4^{wt} indicated a rather heterogeneous degradation pattern, which was most pronounced after 8 hours with a large proportion of cells still showing moderate to high fluorescent intensities (Fig. 3B).

Collectively, we concluded that intracellular uptake of R9-BRC4^{wt} and R9-BRC4^{mut} was efficient and comparable as determined by confocal microscopy, flow cytometry, and SDS-PAGE analysis, thus providing a solid basis for further mechanistic investigations.

BRC4 peptide specifically inhibits RAD51-mediated HR

Conditional overexpression of full-length BRC4 was previously shown to inhibit DNA damage–induced RAD51 foci formation in MCF7 (breast cancer) and chicken DT40 cells (12, 34). Therefore, we wanted to investigate whether the 16-mer BRC4 peptide fused to R9 was able to mimic this phenotype, indicative of effective disruption of RAD51 binding to BRCA2. To this end, HeLa or U2OS cells were first incubated with our peptides and subsequently treated with the DNA topoisomerase I poison camptothecin to induce replication-dependent DSBs. Importantly, we did not detect any significant change in camptothecin-induced ATM and CHK2 phosphorylation as well as γH2AX foci formation upon peptide addition, indicating regular activation of apical DNA damage response kinases (Fig. 4A; Supplementary Fig. S3A and S3B). In contrast, camptothecin-induced RAD51 foci formation in both cell lines was specifically compromised in the presence of BRC4^{wt} but not BRC4^{mut} CPPs (Fig. 4B and C; Supplementary Fig. S3C and S3D). In line with this observation, BRC4^{wt} significantly suppressed RAD51 foci formation following ionizing radiation (Fig. 4D). Notably, intrinsic RAD51 protein stability was not affected by BRC4^{wt} cellular uptake (Supplementary Fig. S3E). To directly examine the impact of BRC4 peptides on DSB repair by HR, we performed repair reporter assays (DR-GFP) in HeLa cells and observed a significant decrease in HR frequency upon repetitive BRC4^{wt} transfections (Fig. 4E). Throughout all experiments reported in this section, we observed that siRNA-mediated BRCA2 depletion conferred much stronger phenotypes compared with delivery of the BRC4^{wt} peptide.

In summary, our findings suggested that delivery of a synthetic BRC4 peptide potently inhibits RAD51 foci formation and HR, most likely as a result of defective BRCA2-mediated RAD51 loading onto resected DSBs.

BRC4 peptide causes MRE11-dependent degradation of stalled replication forks

BRCA2-dependent RAD51 loading is not only critical for HR, but has also been established to protect stalled replication forks from nucleolytic degradation by MRE11 (35, 36). Thus, we examined a potential effect of the BRC4 peptide on replication fork protection by performing dual-labeling DNA fiber assays in the presence of HU, which stalls fork progression. Strikingly, we found that the BRC4^{wt} CPP resulted in shortening of nascent DNA tracts, indicative of increased fork degradation (Fig. 5A). BRC4 intracellular uptake did not interfere with global replication rates, as we could not observe any differences in EdU incorporation (Supplementary Fig. S4). Similar to what has been shown for BRCA2-deficient cells, fork degradation in BRC4 peptide–transduced cells was completely rescued both

Published OnlineFirst April 13, 2018; DOI: 10.1158/1535-7163.MCT-17-1156

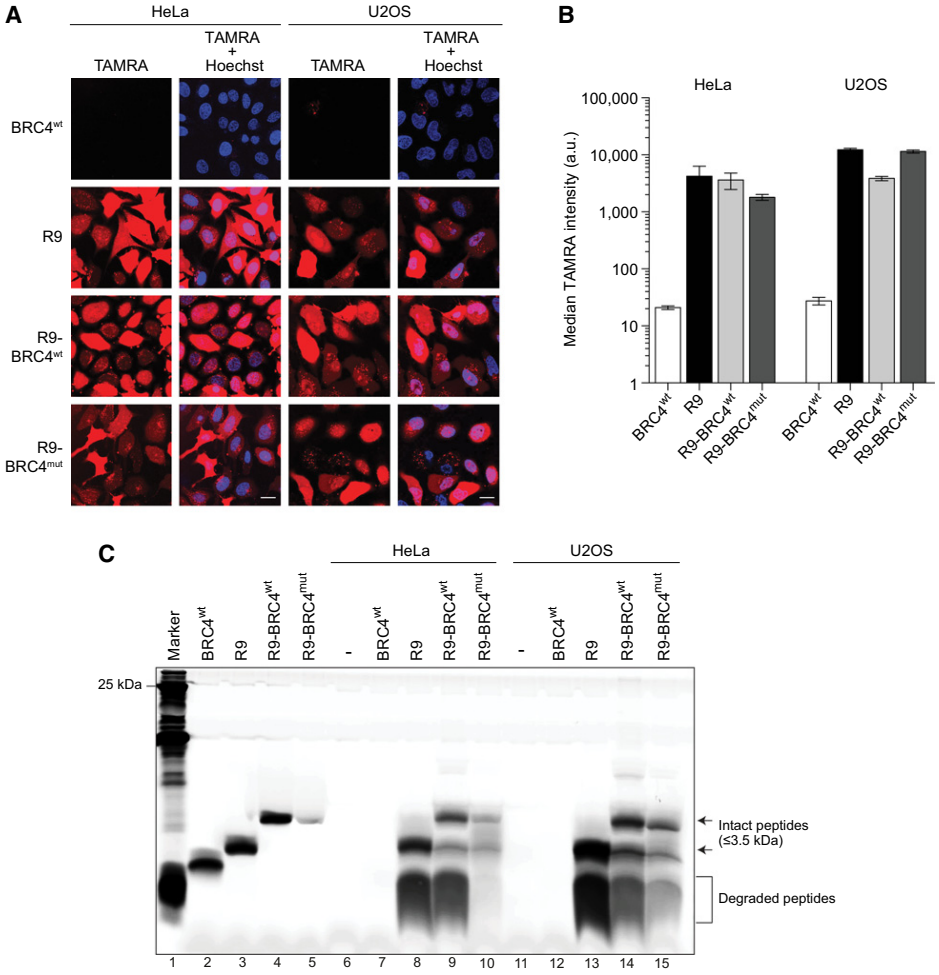

Figure 2.

The CPP nona-arginine (R9) mediates efficient delivery of BRC4 peptides into human cells. **A,** HeLa and U2OS cells were stained for 30 minutes with Hoechst 33342 to visualize nuclei and washed with PBS before adding 10 μmol/L of the indicated TAMRA-labeled peptides. After 1-hour incubation in serum-free medium, cells were washed thoroughly to remove any membrane-bound peptides, and live cells were directly imaged on a confocal microscope. Gains were adjusted for each condition to reduce background fluorescence and to visualize strong and weak signals at the same time. Scale bar, 20 μm. **B,** HeLa and U2OS cells were transfected with 10 μmol/L of the indicated TAMRA-labeled peptides in serum-free medium for 1 hour. Cells were harvested by trypsinization, and TAMRA signal intensities were recorded on a flow cytometer by scoring 20,000 events. Bar graph depicts median TAMRA fluorescence intensity. a.u., arbitrary units. Data, mean ± SD ($n = 3$). **C,** HeLa and U2OS cells were incubated with 10 μmol/L of the indicated TAMRA-labeled peptides. After 1 hour, cells were harvested by trypsinization. Freshly solubilized peptides (10 pmol; lanes 2–5) and whole-cell lysates of 70,000 peptide-transfected cells (lanes 6–15) were loaded onto Tricine SDS-PAGE gel, and TAMRA signals were visualized using a FluorolImager.

by mirin, an MRE11 SMI (Fig. 5B), and by siRNA-mediated MRE11 depletion (Fig. 5C). Of note, BRC4 delivery did not result in additive or synergistic effects when delivered into BRCA2-depleted cells, indicating that peptide-mediated fork degradation resulted most likely from specific targeting of the BRCA2–RAD51 interaction (Fig. 5C).

Published OnlineFirst April 13, 2018; DOI: 10.1158/1535-7163.MCT-17-1156

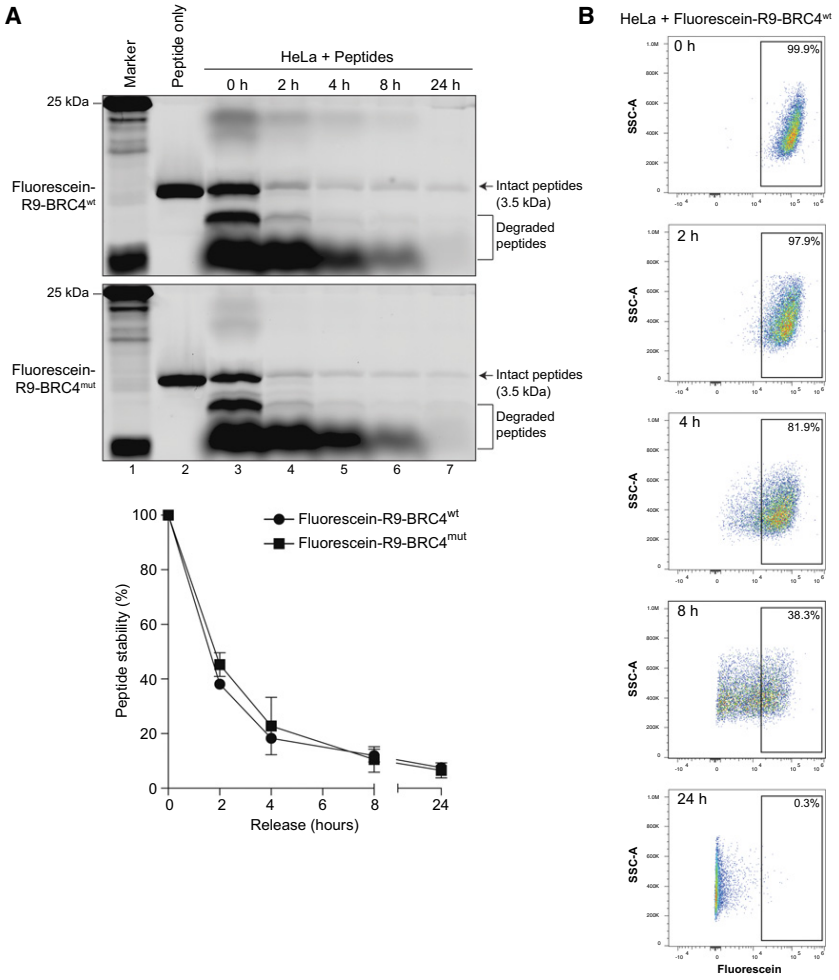

Figure 3.

R9-BRC4 peptides have an approximate half-life of 2 to 4 hours upon cell entry. **A,** HeLa cells were transfected with 10 μmol/L of the indicated Fluorescein-labeled peptides in serum-free DMEM for 1 hour, followed by a release in serum-containing medium for the indicated time points. Top, 10 pmol of freshly solubilized peptides (lane 2) and whole-cell lysates of peptide-transduced cells (lanes 3–7) were loaded onto Tricine SDS-PAGE gel, and Fluorescein signals were analyzed using a FluorolImager. Bottom, quantification of relative Fluorescein signal intensities of intact full-length R9-BRC4^{wt} and R9-BRC4^{mut} peptides. Data, mean ± SD (n = 4). **B,** HeLa cells incubated with Fluorescein-R9-BRC^{wt} peptides as in **A** were analyzed by flow cytometry recording 20,000 events for each condition. The intensity of the Fluorescein signal is plotted against the side-scatter area (SSC-A). Gates display percentages of cells showing moderate to high fluorescent intensities.

BRC4 peptide confers hypersensitivity to PARP inhibition in cancer cell lines

On the basis of our molecular analyses providing robust evidence of the inhibitory effect of the BRC4 peptide on BRCA2 functions in HR and fork protection, we next sought to determine whether it also sensitizes cells to DNA-damaging agents. Profound hypersensitivity of BRCA2-mutant cells to PARP inhibitors has become an emerging therapeutic paradigm

Published OnlineFirst April 13, 2018; DOI: 10.1158/1535-7163.MCT-17-1156

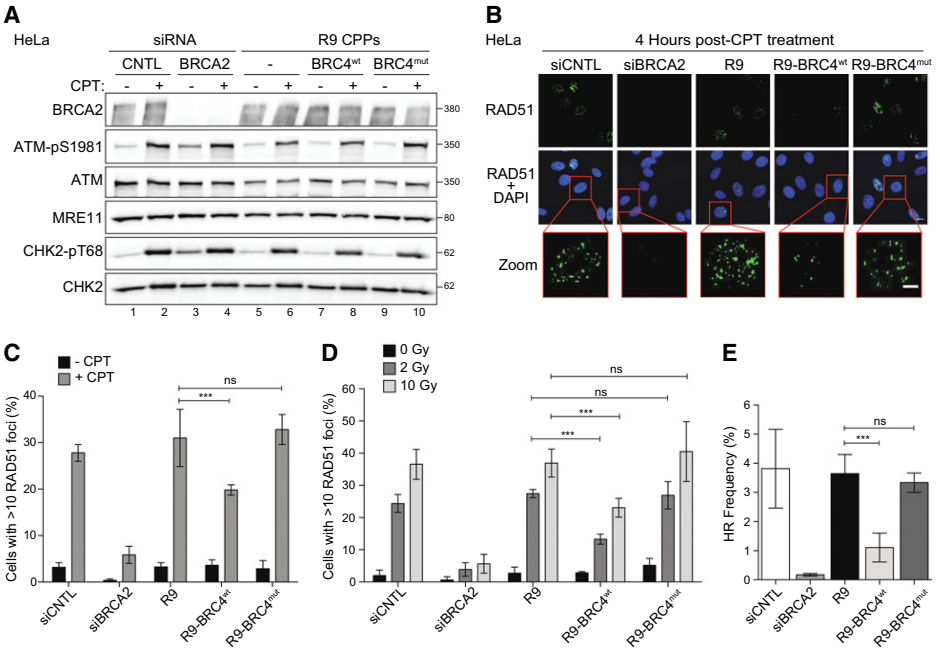

Figure 4.

BRC4 peptide inhibits RAD51 foci formation and HR. **A,** HeLa cells were either transfected with control (CNTL) or BRCA2 siRNA oligos for 48 hours, or incubated with 10 μmol/L of the indicated CPPs for 1 hour before treatment with 100 nmol/L camptothecin (CPT) for 1 hour. Whole-cell lysates were analyzed by immunoblotting using the indicated antibodies. **B** and **C,** Same cells as in **A** were treated with 100 nmol/L camptothecin for 1 hour before transfecting them with the depicted peptides (10 μmol/L) for 1 hour and releasing them for 3 hours in serum-containing medium. Cells were preextracted, fixed, and immunostained for RAD51. **B,** Scale bars, 10 and 5 μm (Zoom). **C,** The graph illustrates the percentage of cells displaying more than 10 RAD51 foci/nucleus. For each condition, at least 100 cells were scored. **D,** Same cells as in **A** were irradiated with increasing doses of IR, peptide-transfected (10 μmol/L), and released for 3 hours in serum-containing medium prior to preextraction, fixation, and immunostaining for RAD51. The graph illustrates the percentage of cells displaying more than 10 RAD51 foci/nucleus. For each condition, at least 100 cells were scored. **E,** HeLa DR-GFP cells were transfected with the *I-SceI* expression plasmid 48 hours post-siRNA transfection. Alternatively, 1-hour incubation periods with 10 μmol/L peptides took place 4, 24, and 34 hours post–*I-SceI* transfection of HeLa DR-GFP cells. A second siRNA transfection was performed 24 hours after I-SceI transfection. Cells were harvested 48 hours post–*I-SceI* transfection, and GFP-positive cells were scored by flow cytometry. A total of 20,000 events were recorded. The graph illustrates the percentage of GFP-positive cells as a readout for HR efficiency. Data in **C–E** display the mean ± SD ($n \geq 3$). Statistical significance (***, $P \leq 0.001$; ns, nonsignificant) was calculated with Tukey multiple comparison test using two-way ANOVA (**C** and **D**) and one-way ANOVA (**E**).

known as synthetic lethality (37). Therefore, we performed clonogenic survival assays in peptide-transfected HeLa cells treated with the PARP inhibitor olaparib (38). Indeed, targeting of the BRCA2–RAD51 interaction by BRC4^{wt} CPPs resulted in a significant reduction in cellular viability in response to chronic PARP inhibition (Fig. 6A and B). Consistent with impaired RAD51 foci formation, delivery of BRC4^{wt} CPPs also sensitized HeLa cells to camptothecin (Supplementary Fig. S5A). Upon treatment with olaparib, we estimated the IC_{50} value of BRC4 to be around 10 μmol/L for HeLa cells (Fig. 6C). Importantly, R9-BRC4^{wt} alone did not decrease cell survival in otherwise undamaged cells (Fig. 6C). Moreover, despite its relatively short half-life, the efficacy of BRC4 CPPs in sensitizing HeLa cells to PARP inhibition was comparable with that of the B02 small-molecule compound, which specifically inhibits RAD51 binding to DNA (Fig. 6D; refs. 23, 39). To further exclude potential off-target effects of the BRC4 CPP in stimulating olaparib-induced cytotoxicity, we employed PEO1 (BRCA2 null) and PEO4 (BRCA2 revertant to wild type) isogenic ovarian cancer cell lines (40). Notably, we observed a strong synergy between PARP inhibition and R9-BRC4 peptides in PEO4 cells, whereas PEO1 cells did not exhibit BRC4-mediated sensitivity toward olaparib (Supplementary Fig. S5B). Differential peptide uptake could be excluded as both cell lines displayed comparable uptake efficiency and intracellular peptide localization (Supplementary Fig. S5B). Finally, in addition to HeLa cells, we observed that BRC4 CPPs elicited olaparib-induced cell death of U2OS human osteosarcoma cells but not of noncancerous

Published OnlineFirst April 13, 2018; DOI: 10.1158/1535-7163.MCT-17-1156

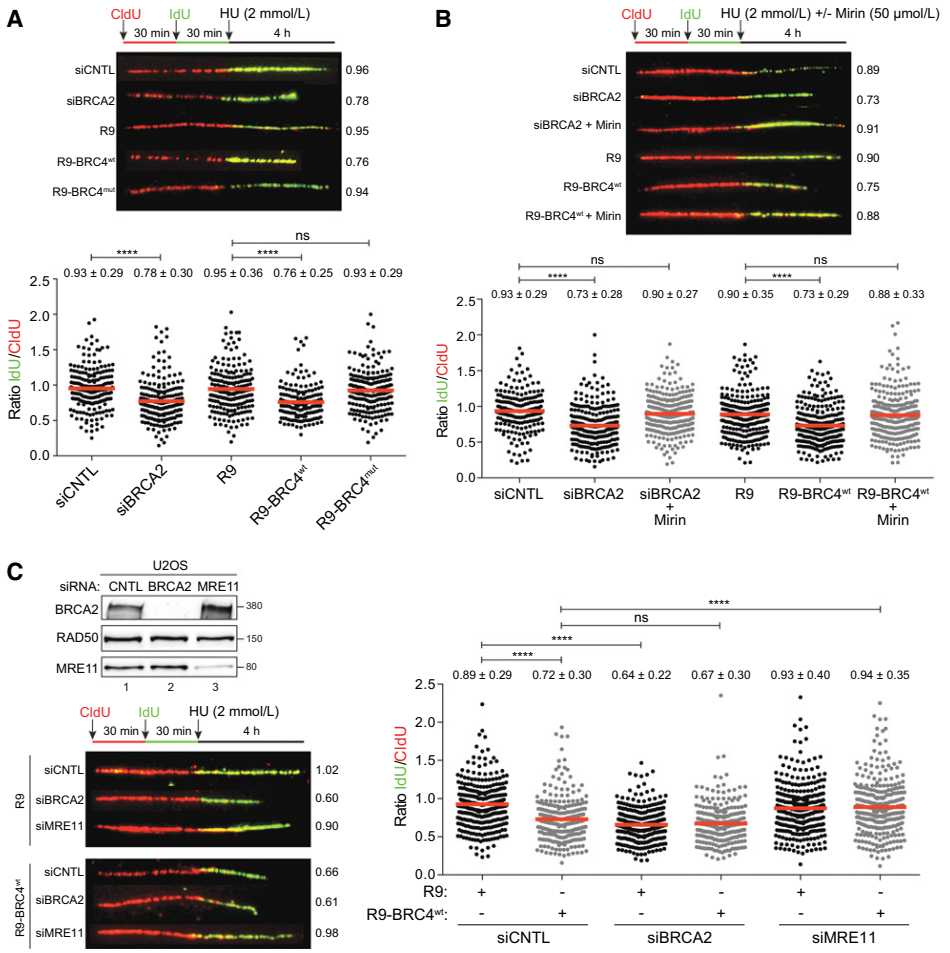

Figure 5.

BRC4 peptide provokes MRE11-dependent degradation of stalled DNA replication forks. **A,** U2OS cells were transfected with indicated siRNA oligos for 48 hours or left untransfected. Subsequently, cells were labeled with CldU and IdU before adding hydroxyurea (HU) together with indicated peptides (10 µmol/L) in serum-free medium for 4 hours followed by DNA fiber spreading. Top, experimental setup, representative DNA fiber images, and their corresponding IdU/CldU ratios, respectively; bottom, IdU/CldU ratios for each condition illustrated by a dot plot with mean ratios denoted as a red line. **B,** Same cells as in **A** were additionally treated with the MRE11 inhibitor mirin. **C,** U2OS cells were transfected with the indicated siRNA oligos for 48 hours before dual labeling and HU treatment in combination with 10 µmol/L R9 or R9-BRC4^{wt} peptides. Representative immunblot is shown to indicate individual knockdown efficiencies. Approximately 250 DNA replication tracks were scored, and numbers indicate the mean ± SD ($n = 2$). Statistical differences (****, $P \leq 0.0001$; ns, nonsignificant) were determined by Mann–Whitney U test.

cell lines, including hTERT-immortalized human retinal pigment epithelial cells (hTERT-RPE1), SV40-immortalized human fetal lung fibroblasts (MRC5) and human breast epithelial cells (MCF10A; Fig. 6E; Supplementary Fig. S6A). This finding could at least in part be explained by an overall low cellular uptake efficiency and predominant endosome trapping of BRC4 peptides in RPE1, MRC5, and MCF10A nontumorigenic cell lines (Supplementary Fig. S6B and S6C).

Published OnlineFirst April 13, 2018; DOI: 10.1158/1535-7163.MCT-17-1156

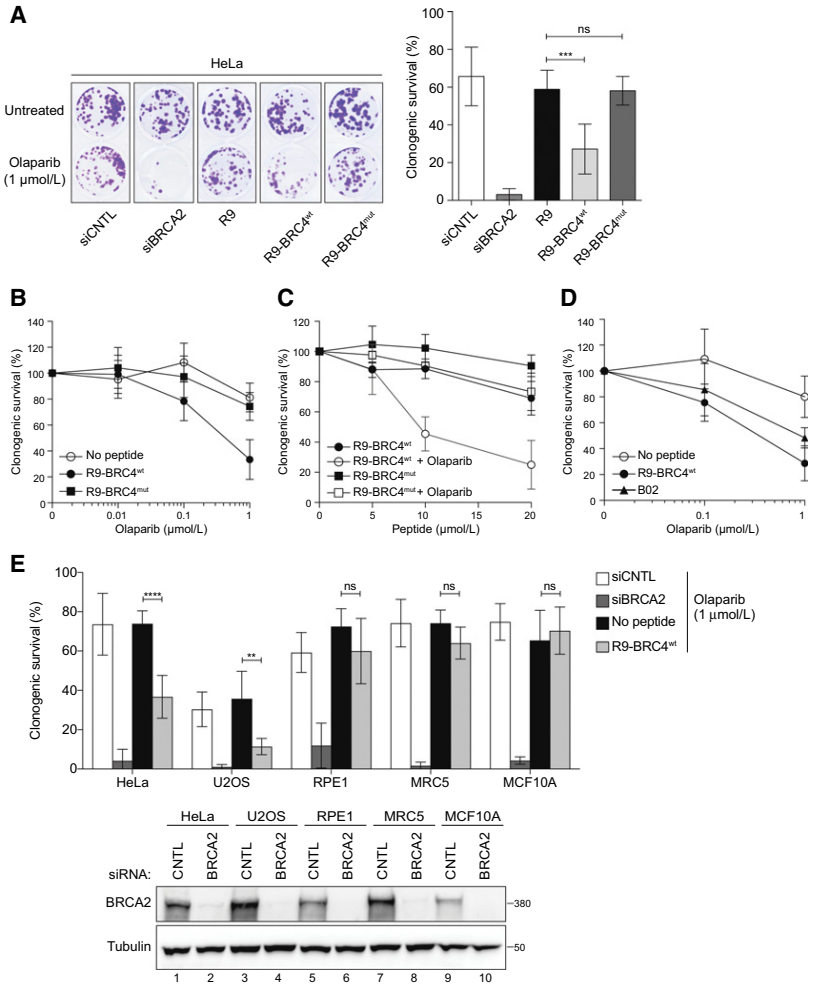

Figure 6.

BRC4 peptide sensitizes cancer cells to PARP inhibition. **A,** HeLa cells were transfected with the indicated siRNAs or left untransfected for standard peptide transduction. Twenty-four hours later, cells were plated at low cell density into 24-well plates. Another 24 hours later, non-siRNA transfected cells were incubated for 1 hour with 10 μmol/L of peptides in serum-free medium supplemented with 1 μmol/L olaparib. Finally, serum-containing medium supplemented with 1 μmol/L olaparib was added, cells were grown for 10 days, and colonies were stained using crystal violet. Representative images of a colony formation assay are shown. Clonogenic survival was determined by quantifying the colony intensity of olaparib-treated relative to untreated and is depicted as bar graph. Data, mean ± SD ($n = 4$). Statistical significance (***, $P \leq 0.001$; ns, nonsignificant) was calculated with Tukey multiple comparison test using one-way ANOVA. **B,** Peptide-transfected HeLa cells as in **A** were treated with increasing concentrations of olaparib, and survival was determined by colony formation assay. **C,** Same cells as in **A** were treated with 1 μmol/L olaparib in combination with increasing concentrations of BRC4 peptides, and survival was determined by colony formation assay. **D,** Same cells as in **B** were treated with 10 μmol/L of the RAD51 inhibitor BO2 under identical experimental conditions as used for the BRC4 peptide, and survival was determined by colony formation assay. Data in **B–D** are represented as mean ± SD ($n \leq 3$). **E,** HeLa, U2OS, RPE1, MRC5, and MCF10A were identically treated as in **A**, and survival was determined by colony formation assay. Bottom, knockdown efficiencies were analyzed by immunoblotting of whole-cell lysates of indicated cell lines; Top, relative clonogenic survival is depicted as mean ± SD ($n = 4$). Statistical significance (****, $P \leq 0.0001$; **, $P \leq 0.01$; ns, nonsignificant) was calculated with Tukey multiple comparison test using one-way ANOVA.

Published OnlineFirst April 13, 2018; DOI: 10.1158/1535-7163.MCT-17-1156

Discussion

PPIs represent attractive but at the same time challenging targets for pharmacologic intervention in cancer therapy. The emergence of successful peptide-based PPI inhibitors seemed promising, yet drug development was faced with the low membrane translocation ability of native peptides. The identification of a wide range of carrier molecules, commonly termed as CPPs or protein transduction domains, provided a possible solution for this major limitation (19).

Here, we designed a 16-amino acid short peptide derived from the N-terminal half of the human BRCA2 BRC4 repeat able to occupy the RAD51 oligomerization interface and thereby potently inhibiting the interaction between BRCA2 and RAD51. Covalent fusion of the BRC4 peptide with the cationic polyarginine R9 CPP resulted in efficient uptake into both cytoplasm and nucleus, causing defects in HR repair, increased fork degradation, and, ultimately, hypersensitivity to DNA-damaging agents.

Detailed biochemical studies have demonstrated that the full-length BRC4 repeat covering both FHTA and LFDE tetrameric cluster motifs selectively interacts with RAD51 and inhibits RAD51–DNA complex formation (15, 41). To increase the likelihood of intracellular peptide uptake (42), we reduced the length of the native BRC4 peptide sequence from 35 to 16 amino acids, including only the first FHTA module, which was shown to mimic the RAD51 oligomerization motif (14). In line with our findings, a similar 17-mer N-terminal BRC4 peptide was reported to compete with full-length BRC4 for RAD51 binding, albeit with modest potency (15). We further corroborated the importance of the FHTA sequence by showing that BRC4 16-mer peptides harboring a mirrored ATHF sequence display greatly reduced RAD51 binding affinity.

Importantly, intracellular BRC4 peptide uptake in the low micromolar range was sufficient to impair BRCA2–RAD51 complex formation. A high uptake efficiency was likely achieved through a combination of the potent CPP R9 with the beneficial biochemical properties of the BRC4 peptide, including its positive net charge, hydrophobicity, and three-dimensional conformation (18). CPP internalization involves both endocytosis and direct translocation, whereby direct cell penetration is preferred because endocytosis can lead to the trapping of peptides in endosomes and their ultimate degradation (18). Multiple factors, including the CPP, cargo identity, concentration, cell type, and differentiation status, influence the balance between both uptake mechanisms (18). We primarily observed a diffuse fluorescent staining and only minor punctuate patterns, indicative of direct translocation as the preferred uptake mechanism. The substantial number of peptide molecules reaching the intracellular space might compensate for the short half-life. Even though only 5% of intact peptides are present 24 hours after transfection, the absolute peptide number per cell at this stage still adds up to 10^6 functional peptides. According to a recent proteomics study in the U2OS cell line, most proteins involved in DSB repair processes, including BRCA2, were shown to be of low to moderate abundance (10^2–10^4 copies/cell; ref. 43). On the basis of these numbers, we speculated that BRC4 peptides are present in high molar excess over their endogenous BRCA2 target protein even 24 hours after uptake.

RAD51 and its property to self-assemble are under dynamic control to enable faithful homology-directed DSB repair. Yu and colleagues proposed the presence of three RAD51 fractions in the cell: a mobile fraction of RAD51 monomers, an immobile oligomerized fraction, and an immobile BRCA2-bound fraction (44). Strikingly, they found the BRCA2-bound fraction to be selectively mobilized upon DNA damage and suggested a dual BRCA2 function of RAD51 sequestration and mobilization. Importantly, the other fractions did not change, suggesting that only the BRCA2-bound RAD51 fraction is involved in DNA repair. Notably, R9-BRC4^{wt} did not affect viability under unstressed growth conditions of conventionally cultured cancer cell lines. Thus, we hypothesize that under normal, undamaged conditions, RAD51 is stably bound to BRCA2 and the peptide's affinity for RAD51 is not high enough to disassemble the protein complex. Accordingly, the BRC4 mimetic peptide is only able to disassemble mobilized BRCA2–RAD51 complexes. We speculate that upon mobilization and ultimate RAD51 loading onto ssDNA, the protein complex becomes increasingly unstable due to an equilibrium change during DNA loading. In this context, the peptide is potent enough to sequester RAD51 transiently dissociated from BRCA2. We further presume that at low levels of DNA damage, requiring only a small fraction of BRCA2-bound RAD51, repair processes are not significantly disturbed by the BRC4 peptide. However, upon increasing DNA damage load and replication stress, when there is a high demand of functional BRCA2–RAD51 complexes, a major pool of RAD51 is sequestered away from BRCA2 by the BRC4 peptide.

Despite its potentially rather high dissociation constant compared with SMIs, BRC4 peptides provided an unexpectedly high degree of specificity. CPPs have often been reported to cause unspecific membrane disruption, which has led to false conclusions regarding their specificity for a number of peptide therapeutics. Because we do not observe a decrease in cell viability upon BRC4 peptide uptake, we can exclude such unspecific CPP-mediated toxicity (45). Furthermore, our finding that MRE11 depletion fully rescued the peptide-induced replication fork degradation phenotype and the lack of synergy between peptides and PARP inhibition in BRCA2-deficient cancer cells argue against potential off-target activity of the BRC4 CPP. Nevertheless, when comparing the outcomes of siRNA-mediated BRCA2 depletion versus R9-BRC4^{wt} peptide delivery, depletion is commonly yielding much more pronounced phenotypes. A possible explanation for this relates to the high susceptibility of peptides to extra- and intracellular protease attacks (17). To improve their pharmacokinetic potential, possible peptide optimizations include various backbone modifications and cyclization (17, 46). Moreover, the BRCA2–RAD51 interaction might not be completely abolished by the BRC4 peptide as it only comprises the first FHTA but lacks the second LFDE tetrameric cluster motif.

The lack of cell-type specificity is commonly reported to present another major limitation of CPP-mediated drug delivery (19, 20). Strikingly, we could not find a synergistic relationship between the PARP inhibitor olaparib and the R9-BRC4 peptide in normal cell lines as compared with cancer cell lines. Interestingly, our peptide uptake data suggest an overall decreased intracellular BRC4 concentration. It is reasonable to speculate that efficient intracellular peptide delivery relies on specific membrane components or lipid compositions that are more uptake responsive in cancer versus noncancerous cell lines. Numerous reports classify lipid metabolic reprogramming as a major source of cell transformation (47). Specifically, the

Published OnlineFirst April 13, 2018; DOI: 10.1158/1535-7163.MCT-17-1156

sphingolipid metabolism, which was suggested to influence R9-mediated peptide uptake, was reported to significantly alter during transformation (48). In addition, cancer cells possess a more negatively charged membrane than normal cells, which is partly caused by a loss in membrane symmetry and the exposure of anionic phosphatidylcholine on the outer leaflet (49). This feature, in combination with higher membrane fluidity (50), might favor the uptake of the cationic R9-BRC4 peptide.

Ultimately, the BRC4 peptide could emerge as a potent radio- and chemosensitizer. Specifically, BRC4 peptide–induced HR deficiency could represent a promising strategy for expanding the utility of PARP inhibitors, successfully applied in breast and ovarian cancer patients with a germline BRCA1 or BRCA2 mutation (51, 52), to BRCA-proficient cancers. Similarly, the BRC4 peptide could resensitize BRCA1/2-mutated tumors that acquired chemoresistance to PARP inhibitors by restoring HR (53). Moreover, malignant cells are frequently compromised in genome stability maintenance pathways that are synthetically lethal with HR deficiency (54). Consequently, monotherapy with the identified BRCA2 peptide inhibitor could provide a promising option for the treatment of these tumors. The BRCA2–BRC4 peptide described in this study could also be applied in combination with proton irradiation, which was shown to be highly advantageous over conventional photon therapy. Notably, it was found that HR-deficient tumor cells exhibit an enhanced susceptibility toward proton versus photon irradiation (55). Drug-induced HR deficiency with the BRC4 peptide inhibitor could make this advantageous effect accessible for patients with HR-proficient tumors. Finally, we reveal a straightforward approach to study distinct PPIs in a biological context without the need of elaborate mutagenesis methodologies and provide a potent research tool to study BRCA2-dependent RAD51 loading to ssDNA in different biological contexts.

Disclosure of Potential Conflicts of Interest

No potential conflicts of interest were disclosed.

Authors' Contributions

Conception and design: A. Trenner, A.A. Sartori
Development of methodology: A. Trenner, A.A. Sartori
Acquisition of data (provided animals, acquired and managed patients, provided facilities, etc.): A. Trenner, J. Godau,
Analysis and interpretation of data (e.g., statistical analysis, biostatistics, computational analysis): A. Trenner, A.A. Sartori
Writing, review, and/or revision of the manuscript: A. Trenner, J. Godau, A.A. Sartori
Study supervision: A.A. Sartori

Acknowledgments

The authors would like to thank Roland Brock (Institute of Molecular Life Sciences, Radboud University Nijmengen, the Netherlands), Martin Pruschy (Clinic of Radiation Oncology, University Hospital Zurich, Zurich, Switzerland), and Stefano Ferrari (Institute of Molecular Cancer Research, University of Zurich, Zurich, Switzerland) for scientific input. We are grateful to Pavel Janscak (Institute of Molecular Cancer Research, University of Zurich) for providing purified, recombinant RAD51 protein and anti-RAD51 rabbit polyclonal antibody and to Fumiko Esashi (Sir William Dunn School of Pathology, University of Oxford, Oxford, United Kingdom) for providing the GST-tagged BRCA2 fusion plasmids. Furthermore, we are grateful to Ross Chapman (Nuffield Department of Medicine, University of Oxford) for providing hTERT-RPE1 cells, Minoru Takata (Radiation Biology Center, Kyoto University, Kyoto, Japan) for the U2OS GFP-RAD51 cell line, Marcel van Vugt (Medical Oncology Department, University Medical Centre Groningen, Groningen, the Netherlands) for HeLa DR-GFP cells, and Steve Jackson (Gurdon Institute, Cambridge, United Kingdom) for MRC5 cells. We also want to thank Antonio Porro (Institute of Molecular Cancer Research, University of Zurich) for critical reading of the manuscript. This study was supported by research grants from the Krebsliga Schweiz (KFS-3845-02-2016, to A.A. Sartori), Swiss National Science Foundation (31003A_156023 and 31003A_176161, to A.A. Sartori), Promedica Stiftung (1317/M to A.A. Sartori), and Novartis Foundation for Medical-Biological Research (#17C155 to A.A. Sartori).

The costs of publication of this article were defrayed in part by the payment of page charges. This article must therefore be hereby marked *advertisement* in accordance with 18 U.S.C. Section 1734 solely to indicate this fact.

Received November 21, 2017; revised March 1, 2018; accepted April 4, 2018; published first April 13, 2018.

References

1. Negrini S, Gorgoulis VG, Halazonetis TD. Genomic instability–an evolving hallmark of cancer. Nat Rev Mol Cell Biol 2010;11:220–8.
2. Ceccaldi R, Rondinelli B, D'Andrea AD. Repair pathway choices and consequences at the double-strand break. Trends Cell Biol 2016;26:52–64.
3. Kolinjivadi AM, Sannino V, de Antoni A, Técher H, Baldi G, Costanzo V. Moonlighting at replication forks - a new life for homologous recombination proteins BRCA1, BRCA2 and RAD51. FEBS Lett 2017;591:1083–100.
4. Hühn D, Bolck HA, Sartori AA. Targeting DNA double-strand break signalling and repair: recent advances in cancer therapy. Swiss Med Wkly 2013;143:w13837.
5. Carvalho JFS, Kanaar R. Targeting homologous recombination-mediated DNA repair in cancer. Expert Opin Ther Targets 2014;18:427–58.
6. Fradet-Turcotte A, Sitz J, Grapton D, Orthwein A. BRCA2 functions: from DNA repair to replication fork stabilization. Endocr Relat Cancer 2016;23:T1–T17.
7. Liu J, Doty T, Gibson B, Heyer WD. Human BRCA2 protein promotes RAD51 filament formation on RPA-covered single-stranded DNA. Nat Struct Mol Biol 2010;17:1260–2.
8. Wong AK, Pero R, Ormonde PA, Tavtigian SV, Bartel PL. RAD51 interacts with the evolutionarily conserved BRC motifs in the human breast cancer susceptibility gene brca2. J Biol Chem 1997;272:31941–4.
9. Esashi F, Galkin VE, Yu X, Egelman EH, West SC. Stabilization of RAD51 nucleoprotein filaments by the C-terminal region of BRCA2. Nat Struct Mol Biol 2007;14:468–74.
10. Davies OR, Pellegrini L. Interaction with the BRCA2 C terminus protects RAD51-DNA filaments from disassembly by BRC repeats. Nat Struct Mol Biol 2007;14:475–83.
11. Carreira A, Kowalczykowski SC. Two classes of BRC repeats in BRCA2 promote RAD51 nucleoprotein filament function by distinct mechanisms. Proc Natl Acad Sci U S A 2011;108:10448–53.
12. Chen CF, Chen PL, Zhong Q, Sharp ZD, Lee WH. Expression of BRC repeats in breast cancer cells disrupts the BRCA2-Rad51 complex and leads to radiation hypersensitivity and loss of G(2)/M checkpoint control. J Biol Chem 1999;274:32931–5.
13. Carreira A, Hilario J, Amitani I, Baskin RJ, Shivji MK, Venkitaraman AR, et al. The BRC repeats of BRCA2 modulate the DNA-binding selectivity of RAD51. Cell 2009;136:1032–43.
14. Pellegrini L, Yu DS, Lo T, Anand S, Lee M, Blundell TL, et al. Insights into DNA recombination from the structure of a RAD51-BRCA2 complex. Nature 2002;420:287–93.

Published OnlineFirst April 13, 2018; DOI: 10.1158/1535-7163.MCT-17-1156

15. Rajendra E, Venkitaraman AR. Two modules in the BRC repeats of BRCA2 mediate structural and functional interactions with the RAD51 recombinase. Nucleic Acids Res 2009;38:82–96.
16. Ivanov AA, Khuri FR, Fu H. Targeting protein-protein interactions as an anticancer strategy. Trends Pharmacol Sci 2013;34:393–400.
17. Tsomaia N. Peptide therapeutics: targeting the undruggable space. Eur J Med Chem 2015;94:459–70.
18. Kristensen M, Birch D, Mørck Nielsen H. Applications and challenges for use of cell-penetrating peptides as delivery vectors for peptide and protein cargos. Int J Mol Sci 2016;17:pii:185.
19. Guidotti G, Brambilla L, Rossi D. Cell-penetrating peptides: from basic research to clinics. Trends Pharmacol Sci 2017;38:406–24.
20. Raucher D, Ryu JS. Cell-penetrating peptides: strategies for anticancer treatment. Trends Mol Med 2015;21:560–70.
21. Tünnemann G, Ter-Avetisyan G, Martin RM, Stöckl M, Herrmann A, Cardoso MC. Live-cell analysis of cell penetration ability and toxicity of oligo-arginines. J Pept Sci 2008;14:469–76.
22. Sato K, Shimomuki M, Katsuki Y, Takahashi D, Kobayashi W, Ishiai M, et al. FANCI-FANCD2 stabilizes the RAD51-DNA complex by binding RAD51 and protects the 5′-DNA end. Nucleic Acids Res 2016;44:10758–71.
23. Huang F, Motlekar NA, Burgwin CM, Napper AD, Diamond SL, Mazin AV. Identification of specific inhibitors of human RAD51 recombinase using high-throughput screening. ACS Chem Biol 2011;6:628–35.
24. Dupré A, Boyer-Chatenet L, Sattler RM, Modi AP, Lee JH, Nicolette ML, et al. A forward chemical genetic screen reveals an inhibitor of the Mre11-Rad50-Nbs1 complex. Nat Chem Biol 2008;4:119–25.
25. Lee M, Daniels MJ, Venkitaraman AR. Phosphorylation of BRCA2 by the Polo-like kinase Plk1 is regulated by DNA damage and mitotic progression. Oncogene 2003;23:865–72.
26. Piwko W, Mlejnkova LJ, Mutreja K, Ranjha L, Stafa D, Smirnov A, et al. The MMS22L-TONSL heterodimer directly promotes RAD51-dependent recombination upon replication stress. EMBO J 2016;35:2584–601.
27. Schägger H. Tricine-SDS-PAGE. Nat Protoc 2006;1:16–22.
28. Steger M, Murina O, Hühn D, Ferretti LP, Walser R, Hänggi K, et al. Prolyl isomerase PIN1 regulates DNA double-strand break repair by counteracting DNA end resection. Mol Cell 2013;50:333–43.
29. Krajewska M, Fehrmann RSN, Schoonen PM, Labib S, de Vries EG, Franke L, et al. ATR inhibition preferentially targets homologous recombination-deficient tumor cells. Oncogene 2015;34:3474–81.
30. Merrick CJ, Jackson D, Diffley JFX. Visualization of altered replication dynamics after DNA damage in human cells. J Biol Chem 2004;279:20067–75.
31. Guzmán C, Bagga M, Kaur A, Westermarck J, Abankwa D. ColonyArea: an ImageJ plugin to automatically quantify colony formation in clonogenic assays. PLoS One 2014;9:e92444.
32. Esashi F, Christ N, Gannon J, Liu Y, Hunt T, Jasin M, et al. CDK-dependent phosphorylation of BRCA2 as a regulatory mechanism for recombinational repair. Nature 2005;434:598–604.
33. Ruttekolk IR, Witsenburg JJ, Glauner H, Bovee-Geurts PH, Ferro ES, Verdurmen WP, et al. The intracellular pharmacokinetics of terminally capped peptides. Mol Pharm 2012;9:1077–86.
34. Abe T, Branzei D. High levels of BRC4 induced by a Tet-On 3G system suppress DNA repair and impair cell proliferation in vertebrate cells. DNA Repair 2014;22:153–64.
35. Schlacher K, Christ N, Siaud N, Egashira A, Wu H, Jasin M. Double-strand break repair-independent role for BRCA2 in blocking stalled replication fork degradation by MRE11. Cell 2011;145:529–42.
36. Hashimoto Y, Ray Chaudhuri A, Lopes M, Costanzo V. Rad51 protects nascent DNA from Mre11-dependent degradation and promotes continuous DNA synthesis. Nat Struct Mol Biol 2010;17:1305–11.
37. Farmer H, McCabe N, Lord CJ, Tutt AN, Johnson DA, Richardson TB, et al. Targeting the DNA repair defect in BRCA mutant cells as a therapeutic strategy. Nature 2005;434:917–21.
38. Menear KA, Adcock C, Boulter R, Cockcroft XL, Copsey L, Cranston A, et al. 4-[3-(4-cyclopropanecarbonylpiperazine-1-carbonyl)-4-fluorobenzyl]-2H-phthalazin-1-one: a novel bioavailable inhibitor of poly(ADP-ribose) polymerase-1. J Med Chem 2008;51:6581–91.
39. Huang F, Mazina OM, Zentner IJ, Cocklin S, Mazin AV. Inhibition of homologous recombination in human cells by targeting RAD51 recombinase. J Med Chem 2012;55:3011–20.
40. Sakai W, Swisher EM, Jacquemont C, Chandramohan KV, Couch FJ, Langdon SP, et al. Functional restoration of BRCA2 protein by secondary BRCA2 mutations in BRCA2-mutated ovarian carcinoma. Cancer Res 2009;69:6381–6.
41. Davies AA, Masson JY, McIlwraith MJ, Stasiak AZ, Stasiak A, Venkitaraman AR, et al. Role of BRCA2 in control of the RAD51 recombination and DNA repair protein. Mol Cell 2001;7:273–82.
42. Renukuntla J, Vadlapudi AD, Patel A, Boddu SH, Mitra AK. Approaches for enhancing oral bioavailability of peptides and proteins. Int J Pharm 2013;447:75–93.
43. Beck M, Schmidt A, Malmstroem J, Claassen M, Ori A, Szymborska A, et al. The quantitative proteome of a human cell line. Mol Syst Biol 2011;7:549.
44. Yu DS, Sonoda E, Takeda S, Huang CL, Pellegrini L, Blundell TL, et al. Dynamic control of Rad51 recombinase by self-association and interaction with BRCA2. Mol Cell 2003;12:1029–41.
45. El-Andaloussi S, Järver P, Johansson HJ, Langel Ü. Cargo-dependent cytotoxicity and delivery efficacy of cell-penetrating peptides: a comparative study. Biochem J 2007;407:285–92.
46. Wójcik P, Berlicki Ł. Peptide-based inhibitors of protein-protein interactions. Bioorg Med Chem Lett 2016;26:707–13.
47. Beloribi-Djefaflia S, Vasseur S, Guillaumond F. Lipid metabolic reprogramming in cancer cells. Oncogenesis 2016;5:e189–9.
48. Verdurmen WP, Thanos M, Ruttekolk IR, Gulbins E, Brock R. Cationic cell-penetrating peptides induce ceramide formation via acid sphingomyelinase: implications for uptake. J Control Release 2010;147:171–9.
49. Jobin ML, Bonnafous P, Temsamani H, Dole F, Grélard A, Dufourc EJ, et al. The enhanced membrane interaction and perturbation of a cell penetrating peptide in the presence of anionic lipids: toward an understanding of its selectivity for cancer cells. Biochim Biophys Acta 2013;1828:1457–70.
50. Sok M, Sentjurc M, Schara M, Stare J, Rott T. Cell membrane fluidity and prognosis of lung cancer. Ann Thorac Surg 2002;73:1567–71.
51. Fong PC, Boss DS, Yap TA, Tutt A, Wu P, Mergui-Roelvink M, et al. Inhibition of poly(ADP-ribose) polymerase in tumors from BRCA mutation carriers. N Engl J Med 2009;361:123–34.
52. Robson M, Im SA, Senkus E, Xu B, Domchek SM, Masuda N, et al. Olaparib for metastatic breast cancer in patients with a germline BRCA mutation. N Engl J Med 2017;377:523–33.
53. Lord CJ, Ashworth A. Mechanisms of resistance to therapies targeting BRCA-mutant cancers. Nat Med 2013;19:1381–8.
54. Chernikova SB, Game JC, Brown JM. Inhibiting homologous recombination for cancer therapy. Cancer Biol Ther 2012;13:61–8.
55. Fontana AO, Augsburger MA, Grosse N, Guckenberger M, Lomax AJ, Sartori AA, et al. Differential DNA repair pathway choice in cancer cells after proton- and photon-irradiation. Radiother Oncol 2015;116:374–80.

Supplementary Information

A short BRCA2-derived cell-penetrating peptide targets RAD51 function and confers hypersensitivity towards PARP inhibition

Anika Trenner, Julia Godau and Alessandro A. Sartori

This PDF file includes:

- Supplementary Tables:
  - Table S1: Primary antibodies
  - Table S2: Secondary antibodies
  - Table S3: siRNA oligos
- Supplementary Figure Legends
- Supplementary References
- Supplementary Figures:
  - Figure S1, related to Figure 1: BRC4 peptide inhibits RAD51 binding to BRCA2 and RAD51 self-oligomerization.
  - Figure S2; related to Figure 2: Efficient cellular uptake of TAMRA- and Fluorescein-labeled R9-BRC4 peptides.
  - Figure S3, related to Figure 4: BRC4 peptide suppresses DNA damage-induced RAD51 foci formation in U2OS cells.
  - Figure S4, related to Figure 5: BRC4 peptide does not affect bulk DNA replication.
  - Figure S5, related to Figure 6: BRC4 peptide confers DNA damage hypersensitivity.
  - Figure S6, related to Figure 6: BRC4 peptide confers olaparib hypersensitivity in cancer cell lines.

Supplementary Tables

Table S1: Primary antibodies

Antibody target	Species	Supplier/Reference	Applications	Dilution
ATM-pS1981	rabbit	Abcam (ab81292)	IB	1:1000
ATM (2C1)	mouse	GeneTex (GTX70103)	IB	1:1000
BRCA2 (OP95)	mouse	Calbiochem	IB	1:1'000
BrdU/IdU (B44)	mouse	BD Biosciences (347580)	DNA Fibers	1:80
BrdU/CIdU	rat	Abcam (ab6326)	DNA Fibers	1:400
CHK2-pT68	rabbit	CellSignaling	IB	1:1'000
CHK2	rabbit	Abcam (ab47433)	IB	1:10'000
Cyclin D1	rabbit	NeoMarkers (MS-210)	IB	1:1'000
GFP (B-2)	mouse	Santa Cruz (sc-9996)	IB	1:100
GST	mouse	Genscript	IB	1:1000
γH2AX	mouse	Millipore	IF	1:400
MRE11 (12D7)	mouse	GeneTex	IB	1:1000
Rad50	mouse	GeneTex (13D3)	IB	1:400
RAD51	rabbit	Abcam	IB	1:2000
RAD51	rabbit	(1)	IF	1:500
Tubulin	mouse	Sigma-Aldrich (T9026)	IB	1:20'000

Table S2: Secondary antibodies

Antibody	Supplier/Reference	Applications	Dilution
HRP-conjugated	GE Healthcare	IB	1:5000
Alexa Fluor-488	Life Technologies	IF/DNA Fibers	1:1'000/1:250
Alexa Fluor-647	Life Technologies	IF	1:1'000
Cy3 anti-rat	Immuno Research	DNA Fibers	1:250

Table S3: siRNA oligos

Name	Sense Sequence (5'-3')	Reference/Cat. No.	Supplier
CNTL	Negative Control No. 2 siRNA	4390846	Ambion
BRCA2	CAGUUGAAAUUAAACGGAA	s2083	Ambion
MRE11	CGACUGCGAGUGGGACUAUA	s8961	Ambion

Supplementary Figure Legends

Figure S1. BRC4 peptide inhibits RAD51 binding to BRCA2 and RAD51 self-oligomerization.

A, Multiple sequence alignment of all 8 BRC repeats in human BRCA2. The two tetrameric RAD51 interaction motifs are highlighted in boxes. **B,** Schematic view of the full-length human BRCA2 protein depicting BRC repeats 1-8 and a C-terminal region implicated in RAD51 interaction. GST-tagged BRCA2 fragments spanning all 8 BRC repeats and the C-term of BRCA2 are shown below. **C,** Indicated GST-BRCA2 fusion proteins were immobilized on GSH beads and added to HeLa nuclear extracts in the absence (-) or presence of the indicated amounts of $BRC4^{wt}$ and $BRC4^{mut}$. **D** and **E,** Lysates of U2OS cells inducibly expressing GFP-RAD51 were supplemented with increasing amounts of the indicated BRC4 peptides and subjected to immunoprecipitation (IP) using anti-GFP affinity resin. Inputs and co-immunoprecipitated protein complexes were analyzed by immunoblotting. SE and LE denote short and long exposure times of the same anti-RAD51 immunoblot.

Figure S2. Efficient cellular uptake of TAMRA- and Fluorescein-labeled R9-BRC4 peptides.

A, Hela and U2OS cells were pre-stained with Hoechst 33342 for 30 minutes to visualize nuclei. After washing, cells were incubated with the indicated concentrations of the R9-BRC4^{wt} peptide for 1 hour in serum-free medium and thoroughly washed. Peptide uptake was analyzed by live cell confocal microscopy. The scale bar represents 20 μm. **B,** Dot plots illustrate representative flow cytometry profiles after incubation of HeLa cells with no peptides or 10 μM of R9-BRC4^{wt}. The intensity of the TAMRA signal is plotted against the side-scatter area (SSC-A). Gate depicts percentage of TAMRA-positive cells. **C,** HeLa and U2OS cells were stained for 30 minutes with Hoechst 33342 to visualize nuclei and washed with PBS before adding 10 μM of Fluorescein-labeled R9-BRC4^{wt} and R9-BRC4^{mut} peptides. After 1-hour incubation in serum-free medium, cells were washed extensively and live cells were directly imaged on a confocal microscope. The scale bar represents 20 μm. **D,** HeLa and U2OS cells were washed with PBS before incubation with 10 μM of the Fluorescein-labeled R9-BRC4 peptides in serum-free medium for 1 hour. Cells were harvested by trypsinization and Fluorescein signal intensities were recorded on a flow cytometer by scoring 20'000 events. Bar graph depicts median Fluorescein fluorescence intensity. a.u. = arbitrary units. Data are presented as the mean ± s.d. (n = 3). **E,** 10 pmol of freshly solubilized peptides (lanes 2 and 3) and whole-cell lysates of 70'000 peptide-transfected cells as described in (D) were loaded onto Tricine-SDS-PAGE gel and Fluorescein signals were analyzed using a FluoroImager.

Figure S3. BRC4 peptide suppresses DNA damage-induced RAD51 foci formation in U2OS cells.

A, U2OS cells were either transfected with control (CNTL) or BRCA2 siRNA oligos for 48 hours or incubated with 10 μM of the indicated cell-penetrating peptides

(CPPs) for 1 hour before treatment with 100 nM camptothecin (CPT) for 1 hour. Whole-cell lysates were analyzed by immunoblotting using the indicated antibodies. **B,** Cells treated as in (A) were pre-extracted, fixed and immunostained for γH2AX. Depicted are representative fluorescent microscopy images. Scale bar represents 10 μM. **C** and **D,** Same cells as in (A) were treated with 100 nM CPT for 1 hour before transfecting them with the depicted peptides (10 μM) and releasing them for 3 hours in serum-containing medium. Cells were pre-extracted, fixed, and immunostained for RAD51. (C) Scale bars represent 10 μm and 5 μm (Zoom). (D) The graph illustrates the percentage of cells displaying more than 10 RAD51 foci/nucleus. For each condition at least 100 cells were scored. Data are presented as the mean ± s.d. (n = 4). Statistical significance (**, p-value ≤ 0.01; ns, non significant) was calculated with Tukey's multiple comparison test using two-way ANOVA. **E,** HeLa cells were incubated for 1 hour with 10 μM R9-BRC4^{wt}. Cells were washed and released for the indicated time points in presence of 50 μg/ml cycloheximide (CHX). Whole-cell lysates were analyzed by immunoblotting using the indicated antibodies.

Figure S4. BRC4 peptide does not affect bulk DNA replication.

U2OS cells were incubated with 10 μM of R9, R9-BRC4^{wt}, or R9-BRC4^{mut} in serum-free medium for 1 hour, washed with PBS and allowed to incorporate EdU (10 μM) for 30 minutes. Cells were harvested, permeabilized, fixed, and immunostained with anti-EdU antibody and DAPI before analysis by flow cytometry. Dot plots represent the intensity of the EdU signals (y-axis) against the DNA content (DAPI) (x-axis). Gates to quantify replicating cells were set with mock-treated sample (no peptide) and the percentage of cells within each gate is indicated. a.u. = arbitrary units.

Figure S5. BRC4 peptide confers DNA damage hypersensitivity.

A, HeLa cells were transfected with the indicated siRNAs or left untransfected for standard peptide transduction. 24 hours later, cells were plated at low cell density into 24-well plates. Another 24 hours later, cells were treated with 1 μM CPT, washed extensively, and subsequently incubated for 1 hour with 10 μM of the indicated peptides. Immediately after, serum-containing medium was added, cells were grown for 10 days and colonies were stained using crystal violet. Left panel, representative images of a colony formation assay are shown. Right panel, relative clonogenic survival is depicted as bar graph. **B,** PEO1 and PEO4 were transfected with indicated siRNAs or left untransfected for subsequent peptide incubation. One day later, cells were seeded at low cell density and 24 hours post-seeding incubated for 1 hour with 10 μM of indicated peptides and 1 μM olaparib in a serum-free environment. Serum-containing medium with 1 μM olaparib was added and cells were grown for 14 days before fixation. Left panel, representative immunoblot is shown. Central panel, bar graph illustrates clonogenic survival relative to untreated conditions. Right panel, PEO1 and PEO4 were stained with Hoechst and transfected with 10 μM R9-BRC4^{wt} prior to confocal image acquisition. The scale bar represents 20 μm. **A** and **B**, Data are represented as mean ± s.d. (n = 3). Statistical significance (****, p-value ≤ 0.0001; ***, p-value ≤ 0.001; ** p-value ≤ 0.01; ns, non significant) was calculated with Tukey's multiple comparison test using one-way ANOVA.

Figure S6: BRC4 peptide confers olaparib hypersensitivity in cancer cell lines.

A, Representative images of colony formation assay shown in Fig. 6E. **B,** HeLa, RPE1, MRC5 and MCF10A cells were stained for 30 minutes with Hoechst 33342 to visualize nuclei, transfected with 10 μM of TAMRA-labeled R9-BRC4^{wt} and directly

imaged on a confocal microscope. The scale bar represents 20 μm. **C,** Same cells as in (B) were harvested by trypsinization and TAMRA signal intensities were recorded on a flow cytometer. Bar graph illustrates median TAMRA intensities. Data are represented as mean ± s.d. (n = 2). a.u. = arbitrary units.

Supplementary References

1. Simandlova J, Zagelbaum J, Payne MJ, Chu WK, Shevelev I, Hanada K, et al. FBH1 helicase disrupts RAD51 filaments in vitro and modulates homologous recombination in mammalian cells. J Biol Chem. 2013;288:34168–80.

Supplementary Figure 1

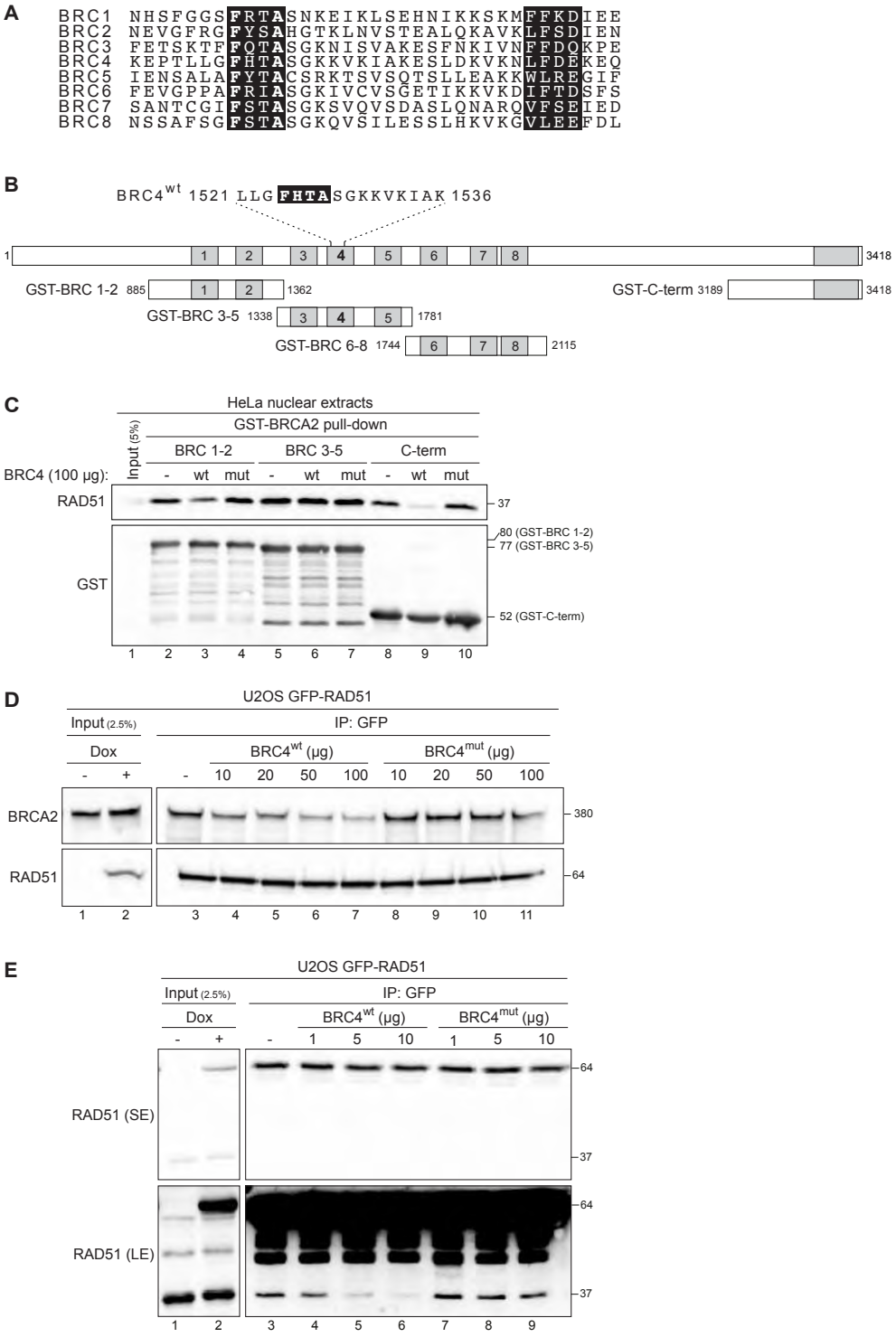

Supplementary Figure 2

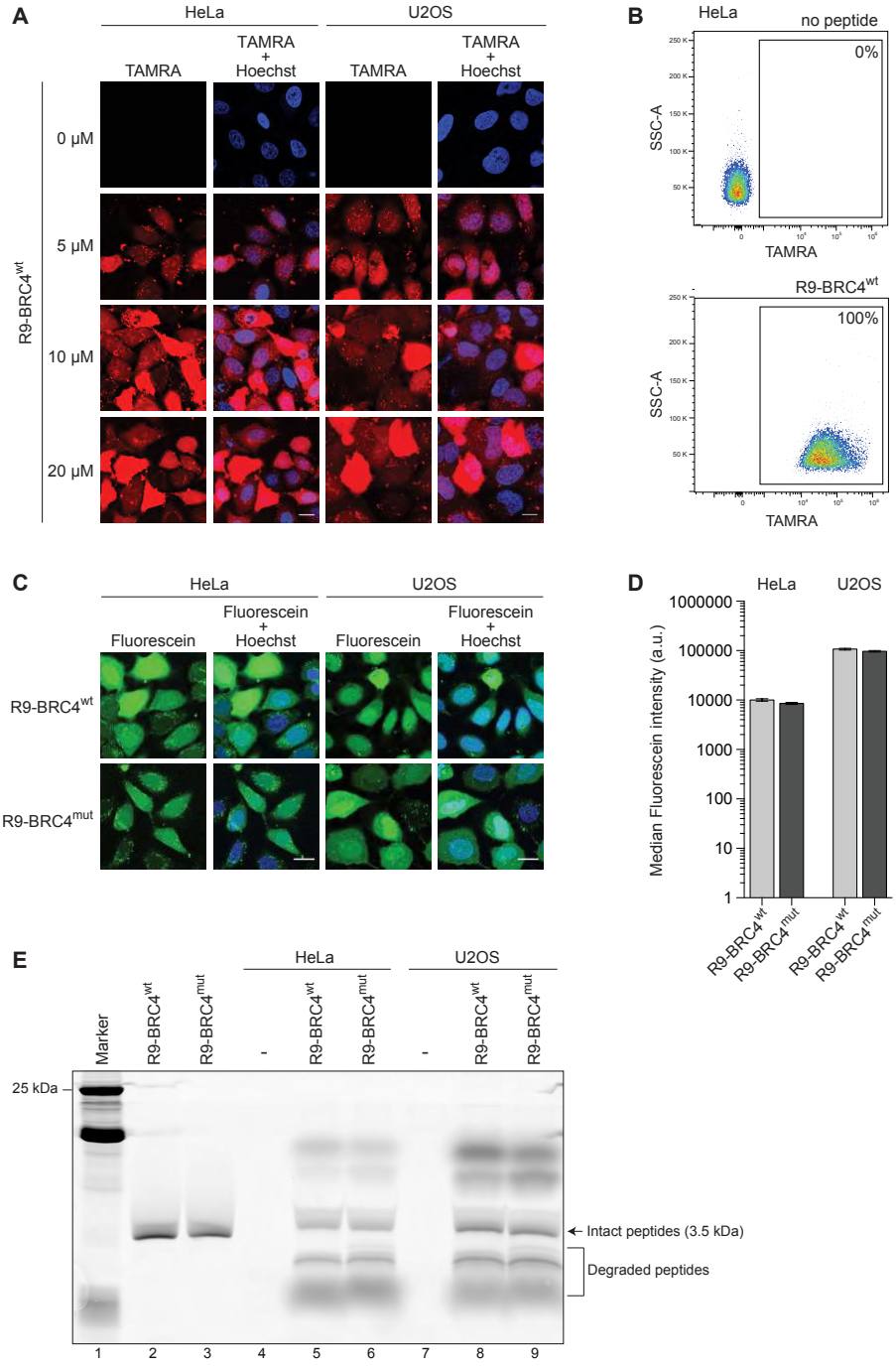

Supplementary Figure 3

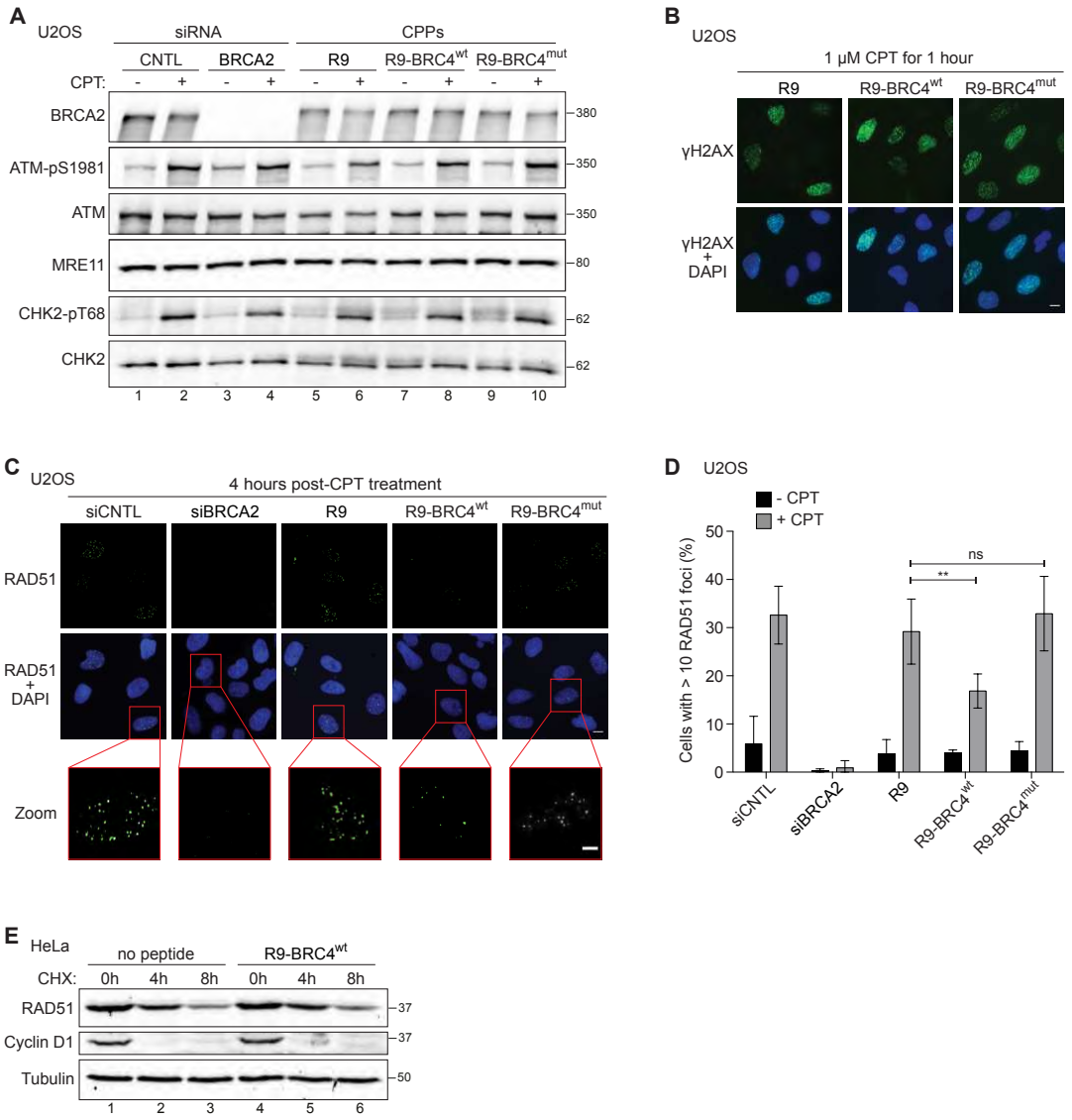

Supplementary Figure 4

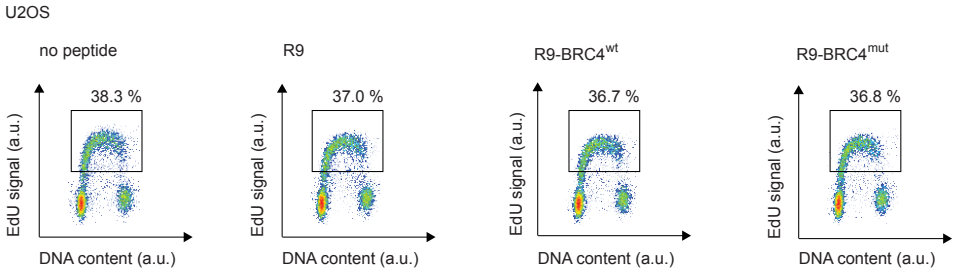

Supplementary Figure 5

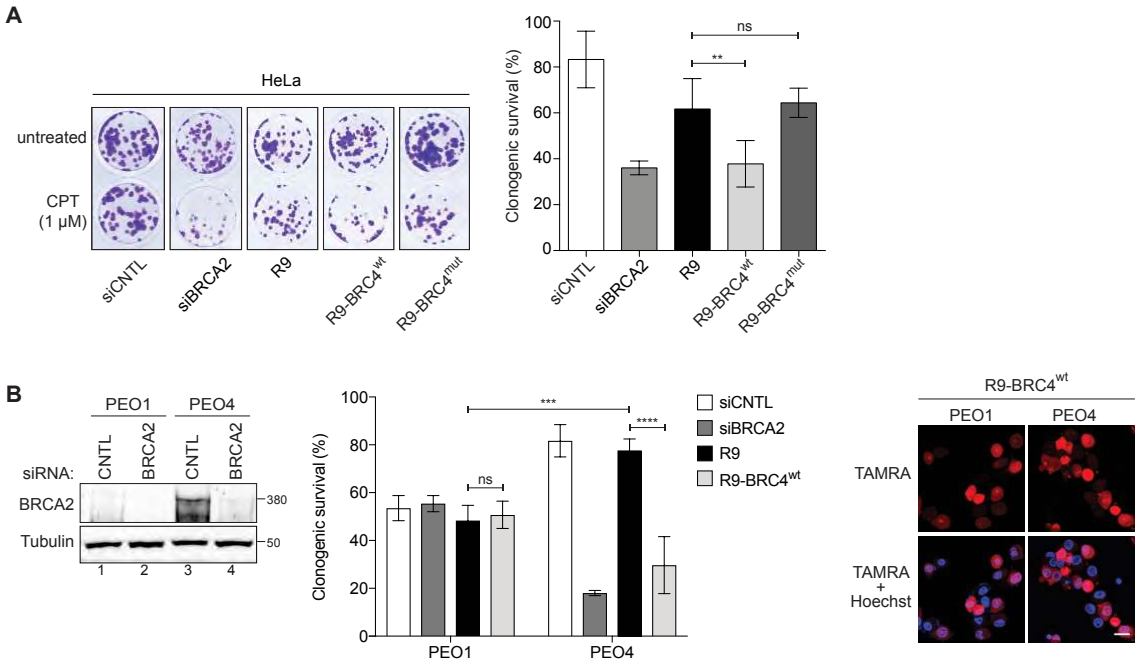

Supplementary Figure 6